INFORMATION TO USERS

This manuscript has been reproduced from the microfilm master. UMI films the text directly from the original or copy submitted. Thus, some thesis and dissertation copies are in typewriter face, while others may be from any type of computer printer.

The quality of this reproduction is dependent upon the quality of the copy submitted. Broken or indistinct print, colored or poor quality illustrations and photographs, print bleedthrough, substandard margins, and improper alignment can adversely affect reproduction.

In the unlikely event that the author did not send UMI a complete manuscript and there are missing pages, these will be noted. Also, if unauthorized copyright material had to be removed, a note will indicate the deletion.

Oversize materials (e.g., maps, drawings, charts) are reproduced by sectioning the original, beginning at the upper left-hand corner and continuing from left to right in equal sections with small overlaps. Each original is also photographed in one exposure and is included in reduced form at the back of the book.

Photographs included in the original manuscript have been reproduced xerographically in this copy. Higher quality 6" x 9" black and white photographic prints are available for any photographs or illustrations appearing in this copy for an additional charge. Contact UMI directly to order.

UMI

A Bell & Howell Information Company
300 North Zeeb Road, Ann Arbor MI 48106-1346 USA
313/761-4700 800/521-0600

UNIVERSITÉ D'OTTAWA
UNIVERSITY OF OTTAWA

KINETICS OF VACANCY ANNEALING IN MONOLAYERS AND INSTABILITIES IN STRESSED MATERIALS

By

Zicong Zhou

A thesis submitted to
the School of Graduate Studies and Research
in partial fulfillment of the requirements
for the degree of Doctor of Philosophy

Department of Physics

University of Ottawa
Ottawa, Ontario
May, 1996

Abstract

Using isothermal-isochore and isoenthalpic-isobaric molecular dynamics simulations, with either periodic boundary conditions or free boundary conditions, we explore in detail the vacancy annealing mechanisms in monolayers with or without substrate. A new mechanism, named dislocation mediated annealing (DMA), is observed. In this mechanism, vacancies condense rapidly into dislocation dipoles, with an associated shear modulus collapse, and anneal out of the system. External pressure, mobility of the vacancies and increased range of the interactions all favour DMA. We find that the other mechanism observed, annealing of the vacancies by the formation of voids, is a slower process, by at least an order of magnitude.

We clarify the concept of reference configuration and volume in the calculation of the elastic constants in "equilibrium" fluctuation methods and give the general expressions. We derive the correct fluctuation formulae for elastic constants in uniform dilation systems. We show that the traditional thermodynamic potentials cannot be used in stability problems for an anisotropically stressed system. We derive general expressions for the mechanical stability criteria of a stressed material. We find that for a system under isotropic initial stress, the elastic stiffness coefficients which govern stress-strain relations can be used as stability criteria. However, for a system under anisotropic initial stress, stability criteria are different from either elastic constants or elastic stiffness coefficients. We show that the stability conditions in the constant pressure ensemble are stronger than in the constant volume ensemble. Exact solutions for perfect systems at zero temperature with three types of interactions of different range are found to be consistent with those obtained from long-wavelength expansion and computer simulations.

We study the rupture of models of solid membranes for several interparticle interactions. We show that rupture at zero temperature occurs at the mechanical instability point. We verify that in general rupture at finite temperature takes place before the mechanical instability point. Two regimes are observed in the variation of the critical rupture pressure (P_c) with temperature (T) for both one and two

dimensional (2D) systems; P_c drops very fast at low T, but relatively slowly at high T. In ideal 2D membranes under isotropic tension, a linear decrease of P_c was observed at high T. The kinetics in non defected systems, involve, just before rupture, the creation of gliding dislocation dipoles. In-grown vacancies reduce the influence of dislocations and can lead to direct cavitation.

Acknowledgements

First of all, I would like to express my deepest thanks to my supervisor, Dr. Béla Joós for his helpful guidance, advice, support, understanding, encouragement and confidence. I highly enjoy having the opportunity to work with Béla, whose superb intuition in physics, his conscientious and meticulous attitude to scientific work extremely impresses me.

I take this opportunity to thank Dr. M. S. Duesbery and Dr. M. Wortis for fruitful discussions and suggestions.

I take this opportunity to thank Qiang Ren and Deyang Qu, a very enthusiastic and friendly couple, for their great help in both my academic and daily life.

I take this opportunity to thank my friends, Yang Cai, Hong Guo, Guowei Zhang, Meizhen Dang, Lixin Dou, G. Nixon, ... for lots of help.

I take this opportunity to thank all the support staff and members of the Department for creating a stimulating atmosphere.

Besides, I would like to take this opportunity to thank the School of Graduate Studies and Research of the University of Ottawa for awarding me a Entrance Research Scholarship, a Partial Tuition Fee Waiver for Foreign Students, and a Special Research Assistantship.

My special thanks must go to my parents, my brothers and sisters. Without their encouragement and support, I could not even enter into the field of physics. Finally, I would like to thank my wife Chiu-Ying Ngai. Without her enduring love and constant support, I would not have been able to finish this work.

Contents

List of Tables

List of Figures

Chapter 1

Introduction

In this thesis we have investigated, with computer simulations on model systems, two phenomena in monolayers out of equilibrium: vacancy annealing and rupture. In the process, since the elastic properties are a valuable measure of the structural response of a system, we have looked in detail into the calculation of elastic constants through computer simulation, and the establishment of stability criteria of an elastic medium.

Vacancy damage is a common occurrence in thin films, membranes and surfaces, more so than in bulk solids due to the direct exchange with the external environment as well as entropic considerations. The fairly high vacancy concentrations may create some serious effects on the structural properties. The phenomenon has been extensively studied experimentally in bulk system but few microscopic studies has been done in either bulk systems or monolayers. The problems of interest to us are: what is the impact of the vacancies on the elastic properties of the system, under what conditions vacancy damage will repair itself, and what are the vacancy annealing kinetics.

When considering structural properties, it is natural to encounter the problem of the calculation of elastic constants and the stability of the material. Elastic constants are not only one of the fundamental mechanical and thermodynamic properties of any material but they are also relevant to their stability. Therefore, how to calculate them correctly and efficiently is an important subject. There exists two sets of "equilibrium" fluctuation formulae for elastic constants, which at first sight do not seem trivially related. The mechanical stability of materials is not only one

of the most central issues in elasticity, but is also an essential consideration in the analysis of structural responses in solids. It has been shown that elastic constants can be used as stability criteria for an unstressed system. However, the validity of these stability criteria for a stressed system is not a simple question. Whether it is possible to find stability criteria within the framework of equilibrium thermodynamics, has also not been well understood.

The rupture of membranes is a common instability phenomenon but theories have been few and usually focus on the response to the mechanical forces neglecting the thermal effects. The rupture kinetics, on a microscopic scale, and its dependence on the range of interparticle interactions and defects composition, are very interesting. On the other hand, the relationship between mechanical instability and rupture is also intriguing.

All these questions have been investigated in the following three closely related projects:

1). Vacancy annealing mechanisms in monolayers using molecular dynamics simulations and elasticity theory. The effects of the range of interparticle interactions, the vacancy concentration, the boundary conditions and the simulation ensembles are investigated. The information obtained from this project provides a full picture of vacancy annealing mechanisms in two dimensions (2D) and may be helpful to a better understanding of bulk annealing kinetics.

2). To clarify the concept of reference state in the calculation of elastic constants and give correct expressions for the "equilibrium" fluctuation formulae for a material under arbitrary loads. On the basis of the laws of thermodynamics and using thermodynamic potentials, the general form of the mechanical stability criteria are derived for a homogeneously deformed material in the microcanonical and the canonical ensembles under specified loading conditions. This project therefore provides not only the basis to calculate elastic constants correctly but also the possibility to predict the critical loading at which the instability occurs.

3). Our final project was to study the rupture of solid membranes with two classes of simple models, a one dimensional (1D) closed membrane (or 2D vesicle) and a flat 2D membrane, using molecular dynamics simulations and the stability criteria developed in 2).

The outline of the thesis is as follows. The next chapter is a brief introduction

to the models in our computer simulations. In chapters 3 and 4, detailed results are presented for the vacancy annealing mechanisms in monolayers, in both infinite and finite systems, respectively. Chapters 5 and 6 provide the results on the calculation of elastic constants and the derivation of stability criteria respectively. Chapter 7 gives the results on rupture. An overall conclusion ends the main part of the thesis. An introduction to the molecular dynamics techniques used in our work is the subject of Appendix A. For convenience, other mathematical details cited in the thesis are presented in remaining appendices.

Chapter 2

Modelling in Computer Simulations

2.1 Introduction

In this Chapter, we will introduce the models used in our computer simulations. We first describe the interparticle interactions used in our simulations. They are, the Lennard-Jones potential (LJP), the nearest - neighbour piecewise linear force potential (PLFP), the 4-8 potential (4-8P), the Steele's potential for the substrate and some potentials for two dimensional (2D) vesicles. The simulation ensembles, the relevant physical quantities and the boundary conditions are then discussed.

2.2 Interparticle Interactions

Monolayers can appear in many forms with various interactions. In this thesis, we focus mainly on monolayers formed of particles interacting with central forces.

2.2.1 Interactions in Two-dimensional Systems

One of the simplest interactions is the nearest-neighbour piecewise linear force potential (PLFP) as shown in Fig. 2.1. The PLFP is a simple, albeit physical interparticle potential, which yields a linear restoring force between the nearest neighbour

particles. The potential is given by:

$$\phi_{PLFP}(r) = \begin{cases} \frac{1}{2}\kappa(r-d_0)^2 - \kappa w^2 & r \leq d_0 + w \\ -\frac{1}{2}\kappa(r-d_0-2w)^2 & d_0 + w < r \leq d_0 + 2w \\ 0 & r > d_0 + 2w \end{cases} \tag{2.1}$$

where r is the distance between atoms, w is taken to be $0.15d_0$ as in reference[1]. For this value of w the dislocation core (the dislocation core is the region where linear elasticity theory fails) has only one broken bond. Smaller values of w lead to more broken bonds in the core. There is no strong core repulsion in this potential. The well-depth is $0.0225\kappa d_0^2$ at lattice constant d_0 and the range of attractive part is very short, only $0.3d_0$ long. Under moderate pressure, there are only nearest neighbour interactions.

The PLFP consists of two parabolic functions and the force derived from this potential is continuous and formed by two linear segments:

$$f_{PLFP}(r) = \begin{cases} -\kappa(r-d_0) & r \leq d_0 + w \\ \kappa(r-d_0-2w) & d_0 + w < r \leq d_0 + 2w \\ 0 & r > d_0 + 2w \end{cases} \tag{2.2}$$

By convention, repulsive forces are positive while attractive forces are negative. For $r \leq 1.15d_0$, this potential is equivalent to a purely harmonic Hooke's law interaction.

Another simple potential, the LJP or 6-12 potential, shown in Fig. 2.2 is also well known. It is given by

$$\phi_{LJP}(r) = 4\epsilon\left[\left(\frac{\sigma}{r}\right)^{12} - \left(\frac{\sigma}{r}\right)^{6}\right]. \tag{2.3}$$

The LJP provides a reasonable description of the properties of rare gases, via computer simulations, if the parameters ϵ and σ are chosen appropriately. The potential has a long-range attractive tail of the form $-1/r^6$, essentially due to corrections from instantaneous configurations of electron clouds surrounding atoms ('van der Waals' or 'London' dispersion). There is a negative well of depth ϵ at $2^{1/6}\sigma$, responsible for cohesion in condensed phases. Finally, there is a steeply repulsive wall at short distances less than $r \sim \sigma$, due to non-bonded overlap between the electron clouds. The force that results from the LJP is

$$f_{LJP} = -\frac{d\phi_{LJP}}{dr} = 24\left(2\left(\frac{\sigma}{r}\right)^{13} - \left(\frac{\sigma}{r}\right)^{7}\right)\frac{\epsilon}{\sigma} \tag{2.4}$$

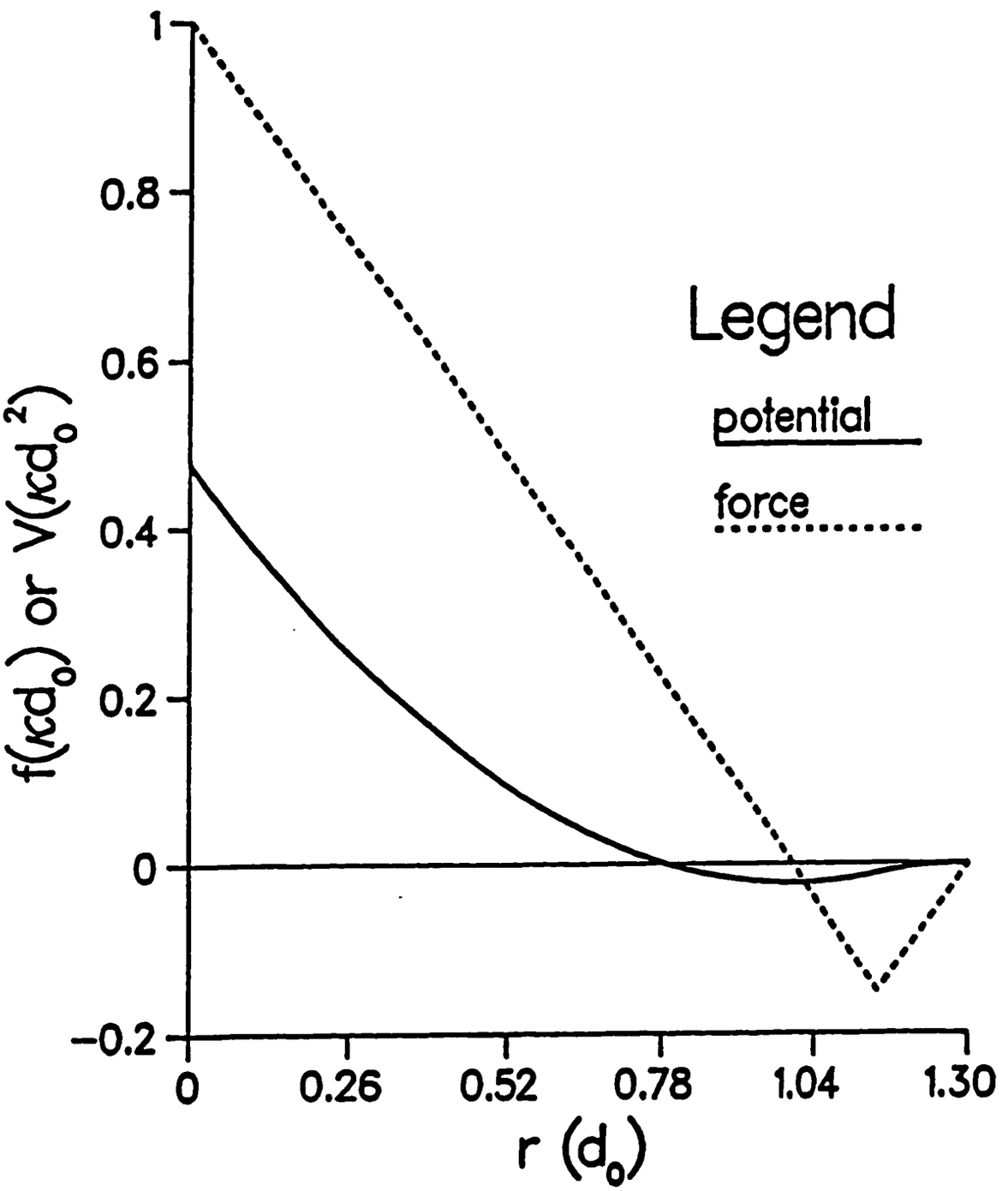

Figure 2.1: The nearest neighbour piecewise linear force potential (PLFP, solid line) and force (dashed line). The unit for potential is κd_0^2 and force is κd_0.

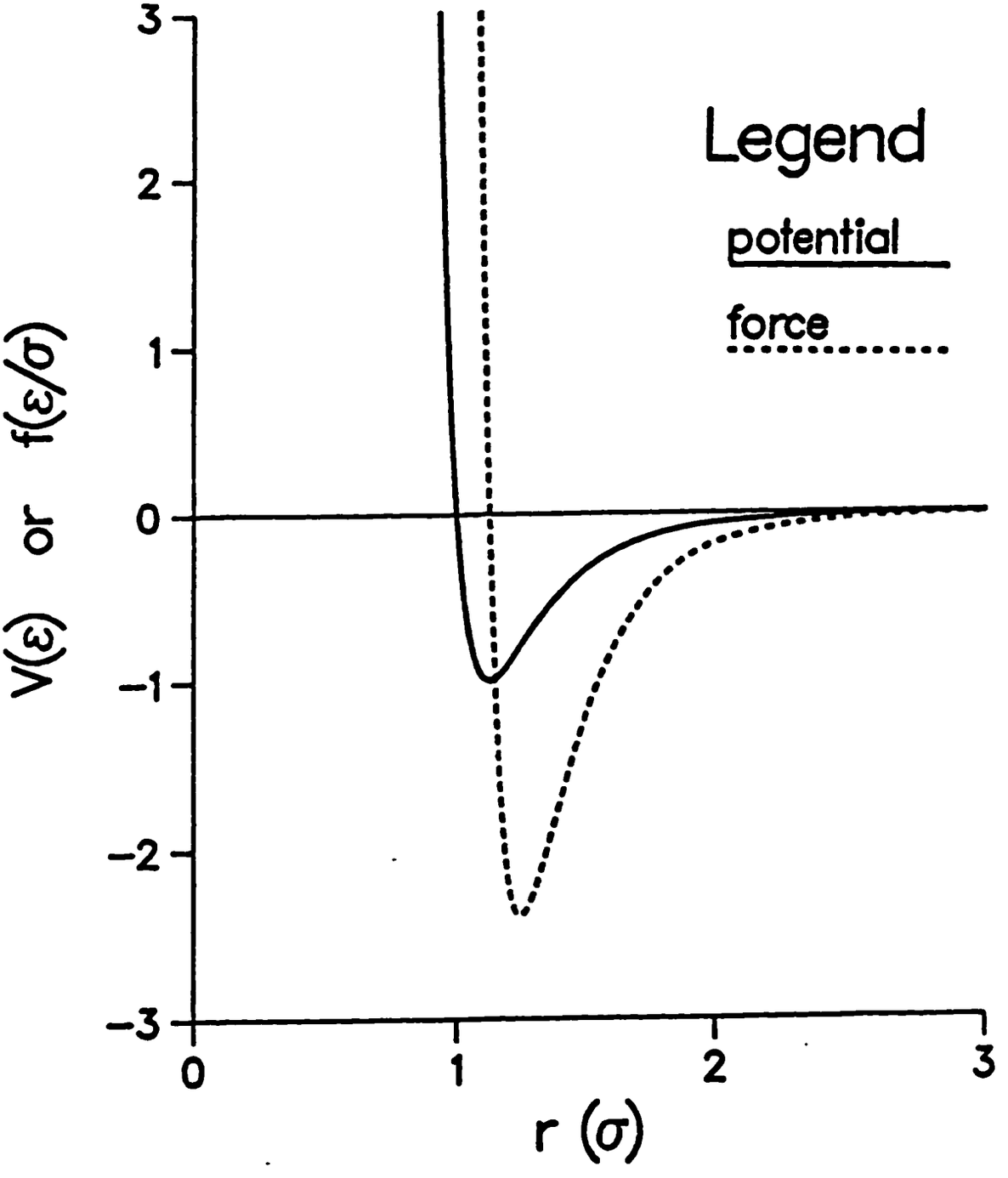

Figure 2.2: The Lennard - Jones potential (LJP, solid line) and force (dashed line). The unit for potential is ϵ and for force is ϵ/σ.

The cut-off for the LJP in most of our simulations with periodic boundary conditions (PBC) was chosen to be $r_c = 2.5\sigma$ but the choice of $r_c = 3.0\sigma$ in some samples does not give noticeable changes. In finite patch studies, we always chose $r_c = 3.0\sigma$.

The LJP and PLFP have been extensively used although for different purposes. The PLFP have been used mostly in simulations of the plasticity of solids [1, 2, 3, 4]. The PLFP system is particularly attractive because, with the triangular lattice in which it usually condenses, it behaves as a continuum model discretized by the finite element method. In contrast, the LJP was used extensively in attempts to understand the nature of the melting transition in two dimensions (for reviews see references [5] and [6]). Recently the melting behaviour of the PLFP was also considered [7]. Due to their simplicity, the PLFP and LJP systems are still the first systems which come to mind when a simple model for a new property of materials is being sought [8, 9].

To explore further the effect of the range of the interaction potential, we also consider the monolayer with a 4-8 potential (4-8P). The reasons for choosing the 4-8P are, that it is easy to compare with the LJP and PLFP, and that it has a longer range than either of the other two. The 4-8P is given by:

$$\phi_{4-8}(r) = 4\epsilon' \left[\left(\frac{\sigma'}{r}\right)^8 - \left(\frac{\sigma'}{r}\right)^4 \right], \tag{2.5}$$

The potential has a very long-range attractive tail of the form $-1/r^4$. There is a negative well of depth ϵ' at $2^{1/4}\sigma$. The force that results from the 4-8P is

$$\phi_{4-8}(r) = 16\epsilon' \left[2\left(\frac{\sigma'}{r}\right)^9 - \left(\frac{\sigma'}{r}\right)^5 \right] \frac{\epsilon'}{\sigma'}, \tag{2.6}$$

As in the LJP system, the cut-off for 4-8P with PBC was chosen to be $r_c = 2.5^{1.5}\sigma'$ but the choice of $r_c = 3.0^{1.5}\sigma'$ in some samples does not give noticeable changes. For a finite patch, we always took $r_c = 3.0^{1.5}\sigma'$.

To investigate the effect of the range of the interaction potential more directly, the three potentials have been chosen to have the same depth, equal to κw^2, and the same minimum ($\sigma = 2^{-\frac{1}{6}} d_0$, $\sigma' = 2^{-\frac{1}{4}} d_0$). For the PLFP the depth is set by the value of w which has been taken as $0.15 d_0$, consequently for the LJP and 4-8 potential $\epsilon = \epsilon' = 0.0225 \kappa d_0^2$.

Using d_0 as the unit of length, the LJP becomes

$$\phi_{LJP}(r) = \epsilon \left[\left(\frac{d_0}{r} \right)^{12} - 2 \left(\frac{d_0}{r} \right)^{6} \right] \tag{2.7}$$

and its force is

$$f_{LJP}(r) = 12 \left[\left(\frac{d_0}{r} \right)^{13} - \left(\frac{d_0}{r} \right)^{7} \right] \frac{\epsilon}{d_0} \tag{2.8}$$

Correspondingly, for the 4-8P

$$\phi_{4-8P}(r) = \epsilon' \left[\left(\frac{d_0}{r} \right)^{8} - 2 \left(\frac{d_0}{r} \right)^{4} \right] \tag{2.9}$$

and its force is

$$f_{4-8P}(r) = 8 \left[\left(\frac{d_0}{r} \right)^{9} - \left(\frac{d_0}{r} \right)^{5} \right] \frac{\epsilon'}{d_0} \tag{2.10}$$

In 2D, monolayers formed of particles interacting with central forces will tend to form triangular lattices, which are isotropic. This is the closest packing in two dimensions and it is favored at densities where the nearest neighbour interparticle distance is close to the minimum of the interparticle interaction. That is the case whenever the pressure is not too large as is the case in our situations. Lattices with fewer nearest neighbours are obtained at very high pressure [7, 10].

2.2.2 Holding Potential of the Substrate

In a real adsorbed system there is always the third degree of freedom. The monolayer will be held by a holding potential which can be weak or strong, and may or may not have significant lateral variations. We shall not consider in this thesis the effects of the lateral variations. We considered the effects of the substrate by applying a smooth (without corrugation) holding potential to the monolayers. The potential chosen is the type occurring in physisorption, a sum of van der Waals interactions. It was first calculated by Steele [11] for a graphite structure and his potential is given by:

$$U_{sub}(z) = \frac{4\pi\epsilon\sigma^6}{a_s d^4} \left(\frac{2}{5} \left(\frac{\sigma}{d} \right)^6 \left(\frac{z}{d} \right)^{-10} - \left(\frac{z}{d} \right)^{-4} - \frac{1}{3} \left(\frac{z}{d} + 0.61 \right)^{-3} \right) \tag{2.11}$$

where a_s is the area of the basal-plane unit cell and d the interlayer spacing. It can be rewritten in reduced units as:

$$U_{sub}(z) = a_0 \left(a_1 z^{-10} - a_2 z^{-4} - \frac{1}{3}(a_3 z + 0.61)^{-3} \right). \tag{2.12}$$

a_0 can be used as a measure of the strength of the holding potential. In our simulations, we took $a_1 = 0.1230$, $a_2 = 0.6148$ and $a_3 = 1.1293$. These would be the values appropriate for Xe adsorbed on graphite. Several values of a_0 were considered, $a_0 = 0.4$, 0.3 and $0.03\kappa d_0^2$. The larger value applies to Xe on graphite but, as we shall see, for that value the potential is already strong enough to prevent any significant change from the case of the ideal flat monolayer. Most calculations were done for $a_0 = 0.3\kappa d_0^2$ which gives a depth of the holding potential of about $V_{sub}(0.8855) = -0.1995\kappa d_0^2$.

2.2.3 Circular Potential Well for Finite Patches

For the finite patch problem, to prevent the particles from drifting apart [12] and to produce the effect of an external pressure we created a circular potential well $V_{ext}(r)$, with a constant potential up to a certain radius r_c, and then a rising parabolic potential:

$$U_{ext}(r) = \begin{cases} 0 & r \le r_c \\ K_{ext}(r - r_c)^2 & r > r_c \end{cases} \tag{2.13}$$

We can change either K_{ext} or r_c to obtain the required pressure, but the pressure is more sensitive to r_c.

2.2.4 Interaction for the One-dimensional (1D) Closed Chain

In the 1D closed chains or 2D vesicles, the particles were assumed to have a main axis n. They interact through the pair potential

$$\phi(\mathbf{r}_1, \mathbf{r}_2) = 4\epsilon \left(\left(\frac{\sigma}{r_{12}} \right)^N - \left(\frac{\sigma}{r_{12}} \right)^M (1 + \gamma f(\mathbf{r}_1, \mathbf{r}_2) \right) \tag{2.14}$$

with

$$f(\mathbf{r}_1, \mathbf{r}_2) = \mathbf{n}_1 \cdot \mathbf{n}_2 - ((\mathbf{n}_1 + \mathbf{n}_2) \cdot (\mathbf{r}_{12}))^2 \tag{2.15}$$

We chose $M = 6, N = 12$ (Lennard Jones-like potential or LJP) and $M = 4, N = 8$ (4-8 potential or 4-8P) to probe the effects of the range of the interaction. The f term in the potential introduces an orientation interaction and γ can be used as a measure of that interaction. $\gamma = 0$ gives the usual $M - N$ potential and the system tends to form a bulk. In our simulations, we chose $\gamma = 0.9$ since for this value the particles can self-assemble into long chains at moderate temperatures. The interaction favours a parallel orientation of the particles (i.e. $\mathbf{n_1} \cdot \mathbf{n_2} = 1$). The cutoff was chosen to be $r_c = 3.0\sigma$ for LJP and $r_c = 3.0^{1.5}\sigma$ for 4-8P. The unit of time in the simulations is $t_0 = \sqrt{m\sigma^2/\epsilon}$.

To deal with the motion of $\mathbf{n}$, we also introduced a rotational inertia I for the particles and took $I = \frac{1}{2}m\sigma^2$ for convenience, where m is the mass of particles.

The pressurizing gas

A pressurizing gas was introduced to simulate the effect of an internal pressure in the vesicle. There is no interaction between the particles of the pressurizing gas. But the pressurizing gas interacts with the particles of the vesicles with a $1/r^{12}$ law. The pressurizing gas is essentially an ideal gas.

2.3 Ensembles in Molecular Dynamics (MD) Simulations

Corresponding to different statistical ensembles, there are also many ensembles in molecular dynamics (MD) simulations. The microcanonical (EVN) ensemble [13, 14, 15, 16], canoncial i.e. isothermal-isochore (TVN) ensemble [17, 18, 19], isoenthalpic-isobaric (HPN) ensemble [20, 21] and isothermal-isobaric (TPN) ensemble [16, 20, 21] are often used to simulate a system under isotropic or hydrostatic pressure. E is the energy, V the volume, N the particle number, T the temperature, H the enthalpy and P the hydrostatic pressure of the system. A more detailed descriptions of the MD ensembles can be found in Appendix A.

The experiments are usually performed in the conditions of isothermal-isochore or isothermal-isobaric and the response functions are the quantities easiest to measure. In principle, the physical results should be independent of the choice of the ensemble for an equilibrium state. However, the response functions, such as the specific heat and the elastic constants, are different in the different ensembles. Though

the response functions can be transformed between ensembles by using thermodynamic equalities [23, 24, 25], such a transformation in computer simulations may be impracticable due to accuracy problems. Furthermore, the critical behaviour of a system may be dependent on the choice of the ensemble. A well known example is that two phase coexistence is allowed in the isothermal-isochore ensemble but prohibited in the isothermal-isobaric ensemble [7, 26, 27]. Therefore, to choose the appropriate ensembles in simulations is not a negligible problem.

Since our systems in 2D with periodic boundary conditions (PBC) are essentially isotropic triangular lattices and we try to explore the effects of the external pressure, the natural choice in our simulations is the TPN ensemble. But to investigate the dependence of our results on the choice of the ensemble we also performed some simulations in the canonical ensemble with PBC. For finite patches we chose the TVN ensemble.

In our simulations, for both the TVN and the TPN ensembles, the damped force method was used to keep the temperature constant. In the second ensemble, the Andersen method was used to maintain the pressure constant (see, for instance, ref. [20] or our Appendix A).

For 2D systems, the half-step Verlet 'leap-frog' algorithm (see Appendix A) was used to integrate the equations of motion. But for 1D systems, the Gear predictor-corrector algorithm was used (see Appendix A).

2.4 Pressure

The pressure is an important thermodynamic quantity. In computer simulations, it can be calculated from the virial theorem

$$P = \frac{1}{3V}\left(\sum_i \frac{1}{m_i}\mathbf{p}_i \cdot \mathbf{p}_i + \sum_{i>j} \mathbf{f}_{ij} \cdot \mathbf{r}_{ij}\right), \tag{2.16}$$

where $\mathbf{p}_i$ is the momentum of particle i, $\mathbf{f}_{ij}$ the force acting on particle i due to particle j and V the volume of the system. In general, the pressure is composed of two parts: (a) the kinetic part due to the momentum carried by the particles and the (b) static part due to the momentum transferred as a result of forces acting

between particles. The 2D version of Eq. (2.16) is given by

$$P = \frac{1}{2A}\left(\sum_i \frac{1}{m_i}\mathbf{p}_i \cdot \mathbf{p}_i + \sum_{i>j} \mathbf{f}_{ij} \cdot \mathbf{r}_{ij}\right) \tag{2.17}$$

where A is the area of the system.

2.5 Reduced Units

In vacancy annealing and 2D rupture problems, we used κd_0^2 as the unit of energy and d_0 as the unit of length. It is also natural to use the mass as another fundamental unit. From these definitions, units of other quantities (pressure, force etc) can be determined.

energy	$E^* = E/\kappa d_0^2$
length	$L^* = L/d_0$
mass	$m^* = 1$
density	$\rho^* = \rho/d_0^2$
pressure	$P^* = P\kappa$
force	$\mathbf{f}^* = \mathbf{f}/(\kappa d_0)$
time	$\sqrt{m/\kappa}$

For the 1D problem, we used ϵ as the unit of energy and σ as the unit of length. Therefore, units of other quantities (pressure, force etc) become

energy	$E^* = E/\epsilon$
length	$L^* = L/\sigma$
mass	$m^* = 1$
density	$\rho^* = \rho/\sigma^2$
pressure	$P^* = P\sigma^2/\epsilon$
force	$\mathbf{f}^* = \mathbf{f}\sigma/\epsilon$
time	$\sqrt{m\sigma^2/\epsilon}$

The use of reduced units avoids the possible embarrassments of conducting essentially duplicate simulations. There are also technical advantages in the use of reduced units. If parameters such as $\epsilon = \kappa d_0^2$ and d_0 have been given a value of unity, they need not appear in a computer simulation program at all; consequently some time will be saved in the calculation of potential energies, forces etc.

2.6 Ensemble Average and Time Average

We assume that the system under consideration has a classical model Hamiltonian $\mathcal{H}$. We denote a state of the system by $\mathbf{r} = (\mathbf{x}^N, \mathbf{p}^N)$, where $\mathbf{x}$ is the coordinate, $\mathbf{p}$ the momentum and N the number of particles in the system. The property $A(\mathbf{r})$ to be calculated should be a function of the states of the system. From statistical mechanics, the macroscopic quantity corresponding to A is then given by

$$\langle A \rangle = \frac{1}{Z} \int_\Omega A(\mathbf{r}) f(\mathcal{H}(\mathbf{r})) d\mathbf{r} \tag{2.18}$$

where Ω is the volume of the phase space constituted by the set of states, the partition function Z is

$$Z = \int_\Omega f(\mathcal{H}(\mathbf{r})) d\mathbf{r} \tag{2.19}$$

and f is the distribution function of the system. Equation (2.18) is the *ensemble average* with the partition function Z. The distribution function f specifies the appropriate ensemble for the problem at hand.

The ensemble average is, however, not accessible in MD simulations. What we can compute in MD is a *time average*

$$\bar{A}_t = \frac{1}{t - t_0} \int_{t_0}^{t} A(\mathbf{r}(\tau)) d\tau \tag{2.20}$$

Assuming ergodicity, we allow the replacement of the ensemble average by a time average

$$\langle A \rangle = \bar{A}_\infty \tag{2.21}$$

At this point, one of the two major limitations of computer simulation methods arises. Clearly a computer simulation cannot follow a path over an infinite time. The *observation time* is limited to a finite duration so that actually the available phase space is a sample of the whole space. To reduce this finite time effect, one and maybe the most common way is to monitor the variations of physical quantities, such as the average of energy, pressure, lattice parameters, with time. Fortunately, in many situations of interest, these averages settle down very fast so we can obtain reasonable results from a moderate simulation time. Another way to reduce this finite time effect is to extrapolate the data to infinite time.

As well as the finite observation time, computer simulation is faced with a second major limitation: *finite system size*. In general, one is interested in the computation of a property in the thermodynamic limit, i.e. the number of particles tends to infinity. Computer simulations allows, however, only system sizes small compared to the thermodynamic limit so that there are possible *finite size effects*. In order to reduce their impact periodic boundary conditions are commonly imposed. They clearly affect some properties.

2.7 Boundary Conditions

2.7.1 Periodic Boundary Conditions (PBC)

Periodic boundary conditions (PBC) are the most popular ones in a simulation of N particles confined to a volume V (we imagine that the volume V is only a small portion of the bulk material). The volume V is called the *primary cell* or *MD cell* in molecular dynamics; it is representative of the bulk material to the extent that the bulk is assumed to be composed of the primary cell surrounded by exact replicas of itself. These replicas are called image cells. The image cells are each the same size and shape as the primary cell and each image cell contains the same N particles, which are *images* of particles in the primary cell. Thus the primary cell is imagined to be periodically replicated in all directions to form a macroscopic sample of the substance of interest. In order to fill all the space, it is important that the shape of volume V is regular. This periodicity extends to the positions and momenta of the images in image cells.

In the course of the simulation, as a particle moves in the primary cell, its images move exactly the same way in the neighbouring image cells. Thus, as a particle leaves the primary cell, one of its images will enter through the opposite face. There are no walls at the boundaries of the primary cell. A two-dimensional version of such a periodic system is shown in Fig. (2.3). The rhombic shape primary cell is labelled A.

It is important to make sure that contributions of the image particles have only a slight effect on the properties of the primary cell which we are interested in. In this case, we have to choose the size of the primary cell carefully to make it big enough to exclude the image effects and small enough to be manageable. The correct size

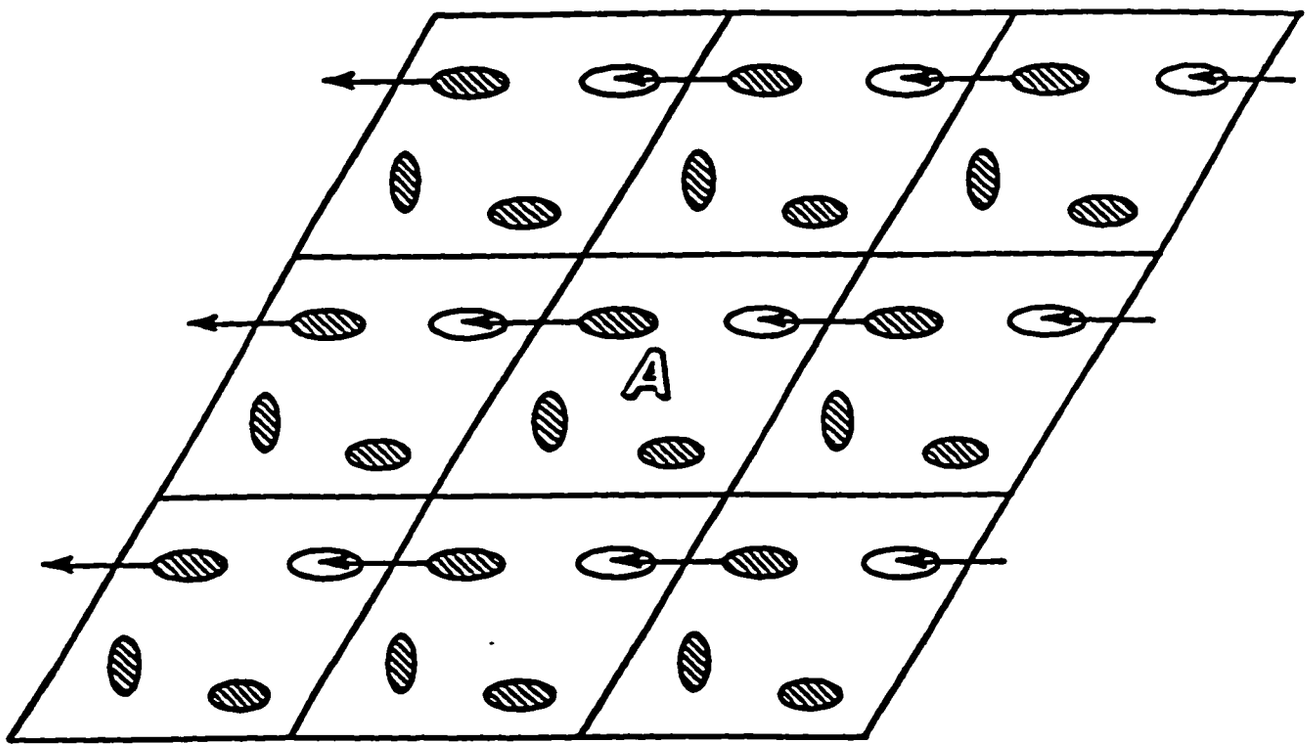

Figure 2.3: A two-dimensional periodic system showing the rhombic shape primary cell *A*. Atoms can enter and leave each cell across each of the four edges. In a three-dimensional system atoms would be free to cross any of the six faces.

of the primary cell depends both on the range of the interaction potential and the properties under investigation. For long range interparticle interactions, the size of the cell tends to be larger. However, if we are only concerned about the average energy of the cell, we can use a small cell. But if what we investigate involves in part of the cell, say, the energy of a dislocation dipole, the size of the cell needs at least to be 2-3 times the length of the dipole.

The use of PBC inhibits the occurrence of long-wavelength fluctuations. For a cube of side L, the periodicity will suppress any density waves with a wavelength greater than L. Thus, it would not be possible to simulate a liquid close to the gas-liquid critical point, where the range of critical fluctuations is macroscopic. Furthermore, transitions which are known to be first order often exhibit the characteristics of higher order transitions when modelled in a small box because of the suppression of fluctuations.

To check if PBC have serious effects on the properties studied, one standard practice is to increase the number of particles and the size of the system but maintain constant density and observe if there is any significant change.

2.7.2 Free Boundary Conditions (FBC)

As discussed above, the PBC are appropriate to study the properties of bulk materials. They eliminate edge effects and hence finite size effects. However, there are problems where edge or finite size effects have to be considered; for instance, crystal growth dynamics, the liquid drop and the crumpling transition in tethered membranes. Also, vacancy annealing is intrinsically a finite size problem, the defects have to be removed from the system. Thus free boundary conditions have to be used in some problems. In using FBC, one has to prevent the particles from drifting apart [12]. One way to solve the problem is to use the reflection walls so that the particle is confined within a box by reversing its velocity should it cross the wall of the box [12]. This method, however, does not work properly if one tries to consider the effects of the external pressure. Instead of the reflection walls, one can use an external field to produce the effect of an external pressure, as we do for vacancy annealing problems in finite patches.

Chapter 3

Vacancy Annealing Mechanisms in Monolayers - Infinite System

3.1 Introduction

Vacancies are the simplest and most common defects in any solid. In thermal equilibrium in an otherwise perfect crystal a certain number of vacancies are always present, because the entropy is increased by the presence of disorder in the structure. In a bulk crystal vacancies have been extensively studied [28, 29, 30]. Vacancies are particularly abundant in thin films, membranes and surfaces where exchange with the environment and damage from external projectiles offer additional avenues for the creation of these defects. In physisorbed monolayers concentrations as high as 10 at. % before melting have been reported [31]. The logical question is, how does a lattice sustain such a high vacancy concentration. From another perspective it is intriguing to determine under what conditions the vacancy damage will repair itself in a two-dimensional system. This question has potentially a wide range of applications. In a protective coating, for instance, one form of lifetime-limiting damage is erosion by bombardment by atmospheric gases or space dust. Or, organic membranes and cells usually show self-repair tendencies and it is intriguing to investigate whether their intrinsic physical structure favors healing. Because vacancies are point defects, the role of the vacancies in the change of the elastic properties has usually been ignored. We attempt to assess their significance.

We show in this Chapter that, although vacancies are local defects, a concentration of just a few percent can have profound consequences on the macroscopic physical properties of a simple monolayer. Specifically we demonstrate, by MD simulation, a unique self-repair mechanism in an ideal (i.e. with in-plane degrees of freedom only) slightly compressed monolayer. The self repair is associated with a shear modulus collapse similar to the melting scenario proposed in the Kosterlitz-Thouless-Halperin-Nelson and Young (KTHNY) [32, 33, 34] theory of two-dimensional melting. In this mechanism, which we could call dislocation mediated healing (DMH), vacancies condense rapidly into dislocation dipoles, repairing the lattice; the dipoles then dissociate inducing an intermediate quasi-fluid state leading eventually to the annealing of the defects at the edges. These effects occur for temperatures just above the self-diffusion temperature. We investigated the conditions which favour DMH, focusing notably on the effects of the range of the interparticle interaction, the pressure and the third degree of freedom (in the direction normal to the plane of the monolayer).

The self-healing mechanism discussed above is seen mainly in the ideal Lennard-Jones potential monolayer (LJM). The other system, the PLFP monolayer (PLFM), exhibits very different behaviour. It usually does not heal but rather tends to develop voids. To explore further the effect of the range of the interacting potential, we also considered the monolayer with a 4-8 potential interaction, in short called the 4-8M. The fact that one potential is very short range (PLFP) and the others relatively long range (LJP, 4-8P) will allow us to determine whether vacancy related properties are significantly altered by the range of the interacting potential.

We first performed simulations in the isothermal-isobaric ensemble (TPN) with periodic boundary conditions (PBC). To investigate the dependence of our results on the choice of the ensemble we also performed some isothermal-isochore (TVN) simulations. The basic time step in our simulations is $0.1t_0$, where t_0 is the unit of time $\sqrt{m/\kappa}$.

The main contents in this Chapter can be found in reference [35].

3.2 Calculation of the Elastic Stiffness Coefficients

The elastic stiffness coefficients $\overset{\circ}{c}_{\alpha\beta\sigma\tau}$ which govern stress-strain relations yield valuable dynamical and mechanical information about the effect of the vacancies on the monolayer. For example, they yield information concerning the stability or strength of the system, and can be used as order parameters to monitor the healing process. In continuum elasticity theory, vacancies have no effect on the elastic properties of a system of particles. Consequently the effects we will be discussing in this work are beyond the predictions of continuum elasticity theory.

For an isotropic solid such as the two dimensional triangular lattice under hydrostatic pressure, there are only two independent elastic stiffness coefficients. Traditionally $\lambda = \overset{\circ}{c}_{1122}$ and $\mu = \overset{\circ}{c}_{1212}$ are chosen to characterize the system. We shall show in Chapter 5 that in the canonical ensemble λ and μ can be calculated by

$$\begin{aligned}
\lambda &= \frac{1}{Ak_BT}\left\{\left\langle\sum\frac{\phi'}{r}(\Delta x)^2\right\rangle\left\langle\sum\frac{\phi'}{r}(\Delta y)^2\right\rangle - \left\langle\sum\frac{\phi'}{r}(\Delta x)^2\otimes\sum\frac{\phi'}{r}(\Delta y)^2\right\rangle\right\} \\
&\quad + \frac{1}{A}\left\langle\sum\frac{\phi''}{r^2}(\Delta x)^2(\Delta y)^2\right\rangle - \frac{1}{A}\left\langle\sum\frac{\phi'}{r^3}(\Delta x)^2(\Delta y)^2\right\rangle \\
&\quad - \frac{1}{2A}\left\langle\sum r\phi'\right\rangle + \frac{Nk_BT}{A}, \qquad (3.1) \\
\mu &= \frac{1}{Ak_BT}\left\{\left\langle\sum\frac{\phi'}{r}\Delta x\Delta y\right\rangle^2 - \left\langle\left(\sum\frac{\phi'}{r}\Delta x\Delta y\right)^2\right\rangle\right\} \\
&\quad + \frac{1}{A}\left\langle\sum\frac{\phi''}{r^2}(\Delta x)^2(\Delta y)^2\right\rangle - \frac{1}{A}\left\langle\sum\frac{\phi'}{r^3}(\Delta x)^2(\Delta y)^2\right\rangle + \frac{1}{2A}\left\langle\sum r\phi'\right\rangle \qquad (3.2)
\end{aligned}$$

where the quantities Δx and Δy represent the x and y coordinates of $\vec{r}_{ij} = \vec{r}_i - \vec{r}_j$, r the modulus of that vector and A the area of the system. The sums are over all pairs of particles. The last thermal average in each equation is required when an external pressure is exerted on the solid. The last term in Equation (3.1) is the kinetic energy contribution.

We shall also show in Chapter 5 and 6 that for a uniform dilation ensemble, which includes our TPN ensemble, Equation (3.2) is still valid.

In the present work, Eqs. (3.1) and (3.2) were used to calculate the bulk modulus $B = \lambda + \mu$ and the shear modulus μ by using the isothermal-isochore ensemble at low temperature ($T = 0.002\kappa d_0^2/k_B$). Equation (3.2) was used to calculate μ in both

the constant-pressure and constant-area ensembles and the results were found to be consistent (see section 3.4.3).

Elastic properties for the two dimensional LJM do not seem to be available in print even for zero temperature. Values are however reported for some rare gas solids [36] which are very close to the LJM. In Chapter 6 of this thesis, we shall derive some simple expressions for λ and μ for LJM and 4-8M (see Eq. (6.53)). From these expressions it follows that for $P = 0.0087\kappa$, $\lambda = 0.865\kappa$ and $\mu = 0.847\kappa$ and for $P = 0.0053\kappa$, $\lambda = 0.843\kappa$ and $\mu = 0.832\kappa$. In contrast, simple analytical results for PLFM at zero temperature have been given [2, 3, 4] (also see Eq. (6.44) in Chapter 6). From Eq. (6.44) we have for a perfect PLFM at a pressure of 0.0053κ $\lambda = 0.446\kappa$ and $\mu = 0.425\kappa$, varying little for a large range of pressures. The LJM, because of its longer range interactions, is a stiffer solid.

3.3 The Dislocation

The concept of the dislocation as an elastic singularity was first introduced by considering the deformation of a body occupying a multiply connected region of space, and a systematic theory was given by Volterra [37], following earlier work by Michell [38], Weingarten [39] and Timpe [40]. Love [41] and Somigliana [42, 43] developed further the elastic theory of dislocations. The first suggestions that dislocations exist in a real crystal arose not from direct observations on structure but in order to interpret experiments on the plastic behaviour of crystals [44, 45]. Dislocations were discussed by Prandtl [46] and Dehlinger [47] as a possible explanation for the large discrepancy between the theoretical and experimental strength of a crystal. The real introduction of the dislocation into physics was done by Taylor [48], Orowan [49] and Polanyi [50] to describe the edge dislocation. Screw dislocations and dislocations of general type were first consided by Burgers [51]. Since then the theory of dislocation has developed rapidly [52]. Experimental techniques such as optical, electron, field ion and X-ray microscopy have provided such an abundance of evidence for dislocations that there can be no doubt that dislocations exist. The discoveries should thus be accorded particular significance in the development of the subject.

The best description of a dislocation is obtained from a study of its formation in the crystalline lattice. Consider Fig. 3.1. In the center, is the starting material, a

perfect, undeformed simple cubic lattice (a simple cubic lattice is used for the sake of clarity). Cut this lattice along any of the planes indicated in the auxiliary cubes. Let the atoms on one side of the cut shift in a direction parallel to the cut surface through a distance, relative to the corresponding atoms on the other side, equal to one atom spacing. Then rejoin the atoms on either side of the cut. The new, distorted lattice is shown in the outer figures. The lattice structure itself actually is almost perfect except near lines AA of the various figures. The line imperfections AA in the lattice are known as dislocation lines.

Three types of dislocations are shown in Fig. 3.1. If the atoms over the cut surface are shifted in a direction perpendicular to the line AA, an edge dislocation is created in the lattice; if the shift is parallel to AA, a screw dislocation is produced; if the shift is neither parallel nor perpendicular to AA but rather at some arbitrary angle, a dislocation called mixed dislocation having the characteristics of both an edge and an screw dislocation is placed into the lattice.

Consider first the Burgers vector of the edge dislocation shown in Fig. 3.2(a). Two circuits have been drawn in this figure. The upper circuit is drawn clockwise, as that is the usual convention, around the edge dislocation; the lower circuit avoids the dislocation. In each circuit the same number of jumps from atom to atom are made upward, as are made downward, to the left as to the right. The starting point and the end point (the atoms shown solid) are one and the same atom in the case of the circuit that does not include the dislocation. However the starting and end points are not at the same atom for the circuit that does enclose the dislocation. Thus there is a closure failure in this circuit. The Burgers vector is defined to be this closure failure. The direction of the vector is from the beginning point of the circuit to its end point. The Burgers vector of an edge dislocation is *perpendicular* to the dislocation line. A circuit about a screw dislocation is shown in Fig. 3.2(b). In this case the closure failure leads to a vector *parallel* to the dislocation line. In the case of a mixed dislocation, the Burgers vector makes some other angle with the dislocation line.

In contrast with three dimensional (3D) solids where two types of dislocations can be found, there is only one kind of dislocation in a two dimensional (2D) system. It is the edge dislocation and it essentially corresponds to a missing extra half line of atoms. Pairs of such dislocations with opposite burgers vector can be viewed

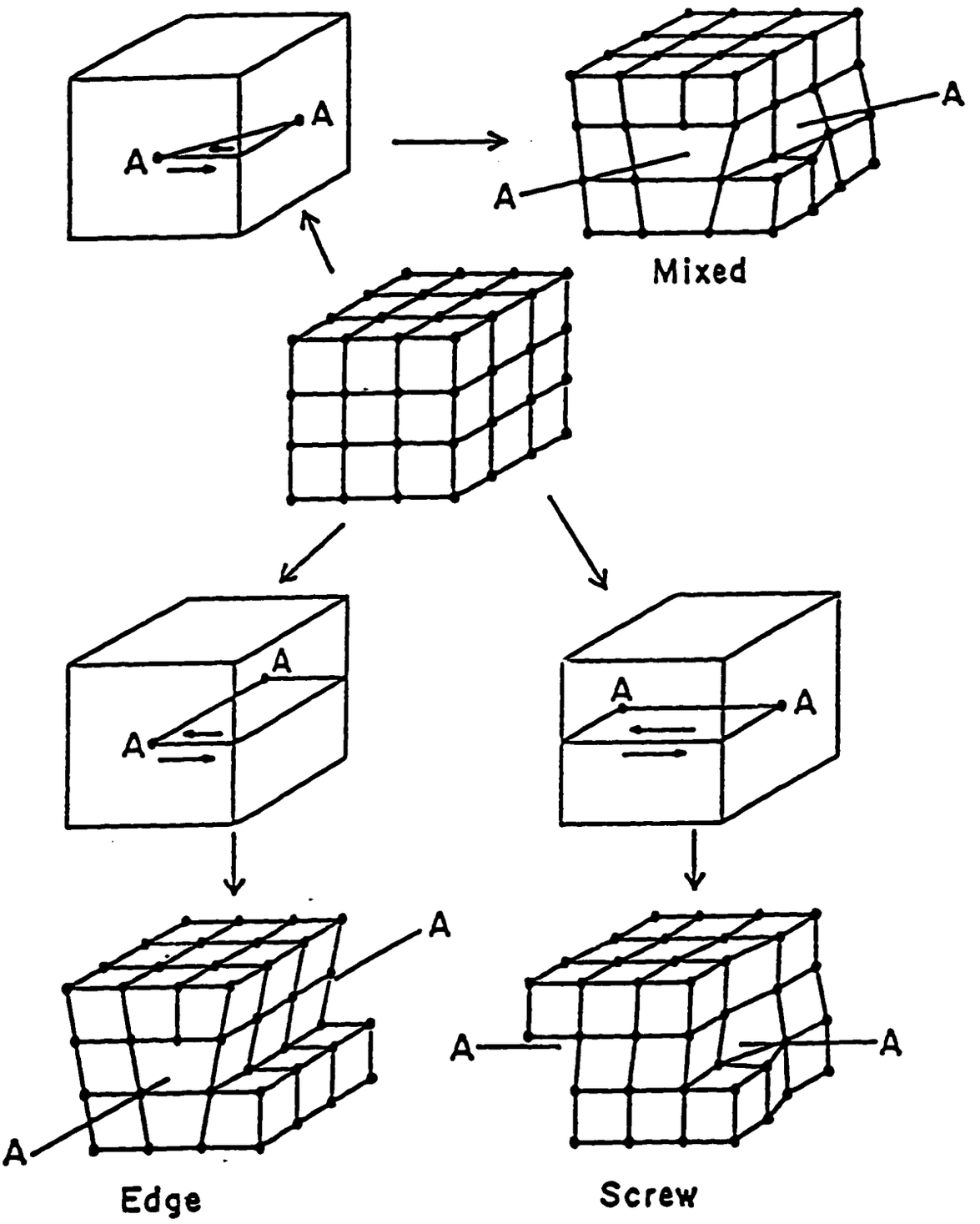

Figure 3.1: The creation of an edge, a screw and a mixed dislocation.

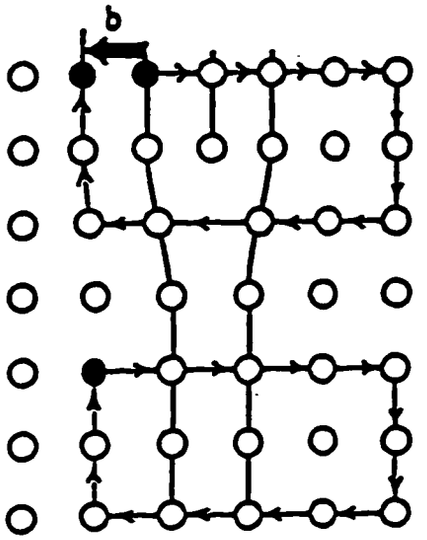

(a)

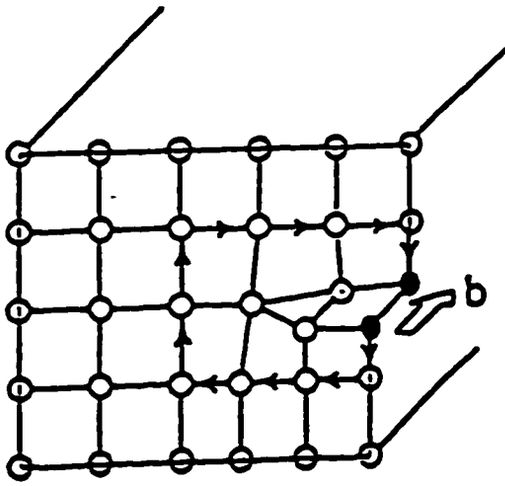

(b)

Figure 3.2: (a) Burgers circuit around edge dislocation. Positive direction of the dislocation line is taken to be out of the plane of the figure. (b) Burgers circuit around screw dislocation.

as rows of vacancies or interstitials. These kinds of defects are low-energy thermal defects, and dislocations are likely to play an important role in 2D phase transitions [6, 32, 33, 34] and also in the self-repair mechanism.

3.4 Results for the Ideal LJM and PLFM

First, we considered the ideal monolayer which has only in-plane degrees of freedom. For the range of pressure of interest, the melting temperature, i.e. the temperature at which the Gibbs free energy of liquid is equal to that of solid [23, 24], is about the same in both systems, specifically $0.010\kappa d_0^2/k_B$ for the LJM [5, 53] and $0.011\kappa d_0^2/k_B$ for the PLFM [7]. In comparison the self diffusion temperature T_D for vacancies in these systems is approximately $0.0055 \pm 0.0005\kappa d_0^2/k_B$, where T_D is defined by assuming that the diffusion coefficient can be written [29]

$$D = D_0 e^{-T_D/T} \tag{3.3}$$

where D_0 is a constant.

To find the exact T_D for vacancies is not a simple task. One way to determine T_D by MD simulations can be found in ref. [54]. But we did not use this method since an exact value of T_D is not necessary for this work. The T_D given above is obtained from a direct observation of the evolution of the configurations with time. For example, we found that, with several different initial configurations, the vacancy moves obviously at about 10000 time steps at a temperature of $0.0055\kappa d_0^2/k_B$ but almost did not change its position over 200000 time steps at a temperature of $0.005\kappa d_0^2/k_B$.

3.4.1 Low Temperature Elastic Stiffness Coefficients (below T_D)

At temperatures below T_D, the vacancies do not move over long time intervals. The elastic stiffness coefficients measure the weakening of the system in the presence of the defects. Fig. 3.3 shows the variation, as a function of vacancy concentration c_n, of the shear modulus (μ) and the bulk modulus ($B = \lambda + \mu$), normalized to their respective perfect lattice values μ_0 and B_0. The temperature was $T = 0.002\kappa d_0^2/k_B$ and vacancy concentrations from 0 to 3.8 at. % (i.e. the number of empty sites is 3.8 % of the total lattice sizes in the initial configuration) were considered. The pressure on the LJM was 0.0087κ while on the PLFM 0.0053κ.

The range of the potential seems to have little effect on the rate of decrease of the shear or bulk modulus with increasing vacancy concentration. The shear modulus loses a fifth of its value for a 4 at. % concentration of vacancies. This corresponds to $\Delta\mu/\mu_0 = (\mu - \mu_0)/\mu_0 = -5c_n$. The bulk modulus decreases at the slightly lower rate $\Delta B/B_0 \simeq -3.5c_n$. As Fig. 3.3 shows, there is a scatter in the data with vacancies present. For each concentration there are many possible configurations of vacancies. Fig. 3.3 shows the average over several configurations for each concentration.

3.4.2 Self-repair Mechanisms (above T_D)

As the temperature is raised, the vacancies start to move. Two types of annealing behaviour, which are illustrated in Fig. 3.4, are observed above the diffusion temperature. Either the vacancies condense rapidly into a dislocation dipole, what we call the dislocation mediated healing (DMH) (Fig. 3.4(b) and (c)). Or they diffuse slowly into small vacancy clusters (Fig. 3.4 (d)) which eventually are removed from the system by aggregating into a large void (Fig. 3.4 (e) and (f)), the void forming (VF) mechanism.

The Lennard Jones Monolayer (LJM)

In the LJM, under slight pressure (specifically 0.0087κ in the runs below) the first scenario occurs when the vacancies are in sufficient number. For fewer than 15 vacancies in a rhombus 28 atoms on the side (or $c_n < 1.9$ at. %) the vacancies diffuse into small vacancy clusters. For 15 vacancies or more (or $c_n \geq 1.9$ at. %) the vacancies are removed by condensing into a "large" vacancy dislocation dipole (separation equal or larger than 15 atomic rows) (see Fig. 3.4(b)) [36, 55]. The periodic boundary conditions introduce a periodicity in the behaviour of our system (see Fig. 3.5(a)). For more than 28 vacancies (or $c_n > 3.6$ at. %) there are more vacancies than would fit into one dipole, so 28 vacancies are annealed out and the remainder form vacancy clusters unless their numbers exceed the minimum required to form a second "large" dipole. When a dipole is present in the sample, the shear modulus collapses (see Fig. 3.5(a)). The dipole appears very quickly, within a few thousand t_0, or a few nanoseconds if parameters appropriate to Xe are used. To complete the process, which means that the average lattice constant and the

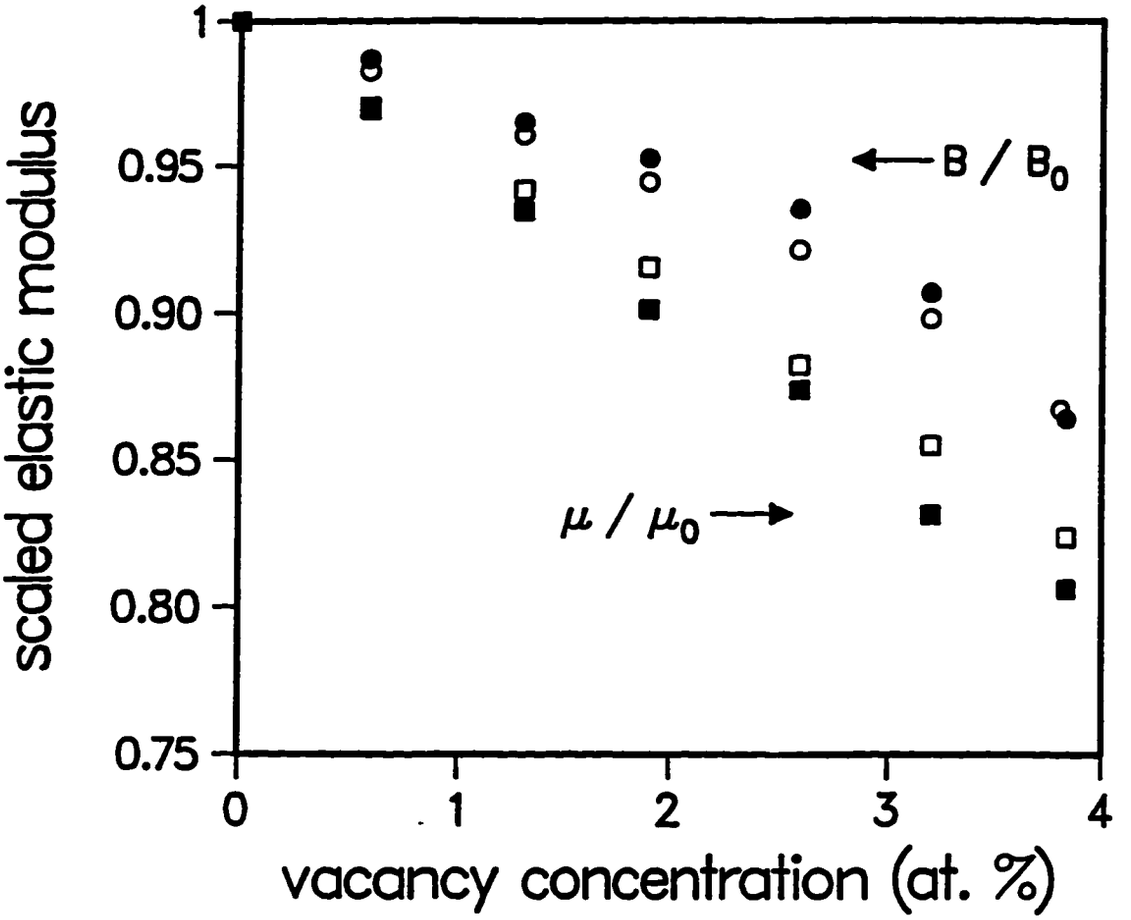

Figure 3.3: Variation of the shear modulus μ (squares) and the bulk modulus $B = \lambda + \mu$ (circles), both normalized to the zero vacancy values μ_0 and B_0 respectively, as a function of vacancy concentration for the LJM (full symbols) and PLFM (open symbols) at the temperature $0.002\kappa d_0^2/k_B$.

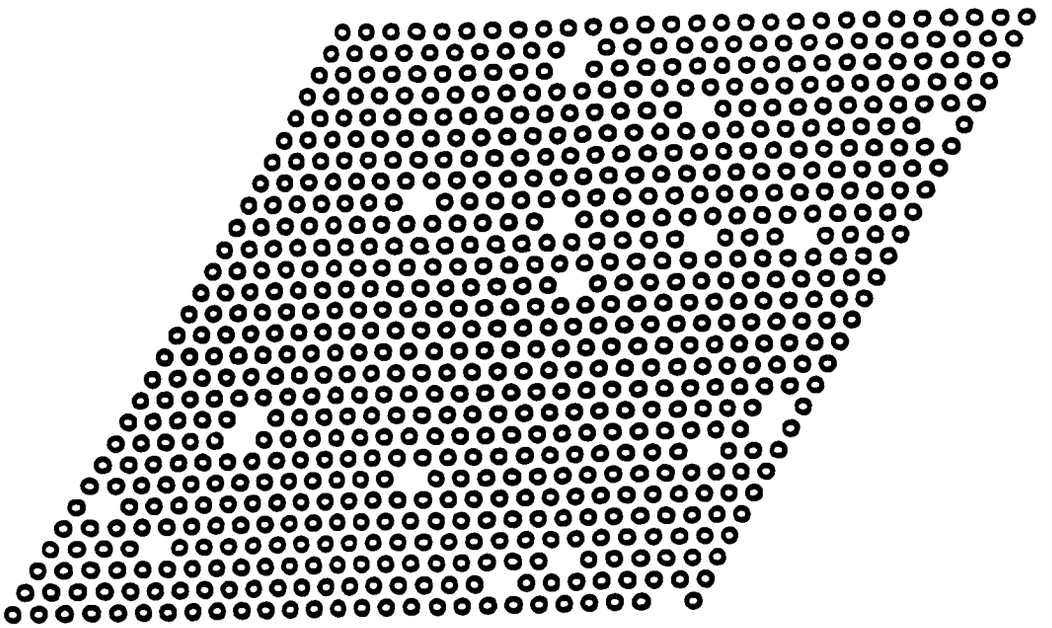

(a)

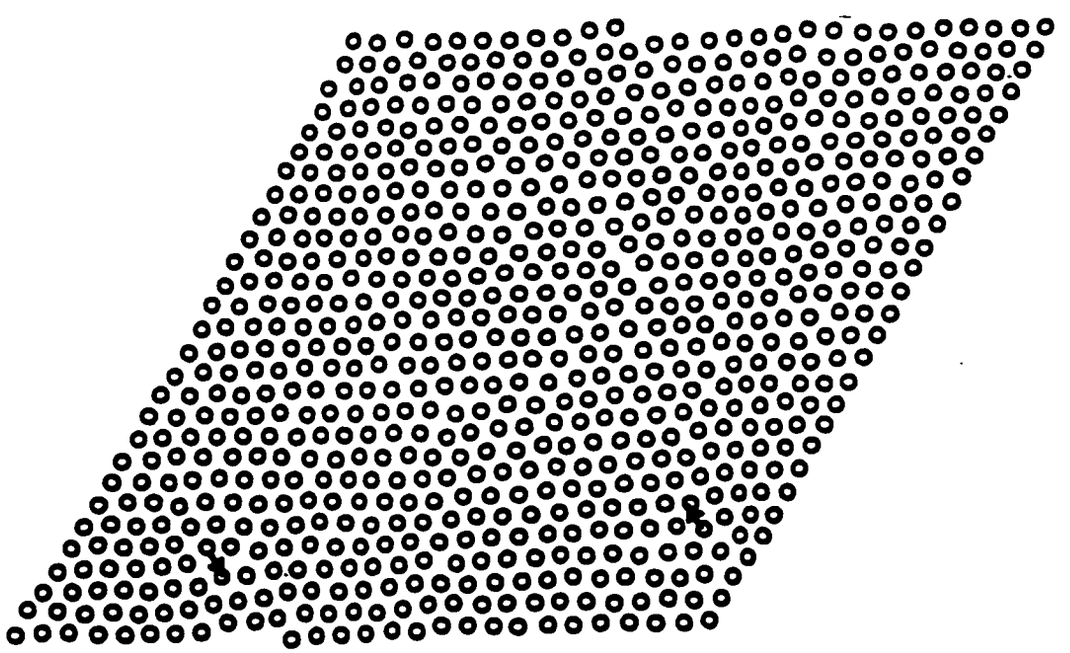

(b)

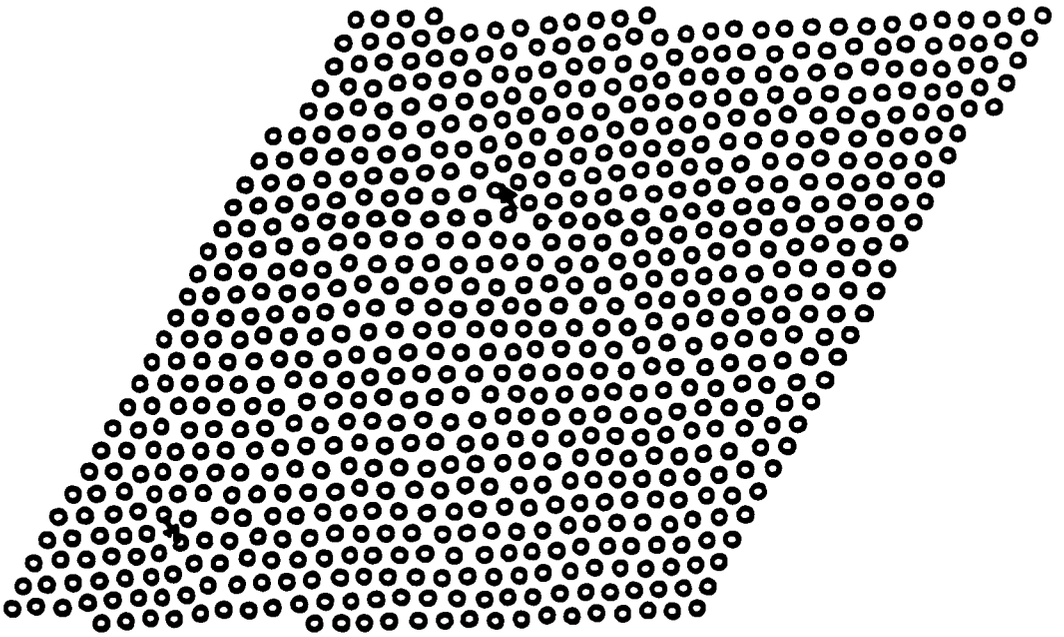

(c)

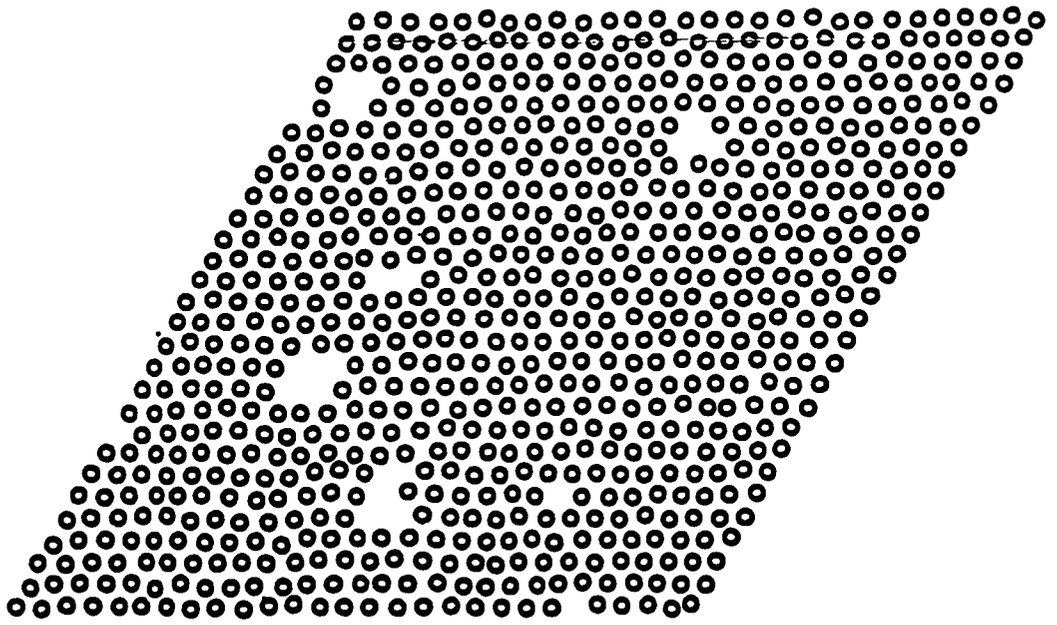

(d)

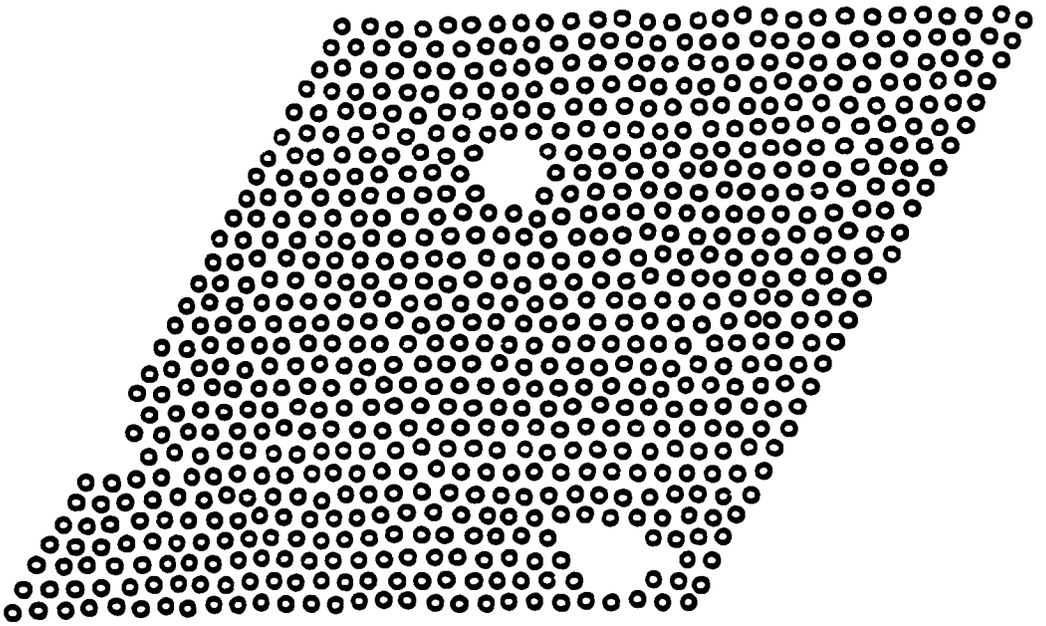

(e)

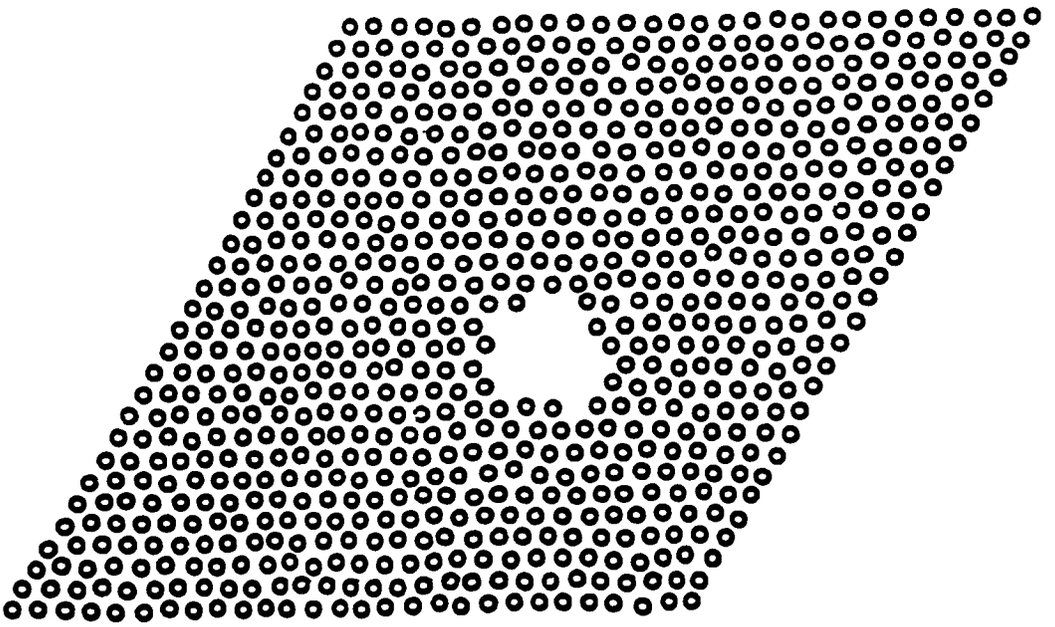

(f)

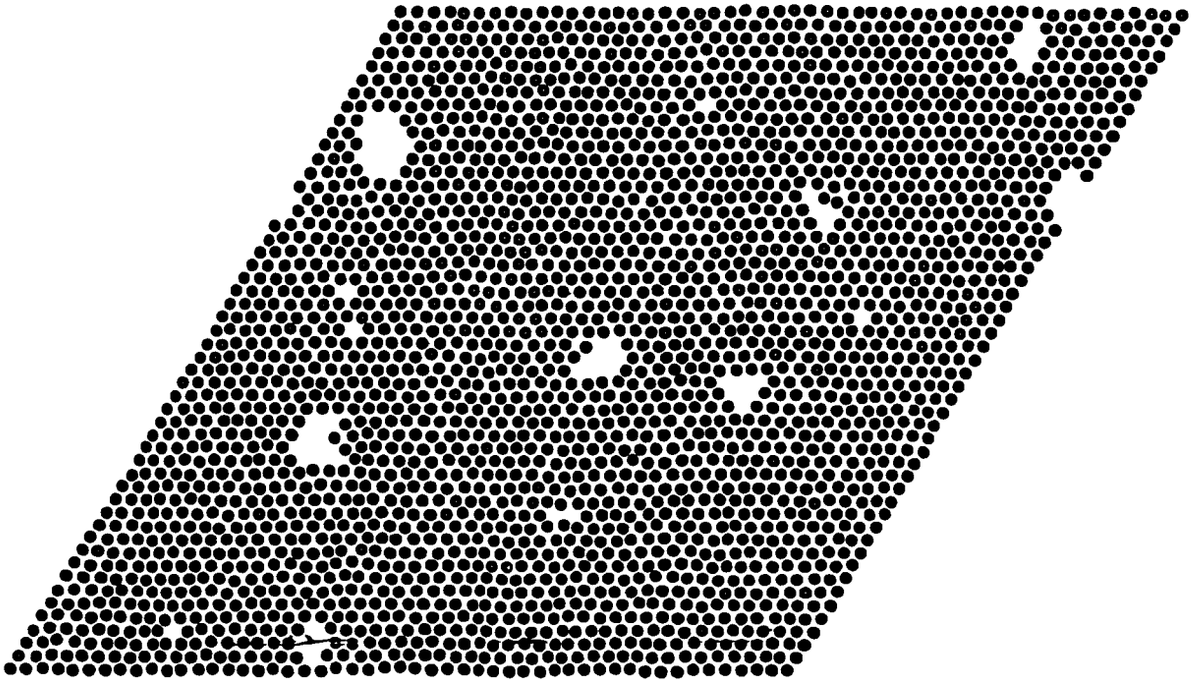

(g)

Figure 3.4: (a) Typical low temperature configuration of atoms for either LJM or PLFM for a vacancy concentration of $c_n = 2.56$ at. %. (b) and (c) same configuration after relaxation during a time $t = 46000t_0$ and $t = 56500t_0$ respectively at the temperature $T = 0.006\kappa d_0^2/k_B$ in LJM with pressure 0.0087κ (the arrows placed at the cores of the dislocations are Burgers vectors). This is an example of dislocation mediated healing (DMH). In (b) we have a 60^0 dipole with the burgers vector making an angle of 60^0 with the vector joining the two dislocations. The vacancies are lined up in a row. In (c) the dislocations have glided along the direction of their burgers vector. (d) to (f) started with the same initial configuration (a) but are for the PLFM at the same temperature as the LJM but with pressure $P = 0.0053\kappa$. They show the different stages of the formation of a large void: (d) at $t = 360000t_0$, (e) at $t = 1118000t_0$ and (f) at $t = 1850000t_0$. (g) is the configuration of atoms of the PLFM system with 51 atoms on the side at $T = 0.006\kappa d_0^2/k_B$, $P = 0.0053\kappa$, $c_n = 2.56$ at. % and $t = 3200000t_0$.

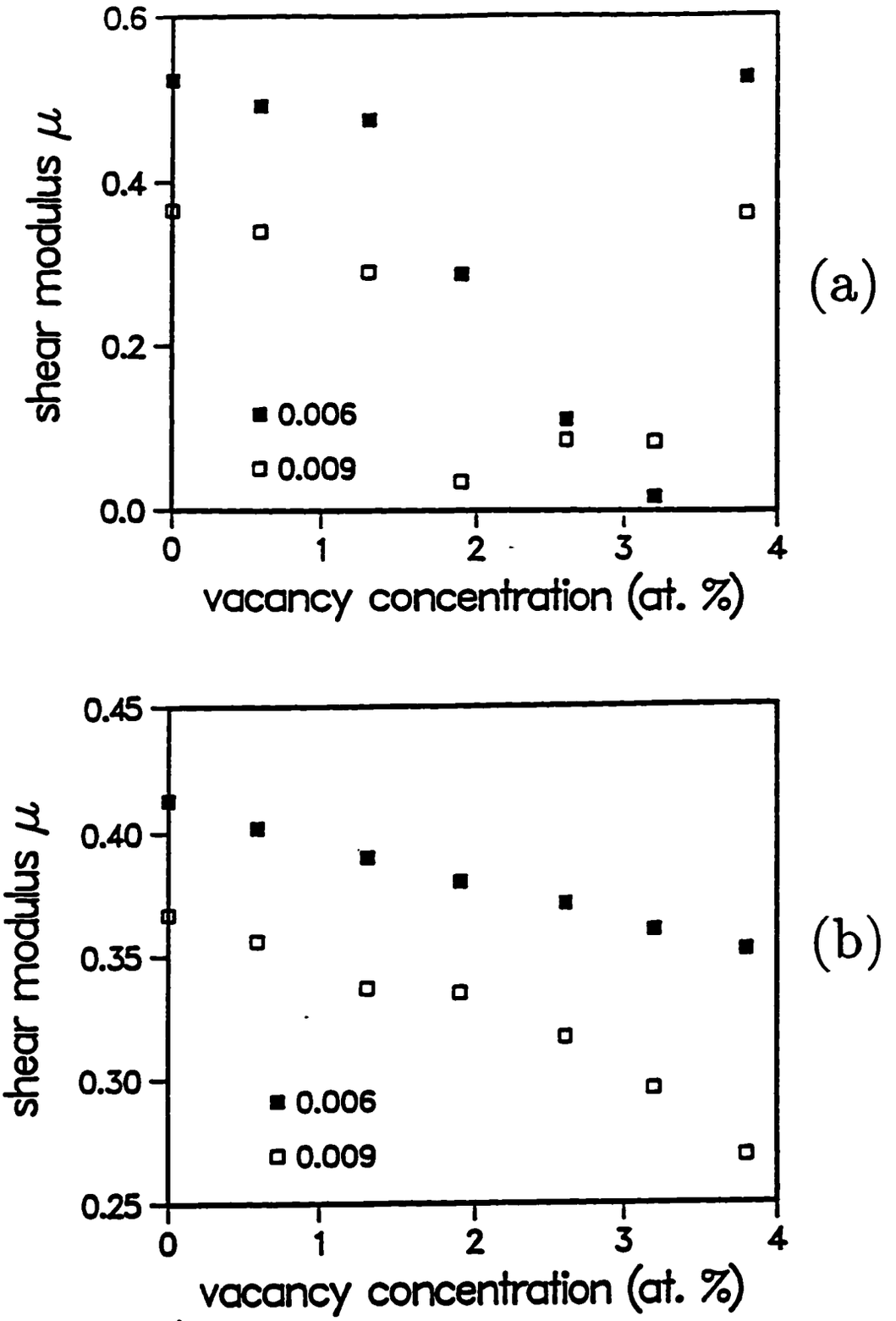

Figure 3.5: Variation of the shear modulus (in units of κ) as a function of vacancy concentration for temperatures of 0.006 and $0.009\kappa d_0^2/k_B$ for (a) the LJM (at a pressure $P = 0.0087\kappa$) and (b) the PLFM ($P = 0.0053\kappa$).

shear modulus have stabilized takes longer, about $30000t_0$ (or about $20ns$ with Xe parameters). The CPU time required for such a run in a IBM RISC system/6000 workstation with CPU type 7011 is about 1 day. This is an upper limit obtained with vacancies uniformly placed on the sample. With other configurations the times were shorter.

The above behaviour is consistent with the properties of dislocation dipoles in LJP type monolayers [36, 55, 56, 57]. In these references it is shown that dipoles containing less than 15 vacancies (or $c_n < 1.9$ at. %) behave more like composite pinned defects than elastic dipoles. They are the favoured defects at very low vacancy concentrations. On the other hand a logarithmic dependence of the energy on size makes "large" dipoles favorable at higher concentrations. These move nearly freely in the direction of their Burgers vector over a wide range of angles (45^o to 135^o) [56, 57]. The high mobility of the dislocations leads to a loss of shear strength and translational order. One dipole is sufficient although the effect may be enhanced by the screening resulting from similar dipoles (in our case in the neighboring cells of our periodic structure). The collapse in the shear modulus is similar to what occurs in the melting mechanism proposed by the KTHNY [32, 33, 34] theory of two dimensional melting where dislocation dipoles are thermally activated, and under the action of their mutual screening dissociate, leading to a collapse of the shear modulus without loss of the bond orientational order.

DMH is observed for all pressures larger than a critical value 0.0066κ for $T = 0.006\kappa d_0^2/k_B$, a temperature just slightly above the diffusion temperature T_D. For smaller pressures void formation is observed. In a typical run the annealing by the formation of a large void occurred within $100000t_0$, quite slower than DMH. In Fig. 3.6 we have mapped out a phase diagram of the LJM showing in the solid phase the regions of DMH and void formation for a vacancy concentration $c_n = 0.0256$ at. %. The line separating regions of DMH and void formation is a function of c_n, moving towards lower pressures with increasing c_n. When the temperature is raised DMH is more rapid and persists to lower pressures. Below $T_D \sim 0.0055\kappa d_0^2/k_B$ vacancy diffusion is very slow and the self diffusion temperature is a natural boundary for DMH. Going to high temperatures the critical line goes to zero as the temperature approaches the tricritical point located at $T = 0.00934\kappa d_0^2/k_B$ close to the zero pressure line [53].

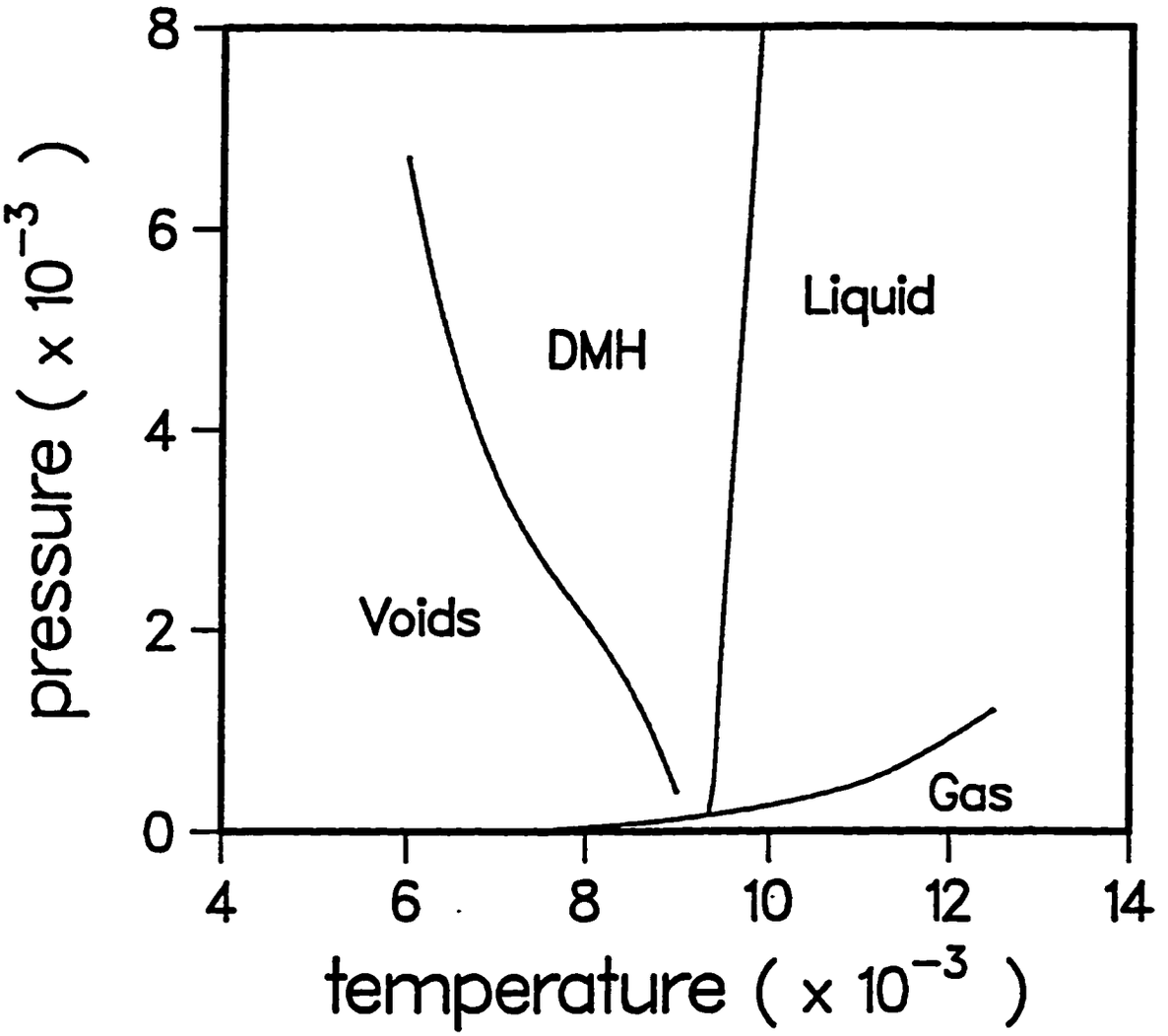

Figure 3.6: Pressure versus temperature phase diagram of the LJM showing regions of dislocation mediated healing (DMH) and void formation in the solid phase for a vacancy concentration $c_n = 0.0256$ at. %. The liquid, solid (note that both DMH and void formation regions are in region of solid state) and gas phase boundaries are Monte Carlo results of Barker et al [53]. (Pressures in units of κ and temperatures in units of $\kappa d_0^2/k_B$. To convert pressures to ϵ/σ^2 and temperatures to ϵ/k_B multiply by 35.28 and 44.44 respectively).

With the increase of the temperature towards the melting line the shear modulus collapse is more complete and occurs at lower vacancy concentrations. This can be seen in Fig. 3.5 (a) for $P = 0.0087\kappa$. It should be noted that the liquid-solid phase boundary is for zero vacancy concentration. In this work we have restricted ourselves to the solid phase. The question of healing in the liquid phase opens up a new range of issues which has not yet been addressed.

The preference for void formation at low pressure can be understood if one notes that as the pressure is decreased and can even become negative, the energies of the vacancy and the short dislocation dipoles drop rapidly [55] making these defects and associated small defect clusters very favorable. These in turn then act as nuclei for a larger void.

The Piecewise Linear Force Monolayer (PLFM)

Void formation (VF) is the usual response of the short range potential system, the PLFM, under vacancy damage. The vacancies form clusters which eventually combine into large voids (see Fig. 3.4(d) and (f)). This typically takes much longer than the DMH or even the void formation in the LJM (at least by an order of magnitude). The precise time depends on the distribution of the vacancies. In the example shown in Fig. 3.4 (f), it was as high as $1.85 \times 10^6 t_0$ at $T = 0.006\kappa d_0^2/k_B$ with a pressure of 0.0053κ, and costed about 20 days of CPU time in a IBM RISC system/6000 workstation with CPU type 7011. The PLFP is nearest neighbour, so as soon as a triangle of vacancies is formed, additional vacancies in the cluster do not add to the energy. In effect, one has a free surface, and the vacancies anneal out but remain within the system. The temperature induced diffusion smoothens out the elastic stiffness coefficients even before the voids are formed (see Fig. 3.5(b)). There is no collapse of the shear modulus, which is reduced only by an amount comparable to the reduction in density. In this system vacancy clusters have lower energies than vacancy dislocation dipoles in contrast to those in the LJM [57].

We have also considered pressures of 0.01κ and 0.02κ for $c_n = 0.0256$ at. % at a temperature of $0.006\kappa d_0^2/k_B$ and still find no DMH. A larger sample size is not expected to make any difference either. A sample of 51×51 atoms for $c_n = 2.56$ at. % showed the same cavitation behaviour (see Fig. 3.4(g)).

Zero and negative pressures were also considered with similar results. While

the system under negative pressure expanded, the zero pressure system contracted. This latter behaviour is a peculiarity of the PLFM. The absence of a hard core in the PLFP favours interstitial types of defects at finite temperature [57].

3.4.3 Constant Pressure vs. Constant Volume

The work described above was done in the TPN ensemble with PBC. To check whether the choice of the ensemble has any influence on the behaviour of the two systems we performed simulations in the TVN ensemble for both the compressed LJM and PLFM with PBC. To avoid biasing the results, we did not use the output data (velocities, coordinates, etc.) of the TPN run as the input data of the TVN run. We started with samples of areas equal to the average area of a constant pressure run with the same number of vacancies after the initial compression which usually only takes about 2000 t_0. This means that there is a slight overcompression in the TVN compared with the corresponding TPN run. The same behaviour is observed as in the TPN runs for the LJM and PLFM but things happen over a longer time scale. It appears that volume fluctuations in the TPN run favor large scale readjustments of the particles and hence accelerate the healing.

Just to emphasize how similar the behaviour in the two ensembles are, we show the shear moduli calculated in the constant volume simulation. As can be seen from Tables 3.1 and 3.2 they are very close to those obtained in the contant pressure runs at the same temperature and average pressure.

Table 3.1: The shear moduli in constant-area (μ_v) and constant-pressure (μ_p) ensembles for the LJM system at $T = 0.006\kappa d_0^2/k_B$ with $P = 0.0087\kappa$.

c_n	μ_v	μ_p
0.0000	0.490 ± 0.005	0.498 ± 0.005
0.0064	0.465 ± 0.005	0.472 ± 0.005
0.0130	0.450 ± 0.005	0.446 ± 0.005
0.0193	0.281 ± 0.005	0.286 ± 0.005

Table 3.2: The shear moduli in constant-area (μ_v) and constant-pressure (μ_p) ensembles for the PLFM system at $T = 0.006\kappa d_0^2/k_B$ with $P = 0.0053\kappa$.

c_n	μ_v	μ_p
0.0000	0.419 ± 0.005	0.419 ± 0.005
0.0256	0.370 ± 0.005	0.370 ± 0.005

3.5 Monolayer with the 4-8 Interaction Potential (4-8M)

Suspecting that the difference in behaviour observed in the LJM and the PLFM was due to the longer range of the LJP with its ensuing consequences on vacancy interactions and dislocation properties, we considered a monolayer with an even longer range interaction than the LJP, the 4-8P defined in Eq. (2.9). This system, the 4-8M, was found to exhibit DMH at all pressures considered, from $P = 0.0087\kappa$ down to -0.0087κ, i.e. a DMH is preferred over the formation of voids *even at negative pressures.* At zero pressure the melting temperature of 4-8M is $0.0095\kappa d_0^2/k_B$ and the self-diffusion temperature $0.0036 \pm 0.0005\kappa d_0^2/k_B$. Typically a vacancy concentration of $c_n = 2.56$ at.% was chosen. The DMH was found to be rapid also at zero pressure with a completion time of $\simeq 30000t_0$ at $T = 0.006\kappa d_0^2/k_B$, a fairly large temperature in this system. With negative pressure the DMH still appears quickly but its completion time is very sensitive to temperature. With $P = -0.0087\kappa$ and $T = 0.0045\kappa d_0^2/k_B$ the lattice parameter stabilizes after $20000t_0$, but after $450000t_0$, the lattice is still partially disordered when $T = 0.006\kappa d_0^2/k_B$.

Contrary to the other two systems with a shorter range potential, partial DMH was observed in the 4-8M below the isolated vacancy diffusion temperature, specifically at $T = 0.0025\kappa d_0^2/k_B$ and $0.0015\kappa d_0^2/k_B$. The healing is not complete. As seen in Fig. 3.7, some isolated vacancies remain in the system.

3.6 Effect of the Third Degree of Freedom

So far we have only considered the ideal monolayer which is constrained to a two dimensional space. In a real adsorbed system there is, however, always the third degree of freedom. The monolayer will be held by a holding potential which can be weak or strong, and may, or may not, have significant lateral variations. We will not consider here the effects of the lateral variations. The third degree of freedom opens up new trajectories to the particles, and if the holding potential is not too strong, we can expect to find some qualitative changes in the healing mechanisms.

To study the changes brought about by the third degree of freedom, we applied a smooth (unmodulating) holding potential as given by Eq. (2.12) to both the LJM and the PLFM at the temperature $0.006\kappa d_0^2/k_B$. We found the behaviours sensitive to the pressure and the strength of the holding potential.

3.6.1 PLFM

For a very weak holding potential, the adsorbed atoms form rapidly a multi-layer film instead of a monolayer. This is what is shown in Fig. 3.8(a) where a_0, the measure of the strength of the holding potential (see Eq. (2.12)), is equal to $0.03\kappa d_0^2$, $c_n = 1.3$ at.%, the pressure $= 0.0053\kappa$, and the configurations are for a time $t = 2000t_0$.

In contrast, with a strong holding potential (such as with $a_0 = 0.4\kappa d_0^2$) the behaviour of the system is similar to that of the ideal monolayer.

For an intermediate strength of the holding potential, something interesting happens. Though the interparticle interaction is short range, we found that the system will exhibit DMH with $a_0 = 0.3\kappa d_0^2$, $c_n = 2.5$ at. % and pressure $= 0.0053\kappa$. Fig. 3.8(b) shows configurations with these conditions at time $167000t_0$. Similar to the ideal compressed monolayer, the vacancies are removed by condensing into a "large" vacancy dislocation dipole.

However, as we have found in the ideal monolayer, when the pressure becomes very low, the system shows no DMH. Cavitation is however quite slow. For a lateral pressure of 0.002κ, after $535000t_0$ as seen in Fig. 3.8(c) the voids are still fairly small and show no haste in condensing into a larger cavity. The same applies for a pressure of 0.0035κ.

3.6.2 LJM

At the intermediate strength of the holding potential $a_0 = 0.3\kappa d_0^2$, DMH is still observed in the LJM and remains pressure dependent. At pressures below 0.0095κ voids are formed. But the time needed to form a large void is still considerably less than in the PLFM. For $P = 0.0095\kappa$, a completed DMH was observed within $20000t_0$. For $P = 0.0087\kappa$ a single large void was formed within less than $100000t_0$.

3.7 Conclusions

In summary, just above the self-diffusion temperature and well below the melting temperature, only a very low concentration of isolated vacancies can be sustained in an ideal monolayer. What happens to the vacancies depends strongly on the range of the interparticle interaction. A short range interaction favours the formation of voids which can eventually combine to form a large cavity. When there is a sufficient number of vacancies, monolayers with long range interparticle interactions heal through the creation of a dislocation dipole, and an intermediate disordered state is formed, a process that we call dislocation mediated healing (DMH). For the system with the 4-8P, the DMH remains rapid at zero pressure and still occurs, albeit slowly, at negative pressures. In the LJM, with the intermediate range LJP, both behaviours are observed. The range of the LJP is not sufficient to permit spontaneous DMH without the application of a little pressure.

The healing is rapid, of the order of nanoseconds when rare gas parameters are used. Void formation is slow, the more so for the shorter range potential.

Dislocations weaken the shear strength of the monolayer but even fairly large voids ($\sim$ 30 atoms) have no dramatic effect on the shear modulus which seems to be mainly a function of the vacancy concentration.

If we consider the effects of the substrate, the situation becomes more complex. We found that a third degree of freedom favours DMH even in the short range force system. This may be due to the increased mobility of the vacancies which facilitates the annealing process. In an actual monolayer adsorbed on a substrate, the corrugation in the substrate field may have to be considered. The substrate corrugation does two things; (i) it screens out the interactions between atoms, decreasing the effective range of the interparticle interaction, and (ii) increases the barrier to

diffusion of the vacancies. Therefore, the effects of the substrate modulating field seem to discourage DMH. The high vacancy concentration observed in some rare gas monolayers adsorbed on graphite indicates significant substrate corrugation effects. The exchange with the gas occurs in a different time scale than the healing of the monolayer and cannot account for the large concentration of vacancies [58]. Structurally these monolayers are therefore quite different from ideal monolayers and are not good candidates for DMH.

It would be interesting to investigate the role that vacancies play in the melting of a physisorbed system in particular one with a weak substrate corrugation, such as Xe on Ag{111} [59]. In an experimental environment thermal vacancies are unavoidable. The vacancies may condense into clusters. Or, they may play a catalytic role in the creation of dislocation dipoles in a form of DMH, producing a melting transition with persistence of bond orientational order as predicted by the KTHNY [32, 33, 34] theory. The melting transition, from a thermodynamic standpoint, may or may not be continuous.

With respect to the self-healing of damaged 2D systems, such as membranes, our studies suggest that several conditions permit physical mechanisms to be operative; diffusion of the vacancies, a long range interparticle interaction and pressure. As we saw above for the PLFM with a third degree of freedom or the 4-8M, the predominance of one property can diminish the reliance on the others. In biological membranes enough of the above conditions may be satisfied to have physical mechanisms of self-healing. The molecules in biological membranes usually form liquid phases, which presumably implies high diffusion coefficients [60]. They are embedded in a pressurizing fluid and long range interactions can be present.

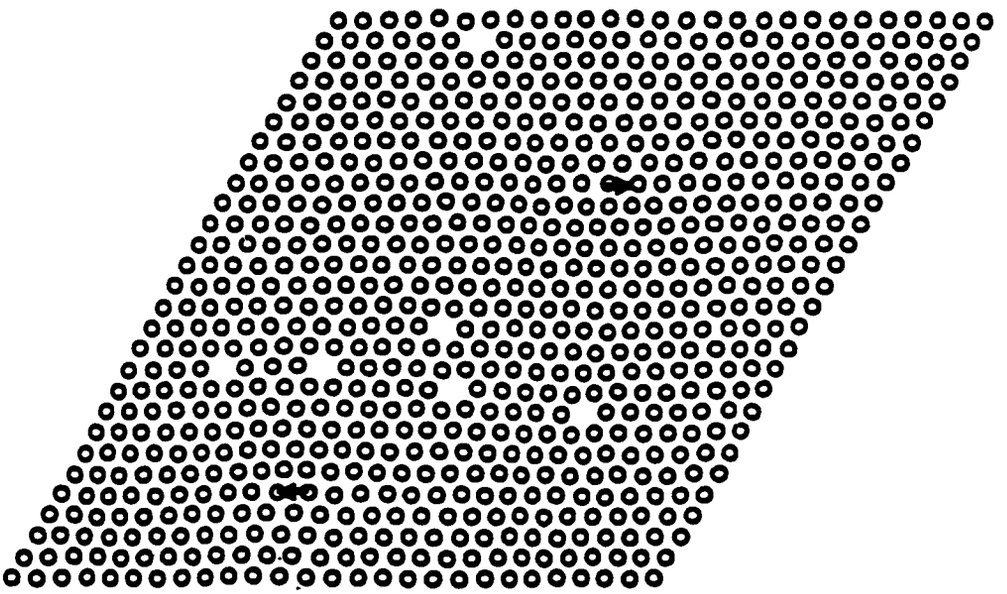

Figure 3.7: Configurations of atoms of the system with the 4-8 interaction potential at $T = 0.0015\kappa d_0^2/k_B$ and $c_n = 2.56$ at. %, at pressure $= -0.0087\kappa$ and at $t = 20000t_0$, $d = 0.9517d_0$.

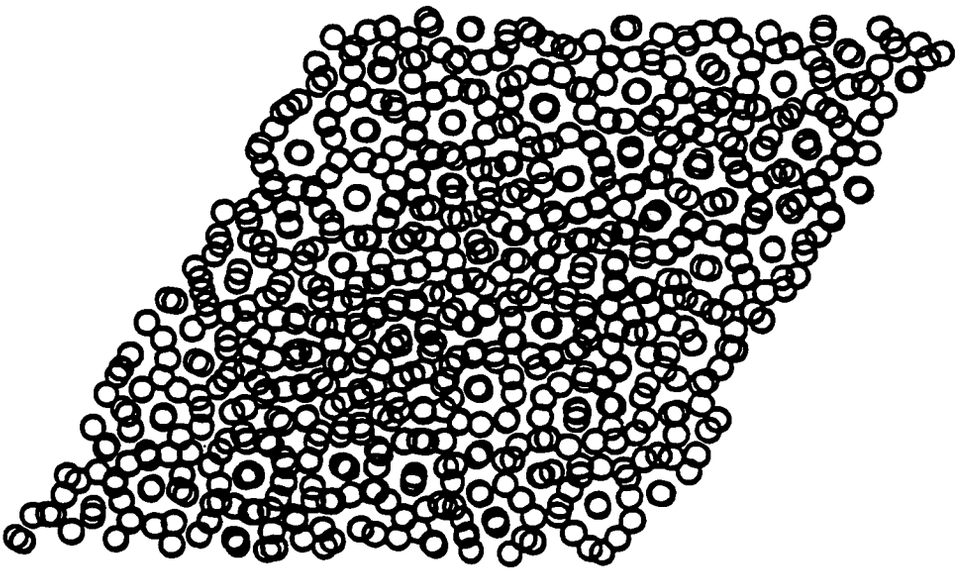

(a)

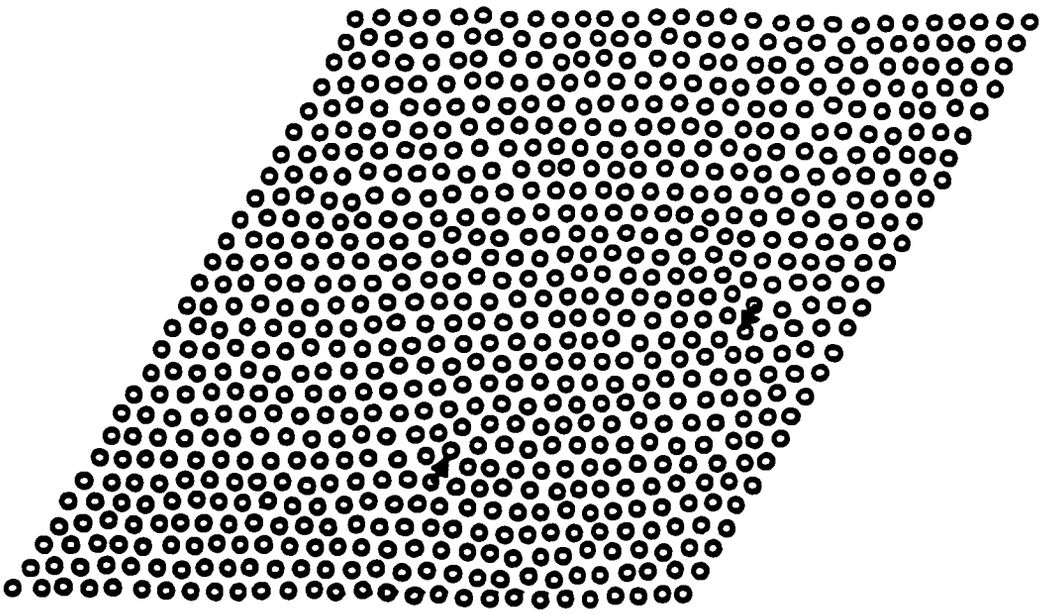

(b)

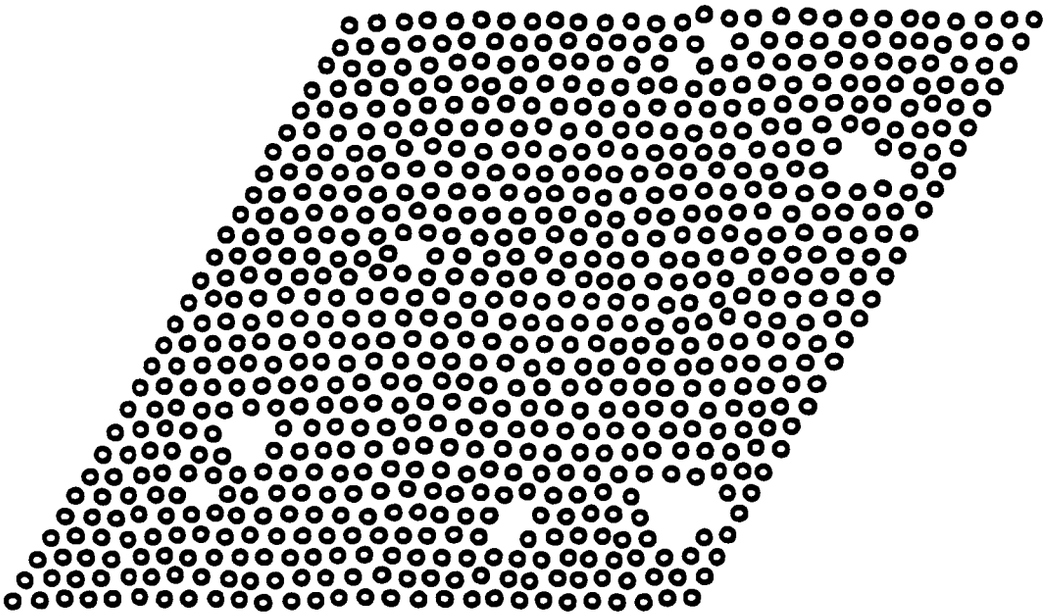

(c)

Figure 3.8: Configurations of atoms for the PLFM with a smooth holding potential at $T = 0.006\kappa d_0^2/k_B$. (a) The potential parameter $a_0 = 0.03\kappa d_0^2$, $c_n = 1.3$ at. %, pressure $= 0.0053\kappa$ and at $t = 2000t_0$, $d = 0.55086d_0$. (b) $a_0 = 0.3\kappa d_0^2$, $c_n = 2.5$ at. %, pressure $= 0.0053\kappa$ and at $t = 167000t_0$, $d = 0.9814d_0$. (c) the same as (b) but the pressure $= 0.0035\kappa$ and $t = 535000t_0$, $d = 0.9957d_0$.

Chapter 4

Vacancy Annealing Kinetics in Monolayers - Finite Patches

4.1 Introduction

In the preceding Chapter, infinite systems were considered. This Chapter completes the study by allowing the dislocations or the voids to anneal out of the system through the edges. It adds another dimension to the work by simulating the process known as annealing, whereby defects such as vacancies are removed from a system. In real situations, its kinetics can be quite varied, depending on the lattice structure, the type of defects and the treatment given to the system, usually known as the annealing sequence. The phenomenon of annealing has been extensively studied experimentally in a variety of classes of bulk systems in particular metallic alloys (see for instance Refs. [28, 61, 62, 63, 64, 65]). But theories have been few and usually specific to a particular type of behaviour in a specific system (for instance Refs. [28, 64, 66]). In this work we looked at a two dimensional model involving vacancies in monolayers consisting of particles interacting with central force potentials. We studied the annealing by directly following the kinetics through MD simulations. The simplicity of the model allows us to consider the role in the process of several important parameters, in particular, the range of the interparticle interaction, the density of vacancies (c_n), the temperature (T) and the pressure (P). Although this work is more revealing of the behaviour of two dimensional systems than bulk

materials, it also brings light to the annealing kinetics which have been observed in bulk materials, as we shall discuss later. In Chapter 3 the self-repair mechanisms in monolayers were studied with periodic boundary conditions (PBC). PBC eliminate edge effects but only partially finite size effects. Annealing is intrinsically a finite size problem, since the defects have to be removed from the system. The results of the Chapter 3 therefore give us the behaviour within the length scale of the periodic cell far away from any edge.

The main contents in this Chapter can be found in reference [67].

4.2 Methods of Calculation

The three interparticle interactions are the same as for the monolayers with PBC and so is the substrate holding potential in the case where a third degree of freedom is allowed. The most notable differences among these three potentials are their range; the piecewise linear force potential (PLFP) is nearest neighbour, the Lennard-Jones potential (LJP) has a range of about three lattice sites whereas a similar potential with the functional form $(r^{-8} - r^{-4})$ has twice that range. The simulations were done in the canonical ensemble. The initial configurations of the system are chosen as a circular patch of roughly 1000, 2000 and 4000 particles placed in a potential well in the form of a circular dish, flat in the middle and parabolic at the edges as given in Eq. (2.13). The constant centripetal force on the periphery of the dish simulates the effect of an external pressure. The circular patch is a natural choice since our system is isotropic. The vacancies are distributed initially randomly. The pressure is calculated by Eq. (2.17) with $A = \pi r_c^2$, where r_c is determined self-consistently to achieve the correct pressure within a precision of 1 % to 2 %. The fluctuations in the pressure are fairly large (may be as large as about $\pm 0.003\kappa$) since most of the configurations investigated were not in the equilibrium state. We tried several different initial configurations for every value of N_s (number of particles), r_c (size of the patch), c_n (the vacancy concentration) and K_{ext} (strength of the confining potential, see Eq. (2.13)).

In most of our simulations the basic time step is $0.1t_0$, where t_0 is the unit of time $\sqrt{m/\kappa}$. We also tried several samples with a basic time step of $0.05t_0$ but no different behaviour was found.

4.3 Vacancy Annealing in the Ideal Monolayer Patches

The edges act as a sink for the vacancies. We looked at three sizes of patches, approximately 1000, 2000 and 4000 particles, and several concentrations of vacancies. In the smallest system the dominant behaviour is direct diffusion of the vacancies to the edges, what we could call vacancy diffusion annealing (VDA). The time scales are obviously very sensitive to system size. For the larger systems we saw more of the behaviour reported for PBC systems. The annealing kinetics are, however, more varied and the effect of inhomogeneities in the distribution of vacancies important. In regions of very low vacancy concentration c_n, VDA dominates. Within the range of c_n considered (from ≈ 1.5 to ≈ 3.7 at. %), it is found that increasing c_n produces no qualitative change in behaviour, only an increase in the number of voids in the void formation (VF) behaviour or in the number of dislocation dipoles in DMH, or both.

Just as a reminder, since they are mentioned in the previous Chapter, here are some reference numbers to help put our choice of parameters in perspective. For the LJM and PLFM, the melting temperature is about the same in the range of pressure of interest, specifically $0.011\kappa d_0^2/k_B$ for the PLFM [7], and $0.010\kappa d_0^2/k_B$ for the LJM [5, 53]. The self diffusion temperature for vacancies for both systems is approximately $0.0055 \pm 0.0005\kappa d_0^2/k_B$. For the 4-8M, the melting temperature is about $0.0095\kappa d_0^2/k_B$ and the self diffusion temperature for vacancies is approximately $0.0036 \pm 0.0005\kappa d_0^2/k_B$ in the absence of external pressure. The self diffusion temperature for vacancies for the 4-8M is considerably lower than for the LJM and PLFM. The melting temperature of the 4-8M is more sensitive to the pressure than the self diffusion temperature. For $P = 0.009\kappa$, the melting temperature has increased to $0.0103\kappa d_0^2/k_B$ but the self diffusion temperature shows no significant change.

4.3.1 The Void Forming System (the Short Range Interaction PLFM)

In the PLFM which always showed VF with PBC, the behaviour is quite simple. The vacancies go to the nearest basin of attraction, whether it be the edge, a void or a region of higher concentration of vacancies. Almost a scaling type of behaviour is observed for the largest systems. Those vacancies not directly attracted to the

edge form voids which condense into larger voids until combining with the largest void of all, the edge.

Simulations were made on the following systems: $N = 965$ with $r_c = 15.902d_0$, $N_s = 1931$ with $r_c = 21.785d_0$, $22.109d_0$ and $22.732d_0$, and $N_s = 3946$ with $r_c = 32.718d_0$. $c_n = 2.56$ at. % and 3.67 at. %. $K_{ext} = 0.2$, 0.5 and 2.5 corresponding to a pressure range of about 0.0030κ to 0.043κ.

The lifetime of a large void can be very long, of the order of $10^4 t_0$ and up. The complete annealing time of the PLFM is over $10^6 t_0$ for patches of about 2000 particles which is, as we shall see, at least one order of magnitude longer than in the LJM or the 4-8M, and needs over 1 month of CPU time in a IBM RISC system/6000 workstation with CPU type 7011.

A typical annealing sequence is shown in Fig. 4.1 where the progressive condensation into larger voids is quite clearly seen. After $2.1 \times 10^6 t_0$ a large void and a divacancy still remain in the patch.

4.3.2 System Exhibiting DMH (the Long Range Interaction 4-8M)

In this system DMH and VDA compete. Only very small vacancy complexes are observed. Above the self-diffusion temperature of vacancies T_D, we get a rapid annealing. Below T_D, incomplete annealing is observed at large enough concentrations. The remaining vacancies stay within the patch at fixed lattice sites.

The simulations were mainly done at two temperatures, one above T_D, $T = 0.0042\kappa d_0^2/k_B$ and the other below, $T = 0.001\kappa d_0^2/k_B$. We also tried $T = 0.006\kappa d_0^2/k_B$, $0.003\kappa d_0^2/k_B$ and $0.002\kappa d_0^2/k_B$. The parameter values were: $r_c = 23.073d_0$ and $N_s = 1911$ for $c_n = 1.90$ at. %, $r_c = 23.078d_0$ and $N_s = 1931$ for $c_n = 2.56$ at. %, and $r_c = 23.030d_0$ and $N_s = 1961$ for $c_n = 3.67$ at. %. $K_{ext} = 0.0\kappa$ in all cases so no external pressure was applied to this system.

The effectiveness of DMH in the 4-8M can be seen in Fig. 4.2 where a very rapid condensation of the vacancies into dislocation dipoles occurs. At already $500t_0$ the last dislocation is leaving the patch on the right hand side (A close look at the dislocation core reveals a very extended core along the Burgers vector direction, a result similar to what is shown in Ref. [57] for the LJM). By $600t_0$ (see Fig. 4.2 (f)) only a few vacancies are left which take a much longer time to anneal out in comparison to the first stage involving the dislocations.

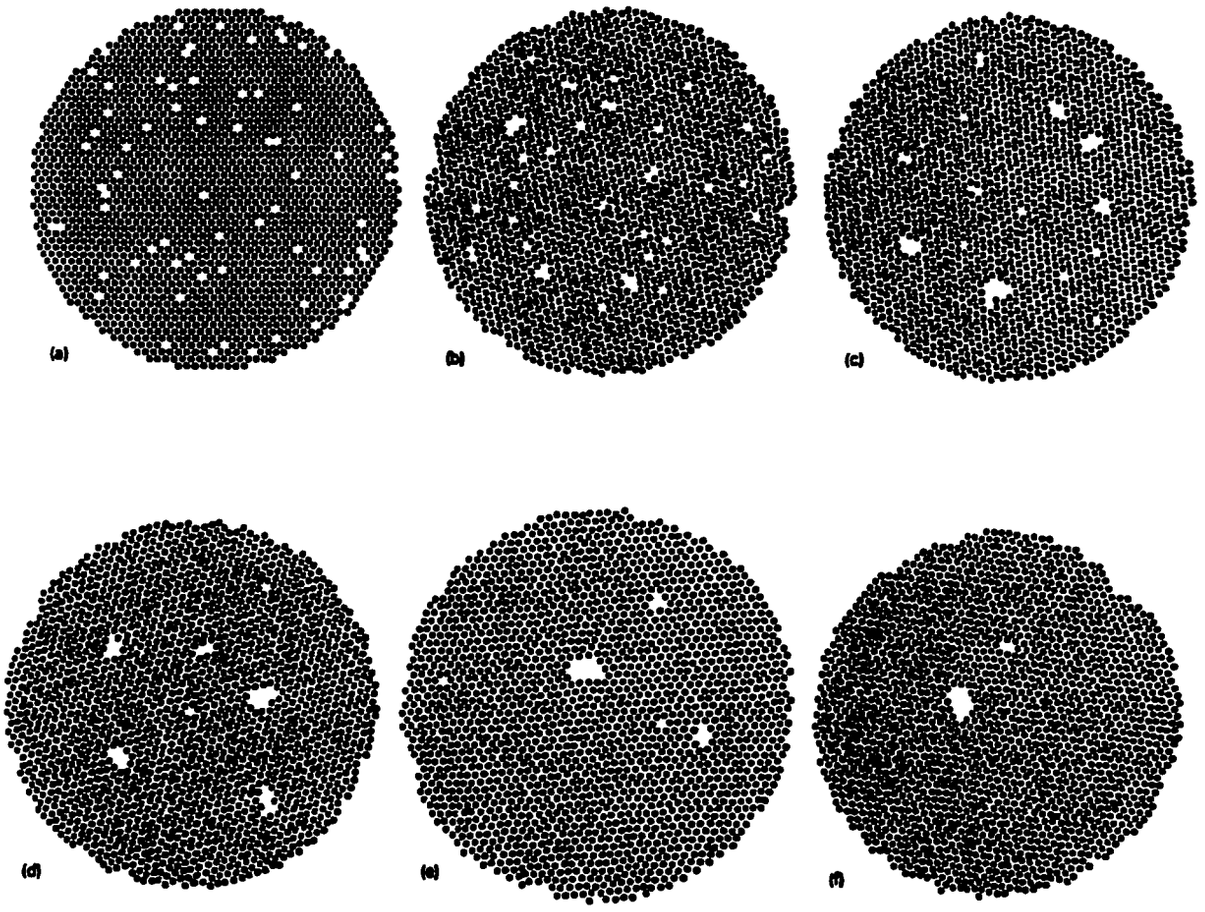

Figure 4.1: Configurations of particles at various times t of a PLFM patch with free boundary conditions at $T = 0.006\kappa d_0^2/k_B$, with $N_s = 1931$, $c_n = 3.67$ at. %, $r_c = 22.60d_0$ and $K_{ext} = 2.5\kappa$ corresponding to a pressure of $P \approx 0.01\kappa$. (a) $t = 0$, (b) $t = 10^4 t_0$, (c) $t = 1.3 \times 10^5 t_0$, (d) $t = 7 \times 10^5 t_0$, (e) $t = 1.75 \times 10^6 t_0$ and (f) $t = 2.1 \times 10^6 t_0$.

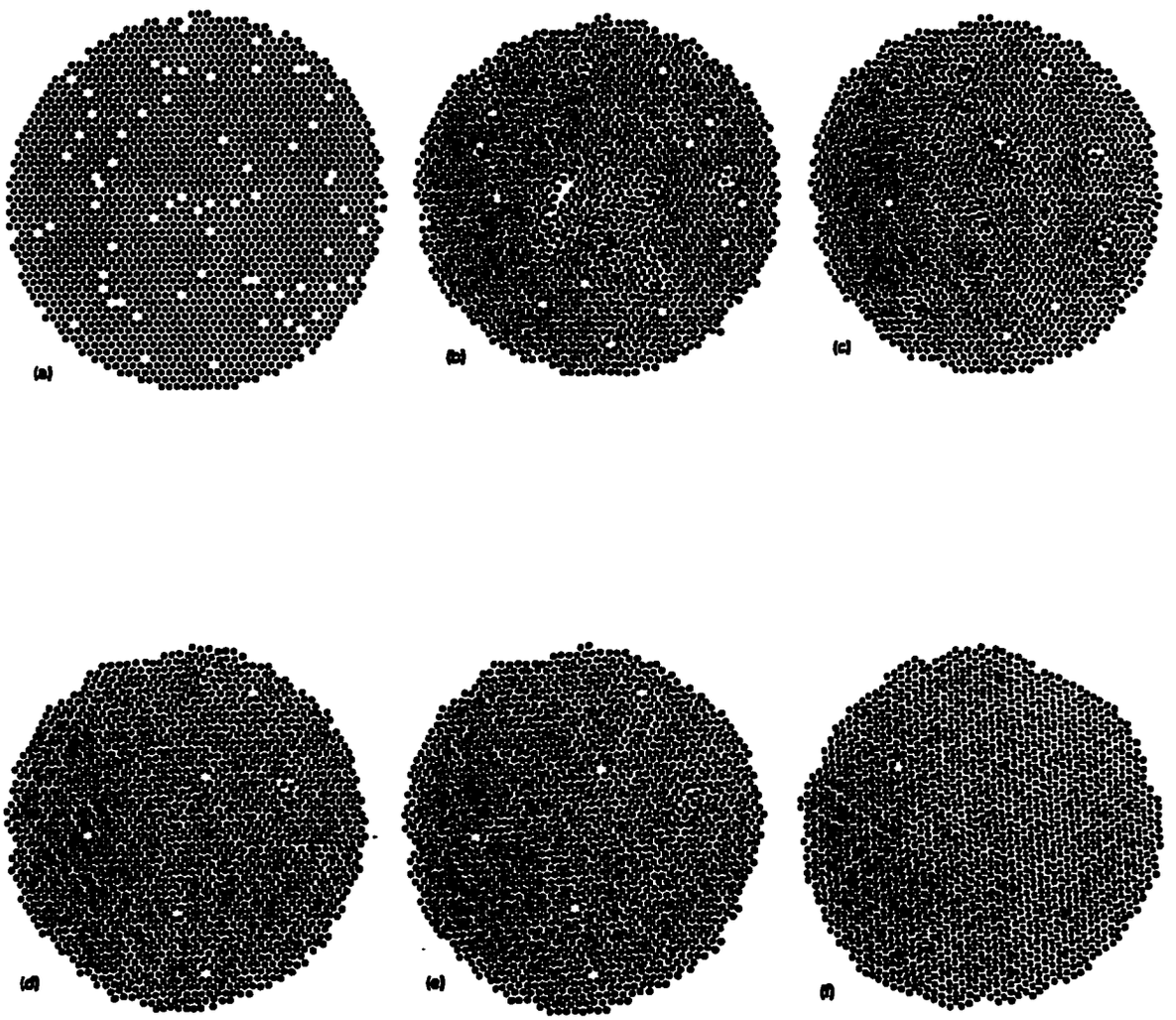

Figure 4.2: Configurations of particles at various times t of a 4-8M patch with free boundary conditions at $T = 0.042\kappa d_0^2/k_B$, $N_s = 1961$, $c_n = 3.67$ at. %, $r_c = 23.52d_0$ and $K_{ext} = 0.0\kappa$. (a) $t = 0$, (b) $t = 100t_0$, (c) $t = 200t_0$, (d) $t = 500t_0$, (e) $t = 600t_0$, and (f) $t = 20600t_0$.

Fig. 4.3 shows an annealing sequence at a temperature below T_D in an intermediate size system with $N = 1961$, $c_n = 3.67$ at. %, $r_c = 23.030d_0$ and $T = 0.001\kappa d_0^2/k_B$. The majority of vacancies are annealed out in $900t_0$ leaving a concentration of $c_n = 0.78$ at. %. At $t = 20225t_0$ no further change occurs. The set of figures 4.3 show the formation of a dislocation dipole, and its climb by absorption of vacancies while gliding towards the edge. During the same time other vacancies diffuse directly to the edges singly or as divacancies. At time $75t_0$ an initial 60^o dipole (see Fig. 4.3 (b)), a linear row of four vacancies (the linear arrangement is the lowest energy configuration for small dipoles [55, 57]) is observed at the center of the patch. By the same time several other dislocations have been generated to the left of patch which because of the large density of vacancies in that region rapidly anneal leaving $50t_0$ later a single dislocation in the upper left corner (see Fig. 4.3 (c)). The central dipole takes the longest to anneal out. One dislocation reaches the edge in about $200t_0$, it is the one which absorbs on its way out the vacancies to its right. The second follows $700t_0$ later.

In these systems the vacancy clusters remain very small. At temperatures above T_D trivacancies already line up as dislocation dipoles. Below T_D the trivacancies appear very stable. It is visible in Figs. 4.3 (b) to (e).

4.3.3 The Lennard Jones Monolayer (LJM)

The LJM exhibits both DMH and VF in its phase diagram. This means that its annealing kinetics will depend sensitively not only upon where the patch under study is located in that phase diagram but also on the distribution of vacancies which can create regions of lower or higher pressure than the average starting pressure. Complex kinetics is therefore expected especially close to the boundaries between the two behaviours.

For the LJM, most of the simulations were done at $T = 0.006\kappa d_0^2/k_B$, $c_n = 1.5$ at.%, $c_n = 2.56$ at.% , and $c_n = 3.73$ at.%. We also tried $T = 0.003\kappa d_0^2/k_B$, a temperature well below the self diffusion temperature of vacancies, with $c_n = 3.73$ at. %. In this case only small voids, di- and tri- vacancies are formed. For $T = 0.006\kappa d_0^2/k_B$ we chose $N_s = 965$, 1931 and 3946. $r_c = 15.935d_0$ and $16.212d_0$ for $N_s = 965$, $r_c = 22.547d_0$, $22.778d_0$, $22.939d_0$ and $23.193d_0$ for $N_s = 1931$ and $r_c = 32.652d_0$ for $N_s = 3946$. $K_{ext} = 0.2$, 0.5 and 2.5κ corresponding to pressures

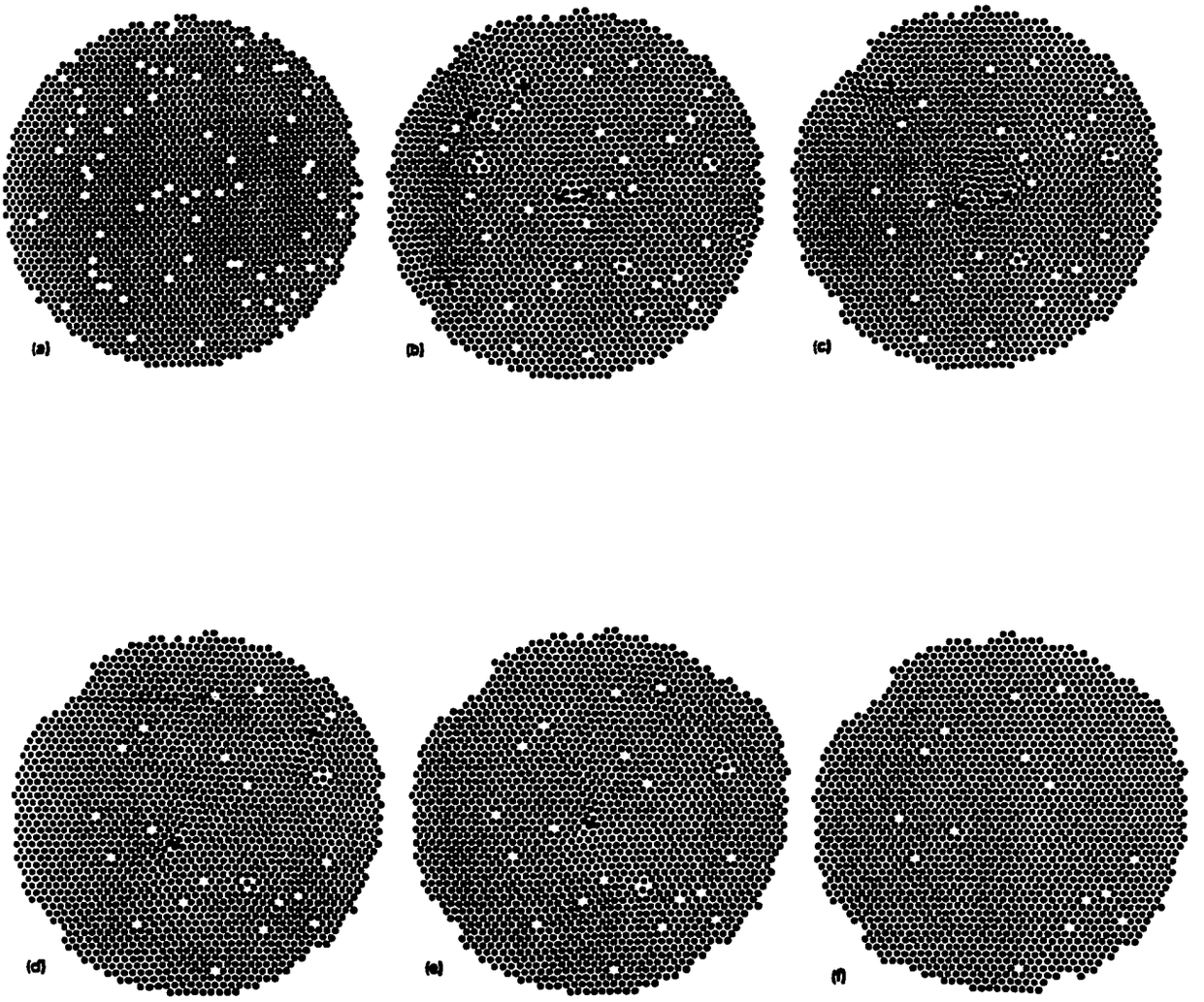

Figure 4.3: Configurations of particles at various times t of a 4-8M patch with free boundary conditions at $T = 0.001\kappa d_0^2/k_B$, $N_s = 1961$, $c_n = 3.67$ at. %, $r_c = 23.03d_0$ and $K_{ext} = 0.0\kappa$. (a) $t = 0$, (b) $t = 75t_0$, (c) $t = 125t_0$, (d) $t = 200t_0$, (e) $t = 225t_0$, and (f) $t = 900t_0$.

ranging from $\approx 0.004\kappa$ to $\approx 0.043\kappa$.

We found that for the larger systems ($N_s = 1931, 3946$), two types of annealing mechanisms coexist, one is the rapid DMH, and the other the slow VDA.

For $T = 0.006\kappa d_0^2/k_B$, the critical pressure P_c separating the two regions of behaviour is $\approx 0.010\kappa$.

For $P > P_c$ the annealing behaviour is very similar to the DMH observed in the 4-8M. The larger the sample size the more effective DMH is, although it takes longer. For $N_s = 1931$ and $P \approx 0.02\kappa$, after $500t_0$, 1.0 at. % of the vacancies were left with a starting concentration of $c_n = 3.73$ at.%. For $N_s = 3946$ at the same pressure DMH took about $6000t_0$ but only about 0.55 at. % of the vacancies remained. Very little difference is seen for the two smaller concentrations, $c_n = 1.5$ at.% and $c_n = 2.56$ at.%.

A full annealing sequence is shown in Fig. 4.4 for the $N_s = 1931$ system with initial $c_n = 3.73$ at.%. A dipole recombination is seen, two dislocations of opposite Burgers vector annihilating. This is about to happen in Fig. 4.4 (c)). In that same figure the dislocation on the left is heading straight to the edge absorbing on its way a few more vacancies. It leaves in Fig. 4.4 (d) a single isolated dislocation. These processes are very fast due to the high mobility of the dislocations in this system [35]. Only the last step takes a little longer, the diffusion of the last dislocation to the edge, although in this size of system it is done within a few $1000t_0$.

It is interesting to note that the preferred dislocation configuration is the five-fold coordinate vacancy (FCV) which was demonstrated to be the lowest energy configuration in ref. [57] as can be seen with the isolated dislocation in Fig. 4.4 (d) and (e)). This configuration is clearer in the LJM than in the 4-8M which is longer range and for this reason the FCV may be a less definite configuration (see Fig. 4.3 (e)).

Below P_c, a unique behaviour is observed similar to what is seen in the PLFM's but with some differences as evidenced in Fig. 4.5 for $N = 1931$, $c_n = 2.56$ at.%, $r_c = 23.193d_0$ and $K_{ext} = 0.5\kappa$, or $P \approx 0.008\kappa$. Vacancies tend to condense into voids but medium size voids i.e. voids containing approximately six vacancies show remnants of DMH behaviour by trying to reform as dislocation dipoles. These conversions do not last long, less than a couple of hundred t_0. The defect remains in the form of a void longer. The oscillation between void and dipole persists for a

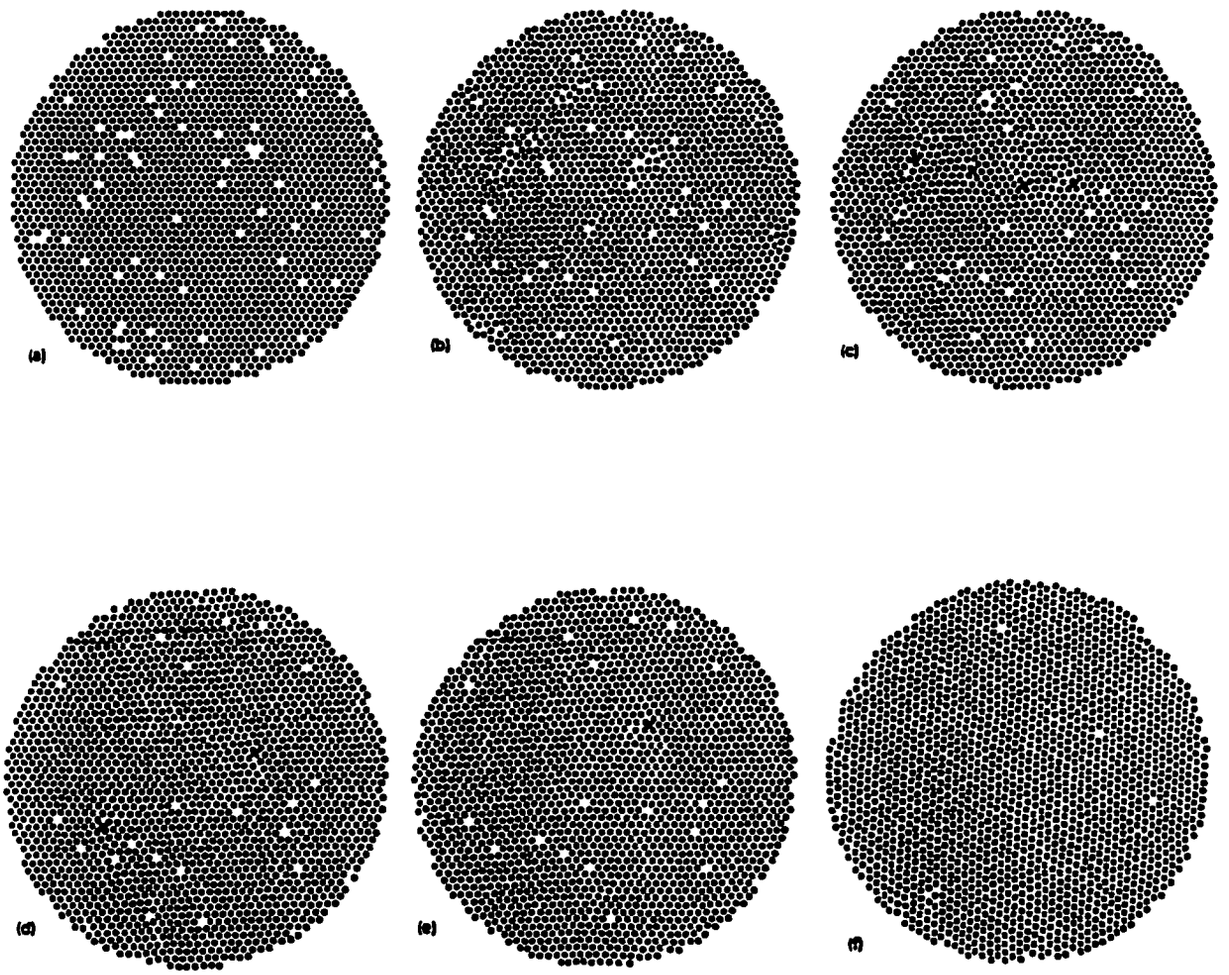

Figure 4.4: Configurations of particles at various times t of a LJM patch with free boundary conditions at $T = 0.006\kappa d_0^2/k_B$, with $N_s = 1931$, $c_n = 3.73$ at.%, $r_c = 22.778d_0$ and $K_{ext} = 2.5\kappa$. This is the regime $P > P_c$. (a) The initial configuration ($t = 0$), (b) $t = 100t_0$, (c) $t = 200t_0$, (d) $t = 300t_0$, (e) $t = 400t_0$, (f) $t = 7000t_0$.

while, up to $3000t_0$ in our simulations. This oscillation stops when the void grows beyond a certain size. It is noteworthy that small dipoles in LJM are more like composite defects than elastic dipoles [55, 56]. In Fig. 4.5 two "dipole - void" oscillations can be seen, one on the left of the patch and the other on the right. On the right hand side the dipole forms for the first time partially as the void absorbs a vacancy at $1050t_0$. By $1250t_0$ it has reformed as a void. At $1500t_0$ the dipole has reappeared. This oscillation continues until $5000t_0$ when the complex breaks up into three small voids which separately reach the edges (see Fig. 4.5 (f)). On the left the starting void is larger. It oscillates once around $1300t_0$ but then remains stable when it has reached the size of eight vacancies.

In LJM's as in 4-8M's only small voids are observed. For $P > P_c$ once the void exceeds five vacancies it will collapse into a dislocation dipole. When $P < P_c$ "dipole - void oscillation" may be observed followed by growth of the void.

In both cases in regions of low vacancy concentration the annealing occurs slowly through VDA. Some of the vacancies condense into small voids (consisting of fewer than 5 vacancies) first and then these voids as well as the remaining isolated vacancies move to the edges by self diffusion. This can take between 10^4t_0 and 10^5t_0 depending on the size of the vacancy complexes.

4.4 Vacancy Annealing in the Presence of a Third Degree of Freedom

As in the studies on systems with PBC the only significant difference occurred with the PLFM patches. We report on studies with $a_0 = 0.3\kappa d_0^2$ which gives enough vertical mobility to produce new qualitative behaviour without destroying in plane order. The simulations were done at $T = 0.006\kappa d_0^2/k_B$.

4.4.1 LJM

For the LJM, the characteristics of the patch were; (i) with $c_n = 3.63$ at. %; $N_s = 1955$, $r_c = 22.814d_0$ and $23.233d_0$, (ii) with $c_n = 2.56$ at. %; $N_s = 1939$, $r_c = 23.351d_0$ and $N_s = 1945$, $r_c = 22.924d_0$. $K_{ext} = 0.01$, 0.2, 2.0 and 2.5κ. Consequently, the pressure ranged from $\sim 0.0\kappa$ to $\sim 0.040\kappa$.

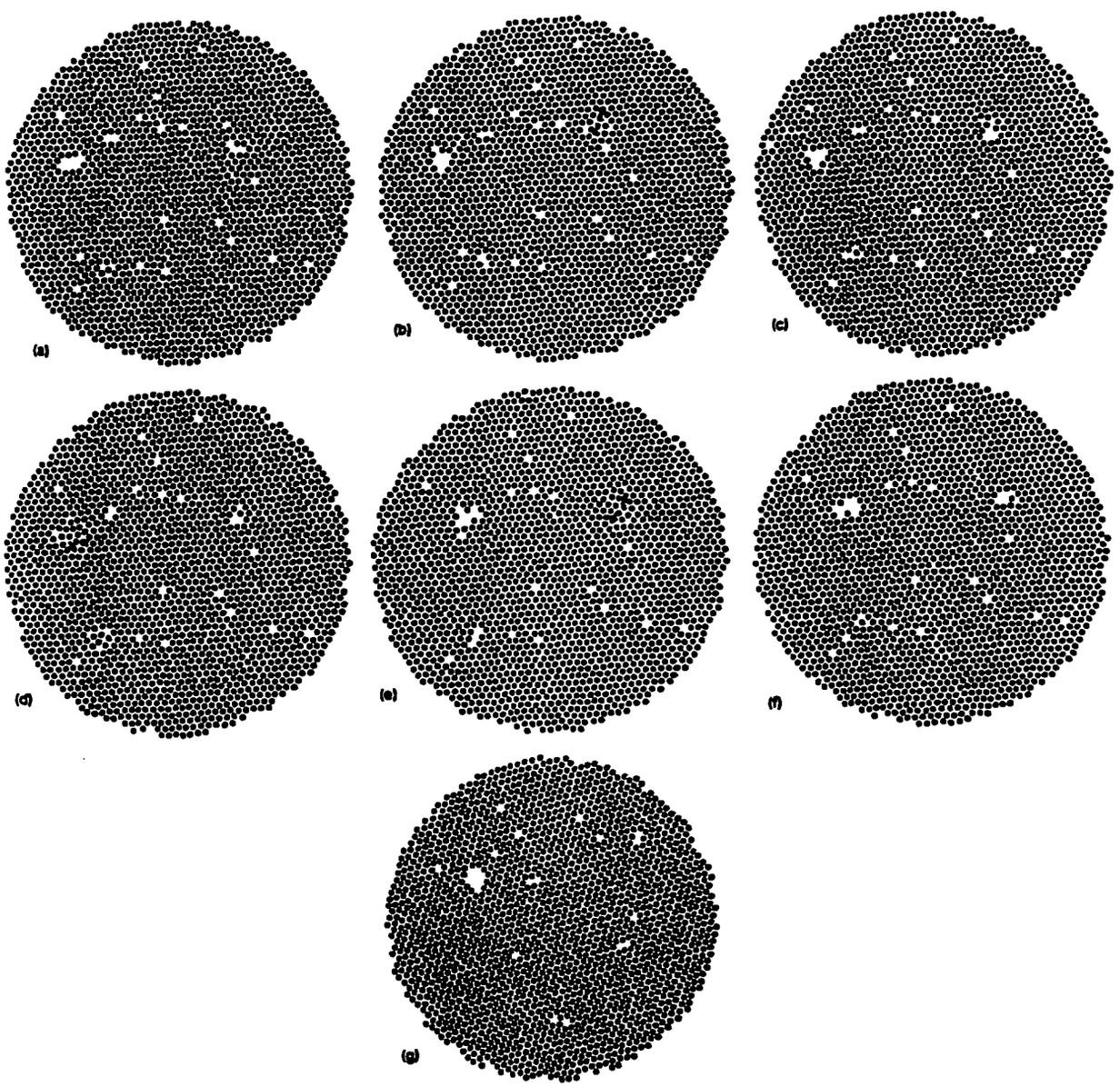

Figure 4.5: Configurations of particles at various times t of a LJM patch with free boundary conditions at $T = 0.006\kappa d_0^2/k_B$, $N_s = 1931$, $c_n = 2.56$ at. %, $r_c = 23.193 d_0$ and $K_{ext} = 0.5\kappa$. This is the regime $P < P_c$. (a) $t = 850t_0$, (b) $t = 1050t_0$, (c) $t = 1250t_0$, (d) $t = 1300t_0$, (e) $t = 1500t_0$, (f) $t = 1600t_0$ and (g) $t = 5400t_0$.

The additional degree of freedom brings no change in the behaviour of the LJM patch. DMH and VDA coexist again. In regions where the vacancy concentration is larger than some critical value, there is still a nonzero critical pressure $P_c \approx 0.010\kappa$. Below P_c, the 'dipole - void oscillation' was observed and large voids (containing about 10 vacancies) can be observed. But above P_c dipoles are stable and no large void appeared. The "dipole - void oscillation" was also observed above P_c. In regions where the vacancy concentration is low, annealing occurs through VDA.

The lifetime of the dislocation dipole and the free dislocation are not obviously different from that of the ideal monolayer and neither is the total annealing time.

4.4.2 PLFM

With the PLFM, we tried $r_c = 22.721d_0$, $22.884d_0$ and $23.047d_0$ for $N_s = 1955$ and $C_n = 3.63$ at. %. $K_{ext} = 0.01$, 0.2, and 0.5κ. The pressure then ranges from $\approx 0.0020\kappa$ to $\approx 0.010\kappa$.

As we have found with PBC [35], DMH can occur with a third degree of freedom for pressures larger than 0.005κ. However, there are still some obvious differences between the PLFM and for instance the LJM. First,the lifetime of a dislocation dipole (about $10^3 t_0$) is obviously longer. Secondly, large voids (consisting of more than 5 vacancies) can coexist with the dislocation dipole and have a very long life time ($> 10^4 t_0$). Thirdly no "dipole-void oscillation" is observed at any pressure. Moreover, DMH in the PLFM is less effective than in the LJM. Finally the complete annealing time (over $10^6 t_0$) is still much longer than in the LJM. Fig. 4.6 shows typical snapshots with $N_s = 1955$, $c_n = 3.63$ at. % , $r_c = 22.721d_0$ and $K_{ext} = 0.5\kappa$ so that $P \approx 0.01\kappa$. Fig. 4.6(a) shows the configuration at $3600t_0$ where we can see a dipole coexisting with many voids. DMH is only part of the annealing process. Large voids are still part of the process. After $5800t_0$ the dipole has disappeared and the voids remain Fig. 4.6(b). The rest of the annealing process is essentially VF.

4.5 Conclusion

These studies on monolayer patches show the effectiveness of the condensation of vacancies into dislocation dipoles in the annealing process of damaged monolayers.

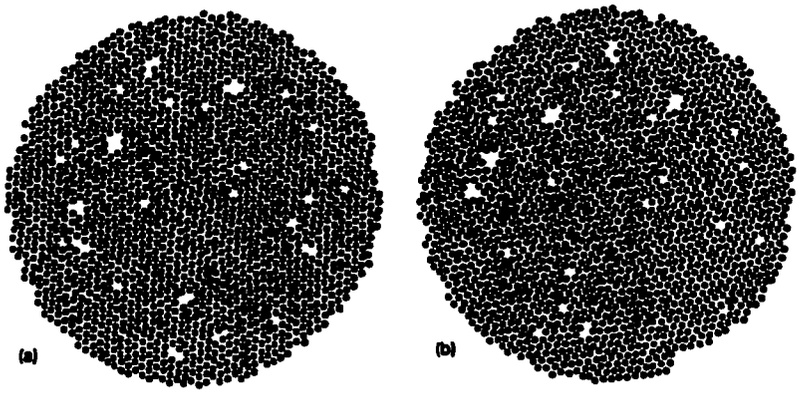

Figure 4.6: Configurations of particles at various times t of a PLFM patch with free boundary conditions at $T = 0.006\kappa d_0^2/k_B$, $N_s = 1955$, $c_n = 3.63$ at. % , $r_c = 22.721 d_0$ and $K_{ext} = 0.5\kappa$. (a) $t = 3600 t_0$ and (b) $t = 5800 t_0$.

Our models are two dimensional with central force interactions, i.e. pairwise interactions with no bond angle stiffness. In this class of system the key to obtaining DMH is a long range interaction. Pressure, temperature, a high local density of vacancies and an additional degree of freedom will, however, favour the phenomenon. DMH is associated with the early collapse of voids into dislocation dipoles. In monolayers with more complex interactions, incorporating for instance bond angle stiffness, the dislocation mobility may be hampered, and this would hinder DMH. The above results are in accord with what was found using PBC and complete that earlier work by including the effect of free edges.

The findings of this work can be related with the behaviour reported in bulk materials. Metals can be considered as long range force systems while semiconductors, short range with strong bond angle stiffness. The clustering of vacancies has been extensively studied in f.c.c. metals [28, 61, 62, 63, 65]. Almost every article in Ref. [28] discusses the clustering of vacancies and the collapse of voids into dislocation loops, the three dimensional equivalent of the dislocation dipole in two dimensions, in the first stage of annealing. The specific defect obtained depends on such factors as the stacking fault energy. A low stacking fault energy favours a tetrahedra of

{111} planes of stacking faults. With high stacking fault energies, such as in Al, the collapse of the voids into dislocation loops in the {111} plane begins to occur even with clusters of a few vacancies. In a second stage at a higher temperature the loops are annealed out.

In semiconductors, systems where dislocations have high Peierls energies due to the covalent bonding, studies have focussed on the kinetics resulting from radiation damage and the kinetics is dominated by interstitials, vacancies, divacancies and other small complexes [68].

There is a related problem, the generation of dislocations by condensation of vacancies during the growth process, which is discussed in a review article by Muftatschiev [69]. This nucleation process may obey the same physical principles.

All in all we have showed some basic kinetic scenarios which focus on the competition between voids, circular aggregates of vacancies, and dislocation dipoles, linear aggregates of vacancies.

Chapter 5

Calculation of Elastic Constants

5.1 Introduction

Elastic constants yield valuable dynamical and mechanical information about materials. For example, they yield information concerning the stability and strength of materials. Furthermore, the comparison of experimentally measured and theoretically calculated elastic constants has been widely used as an important means of probing the interactomic forces [70]. In cases where well established potentials are available one should be able to predict the behaviour of the material under various conditions of normal or extreme loading.

For comparison of experimental results with theory, it is necessary not only to have accurate experimental data, but also to have a reliable method of calculation. Recent advances in computer-simulation techniques and formalism have made this possible [70]-[79].

At zero temperature and zero stress the calculation of elastic constants follows the arguments first given by Born and Huang [70] and also found in reference [80]. The elastic constants are obtained from the long wavelength limit of the elastic waves.

To obtain an expression for the elastic constants which is valid at finite temperatures, an approach different from the one used in the zero temperature is necessary. Squire, Holt and Hoover [71] showed in 1969 that expressions in the canonical ensemble and free of stress can be easily derived by noticing that the elastic constants

are the second derivatives of the Helmholtz free energy. They were the first to derive what are known as the "equilibrium" fluctuation formulae. Their method was further extended by many people to more complex systems [73]-[79]. However, the definition of elastic constants in most papers (for instance, see Refs. [25], [71]-[79]) requires implicitly the natural (stress-free) reference (initial) configurations, therefore a priori their expressions are only valid for systems under moderate stress.

Elastic constants were often identified to the elastic stiffness coefficients which govern stress-strain relations and used as stability criteria. T. Barron and M. Klein [81] were the first to clarify this situation. They pointed out that the traditional definition of the elastic constants derived from the internal energy or Helmholtz free energy cannot be directly applied to the study of the stress-strain relationship of a stressed state. They derived the correct form of the stress-strain relations for a stressed system in the microcanonical or canonical ensembles. They have in fact given the correct reference state for the definition of elastic constants but they did not derive the fluctuation formulae.

Following T. Barron and M. Klein, for systems under arbitrary stress, we clarify some points concerning the calculation of the elastic constants when using fluctuation formulae. This is particularly important when the stressed systems are far from their natural configuration. We shall also prove in the next Chapter that elastic constants cannot be used as stability criteria for a stressed state.

The purposes of this chapter are threefold. First, we emphasize that, when using fluctuation formulae for the calculation of the elastic constants, the reference configuration (i.e. before virtual deformations are applied to the system) must be the current (stressed) one. Second, with a single shape tensor simple fluctuation formulae convenient for computer simulations are obtained for a system under arbitrary stress in the canonical ensemble. We shall also reconcile the apparent difference between the expressions obtained from two equivalent ways. And finally we derive the correct fluctuation formulae for elastic constants in the uniform dilation system. The exact results for some two dimensional perfect systems at zero temperature will be presented in the next chapter, together with the stability criteria.

The main contents of this Chapter can be found in reference [82].

5.2 Fundamental Concepts in Elasticity Theory

We first recall some fundamental concepts to introduce the formulae on which our discussion is based. The variety of terminology and symbols used in this field make this presentation necessary.

5.2.1 Strain

In the theory of elastic continuum, we can assign to every point in the material a coordinate x [25, 70, 81, 83]. After deformation, the displacement of a point initially at $\mathring{\mathbf{x}}$ is

$$\mathbf{u}(\mathring{\mathbf{x}}) \;=\; \mathbf{x}(\mathring{\mathbf{x}}) - \mathring{\mathbf{x}}$$

or

$$u_\alpha(\mathring{\mathbf{x}}) \;=\; x_\alpha(\mathring{\mathbf{x}}) - \mathring{x}_\alpha, \qquad \alpha = 1,2,3. \tag{5.1}$$

$\mathring{\mathbf{x}}$ is also referred to as the reference position of x. The reference state can be either stressed or stress-free.

We should note that the deformation parameters can be viewed as pure geometric quantities, so their definition are quite arbitrary [84, 85, 86] in the meaning of the choice of both the coordinate system and the reference states. One can choose generalized coordinates instead of the Cartesian coordinates to describe the deformation. For instance, for Milstein [85, 86] the variables are the cell edges and their included angles. Hill gave in detail the relationship between the strains defined in different coordinate systems [84]. Since computer simulations are always performed in Cartesian coordinate systems, we shall not discuss more the choice of the coordinate system, but only note that *the physical results must be independent of the choice of the coordinate system.* On the other hand, many authors like to use the stress-free state as an absolute reference state for deformation parameters and strains [71]-[79]. However, such a choice may lead to some confusion about the expressions of the stress and relevant elastic quantities, as we shall discuss.

For a small deformation, we can write

$$u_\alpha(\mathring{\mathbf{x}}) = \frac{\partial u_\alpha(\mathring{\mathbf{x}})}{\partial \mathring{x}_\beta}\, \mathring{x}_\beta \equiv u_{\alpha\beta}(\mathring{\mathbf{x}})\, \mathring{x}_\beta \,. \tag{5.2}$$

In this equation, and all subsequent ones, the Einstein summation convention for repeated suffices is followed. Note that in general $u_{\alpha\beta} \neq u_{\beta\alpha}$. Sometimes the deformation parameters $u_{\alpha\beta}$ are also called the strain tensor (for instance, see Refs. [83, 87]).

For simplicity, we shall consider only systems under homogeneous deformation [25, 70, 80, 81, 83] so the $u_{\alpha\beta}(\mathring{\mathbf{x}})$ are independent of $\mathring{\mathbf{x}}$.

The $u_{\alpha\beta}$ can be written as

$$u_{\alpha\beta} = e_{\alpha\beta} + \omega_{\alpha\beta} \tag{5.3}$$

with

$$e_{\alpha\beta} = \frac{1}{2}(u_{\alpha\beta} + u_{\beta\alpha}) = e_{\beta\alpha} \tag{5.4}$$

and

$$\omega_{\alpha\beta} = \frac{1}{2}(u_{\alpha\beta} - u_{\beta\alpha}) = -\omega_{\beta\alpha}, \tag{5.5}$$

where the $e_{\alpha\beta}$ are the components of the elongation or pure strain tensor and the $\omega_{\alpha\beta}$ those of the rotation tensor [25, 81]. In general, the $\omega_{\alpha\beta}$ are disregarded for a small deformation since they represent an infinitesimal rotation of the whole system, and in the absence of internal torques cannot give rise to stress.

The elongation $e_{\alpha\beta}$ is preferably used in experiment since it is what is measured. In contrast, another strain, the Lagrangian strain tensor [25, 81] defined by

$$\eta_{\alpha\beta} \equiv \frac{1}{2}(u_{\alpha\beta} + u_{\beta\alpha} + u_{\gamma\alpha}u_{\gamma\beta}) = \eta_{\beta\alpha} \tag{5.6}$$

is more often used in theoretical models as it can completely determine the deformation of the system [25, 81, 83]. An advantage of the Lagrangian strain tensor is that if we expand a function in power series of η, the expansion coefficients will automatically satisfy the requirement of rotational invariance [83].

In the following, when we refer to strain we shall refer to the Lagrangian strain tensor. Another often used symbol for the Lagrangian strain tensor is $\epsilon_{\alpha\beta}$ [74, 75, 76, 77].

5.2.2 Elastic Constants

Elastic constants, or more exactly, second order elastic constants are in general defined by

$$\mathring{C}_{\alpha\beta\sigma\tau} \equiv \frac{1}{V_o}\left(\frac{\partial^2 W}{\partial\eta_{\alpha\beta}\partial\eta_{\sigma\tau}}\right)_{\eta=0}, \tag{5.7}$$

where W is the strain-energy. It can refer either to the Helmholtz free energy F in the derivation of isothermal elastic constants (the canonical ensemble) or to the internal energy E in the derivation of adiabatic elastic constants (the microcanonical ensemble). V_o is the reference value of the volume V i.e. before deformation.

We have to point out that the subscript $\eta = 0$ in Eq. (5.7) is missing in many publications. This omission causes confusion about the reference state. Note that $\mathring{C}_{\alpha\beta\sigma\tau}$ is essentially an expansion coefficient. Such a subscript is therefore a necessary.

By definition the elastic constants have the following symmetries;

$$\mathring{C}_{\alpha\beta\sigma\tau} = \mathring{C}_{\sigma\tau\alpha\beta} = \mathring{C}_{\alpha\beta\tau\sigma}\,. \tag{5.8}$$

Eq. (5.8) reduces the number of independent elastic constants from 81 to 21 which are often expressed in the condensed Voigt notation (for instance $\mathring{C}_{1111}$=$\mathring{C}_{11}$, $\mathring{C}_{1122}$=$\mathring{C}_{12}$, $\mathring{C}_{1212}$=$\mathring{C}_{44}$ etc ...).

For a central force system, we can derive $\mathring{C}_{\alpha\beta\sigma\tau}$ straightforwardly from its definition since the strain-energy W can be written explicitly as a function of η by using [25, 70, 81]

$$\mathbf{x}^2 - \mathring{\mathbf{x}}^2 = 2\eta_{\alpha\beta}\,\mathring{x}_\alpha\mathring{x}_\beta\,. \tag{5.9}$$

But for a non-central force system, we have to use a different approach since in general it is impossible to express the strain-energy explicitly as a function of η. Instead, we can expand $\frac{W-W_o}{V_o}$ as a Taylor series [70]

$$\frac{W-W_o}{V_o} = \mathring{S}_{\alpha\beta}\,u_{\alpha\beta} + \frac{1}{2}\,\mathring{S}_{\alpha\beta\sigma\tau}\,u_{\alpha\beta}u_{\sigma\tau} + \ldots \tag{5.10}$$

$$= \mathring{c}_{\alpha\beta}\,\eta_{\alpha\beta} + \frac{1}{2}\,\mathring{C}_{\alpha\beta\sigma\tau}\,\eta_{\alpha\beta}\eta_{\sigma\tau} + \ldots, \tag{5.11}$$

where W_o is the reference value of W. $\mathring{S}_{\alpha\beta}$ is the component of the applied stress tensor [25, 81, 83] for the reference state.

Note that Eqs. (5.10) and (5.11) give some constraints on V_o and the reference state. If we want to calculate the elastic constants at a stressed state, the expansion must be done around this stressed state which acts as the reference state, so that V_o must be the volume of this reference state instead of the volume of the stress-free state. Also, $\eta_{\alpha\beta}$ must use this stressed state as reference. We can see this point more clearly from Eq. (5.9). If the $\eta_{\alpha\beta}$ use the stress-free state as reference, $\mathring{x}_\alpha$ must also be the coordinates in the stress-free state so that the expansion is around the stress-free state and not about the point of interest.

As we mentioned in section 5.2.1, one can use the stress-free state as the absolute reference for the definition of the strains. Correspondingly, Eq. (5.9) becomes

$$\mathbf{x}^2 - \mathring{\mathbf{x}}^2 = 2\delta\eta_{\alpha\beta}\,\mathring{x}_\alpha\mathring{x}_\beta\,. \tag{5.12}$$

and Eq. (5.11) should be written

$$\frac{W - W_o}{V_o} = \mathring{c}'_{\alpha\beta}\,\delta\eta_{\alpha\beta} + \frac{1}{2}\,\mathring{C}'_{\alpha\beta\sigma\tau}\,\delta\eta_{\alpha\beta}\delta\eta_{\sigma\tau} + ..., \tag{5.13}$$

where $\delta\eta = \eta - \eta_0$ and η_0 is the strains at the expansion point. However, now

$$\mathring{c}'_{\alpha\beta} = \frac{1}{V_o}\left(\frac{\partial W}{\partial \eta_{\alpha\beta}}\right)_{\eta=\eta_0} \tag{5.14}$$

In this way, the meaning of $\mathring{c}'_{\alpha\beta}$ is questionable. We shall show in section 5.3.1 that $\mathring{c}'_{\alpha\beta}$ cannot be identified with the physical stress except in the case of $\eta_0 = 0$. As a consequence, it is inappropriate to use $\mathring{C}'_{\alpha\beta\sigma\tau}$ to characterize the relationship between stress and strains. This complication is due to the fact that the transformation of strains between different reference states is nonlinear. For instance, consider a deformation in which a point initially at $\mathring{\mathbf{x}}$, was moved to $\mathbf{x}'$ first and finally to $\mathbf{x}$, we can write

$$\begin{aligned} x_\alpha &= (\delta_{\alpha\gamma} + \omega_{\alpha\gamma})\,\mathring{x}_\gamma = \mathring{x}_\alpha + \omega_{\alpha\gamma}\,\mathring{x}_\gamma \\ &= (\delta_{\alpha\beta} + v_{\alpha\beta})(\delta_{\beta\gamma} + u_{\beta\gamma})\,\mathring{x}_\gamma = \mathring{x}_\alpha + (u_{\alpha\gamma} + v_{\alpha\gamma} + v_{\alpha\beta}u_{\beta\gamma})\,\mathring{x}_\gamma \end{aligned} \tag{5.15}$$

where w and u use $\mathring{\mathbf{x}}$ as reference but v uses $x'_\alpha = (\delta_{\alpha\gamma} + u_{\alpha\gamma})\,\mathring{x}_\gamma$ as reference. Therefore,

$$\omega_{\alpha\gamma} - u_{\alpha\gamma} = v_{\alpha\gamma} + v_{\alpha\beta}u_{\beta\gamma} \neq v_{\alpha\gamma} \tag{5.16}$$

It is this absolute reference value for strains which causes some confusion about the calculations of the elastic constants .

The higher order tensors $\mathring{S}_{\alpha\beta\sigma\tau}$ related to the elastic constants are sometimes called displacement gradient moduli. We do not discuss the higher order terms of Eqs. (5.10)-(5.11). However, our comments about the reference state must be also applied to them.

Substituting Eq. (5.6) in Eq. (5.11) and using Eq. (5.10) we find [81]

$$\mathring{c}_{\alpha\beta}=\mathring{S}_{\alpha\beta} \quad \text{and} \quad \mathring{C}_{\alpha\beta\sigma\tau}=\mathring{S}_{\alpha\beta\sigma\tau} - \mathring{S}_{\beta\tau}\,\delta_{\alpha\sigma}. \tag{5.17}$$

5.2.3 Stress-strain Relations

In thermodynamics, a thermodynamic stress tensor $t_{\alpha\beta}$, defined by

$$t_{\alpha\beta} = \frac{1}{V_o}\frac{\partial W}{\partial \eta_{\alpha\beta}} = \mathring{S}_{\alpha\beta} + \mathring{C}_{\alpha\beta\sigma\tau}\,\eta_{\sigma\tau}, \tag{5.18}$$

is introduced [25, 83, 88]. (Often the opposite sign for $t_{\alpha\beta}$ is used as in Refs. [74, 77]). $t_{\alpha\beta}$ should not be confused with the applied stress $T_{\alpha\beta}$.

The actual internal stress $T_{\alpha\beta}$ corresponds to the strained system [81] and its reference configuration is different from that of $\mathring{C}_{\alpha\beta\sigma\tau}$. $T_{\alpha\beta}$ is formally equal to

$$T_{\alpha\beta} = \frac{1}{V(u)}\left(\frac{\partial W(u_{\alpha\beta}, v_{\alpha\beta})}{\partial v_{\alpha\beta}}\right)_{v_{\alpha\beta}=0}. \tag{5.19}$$

The reference configuration is the system deformed by $u_{\alpha\beta}$, and $v_{\alpha\beta}$ is the small deformation made on that system.

Using

$$x_\alpha(\mathring{\mathbf{x}}) = (\delta_{\alpha\beta} + u_{\alpha\beta})(\delta_{\beta\gamma} + v_{\beta\gamma})\,\mathring{x}_\gamma \tag{5.20}$$

an expansion of $W(u_{\alpha\beta}, v_{\alpha\beta})$ leads, as shown by Barron and Klein [81], to

$$\begin{aligned} T_{\alpha\beta} &= \mathring{S}_{\alpha\beta} + (\mathring{S}_{\alpha\beta\sigma\tau} - \mathring{S}_{\alpha\beta}\,\delta_{\sigma\tau} + \mathring{S}_{\alpha\tau}\,\delta_{\beta\sigma})u_{\sigma\tau} \\ &= \mathring{S}_{\alpha\beta} + \mathring{c}_{\alpha\beta\sigma\tau}\,\eta_{\sigma\tau} + \mathring{S}_{\beta\tau}\,\omega_{\alpha\tau} + \mathring{S}_{\alpha\tau}\,\omega_{\beta\tau} \end{aligned} \tag{5.21}$$

where they introduce another symbol, the elastic stiffness coefficient [89]

$$\begin{aligned} \mathring{c}_{\alpha\beta\sigma\tau} \equiv\ & \mathring{C}_{\alpha\beta\sigma\tau} - \frac{1}{2}(2\,\mathring{S}_{\alpha\beta}\,\delta_{\sigma\tau} - \mathring{S}_{\alpha\sigma}\,\delta_{\beta\tau} - \mathring{S}_{\alpha\tau}\,\delta_{\beta\sigma} \\ & - \mathring{S}_{\beta\tau}\,\delta_{\alpha\sigma} - \mathring{S}_{\beta\sigma}\,\delta_{\alpha\tau}). \end{aligned} \tag{5.22}$$

$\mathring{c}_{\alpha\beta\sigma\tau}$ are symmetric with respect to the interchanges (α,β) or (σ,τ). However, it does not have the full symmetry of Eq. (5.8). Instead, it satisfies the equalities

$$\mathring{c}_{\alpha\beta\sigma\tau} - \mathring{c}_{\sigma\tau\alpha\beta} = \mathring{S}_{\sigma\tau}\,\delta_{\alpha\beta} - \mathring{S}_{\alpha\beta}\,\delta_{\sigma\tau}. \tag{5.23}$$

The thermodynamic stress $t_{\alpha\beta}$ and the applied stress $T_{\alpha\beta}$ are related by the relation [25, 83, 88]

$$t_{\alpha\beta} = \det(J)\cdot J^{-1}_{\alpha\sigma} J^{-1}_{\beta\tau} T_{\sigma\tau}, \tag{5.24}$$

where

$$J_{\alpha\beta} = \delta_{\alpha\beta} + u_{\alpha\beta} \tag{5.25}$$

$\det(J)$ is the ratio V/V_0.

In a direct experiment $T_{\alpha\beta}$ and $e_{\alpha\beta}$ are measured and hence $\mathring{c}_{\alpha\beta\sigma\tau}$.

5.2.4 The Unstressed System

For an unstressed system, $\mathring{S}_{\alpha\beta}= 0$, therefore, we have

$$\mathring{C}_{\alpha\beta\sigma\tau} = \mathring{S}_{\alpha\beta\sigma\tau} = \mathring{c}_{\alpha\beta\sigma\tau} \tag{5.26}$$

$$T_{\alpha\beta} = \mathring{C}_{\alpha\beta\sigma\tau}\, u_{\sigma\tau} = \mathring{C}_{\alpha\beta\sigma\tau}\, \eta_{\sigma\tau} = t_{\alpha\beta} \tag{5.27}$$

$$\frac{W - W_o}{V_o} = \frac{1}{2}\,\mathring{C}_{\alpha\beta\sigma\tau}\,\eta_{\alpha\beta}\eta_{\sigma\tau}. \tag{5.28}$$

In this situation, the different definitions of the elastic constants are identical.

The symmetry of the crystal reduces the number of independent elastic constants to less than 21. For example, for an isotropic system, there are only two independent elastic constants. Traditionally $\lambda = \mathring{C}_{1122} \equiv \mathring{C}_{12}$ and $\mu = \mathring{C}_{1212} \equiv \mathring{C}_{44}$ are chosen to characterize the system.

5.3 Fluctuation Formulae in the Canonical Ensemble

There are various approaches to calculating elastic constants in computer simulations: direct computation of the stress-strain relations by deformation of the simulation cell, strain-strain fluctuation methods which work on the constant stress ensembles, where the elastic constants are extracted from the fluctuations in the shape

of the simulation cell, and the "equilibrium" fluctuation method. It is this last technique that we shall discuss in this section. The canonical ensemble is used because it is the most commonly used ensemble and the most appropriate for the calculation of elastic constants. As pointed out by Sprik et al. [90] and others, [74, 76] the rate of convergence of elastic constants from stress-strain relations or strain-strain fluctuation methods is unsatisfactory. It is much more efficient to first determine the equilibrium lattice constant for the pressure of interest using a constant pressure simulation, and then do a simulation in the corresponding canonical (constant volume) ensemble [76] using formulae obtained from the "equilibrium" fluctuation method. This can be understood if one observes that strain-strain fluctuation methods follow the fluctuations in a macroscopic quantity which evolves slowly, especially in a large system. In contrast, the "equilibrium" fluctuation method calculates the elastic constants by probing microscopic features of the system where fluctuations occur on a shorter time scale. In this method, a formal expression is derived for the elastic constants, from the second derivative of the free energy (see Eq. (5.7)). The elastic constants are directly obtained from the microscopic fluctuations within the system. The method has the advantage that no actual deformations are made, so no symmetry breaking occurs, and all elastic constants can be obtained from a single run. It must be emphasized that the derivatives are taken with respect to a reference configuration, the one on which virtual deformations $\eta_{\alpha\beta}$ are applied for the purpose of calculating the elastic constants. Hence at every step of a computer run, *the reference configuration and volume are the instantaneous one.*

There are some limitations to the method, though. In a system where elasticity has an entropic origin, such as in a crosslinked polymer melt, the absence of equilibrium positions about which particles vibrate, causes some difficults. In such cases a macroscopic measurement may be more appropriate [91].

5.3.1 General Formalism

In the canonical ensemble, W is the Helmholtz free energy F. With the Hamiltonian $\mathcal{H}$

$$\mathcal{H} = \mathcal{H}(\mathbf{x}, \mathbf{p}, N) = \sum_i \frac{\mathbf{p}_i^2}{2m} + U(\mathbf{x}_1, \mathbf{x}_2, ..., \mathbf{x}_N) \tag{5.29}$$

where $\mathbf{x}$ and $\mathbf{p}$ represent the coordinates and momenta of the N particles,

$$\begin{aligned} F &= -k_B T \ln Z \\ Z &= \frac{1}{C}\int e^{-\mathcal{H}/k_B T} d\tau \end{aligned} \tag{5.30}$$

where C is a constant, $d\tau$ the differential volume element in the 6-N-dimensional phase space and k_B the Boltzmann constant.

There are in general two ways to derive the fluctuation formulae for elastic constants from the definition. The first was adopted by Squire, Holt and Hoover [71] for a cubic crystal with pair force system and later extended by Klein and Murphy [73] to three-body force systems. The second was used by Ray and Rahman [75] for the central force system and later extended by Lutsko [79] to general cases.

Of course, the two approaches should produce equivalent expressions.

The first method works on the real phase space. It is a straightforward derivation of the elastic constants from Eqs. (5.7) and (5.30) [73] :

$$\begin{aligned} \mathring{S}_{\alpha\beta} = \mathring{c}_{\alpha\beta} &= \frac{1}{V_0}\left\langle \frac{\partial \mathcal{H}}{\partial \eta_{\alpha\beta}} \right\rangle_{\eta=0} - \frac{N k_B T}{V_o}\left(\frac{\partial \ln V}{\partial \eta_{\alpha\beta}}\right)_{\eta=0} \\ &= \frac{1}{V_0}\left\langle \frac{\partial \mathcal{H}}{\partial \eta_{\alpha\beta}} \right\rangle_{\eta=0} - \frac{N k_B T}{V_o}\delta_{\alpha\beta}, \end{aligned} \tag{5.31}$$

where we have used $\left(\frac{\partial \ln V}{\partial \eta_{\alpha\beta}}\right)_{\eta=0} = \delta_{\alpha\beta}$ (also see Eq. (B.7) in Appendix B), and

$$\begin{aligned} \mathring{C}_{\alpha\beta\sigma\tau} &= \frac{1}{V_o}\left\langle \frac{\partial^2 \mathcal{H}}{\partial \eta_{\alpha\beta}\partial \eta_{\sigma\tau}} \right\rangle_{\eta=0} - \frac{1}{k_B T V_o}\left\langle \delta\left(\frac{\partial \mathcal{H}}{\partial \eta_{\alpha\beta}}\right)\delta\left(\frac{\partial \mathcal{H}}{\partial \eta_{\sigma\tau}}\right)\right\rangle_{\eta=0} \\ &\quad + \frac{N k_B T}{V_o}(\delta_{\alpha\sigma}\delta_{\beta\tau} + \delta_{\alpha\tau}\delta_{\beta\sigma}), \end{aligned} \tag{5.32}$$

where the $< \ldots >$ designate configurational averages and $\delta(A) = A - < A >$. The last term comes from the identity (also see Eq. (B.8) in Appendix B)

$$\left(\frac{\partial^2 \ln V}{\partial \eta_{\alpha\beta}\partial \eta_{\sigma\tau}}\right)_{\eta=o} = -(\delta_{\alpha\sigma}\delta_{\beta\tau} + \delta_{\alpha\tau}\delta_{\beta\sigma}). \tag{5.33}$$

The $\frac{N k_B T}{V_o}$ terms has often been called "kinetic term" because in a formalism which is constructed with scaled momenta and scaled positions (see Appendix C), it comes out of the kinetic energy contribution to $\frac{\partial \mathcal{H}}{\partial \eta}$. Physically it can be understood as

measuring the mechanical effects of the confinement of the particles. One way to look at it, is if the spatial coordinates are scaled to the simulation box coordinates to maintain them constant under deformations, a V^N appears in front of the partition function leading to a $N \ln V$ term in the free energy. In this way we can avoid the use of the scaled momenta used in Refs. [74, 75, 76, 77, 78, 79] and the kinetic energy term in the Hamiltonian does not depend on the strain.

Now we can see the problem caused with the choice of an absolute reference value for strains. With such a choice, by using the expressions in Appendix B, it is clear that

$$\left(\frac{\partial \ln V}{\partial \eta_{\alpha\beta}}\right)_{\eta=\eta_0} \neq \delta_{\alpha\beta} \tag{5.34}$$

As a consequence, except for $\eta_0 = 0$ i.e. the stress-free state, the $\overset{\circ}{c}{}'_{\alpha\beta}$ defined by Eq. (5.14) cannot be reduced to the form of Eq. (5.31) which is well accepted as the expression for external stress and can be derived independently from kinetic theory [92, 93]. Therefore, to use an absolute reference for strains may lead to some confusion.

From Eq. (5.22) we get the elastic stiffness coefficients which are the quantities determined from direct experiment;

$$\begin{aligned}
\overset{\circ}{c}_{\alpha\beta\sigma\tau} &= \frac{1}{V_o}\left\langle \frac{\partial^2 \mathcal{H}}{\partial \eta_{\alpha\beta}\partial \eta_{\sigma\tau}} \right\rangle_{\eta=0} - \frac{1}{k_B T V_o}\left\langle \delta\left(\frac{\partial \mathcal{H}}{\partial \eta_{\alpha\beta}}\right)\delta\left(\frac{\partial \mathcal{H}}{\partial \eta_{\sigma\tau}}\right)\right\rangle_{\eta=0} \\
&\quad -\frac{1}{2}\left(2\left\langle \frac{\partial \mathcal{H}}{\partial \eta_{\alpha\beta}}\right\rangle_{\eta=0}\delta_{\sigma\tau} - \left\langle \frac{\partial \mathcal{H}}{\partial \eta_{\alpha\sigma}}\right\rangle_{\eta=0}\delta_{\beta\tau} - \left\langle \frac{\partial \mathcal{H}}{\partial \eta_{\alpha\tau}}\right\rangle_{\eta=0}\delta_{\beta\sigma}\right. \\
&\quad \left. - \left\langle \frac{\partial \mathcal{H}}{\partial \eta_{\beta\tau}}\right\rangle_{\eta=0}\delta_{\alpha\sigma} - \left\langle \frac{\partial \mathcal{H}}{\partial \eta_{\beta\sigma}}\right\rangle_{\eta=0}\delta_{\alpha\tau}\right) + \frac{N k_B T}{V_o}\delta_{\alpha\beta}\delta_{\sigma\tau}.
\end{aligned} \tag{5.35}$$

For convenience, we also present here the stability criteria defined by $C_{\alpha\beta\sigma\tau} \equiv \frac{1}{2}(\overset{\circ}{c}_{\alpha\beta\sigma\tau} + \overset{\circ}{c}_{\sigma\tau\alpha\beta})$. We will derive this stability criteria in the next chapter. Replacing $2\left\langle \frac{\partial \mathcal{H}}{\partial \eta_{\alpha\beta}}\right\rangle_{\eta=0}\delta_{\sigma\tau}$ in the above expression by $\left\langle \frac{\partial \mathcal{H}}{\partial \eta_{\alpha\beta}}\right\rangle_{\eta=0}\delta_{\sigma\tau} + \left\langle \frac{\partial \mathcal{H}}{\partial \eta_{\sigma\tau}}\right\rangle_{\eta=0}\delta_{\alpha\beta}$, we can get the elements of the positive definite tensor $C_{\alpha\beta\sigma\tau}$ which determines stability:

$$C_{\alpha\beta\sigma\tau} = \frac{1}{V_o}\left\langle \frac{\partial^2 \mathcal{H}}{\partial \eta_{\alpha\beta}\partial \eta_{\sigma\tau}} \right\rangle_{\eta=0} - \frac{1}{k_B T V_o}\left\langle \delta\left(\frac{\partial \mathcal{H}}{\partial \eta_{\alpha\beta}}\right)\delta\left(\frac{\partial \mathcal{H}}{\partial \eta_{\sigma\tau}}\right)\right\rangle_{\eta=0}$$

$$-\frac{1}{2}\left(\left\langle\frac{\partial\mathcal{H}}{\partial\eta_{\alpha\beta}}\right\rangle_{\eta=0}\delta_{\sigma\tau}+\left\langle\frac{\partial\mathcal{H}}{\partial\eta_{\sigma\tau}}\right\rangle_{\eta=0}\delta_{\alpha\beta}-\left\langle\frac{\partial\mathcal{H}}{\partial\eta_{\alpha\sigma}}\right\rangle_{\eta=0}\delta_{\beta\tau}\right.$$
$$\left.-\left\langle\frac{\partial\mathcal{H}}{\partial\eta_{\alpha\tau}}\right\rangle_{\eta=0}\delta_{\beta\sigma}-\left\langle\frac{\partial\mathcal{H}}{\partial\eta_{\beta\tau}}\right\rangle_{\eta=0}\delta_{\alpha\sigma}-\left\langle\frac{\partial\mathcal{H}}{\partial\eta_{\beta\sigma}}\right\rangle_{\eta=0}\delta_{\alpha\tau}\right)$$
$$+\frac{Nk_BT}{V_o}\delta_{\alpha\beta}\delta_{\sigma\tau} \tag{5.36}$$

The first term in $C_{\alpha\beta\sigma\tau}$ is referred to as the "Born term" since it corresponds to the elastic constants at zero temperature. The second term is the "fluctuation term". The third arises from the effect of the stress. And the last is sometimes called "the kinetic term" [71].

This method is especially convenient for a central force system due to Eq. (5.9). For a non-central force system, one has to derive the analogous expressions for $\mathring{S}_{\alpha\beta\sigma\tau}$ first and then find elastic constants from Eq. (5.17). The expressions for a non-central force system from this method seem to be unavailable in print.

However, this method does not work properly for microcanonical or isoenthalpic-isobaric ensembles because the size effects cannot be obtained as we did above.

The second method works on a scaled space by using scaled coordinates $\mathbf{q}_i$ and scaled momenta $\tilde{\mathbf{p}}_i$ defined by

$$\mathbf{x}_i = h\mathbf{q}_i \tag{5.37}$$
$$\tilde{\mathbf{p}}_i = \mathbf{p}_i h^{-1} \tag{5.38}$$

where $h = (\mathbf{a}, \mathbf{b}, \mathbf{c})$, $\mathbf{a}$, $\mathbf{b}$ and $\mathbf{c}$ are the three vectors forming the MD cell. The strain tensor is defined by

$$\eta = \frac{1}{2}(h_0'^{-1}Gh_0^{-1} - I) \tag{5.39}$$

where h_0 is the reference value of h, h' the transpose of h and $G = h'h$ is called the metric tensor. I is the unit tensor. Eq. (5.39) is equivalent to Eq. (5.6) so our comments about the reference state should also be applied to this definition.

This method essentially transforms the size effects related to h into the kinetic term of the Hamiltonian so the integral limit in Eq. (5.30) is independent of the size of the system. The derivation using this method is a little complex. We give in Appendix C a detailed derivation for a central force system. However, this method

works well in the microcanonical or isoenthalpic-isobaric ensembles where the size effects cannot be factored out directly, as in the first method.

Lutsko derived the general expressions using this method for an arbitrary potential system. His expressions can be written, from Eqs. (20), (26) - (28), (33a), (33b), (35) and (37) in his paper [79]

$$\mathring{C}_{\alpha\beta\sigma\tau} = (h_0 h^{-1})_{\alpha\alpha'}(h_0 h^{-1})_{\beta\beta'}\,\mathring{C}'_{\alpha'\beta'\sigma'\tau'}\,(h_0 h^{-1})_{\sigma\sigma'}(h_0 h^{-1})_{\tau\tau'} \tag{5.40}$$

$$\begin{aligned}\mathring{C}'_{\alpha\beta\sigma\tau} &= \mathring{C}^{B}{}_{\alpha\beta\sigma\tau} - \frac{1}{k_B T}\left(\left\langle \tilde{t}^{U}_{\alpha\beta}\tilde{t}^{U}_{\sigma\tau}\right\rangle - \left\langle \tilde{t}^{U}_{\alpha\beta}\right\rangle\left\langle \tilde{t}^{U}_{\sigma\tau}\right\rangle\right) \\ &\quad + \frac{N k_B T}{V_o}(\delta_{\alpha\sigma}\delta_{\beta\tau} + \delta_{\alpha\tau}\delta_{\beta\sigma})\end{aligned} \tag{5.41}$$

$$\mathring{C}^{B}{}_{\alpha\beta\sigma\tau} = S\left(\frac{1}{V_o}\left\langle \sum_{i,j} 2x_{i\beta}x_{j\tau}\frac{\partial^2 U}{\partial x_{j\sigma}\partial x_{i\alpha}}\right\rangle + \left\langle \tilde{t}^{U}_{\alpha\sigma}\right\rangle\delta_{\beta\tau}\right) \tag{5.42}$$

$$\tilde{t}^{U}_{\alpha\beta} = -\frac{1}{V_o}\sum_{i}\left(x_{i\alpha}\frac{\partial U}{\partial x_{i\beta}} + x_{i\beta}\frac{\partial U}{\partial x_{i\alpha}}\right) \tag{5.43}$$

where we use the convention that Greek indices refer to Cartesian components while Latin indices shall refer to particle numbers. S is a symmetrizing operator defined by its action on Cartesian coordinates:

$$S(A_{\alpha\beta\sigma\tau}) = \frac{1}{4}(A_{\alpha\beta\sigma\tau} + A_{\beta\alpha\sigma\tau} + A_{\alpha\beta\tau\sigma} + A_{\beta\alpha\tau\sigma}) \tag{5.44}$$

We have to point out that there are some misprints in Lutsko's paper. First, there is a bar ($^-$) missing on the lefthand side of the first equation in his Eq. (27). Secondly, two constant factors of 2 are missing in the first two terms on the righthand side of the second equation in his Eq. (27). Without these factors, it is impossible to get his Eq. (27') in which a factor of 2 is missing in the first term of the righthand side. We can check this by using his Eq. (25). Third, the sign of his Eq. (35) i.e. the sign for the expression $\tilde{t}^{U}_{\alpha\beta}$ is wrong. We can see this from his Eq. (20).

Note that Eqs. (5.40) - (5.43) need a reference value h_0. Lutsko, as many others [74, 75, 76, 77, 78]), requires h_0 to be the value of the natural (stress-free) configuration, therefore a priori his expressions are only valid for systems under moderate stress. By definition, from Eq. (5.7), its reference value h_0 must have the value for the instantaneous stressed system. In other words $h_0 = h$ and therefore we finaly find $\mathring{C}_{\alpha\beta\sigma\tau} \equiv \mathring{C}'_{\alpha\beta\sigma\tau}$.

With $h_0 = h$, these two methods produce exactly the same results. We shall verify this for the central force system in Appendix C.

We should also note that, if $h_0 \neq h$, the expressions for the elastic constants derived from these two methods will be inconsistent since it is obvious that in the final results using the first method only V_0 appears. We can see this difference more clearly in Appendix C for the central force system. For the simplest case of isotropic stress they will differ by an additional unrequired factor $\left(\frac{V}{V_0}\right)^{4/3}$. Moreover, it is easy to show that neither $t_{\alpha\beta}$ nor $T_{\alpha\beta}$ obtained from this method has the proper isotropic limit i.e. neither of them can be identified as the hydrostatic pressure in the isotropic case since it is obvious that both of them are dependent on h_0 but the hydrostatic pressure is not. This conclusion is consistent with that obtained in the first method.

For convenience we also present here the expression for the stress

$$\mathring{S}_{\alpha\beta} = \frac{1}{V_o}\sum_i \left(x_{i\alpha}\frac{\partial U}{\partial x_{i\beta}} + x_{i\beta}\frac{\partial U}{\partial x_{i\alpha}} \right) - \frac{Nk_BT}{V_o}\delta_{\alpha\beta} \tag{5.45}$$

Note that Eq. (5.45) can be derived from kinetic theory without using the condition of homogeneous deformation [93].

5.3.2 Special Case of the Central Force System

For a central force system,

$$\mathcal{H} = \sum_i \frac{p_i^2}{2m} + \sum_{i<j} \Phi(|\,\mathbf{x}_i - \mathbf{x}_j\,|). \tag{5.46}$$

By using Eqs. (5.9) and (5.31)-(5.46), it is straightforward to derive (an alternate derivation using method 2 is given in Appendix C)

$$\mathring{S}_{\alpha\beta} = \mathring{c}_{\alpha\beta} = \frac{1}{V}\left\langle \sum_{i<j} \Delta x_\alpha(ij)\Delta x_\beta(ij)\frac{\Phi'}{r} \right\rangle - \frac{Nk_BT}{V}\delta_{\alpha\beta} \tag{5.47}$$

$$\begin{aligned} \mathring{C}_{\alpha\beta\sigma\tau} = {} & \frac{1}{V}\left\langle \sum_{i<j} \Delta x_\alpha(ij)\Delta x_\beta(ij)\Delta x_\sigma(ij)\Delta x_\tau(ij)\frac{1}{r^2}\left(\Phi'' - \frac{\Phi'}{r}\right) \right\rangle \\ & - \frac{1}{k_BTV}\left\langle \delta\left(\sum_{i<j} \Delta x_\alpha(ij)\Delta x_\beta(ij)\frac{\Phi'}{r}\right)\delta\left(\sum_{i<j} \Delta x_\sigma(ij)\Delta x_\tau(ij)\frac{\Phi'}{r}\right) \right\rangle \end{aligned}$$

$$+\frac{Nk_BT}{V}(\delta_{\alpha\sigma}\delta_{\beta\tau}+\delta_{\alpha\tau}\delta_{\beta\sigma}) \tag{5.48}$$

$$\begin{aligned}
\mathring{c}_{\alpha\beta\sigma\tau} &= \frac{1}{V}\left\langle\sum_{i<j}\Delta x_\alpha(ij)\Delta x_\beta(ij)\Delta x_\sigma(ij)\Delta x_\tau(ij)\frac{1}{r^2}\left(\Phi''-\frac{\Phi'}{r}\right)\right\rangle \\
&-\frac{1}{k_BTV}\left\langle\delta\left(\sum_{i<j}\Delta x_\alpha(ij)\Delta x_\beta(ij)\frac{\Phi'}{r}\right)\right. \\
&\left.\delta\left(\sum_{i<j}\Delta x_\sigma(ij)\Delta x_\tau(ij)\frac{\Phi'}{r}\right)\right\rangle-\frac{1}{2V}\left(2\left\langle\sum_{i<j}\Delta x_\alpha(ij)\Delta x_\beta(ij)\frac{\Phi'}{r}\right\rangle\delta_{\sigma\tau}\right. \\
&-\left\langle\sum_{i<j}\Delta x_\alpha(ij)\Delta x_\sigma(ij)\frac{\Phi'}{r}\right\rangle\delta_{\beta\tau}-\left\langle\sum_{i<j}\Delta x_\alpha(ij)\Delta x_\tau(ij)\frac{\Phi'}{r}\right\rangle\delta_{\beta\sigma} \\
&\left.-\left\langle\sum_{i<j}\Delta x_\beta(ij)\Delta x_\tau(ij)\frac{\Phi'}{r}\right\rangle\delta_{\alpha\sigma}-\left\langle\sum_{i<j}\Delta x_\beta(ij)\Delta x_\sigma(ij)\frac{\Phi'}{r}\right\rangle\delta_{\alpha\tau}\right)
\end{aligned} \tag{5.49}$$

$$+\frac{Nk_BT}{V}\delta_{\alpha\beta}\delta_{\sigma\tau}$$

where we have dropped the symbol "o" for the reference state and $\eta = 0$ on the averages for simplicity. In addition $\Delta x_\alpha(ij)$ and r were defined as

$$\Delta x_\alpha(ij) = x_\alpha(i) - x_\alpha(j), \tag{5.50}$$

$$r^2 = |\,\Delta x_\alpha(ij)\,|^2, \tag{5.51}$$

$C_{\alpha\beta\sigma\tau}$ is obtained by replacing the terms $2\Delta x_\alpha(ij)\Delta x_\beta(ij)\frac{\Phi'}{r}\delta_{\sigma\tau}$ in $\mathring{c}_{\alpha\beta\sigma\tau}$ with $\Delta x_\alpha(ij)\Delta x_\beta(ij)\frac{\Phi'}{r}\delta_{\sigma\tau}+\Delta x_\sigma(ij)\Delta x_\tau(ij)\frac{\Phi'}{r}\delta_{\alpha\beta}$.

It is interesting to note that for the central force system, the Cauchy relations [70] (in Voigt's notation),

$$\mathring{C}_{23} = \mathring{C}_{44}\,,\quad \mathring{C}_{31}=\mathring{C}_{55},\quad \mathring{C}_{12}=\mathring{C}_{66},\quad \mathring{C}_{14}=\mathring{C}_{56},\quad \mathring{C}_{25}=\mathring{C}_{64}\quad \mathring{C}_{36}=\mathring{C}_{45}\,,$$

hold at zero temperature for arbitrary stress but for $\mathring{c}_{\alpha\beta\sigma\tau}$ and $C_{\alpha\beta\sigma\tau}$ the Cauchy relations require both the conditions of zero temperature and zero stress.

For a cubic crystal under hydrostatic pressure $\mathring{S}_{\alpha\beta}= -p\delta_{\alpha\beta}$, $\mathring{C}_{\alpha\beta\sigma\tau}$ in Eq. (5.49) reduces to the form obtained by Squire, Holt and Hoover [71] and is valid even for high pressures. The relevant quantities for stability are the related $C_{\alpha\beta\sigma\tau}$. The three independent ones in the condensed notation ($C_{1111} = C_{11}$, $C_{1122} = C_{12}$, and

$C_{1212} = C_{44}$) are

$$C_{11} = \frac{1}{k_B T V}\left\{\left\langle\sum\frac{\phi'}{r}(\Delta x)^2\right\rangle^2 - \left\langle\left(\sum\frac{\phi'}{r}(\Delta x)^2\right)^2\right\rangle\right\} + \frac{1}{V}\left\langle\sum\frac{\phi''}{r^2}(\Delta x)^4\right\rangle$$
$$-\frac{1}{V}\left\langle\sum\frac{\phi'}{r^3}(\Delta x)^4\right\rangle + \frac{1}{3V}\left\langle\sum r\phi'\right\rangle + \frac{Nk_BT}{V} = \mathring{C}_{11} - p \tag{5.52}$$

$$\lambda \equiv C_{12} = \frac{1}{k_B T V}\left\{\left\langle\sum\frac{\phi'}{r}(\Delta x)^2\right\rangle\left\langle\sum\frac{\phi'}{r}(\Delta y)^2\right\rangle - \left\langle\sum\frac{\phi'}{r}(\Delta x)^2\cdot\sum\frac{\phi'}{r}(\Delta y)^2\right\rangle\right\}$$
$$+\frac{1}{V}\left\langle\sum\frac{\phi''}{r^2}(\Delta x)^2(\Delta y)^2\right\rangle - \frac{1}{V}\left\langle\sum\frac{\phi'}{r^3}(\Delta x)^2(\Delta y)^2\right\rangle - \frac{1}{3V}\left\langle\sum r\phi'\right\rangle$$
$$+\frac{Nk_BT}{V} = \mathring{C}_{12} + p \tag{5.53}$$

$$\mu \equiv C_{44} = \frac{1}{k_B T V}\left\{\left\langle\sum\frac{\phi'}{r}\Delta x\Delta y\right\rangle^2 - \left\langle\left(\sum\frac{\phi'}{r}\Delta x\Delta y\right)^2\right\rangle\right\} + \frac{1}{V}\left\langle\sum\frac{\phi''}{r^2}(\Delta x)^2(\Delta y)^2\right\rangle$$
$$-\frac{1}{V}\left\langle\sum\frac{\phi'}{r^3}(\Delta x)^2(\Delta y)^2\right\rangle + \frac{1}{3V}\left\langle\sum r\phi'\right\rangle = \mathring{C}_{44} - p. \tag{5.54}$$

The pressure p is obtained from Eq. (5.47). For a two-dimensional system, we need to change the volume to area A and the $3V$ in the pressure term into $2A$. We have used these formulae in Chapter 3.

5.4 Fluctuation Formulae for Uniform Dilation System

Uniform dilation ensembles, such as isoenthalpic-isobaric (HPN) [20, 21] and isothermal-isobaric (TPN) ensembles [16, 20, 21] are among the most widely used MD ensembles. In these ensembles, the shape of the MD cell is fixed and the variations of the MD cell lengths, l_1, l_2 and l_3 satisfy $l_1/l_{0_1} = l_2/l_{0_2} = l_3/l_{0_3}$. Traditionally, the formulae to calculate the elastic constants in these ensembles were regarded to be the same as those in the constant stress ensembles [94] i.e. should be obtained from strain-strain fluctuation methods

$$\frac{k_BT}{V_0}(\mathring{C}^T)^{-1}_{\alpha\beta\sigma\tau} = \langle\eta_{\alpha\beta}\cdot\eta_{\sigma\tau}\rangle - \langle\eta_{\alpha\beta}\rangle\langle\eta_{\sigma\tau}\rangle \tag{5.55}$$

However, as we will show, the strain-strain fluctuation method is inappropriate for these ensembles if we want to find the shear modulus since the shear strains in these

ensembles do not fluctuate. We shall derive the appropriate fluctuation formulae for these ensembles in this section.

5.4.1 Conditions for Constant Shear Strain

First of all, we prove that uniform dilation corresponds to keeping a zero shear strain. The definition of strain adopted in this section is given in Eq. (5.39).

If we consider a system with the constraint of constant angle [95], h can be written

$$\begin{aligned} h &= gL \\ h_0 &= gL_0 \end{aligned} \tag{5.56}$$

where g is a constant matrix, and L_0 and L are diagonal matrices; $L_{0_{ij}} = l_{0_i}\delta_{ij}$ and $L_{ij} = l_i\delta_{ij}$. In this case,

$$\eta = \frac{1}{2}(h_0'^{-1}Gh_0^{-1} - I) = \frac{1}{2}(g'^{-1}L_0'^{-1}L'g'gLL_0^{-1}g^{-1} - I). \tag{5.57}$$

Now, one can show that η is diagonal, if and only if, one of the following three conditions is satisfied:

1. $l_1/l_{0_1} = l_2/l_{0_2}$ and c is perpendicular to both a and b so one can write $g_{3i} = g_{i3} = \delta_{i3}$. It includes the system of either hexagonal or tetragonal symmetry.

2. g is a unit matrix, i.e. a system of either tetragonal or orthogonal symmetry.

3. $l_1/l_{0_1} = l_2/l_{0_2} = l_3/l_{0_3}$, i. e. a system of uniform dilation.

So for a system under uniform dilation η is diagonal or the off-diagonal shear strain terms are zero. The above three conditions contain all situations of interest in the constant angle simulations. But in general the constraint of constant angle does not lead to a zero shear strain, nor even a constant shear strain. This illustrates the point that one has to be very careful in specifying the ensemble to which a constrained system belongs.

From the above result, in the MD simulation, the uniform dilation system is a special case of the constant shear strain ensemble. In this ensemble the independent variables must be $t_{\alpha\alpha}$ and $\eta_{\alpha\beta}$ with $\alpha \neq \beta$ (in our case these $\eta_{\alpha\beta} = 0$. Eq. (5.55) is

obviously inappropriate for the elastic constants related to the shear strains which do not fluctuate. An interesting thing is that this is an ensemble 'between' constant t and constant h so that we can expect to get formulae partly the same as those of the constant stress ensemble and partly the same as those of the constant h ensemble. Moreover, we can introduce a pair of new ensembles, one is the constant temperature and constant shear strain ensemble and the other is the constant enthalpy and constant shear strain ensemble. We focus on the constant temperature and constant shear strain in this section. The expressions for the constant enthalpy and constant shear strain ensembles are quite similar to those of the constant T and constant shear strain ensembles but the derivations are more complex so we shall present them in Appendix D.

5.4.2 Formalism in Constant T and Constant Shear Strain Ensemble

In this ensemble, the thermodynamic potential $\mathbf{A}$ has to be written in the form of

$$\mathbf{A} = E - TS - V_0 \sum_{\alpha} t_{\alpha\alpha}\eta_{\alpha\alpha} \tag{5.58}$$

Note that $\mathbf{A}$ is neither the usual Helmholtz free energy nor the Gibbs free energy. Therefore, from the first law of thermodynamics [24, 25], we obtain

$$d\mathbf{A} = -SdT - V_0 \sum_{\alpha} \eta_{\alpha\alpha} dt_{\alpha\alpha} + V_0 \sum_{\alpha\neq\beta} t_{\alpha\beta} d\eta_{\alpha\beta} \tag{5.59}$$

from which follow:

$$\begin{aligned} t_{\alpha\beta} &= \frac{1}{V_0}\left(\frac{\partial \mathbf{A}}{\partial \eta_{\alpha\beta}}\right)_{T,t_{\alpha\alpha}} \\ \eta_{\alpha\alpha} &= -\frac{1}{V_0}\left(\frac{\partial \mathbf{A}}{\partial t_{\alpha\alpha}}\right)_{T,\eta_{\alpha\beta}} . \end{aligned} \tag{5.60}$$

The fundamental connection between thermodynamics and statistical mechanics gives

$$\mathbf{A} = -k_B T \ln \Theta. \tag{5.61}$$

with

$$\Theta = \frac{1}{C}\int e^{-(\mathcal{H} - V_0 \sum_i t_{\alpha\alpha}\epsilon_{\alpha\beta})/k_B T} d\Gamma \tag{5.62}$$

where the integral in Eq. (5.62) is over all $3N$ coordinates, $3N$ momenta and 3 independent diagonal microscopic strain components $\epsilon_{\alpha\alpha}$.

Using the fact that the reference configuration for shear strains must be the instantaneous one, it is straightforward to derive

$$\frac{k_B T}{V_0}(\mathring{C}^T)^{-1}_{\alpha\alpha\beta\beta} = \langle \eta_{\alpha\alpha} \cdot \eta_{\beta\beta} \rangle - \langle \eta_{\alpha\alpha} \rangle \langle \eta_{\beta\beta} \rangle \tag{5.63}$$

$$\begin{aligned} \mathring{C}^T{}_{\alpha\beta\sigma\tau} &= \frac{1}{V_o}\left\langle \frac{\partial^2 \mathcal{H}}{\partial \eta_{\alpha\beta}\partial \eta_{\sigma\tau}} \right\rangle_{\eta=0} - \frac{1}{k_B T V_o}\left\langle \delta\left(\frac{\partial \mathcal{H}}{\partial \eta_{\alpha\beta}}\right)\delta\left(\frac{\partial \mathcal{H}}{\partial \eta_{\sigma\tau}}\right)\right\rangle_{\eta=0} \\ &\quad + \frac{N k_B T}{V_o}(\delta_{\alpha\sigma}\delta_{\beta\tau} + \delta_{\alpha\tau}\delta_{\beta\sigma}) \quad \text{for} \quad \alpha \neq \beta, \sigma \neq \tau \end{aligned} \tag{5.64}$$

We have to say a few words about the choice of V_0 in Eqs. (5.63) and (5.64). Since V_0 appears in the thermodynamic potential **A**, it must be a macroscopic quantity i.e. an ensemble average. Furthermore, to be consistent with the results in the canonical ensemble, V_0 must be taken as the average volume in the current (stressed) state, instead of the average volume in the stress-free state.

It is interesting to note that Eq. (5.63) is the same as Eq. (5.55) and Eq. (5.64) is the same as Eq. (5.32). This is a natural result since the constant shear strain ensemble is just 'between' constant h and constant stress ensembles.

For a central force system, Eq. (5.64) will again be reduced to Eq. (5.48). We have used these results in Chapter 3.

We should also note that the remaining parts of the elastic constants (i. e. the crossover part with $\alpha = \beta$ but $\sigma \neq \tau$ or $\alpha \neq \beta$ but $\sigma = \tau$) cannot be obtained in this ensemble. It is because these quantities are related to the differential of the independent variables $t_{\alpha\alpha}$ or (and) $\eta_{\alpha\beta}$, which do not fluctuate in this ensemble. However, in a system of isotropic, cubic, hexagonal, or orthogonal symmetry, we do not need to find these crossover parts due to symmetry.

5.5 Conclusion

We have clarified the problem of the choice of the reference configuration for elastic quantities (it has to be the instantaneous one) when fluctuation formulae are used. We also point out that the choice of an absolute reference state for strains is inappropriate since it may introduce some unphysical 'stress'. It is especially important

for a system subject to a large deformation. Simple fluctuation formulae are given for the elastic constants under arbitrary stress in the canonical ensemble, as shown in Eqs. (5.41) - (5.43) but we replace $\mathring{C}'$ in Eq. (5.41) by $\dot{C}$. We also derive the correct fluctuation formulae for the constant shear strain ensembles which include the uniform dilation ensemble.

Chapter 6

Mechanical Stability Criteria for Stressed Materials

6.1 Introduction

The mechanical stability of a solid is not only one of the most central issues in elasticity but also an essential consideration in the analysis of structural responses, ranging from polymorphism, amorphization, melting, to fracture.

The first systematic analysis of lattice stability is generally attributed to Born [96], who showed that by expanding the internal energy of a crystal in a power series in the strain and by requiring the energy to be minimum, one obtains stability criteria in the form of a set of conditions on the elastic constants appropriate to the crystal. Since, from the thermodynamics theory, the internal energy is not a proper thermodynamic potential to describe a system under stress, Born's criteria are in fact valid only for an unstressed system. This fact has not been always appreciated [85, 97, 98].

Hill [84] was the first to point out that elastic constants are not the appropriate quantities to determine the stability of a stressed solid. He noted correctly that the problem lies in that, when the crystal is under load, the first-order changes in the surface tractions in an incremental deformation have to be specified, as the change in the *internal energy* are evaluated to second order. However, by requiring the internal energy to be *convex* [84], [99] - [104], he concluded that the mechanical stability is

dependent on the *choice of the coordinate system or the definition of strains or the choice of the generalized stresses.* This conclusion is obviously unphysical.

Wang et al. [89, 104] demonstrated that elastic constants cannot be used as stability criteria for a constant stressed system. They suggest the use of elastic stiffness coefficients as stability criteria for isotropic stress. For anisotropic stress, they obtain a more general form from path dependent finite displacements [104]. We establish the thermodynamic foundation of their argument and elaborate on their significance. We also show that stability conditions are dependent on the ensemble used. In particular, stability conditions are stronger in the constant pressure ensemble than in the constant volume ensemble, i.e. a state can be stable in the constant volume ensemble but unstable in the constant pressure ensemble. In systems with anisotropic stress, several ensembles can also be envisaged. We provide an exact solution to support our results. We also derive some simple expressions for elastic moduli in some 2D perfect systems at zero temperature and hydrostatic pressure.

The main contents of this Chapter are also found in reference [82].

6.2 Thermodynamic Potentials and Stability Conditions

Thermodynamics describes the behaviour of systems with many degrees of freedom after they have reached a state of thermal equilibrium – a state in which all past history is forgotten and all macroscopic quantities cease to change. The amazing feature of such a system is that, even though they contain many degrees of freedom ($\sim 10^{23}$) in chaotic motion, their thermodynamic state can be specified completely in terms of a few parameters – called *state variables.* In general, there are many state variables which can be used to specify the equilibrium state of a system, but only a few are independent. The relationship among state variables is called equation of state. In practice, one chooses state variables which are accessible to experiment and obtain relations between them. One should also note that an equilibrium state implies that it must be stable.

The thermodynamic potentials, as functions of independent state variables, can be used to describe the behaviour and stability of thermodynamic systems. There are a number of different thermodynamic potentials. Which thermodynamic potential to use depends on the type of constraint imposed on the system, or equivalently,

depends on the choice of the independent state variables. The five most commonly used thermodynamic potentials are the internal energy (E), the enthalpy (H), the Helmholtz free energy (F), the Gibbs free energy (G) and the grand potential. In general, one can use Legendre transforms [105] to construct new thermodynamic potentials.

The stability of any system is essentially determined by the second law of thermodynamics. For a system with a fixed number of particles undergoing an arbitrary but small transformation from state A to state B, the second law says [22, 23, 24]

$$\Delta \mathcal{W} \geq \Delta E - T\Delta S = \Delta F \tag{6.1}$$

where $-\Delta \mathcal{W}$ is the work done by the system during the transformation. The equality sign applies for reversible transformations. If state A is an equilibrium configuration, stability requires that in moving to a nearby state $\Delta F - \Delta \mathcal{W} > 0$

For a mechanically isolated i.e. constant volume system, or unstressed system, $\Delta \mathcal{W} = 0$ and Eq. (6.1) leads to the requirement that W (E or F) be minimum in the microcanonical or canonical ensembles for stability.

In the same way, for a stressed system, Eq. (6.1) leads to the requirement that $H = W - \mathcal{W}$ be minimum in constant stress ensembles for stability.

For a system under constant hydrostatic pressure, $-\mathcal{W} = pV$ so that the stability criteria can be derived by requiring traditional Gibbs' free energy or enthalpy be minimum. It is equivalent to finding the minimum of the Legendre transform [105] of W, i.e. $H = W + pV$ and use p instead of V as *independent state variables.* However, for a system under anisotropic loading, the traditional Gibbs' free energy or enthalpy requires a more careful definition. We will discuss this point in detail later.

To use thermodynamic potentials as stability criteria is however inconvenient since they are not easy to measure in experiments or computer simulations. The quantities easiest to measure, are the response functions such as specific heat, compressibility, magnetic susceptibility, thermal expansivity, and elastic stiffness coefficients. Generally, we change one parameter or state variable in the system and see how another parameter responds to that change, under highly controlled conditions. The quantity that measures the way in which the system responds is called a response function. Therefore, it is more convenient to use response functions as

stability criteria.

It is also valuable to remember that *the minimum of a function is independent of the choice of the coordinate system.*

6.3 Stability Criteria for the Unstressed System

One of the most important applications of elastic constants in theoretical models is as stability criteria for unstressed systems. For W in Eq. (5.28) to be a minimum in the absence of stress $\mathring{C}_{\alpha\beta\sigma\tau}$ must be a positive definite tensor [70], i.e. all of its eigenvalues must be positive.

Explicitly the stability conditions for a three dimensional (3D) cubic solid are [89]:

$$\mathring{C}_{11} + 2\,\mathring{C}_{12} > 0, \qquad \mathring{C}_{44} > 0, \qquad \mathring{C}_{11} - \mathring{C}_{12} > 0. \tag{6.2}$$

For an isotropic solid, $\mathring{C}_{11} - \mathring{C}_{12} = 2\,\mathring{C}_{44}$, and conditions (6.2) reduce to

$$3B = 2\,\mathring{C}_{44} + 3\,\mathring{C}_{12} > 0, \qquad \mathring{C}_{44} > 0, \tag{6.3}$$

where B is the bulk modulus and C_{44} the shear modulus. Similar conditions are obtained for two dimensional isotropic solids (2D) to which belongs the triangular lattice:

$$B = \mathring{C}_{44} + \mathring{C}_{12} > 0, \qquad \mathring{C}_{44} > 0. \tag{6.4}$$

6.4 Stability Criteria for a Stressed System

6.4.1 System with Isotropic Initial Stress and Constant Volume

For a system with isotropic reference stress [25]

$$\mathring{S}_{\alpha\beta} = -p\delta_{\alpha\beta} \tag{6.5}$$

where p is the isotropic stress, *positive for compression.*

To study the problem of stability in both microcanonical and canonical ensembles, we need to check if W is minimum. In those ensembles the minimum of W must

be achieved at constant volume so shape changes are allowed without volume fluctuations. The instantaneous volume V can be written as $V = V_o \det(\delta_{\alpha\beta} + u_{\alpha\beta})$[25] where V_0 is the volume of the stressed system before deformation. This leads to (see Appendix B)

$$\frac{V - V_o}{V_o} = \eta_{\alpha\alpha} + \frac{1}{2}(\delta_{\alpha\beta}\delta_{\sigma\tau} - \delta_{\alpha\sigma}\delta_{\beta\tau} - \delta_{\alpha\tau}\delta_{\beta\sigma})\eta_{\alpha\beta}\eta_{\sigma\tau} \tag{6.6}$$

to second order in the strain. To fix the volume requires $V - V_o = 0$ or

$$\eta_{\alpha\alpha} = -\frac{1}{2}(\delta_{\alpha\beta}\delta_{\sigma\tau} - \delta_{\alpha\sigma}\delta_{\beta\tau} - \delta_{\alpha\tau}\delta_{\beta\sigma})\eta_{\alpha\beta}\eta_{\sigma\tau}. \tag{6.7}$$

Substituting Eq. (6.7) into Eq. (5.11) leads to

$$\frac{W - W_o}{V_o} = \frac{1}{2}C_{\alpha\beta\sigma\tau}\eta_{\alpha\beta}\eta_{\sigma\tau}, \tag{6.8}$$

where

$$C_{\alpha\beta\sigma\tau} \equiv \mathring{C}_{\alpha\beta\sigma\tau} + p(\delta_{\alpha\beta}\delta_{\sigma\tau} - \delta_{\alpha\sigma}\delta_{\beta\tau} - \delta_{\alpha\tau}\delta_{\beta\sigma}). \tag{6.9}$$

Eq. (6.8) has to be a positive definite quadratic form, with the constraints given by Eq. (6.7).

Note that the $C_{\alpha\beta\sigma\tau}$ have the same symmetry as the elastic constants so they can be condensed using the Voigt notation. Combining Eqs. (6.7) and (6.8), we find

$$\frac{W - W_o}{V_o} = \frac{1}{2}f_{\alpha\beta}S_\alpha S_\beta, \qquad \alpha, \beta = 2, 6 \tag{6.10}$$

where

$$\begin{aligned}
f_{22} &= C_{11} + C_{22} - 2C_{12}, \\
f_{23} &= f_{32} = C_{11} + C_{23} - C_{12} - C_{13}, \\
f_{24} &= f_{42} = C_{24} - C_{14}, \quad f_{25} = f_{52} = C_{25} - C_{15}, \\
f_{26} &= f_{62} = C_{26} - C_{16}, \quad f_{33} = C_{11} + C_{33} - 2C_{13}, \\
f_{34} &= f_{43} = C_{34} - C_{14}, \quad f_{35} = f_{53} = C_{35} - C_{15}, \\
f_{36} &= f_{63} = C_{36} - C_{16}, \quad f_{44} = C_{44}, \\
f_{45} &= f_{54} = C_{45}, \quad f_{46} = f_{64} = C_{46}, \\
f_{55} &= C_{55}, \quad f_{56} = f_{65} = C_{56}, \quad f_{66} = C_{66},
\end{aligned} \tag{6.11}$$

and

$$\begin{aligned} S_2 &= \eta_{22}, \quad S_3 = \eta_{33}, \quad S_4 = 2\eta_{23}, \\ S_5 &= 2\eta_{31}, \quad S_6 = 2\eta_{12}, \end{aligned} \tag{6.12}$$

where the S_α are a set of independent strains. Stability requires that Eq. (6.10) be a positive definite quadratic form so the stability conditions reduce to an eigenvalue problem for the $f_{\alpha\beta}$.

Explicitly the stability conditions for a three dimensional cubic solid are:

$$C_{44} > 0 \qquad \text{and} \qquad C_{11} - C_{12} > 0 \tag{6.13}$$

For an isotropic solid, either in two or three dimensions, it reduces to

$$C_{44} > 0 \tag{6.14}$$

6.4.2 System with Isotropic Initial Stress and Allowing Volume Fluctuations

Keeping the volume constant is, however, too restrictive. In general, instability is always accompanied by volume fluctuations. To allow for volume fluctuations we study the minimum of the Legendre transform of W, i.e., $H = W + pV$ which is the enthalpy or the Gibbs' free energy and fix the pressure instead of the volume.

This problem is quite similar to the stability problem in the study of membranes using the curvature model [106, 107, 108], in which the Legendre transform requires two parameters, one is the surface tensile stress and the other the pressure. M. A. Peterson [108] clarified the distinction between the conditions of fixed volume and fixed pressure.

By using Eqs. (5.11), (6.5) and (6.6), we obtain

$$\frac{H - H_o}{V_o} = \frac{1}{2} C_{\alpha\beta\sigma\tau} \eta_{\alpha\beta} \eta_{\sigma\tau} \tag{6.15}$$

and hence the same quadratic form as in Eq. (6.8) but now without the volume constraints and the stability conditions reduce to an eigenvalue problem for the $C_{\alpha\beta\sigma\tau}$ tensor instead of $\mathring{C}_{\alpha\beta\sigma\tau}$.

From Eqs. (5.22), (6.5), and (6.9), it is easy to show that in this case, $C_{\alpha\beta\sigma\tau}$ is identical to $\mathring{c}_{\alpha\beta\sigma\tau}$, the elastic stiffness coefficient. Since the stress-strain relations are still linear in the strains, with Eq. (5.17) simplifying to

$$T_{\alpha\beta} = -p\delta_{\alpha\beta} + \mathring{c}_{\alpha\beta\sigma\tau}\, u_{\sigma\tau} = -p\delta_{\alpha\beta} + \mathring{c}_{\alpha\beta\sigma\tau}\, \eta_{\sigma\tau}, \tag{6.16}$$

$\mathring{c}_{\alpha\beta\sigma\tau}$ and hence also $C_{\alpha\beta\sigma\tau}$ and $\mathring{C}_{\alpha\beta\sigma\tau}$ have the same symmetry relations as in the unstressed state. Moreover, we can expect that $C_{\alpha\beta\sigma\tau}$ will yield the same stability conditions as those obtained from the long acoustic lattice wave theory as the latter contains the effects of stress. This point will be illustrated in the next section with an example of a central force system. We can also confirm this, by noticing, that the equations of motion in the isotropic state, can be reduced to [81]

$$\mathring{\rho}\, \frac{\partial^2 u_\alpha(\mathring{\mathbf{x}})}{\partial t^2} = \mathring{c}_{\alpha\beta\sigma\tau}\, \frac{\partial^2 u_\sigma(\mathring{\mathbf{x}})}{\partial\, \mathring{x}_\beta\, \partial\, \mathring{x}_\tau} \tag{6.17}$$

where $\mathring{\rho}$ is the reference density, and $\mathring{c}_{\alpha\beta\sigma\tau}$ plays the same role as the elastic constants in the stress-free state.

The stability conditions follow straightforwardly from those of the unstressed system, $C_{\alpha\beta\sigma\tau}$, or $\mathring{c}_{\alpha\beta\sigma\tau}$ replacing $\mathring{C}_{\alpha\beta\sigma\tau}$. Explicitly, for a cubic system, the relevant elastic constants are:

$$\begin{aligned} C_{11} &= \mathring{C}_{11} - p, \\ C_{12} &= \mathring{C}_{12} + p = \lambda, \\ C_{44} &= \mathring{C}_{44} - p = \mu. \end{aligned} \tag{6.18}$$

And the stability conditions are obtained by substituting in Eqs. (6.2), (6.3), and (6.4), the $\mathring{C}$'s with the C's. This is what has been suggested by J. Wang et al. [89].

It is interesting to note that Eq. (6.8) or Eq. (6.10) will be a positive definite quadratic form provided Eq. (6.15) is but the converse is not necessarily true. Therefore, we can conclude that the condition of stability for the constant pressure ensemble is stronger than in the constant volume ensemble. For instance, for an isotropic solid, in the constant pressure ensemble, $B > 0$ is necessary for stability but it is not required with constant volume. As a consequence, a state stable in the constant volume ensemble may be unstable in the constant pressure ensemble. This

may account for the fact that in a first order phase transition two phase coexistence is allowed in the constant volume ensemble but prohibited in the constant pressure ensemble [7, 26, 27]. The reason is simple, the first order phase transition must be accompanied by a volume change which is prohibited in a constant volume ensemble.

6.4.3 System with Anisotropic Initial Stress

For a system under anisotropic stress, it is even more crucial to consider volume fluctuations since a system without size and shape fluctuations is always in mechanical equilibrium, no stability criteria is required. In general the shape fluctuations require mechanical work so that stability is not achieved by requiring W to be minimum.

System with Constant $t_{\alpha\beta}$

At first thought, one could try using the traditional Gibbs' free energy $G = F - V_o t_{\alpha\beta}\eta_{\alpha\beta}$ or enthalpy $= E - V_o t_{\alpha\beta}\eta_{\alpha\beta}$ [25, 83, 88] to determine the stability of an anisotropic stressed system as we did in the last two sections. But since the quantity conjugate to the strain $\eta_{\alpha\beta}$ is the thermodynamic stress tensor $t_{\alpha\beta}$, the minimum must be achieved under the condition of *constant* $t_{\alpha\beta}$. In this case it follows from Eqs. (5.11) and (5.17) that stability requires that the elastic constant tensor $\mathring{C}_{\alpha\beta\sigma\tau}$ be a positive definite tensor. This constant $t_{\alpha\beta}$ ensemble can be realized in computer simulations [74, 75]. However, as seen from Eq. (5.24) the applied stress $T_{\alpha\beta}$ fluctuates in this ensemble. And a diagonal $t_{\alpha\beta}$ does not lead to a diagonal, or isotropic, $T_{\alpha\beta}$ and this is why the corresponding stability criteria are different from those obtained in the last two sections. Therefore, this constant $t_{\alpha\beta}$ ensemble is not equivalent to the ensemble of constant applied stress and so one has to be careful in comparing the results obtained from this ensemble with experiments or theory. We can also see this point by noting that under constant loading, $\Delta\mathcal{W} \neq V_o t_{\alpha\beta}\eta_{\alpha\beta}$. Instead, for a quasi-static process [25, 83, 88, 104]

$$\Delta\mathcal{W} = V_o \int \det(J) J^{-1}_{\alpha\sigma} J^{-1}_{\beta\tau} T_{\sigma\tau} d\epsilon_{\alpha\beta} = V_o T_{\alpha\beta}\xi_{\alpha\beta} \tag{6.19}$$

where

$$\xi_{\alpha\beta} = \int \det(J) J^{-1}_{\sigma\alpha} J^{-1}_{\tau\beta} d\epsilon_{\sigma\tau} \tag{6.20}$$

are variables conjugate to $T_{\alpha\beta}$ and the $\epsilon_{\alpha\beta}$ vary along some path from $\epsilon_{\alpha\beta} = 0$ to $\epsilon_{\alpha\beta} = \eta_{\alpha\beta}$. So that the minimum of the traditional Gibbs' free energy or enthalpy are in general different from that of $H = W - \mathcal{W}$.

System with Constant Applied Stress

From the above discussion, for the constant loading ensemble we need a thermodynamic potential using the $T_{\alpha\beta}$ instead of the $t_{\alpha\beta}$ as independent state variables and stability criteria can then be derived by requiring this thermodynamic potential to be minimum. Such a thermodynamic potential can be obtained by a Legendre transform [105]

$$H = W - V_o T_{\alpha\beta}\xi_{\alpha\beta} \tag{6.21}$$

To find the stability criteria, we need to consider a small deformation from some reference configuration. To first order in $u_{\alpha\beta}$, we have

$$\begin{aligned} \det(J)J^{-1}_{\sigma\alpha}J^{-1}_{\tau\beta} &= (1+u_{ii})(\delta_{\sigma\alpha} - u_{\sigma\alpha})(\delta_{\tau\beta} - u_{\tau\beta}) \\ &= (1+u_{ii})(\delta_{\sigma\alpha}\delta_{\tau\beta} - u_{\sigma\alpha}\delta_{\tau\beta} - u_{\tau\beta}\delta_{\sigma\alpha}) \\ &= \delta_{\sigma\alpha}\delta_{\tau\beta} + \delta_{\sigma\alpha}\delta_{\tau\beta}u_{ii} - u_{\sigma\alpha}\delta_{\tau\beta} - u_{\tau\beta}\delta_{\sigma\alpha} \end{aligned} \tag{6.22}$$

Neglecting the rotational terms $\omega_{\alpha\beta}$, it becomes

$$\det(J)J^{-1}_{\sigma\alpha}J^{-1}_{\tau\beta} = \delta_{\sigma\alpha}\delta_{\tau\beta} + \eta_{ii}\delta_{\sigma\alpha}\delta_{\tau\beta} - \eta_{\sigma\alpha}\delta_{\tau\beta} - \eta_{\tau\beta}\delta_{\sigma\alpha} \tag{6.23}$$

Therefore, to second order in $\eta_{\alpha\beta}$, from Eqs. (6.20) and (6.23)

$$\begin{aligned} \xi_{\alpha\beta} &= \int(\delta_{\sigma\alpha}\delta_{\tau\beta} + \epsilon_{ii}\delta_{\sigma\alpha}\delta_{\tau\beta} - \epsilon_{\sigma\alpha}\delta_{\tau\beta} - \epsilon_{\tau\beta}\delta_{\sigma\alpha})d\epsilon_{\sigma\tau} \\ &= \eta_{\alpha\beta} + \int(\epsilon_{\sigma\sigma}d\epsilon_{\alpha\beta} - \epsilon_{\sigma\alpha}d\epsilon_{\sigma\beta} - \epsilon_{\sigma\beta}d\eta_{\sigma\alpha}) \\ &= \eta_{\alpha\beta} + \frac{1}{2}\int(\epsilon_{\sigma\sigma}d\epsilon_{\alpha\beta} + \epsilon_{\alpha\beta}d\epsilon_{\sigma\sigma} + \epsilon_{\sigma\sigma}d\epsilon_{\alpha\beta} - \epsilon_{\alpha\beta}d\epsilon_{\sigma\sigma} - 2d(\epsilon_{\alpha\sigma}\epsilon_{\beta\sigma})) \\ &= \eta_{\alpha\beta} + \frac{1}{2}\eta_{\sigma\sigma}\eta_{\alpha\beta} - \eta_{\alpha\sigma}\eta_{\beta\sigma} + \frac{1}{2}\int(\epsilon_{\sigma\sigma}d\epsilon_{\alpha\beta} - \epsilon_{\alpha\beta}d\epsilon_{\sigma\sigma}) \end{aligned} \tag{6.24}$$

and

$$\begin{aligned} T_{\alpha\beta}\xi_{\alpha\beta} &= T_{\alpha\beta}(\eta_{\alpha\beta} + \frac{1}{2}\eta_{\sigma\sigma}\eta_{\alpha\beta} - \eta_{\alpha\sigma}\eta_{\beta\sigma}) + \frac{1}{2}T_{\alpha\beta}\int(\epsilon_{\sigma\sigma}d\epsilon_{\alpha\beta} - \epsilon_{\alpha\beta}d\epsilon_{\sigma\sigma}) \\ &= T_{\alpha\beta}(\eta_{\alpha\beta} + \frac{1}{2}\eta_{\sigma\sigma}\eta_{\alpha\beta} - \eta_{\alpha\sigma}\eta_{\beta\sigma}) + \frac{1}{2}\mathcal{B}_{\alpha\beta\sigma\tau}\int\epsilon_{\sigma\tau}d\epsilon_{\alpha\beta} \end{aligned} \tag{6.25}$$

where

$$\mathcal{B}_{\alpha\beta\sigma\tau} = T_{\alpha\beta}\delta_{\sigma\tau} - T_{\sigma\tau}\delta_{\alpha\beta} = -\mathcal{B}_{\sigma\tau\alpha\beta} \tag{6.26}$$

The last term in Eqs. (6.24) - (6.25), $T_{\alpha\beta}\xi'_{\alpha\beta}$, with

$$\xi'_{\alpha\beta} \equiv \int \epsilon_{\sigma\sigma} d\epsilon_{\alpha\beta} - \epsilon_{\alpha\beta} d\epsilon_{\sigma\sigma}, \tag{6.27}$$

is path dependent and of the same order of magnitude as $\eta_{\alpha\beta}\eta_{\sigma\tau}$. The deformation-path-dependent nature of $\xi'_{\alpha\beta}$ was first pointed out by Wang et al. [104]. For instance, along a path defined by

$$\epsilon_{\alpha\beta} = \begin{cases} \eta_{\alpha\beta}(1 - \cos\frac{\pi}{2}x) & \alpha \neq \beta \\ \eta_{\alpha\beta}\sin\frac{\pi}{2}x & \alpha = \beta \end{cases} \tag{6.28}$$

$\xi'_{\alpha\beta} = (\frac{\pi}{2} - 1)(1 - \delta_{\alpha\beta})\eta_{\alpha\beta}\eta_{\sigma\sigma}$ (no summation for α and β). Eq. (6.27) can be rewritten as

$$\xi'_{\alpha\beta} = \int (\epsilon_{\sigma\sigma})^2 d\left(\frac{\epsilon_{\alpha\beta}}{\epsilon_{\sigma\sigma}}\right). \tag{6.29}$$

Along a straight line it is trivial to see that $\xi'_{\alpha\beta} = 0$. The same applies to volume preserving paths ($\epsilon_{\sigma\sigma} = 0$). And if one considers $T_{\alpha\beta}\xi'_{\alpha\beta}$, it will be zero if $T_{\alpha\beta}\epsilon_{\alpha\beta}$ is proportional to the volume change $\epsilon_{\alpha\alpha}$. This is similar to the isotropic case, where the work is always proportional to the volume change.

The important thing for our purpose is that paths can be paired. To every path l

$$\begin{aligned} \epsilon_{\alpha\beta} &= f_{\alpha\beta}(x), \qquad f_{\alpha\beta}(0) = 0, \quad f_{\alpha\beta}(1) = \eta_{\alpha\beta} \\ \xi'_{\alpha\beta}(l) &= \int_0^1 (f_{\sigma\sigma}(x) f'_{\alpha\beta}(x) - f_{\alpha\beta}(x) f'_{\sigma\sigma}(x)) dx \\ f'_{\alpha\beta}(x) &= \frac{df_{\alpha\beta}(x)}{dx} \end{aligned} \tag{6.30}$$

there exists another path l'

$$\epsilon_{\alpha\beta} = \eta_{\alpha\beta} - f_{\alpha\beta}(1 - x) \tag{6.31}$$

such that $\xi'_{\alpha\beta}(l) + \xi'_{\alpha\beta}(l') = 0$. From which it follows that

$$< \xi'_{\alpha\beta} >= 0 \tag{6.32}$$

This allows us to define a thermodynamic potential for each point in spite of the path dependence of the work. We define the change in H, in going from one point to another, as an average over all possible paths. The path dependent term is eliminated because $< \xi'_{\alpha\beta} >= 0$. This is also what is obtained by following a straight line between two points. Choosing the average is more convenient than looking for the minimum. As discussed in Appendix E, extrema of $T_{\alpha\beta}\xi'_{\alpha\beta}$ do not usually exist for general deformations in the anisotropic case.

In discussing stability the $T_{\alpha\beta}\xi'_{\alpha\beta}$ term is not required. Stability criteria are always with respect to infinitesimal displacements from some equilibrium configuration; displacements, in such limits, are linear, hence the $T_{\alpha\beta}\xi'_{\alpha\beta}$ term is zero.

Therefore, up to second order in $\eta_{\alpha\beta}$, $H = W - V_o T_{\alpha\beta}\xi_{\alpha\beta}$ can be written as

$$H = W - V_o T_{\alpha\beta}\xi_{\alpha\beta} = W - V_o T_{\alpha\beta}\eta_{\alpha\beta} - \frac{1}{2}V_o \mathcal{A}_{\alpha\beta\sigma\tau}\eta_{\alpha\beta}\eta_{\sigma\tau} \tag{6.33}$$

with

$$\xi_{\alpha\beta} = \eta_{\alpha\beta} - \eta_{\alpha\sigma}\eta_{\beta\sigma} + \frac{1}{2}\eta_{\alpha\beta}\eta_{\sigma\sigma} \tag{6.34}$$

and

$$2\mathcal{A}_{\alpha\beta\sigma\tau} = T_{\alpha\beta}\delta_{\sigma\tau} + T_{\sigma\tau}\delta_{\alpha\beta} - T_{\tau\beta}\delta_{\alpha\sigma} - T_{\tau\alpha}\delta_{\beta\sigma} - T_{\alpha\sigma}\delta_{\beta\tau} - T_{\beta\sigma}\delta_{\alpha\tau} \tag{6.35}$$

$\mathcal{A}_{\alpha\beta\sigma\tau}$ has the same symmetry as the elastic constants.

Between any two points in configuration space, the difference in this thermodynamic potential H is the change in the free energy W minus the average work between the two points, which is the same as the work along a direct straight line segment joining the two points. One has to be careful not to infer from this that, when connecting two points by a trajectory made of small straight line segments that the work done by the system, is the same as if the points had been connected by a single direct straight line segment. The path dependence of the work requires always to consider the work as being an average over all trajectories connecting the two points.

Requiring that H_o be minimum leads, from Eqs. (5.11) and (5.17), to

$$T_{\alpha\beta} = \mathring{S}_{\alpha\beta} \tag{6.36}$$

and the corresponding energy variation close to the minimum is of the form

$$\frac{H - H_o}{V_o} = \frac{1}{2} C_{\alpha\beta\sigma\tau} \eta_{\alpha\beta} \eta_{\sigma\tau} \tag{6.37}$$

where $\mathring{S}_{\alpha\beta}$ is fixed and not usually diagonal, and

$$\begin{aligned} C_{\alpha\beta\sigma\tau} &\equiv \mathring{C}_{\alpha\beta\sigma\tau} - \mathcal{A}_{\alpha\beta\sigma\tau} \equiv \frac{1}{2}(\mathring{c}_{\alpha\beta\sigma\tau} + \mathring{c}_{\sigma\tau\alpha\beta}) \\ &= \mathring{C}_{\alpha\beta\sigma\tau} - \frac{1}{2}(\mathring{S}_{\alpha\beta}\,\delta_{\sigma\tau} + \mathring{S}_{\sigma\tau}\,\delta_{\alpha\beta} - \mathring{S}_{\alpha\sigma}\,\delta_{\beta\tau} \\ &\quad - \mathring{S}_{\alpha\tau}\,\delta_{\beta\sigma} - \mathring{S}_{\beta\tau}\,\delta_{\alpha\sigma} - \mathring{S}_{\beta\sigma}\,\delta_{\alpha\tau}) \end{aligned} \tag{6.38}$$

is the positive definite quantity for stability. Note that the only difference between $\mathring{c}_{\alpha\beta\sigma\tau}$ and $C_{\alpha\beta\sigma\tau}$ is that the terms $2\,\mathring{S}_{\alpha\beta}\,\delta_{\sigma\tau}$ in $\mathring{c}_{\alpha\beta\sigma\tau}$ are replaced by $\mathring{S}_{\alpha\beta}\,\delta_{\sigma\tau} + \mathring{S}_{\sigma\tau}\,\delta_{\alpha\beta}$.

It is easy to check that $C_{\alpha\beta\sigma\tau}$ has the proper isotropic limit. Condensed expressions in terms of the Voigt notation are still possible, but the number of independent elements, determined not only by the symmetry of the crystal but also by the symmetry of the applied stress $T_{\alpha\beta}$, will likely be increased. In general also, the reference state will have a lower symmetry and more elastic constants $\mathring{C}_{\alpha\beta\sigma\tau}$ will be required.

It should be noted that for a stressed system $C_{\alpha\beta\sigma\tau}$, $\mathring{c}_{\alpha\beta\sigma\tau}$ and $\mathring{C}_{\alpha\beta\sigma\tau}$ are dependent on the stress. They are no longer intrinsic properties of the system and hence cannot be used as probes of the interatomic forces.

This result is the same as the one recently obtained by Wang et al. [104] for an isothermal system. They considered the $\Delta\mathcal{G} = \Delta F - \Delta\mathcal{W}$ and required $\Delta\mathcal{G} > 0$ for stablility, a condition identical to minimizing $\mathcal{G} = F - \mathcal{W}$. We strengthen their argument by considering in detail the effect of the deformation path dependent term $\xi'_{\alpha\beta}$. As pointed out above, without considering it, the positive definiteness of $C_{\alpha\beta\sigma\tau}$ does not automatically lead to $\Delta\mathcal{G} > 0$ or $\mathcal{G}$ minimum.

6.5 Exact Results for Some Two-dimensional Perfect Systems at Zero Temperature

For a 2D simple Bravais lattice at zero temperature and hydrostatic pressure P, using periodic boundary conditions, the expressions for λ, μ and P for a central

force system can be further simplified to

$$\begin{aligned} \lambda &= \lambda_0 + p \qquad \text{and} \qquad \mu = \lambda_0 - p \\ \lambda_0 &= \frac{1}{2a}\sum_{r_i \neq 0}\left(\frac{\phi''(r_i)}{r_i^2} - \frac{\phi'(r_i)}{r_i^3}\right) x_i^2 y_i^2 \\ p &= -\frac{1}{4a}\sum_{r_i \neq 0} r_i \phi'(r_i) \end{aligned} \tag{6.39}$$

where a is the area of the unit cell; the origin of the coordinate system is a lattice point and the summation is over the coordinate of all lattice points except the origin. $\lambda_0 = \mathring{C}_{44} = \mathring{C}_{12}$ is the elastic constant.

From the above equations, we see that $(\lambda + \mu) - 2\mu = 2p$. Therefore, if $p > 0$ (compression) $\lambda + \mu > 2\mu$ so that the shear instability will occur prior to the spinodal instability (characterized by the bulk modulus $= \lambda + \mu = 0$). In contrast, if $p < 0$ (tensile) then $\lambda + \mu < 2\mu$ and the spinodal instability will occur prior to the shear instability.

As we discussed in Chapter 2, monolayers formed of particles interacting with central forces will tend to form triangular lattices. Therefore, here we consider triangular lattices only. It is easy to derive the analogous results for other kinds of lattices.

6.5.1 PLFP System

The PLFP energy between two atoms at a distance r from each other is given by Eq. (2.1).

Therefore, for a perfect system of lattice constant $d < 1.15d_0$, $\phi' = d - d_0$, $\phi'' = 1$, $a = \frac{\sqrt{3}}{2}d^2$ and note that for $d \geq 0.75d_0$ we only need to consider 6 nearest neighbours

$$\begin{aligned} \lambda &= \frac{1}{2a}\sum_{(n.n.)}\left(\frac{1}{d^2} - \frac{d-d_0}{d^3}\right)x_i^2 y_i^2 - \frac{1}{4a}\sum_{(n.n.)} d(d-d_0) \\ &= \frac{1}{2a}\left(\frac{1}{d^2} - \frac{d-d_0}{d^3}\right)\sum_{(n.n.)} x_i^2 y_i^2 - \frac{6}{4a}d(d-d_0) \\ &= \frac{d_0}{2ad^3}\cdot\frac{3}{4}d^4 - \frac{6}{4a}d(d-d_0) = \frac{\sqrt{3}}{4}(5\rho^{1/2} - 4) \end{aligned} \tag{6.40}$$

where $\rho = (d_0/d)^2$ is the density relative to the stress free state and we used

$$\sum_{(n.n.)} x_i^2 y_i^2 = \frac{3}{4} d^4. \tag{6.41}$$

In the same way

$$\mu = \frac{1}{2a} \sum_{(n.n.)} \left(\frac{1}{d^2} - \frac{d - d_0}{d^3}\right) x_i^2 y_i^2 + \frac{1}{4a} \sum_{(n.n.)} d(d - d_0) = \frac{\sqrt{3}}{4}(4 - 3\rho^{1/2}), \tag{6.42}$$

and

$$p = \sqrt{3}(\rho^{1/2} - 1). \tag{6.43}$$

In this way, we finally obtain

$$\lambda = \begin{cases} \frac{\sqrt{3}}{4}(5\rho^{1/2} - 4)\kappa & 0.75d_0 \le d \le 1.15d_0 \\ \frac{\sqrt{3}}{4}(4 - 6.5\rho^{1/2})\kappa & 1.15d_0 < d \le 1.3d_0 \\ 0 & d > 1.3d_0 \end{cases} \tag{6.44}$$

$$\mu = \begin{cases} \frac{\sqrt{3}}{4}(4 - 3\rho^{1/2})\kappa & 0.75d_0 \le d \le 1.15d_0 \\ \frac{\sqrt{3}}{4}(3.9\rho^{1/2} - 4)\kappa & 1.15d_0 < d \le 1.3d_0 \\ 0 & d > 1.3d_0 \end{cases} \tag{6.45}$$

$$p = \begin{cases} \sqrt{3}(\rho^{1/2} - 1)\kappa & 0.75d_0 \le d \le 1.15d_0 \\ \sqrt{3}(1 - 1.3\rho^{1/2})\kappa & 1.15d_0 < d \le 1.3d_0 \\ 0 & d > 1.3d_0 \end{cases} \tag{6.46}$$

The results for $0.75d_0 \le d \le 1.15d_0$ agree with those obtained from long-wave expansion [10] and give the correct shear instability at $\rho = \frac{16}{9}$ where the lattice transform from triangular to square symmetry. In contrast,

$$\dot{C}_{44} = \dot{C}_{12} = \frac{\sqrt{3}}{4}\rho^{1/2}\kappa \tag{6.47}$$

does not show any instability. From Eqs. (6.44) - (6.45) we can also find a spinodal instability at $d = 1.15d_0$. This spinodal instability coincides with the rupture of system as demonstrated in our computer simulations (see Chapter 7).

6.5.2 LJP System

Choose the unit of length as $d_0 = 2^{\frac{1}{6}}\sigma$, $\epsilon = 0.0225\kappa d_0^2$, the Lennard-Jones potential (Eq. (2.7)) becomes

$$\phi_{LJP}(r) = \epsilon\left(\frac{1}{r^{12}} - \frac{2}{r^6}\right) \tag{6.48}$$

so

$$\begin{aligned} \frac{\phi''_{LJP}}{r^2} - \frac{\phi'_{LJP}}{r^3} &= 24\epsilon\left(\frac{7}{r^{16}} - \frac{4}{r^{10}}\right) \\ r\phi'_{LJP} &= 12\epsilon\left(\frac{1}{r^6} - \frac{1}{r^{12}}\right) \end{aligned} \tag{6.49}$$

From Fig. 6.1 it is easy to construct r_i and $\sum x_i^2 y_i^2$, up to the 11th neighbours, as shown in Table 6.1. Z in Table 6.1 is the number of neighbours.

Table 6.1: r_i and $\sum x_i^2 y_i^2$ for the triangular lattice up to the 11th neighbours.

Neighbour	1st	2nd	3rd	4th	5th	6th	7th	8th	9th	10th	11th
Z	6	6	6	12	6	6	12	6	12	12	6
r_i/d	1	$\sqrt{3}$	2	$\sqrt{7}$	3	$\sqrt{12}$	$\sqrt{13}$	4	$\sqrt{19}$	$\sqrt{21}$	5
$\sum x_i^2 y_i^2/d^4$	0.75	6.75	12	37.5	60.75	108	253.5	192	805.5	843.75	468.75

Therefore

$$\begin{aligned} p &= \frac{3\epsilon}{a}\sum_i\left(\frac{1}{r_i^{12}} - \frac{1}{r_i^6}\right) \\ &= \frac{3\epsilon}{a}\Big(6(\frac{1}{d^{12}} - \frac{1}{d^6}) + 6(\frac{1}{3^6 d^{12}} - \frac{1}{3^3 d^6}) + 6(\frac{1}{2^{12}d^{12}} - \frac{1}{2^6 d^6}) + 12(\frac{1}{7^6 d^{12}} - \frac{1}{7^3 d^6}) \\ &\quad + 6(\frac{1}{3^{12}d^{12}} - \frac{1}{3^6 d^6}) + 6(\frac{1}{12^6 d^{12}} - \frac{1}{12^3 d^6}) + 12(\frac{1}{13^6 d^{12}} - \frac{1}{13^3 d^6}) + 6(\frac{1}{4^{12}d^{12}} - \frac{1}{4^6 d^6}) \\ &\quad + 12(\frac{1}{19^6 d^{12}} - \frac{1}{19^3 d^6}) + 12(\frac{1}{21^6 d^{12}} - \frac{1}{21^3 d^6}) + 6(\frac{1}{5^{12}d^{12}} - \frac{1}{5^6 d^6})\Big) \\ &= \frac{18\epsilon}{a}\Big(\Big(1 + \frac{1}{3^6} + \frac{1}{2^{12}} + \frac{2}{7^6} + \frac{1}{3^{12}} + \frac{1}{12^6} + \frac{2}{13^6} + \frac{1}{4^{12}} + \frac{2}{19^6} + \frac{2}{21^6} + \frac{1}{5^{12}}\Big)\cdot\frac{1}{d^{12}} \\ &\quad - \Big(1 + \frac{1}{3^3} + \frac{1}{2^6} + \frac{2}{7^3} + \frac{1}{3^6} + \frac{1}{12^3} + \frac{2}{13^3} + \frac{1}{4^6} + \frac{2}{19^3} + \frac{2}{21^3} + \frac{1}{5^6}\Big)\cdot\frac{1}{d^6}\Big) \end{aligned} \tag{6.50}$$

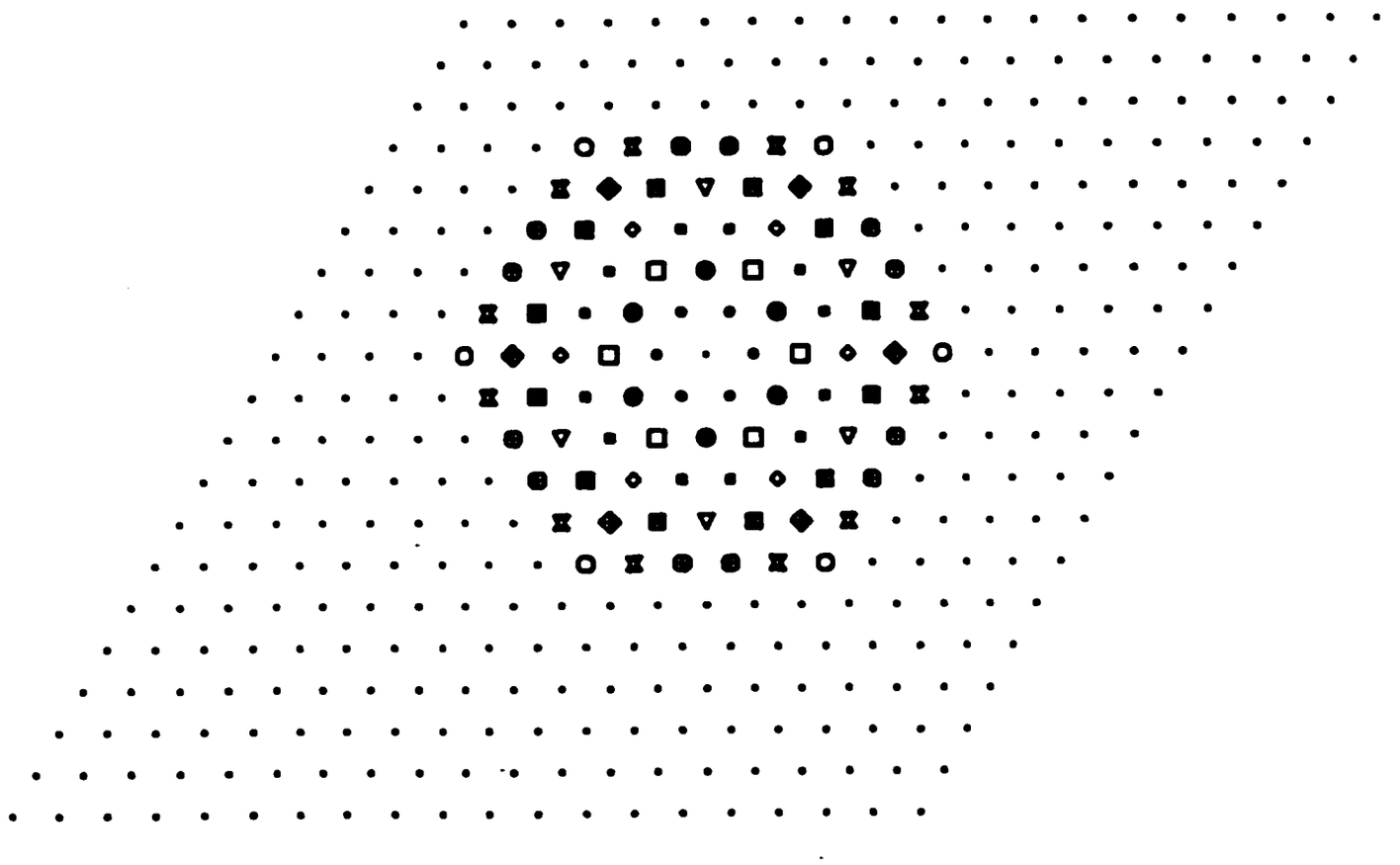

Figure 6.1: Figure to count the number of neighbours for a triangular lattice point. o : the nearest neighbours; •: the next nearest neighbours; □: the 3th neighbours; ■ : the 4th neighbours; ◇: the 5th neighbours; ▽ : the 6th neighbours; ⊠: the 7th neighbours; ⊕: the 8th neighbours; ⊗ the 9th neighbours; ⧖: the 10th neighbours; ◯ : the 11th neighbours;

and

$$\begin{aligned}\lambda_0 &= \frac{12\epsilon}{a}\Big((\frac{7}{d^{12}}-\frac{4}{d^6})\cdot 0.75+(\frac{7}{3^5d^{12}}-\frac{4}{3^2d^6})\cdot 0.25+(\frac{7}{2^{14}d^{12}}-\frac{1}{2^6d^6})\cdot 3\\ &+(\frac{1}{7^7d^{12}}-\frac{4}{7^5d^6})\cdot 37.5+(\frac{7}{3^{11}d^{12}}-\frac{4}{3^5d^6})\cdot 0.25+(\frac{1}{12^8d^{12}}-\frac{4}{12^5d^6})\cdot 108\\ &+(\frac{7}{13^8d^{12}}-\frac{4}{13^5d^6})\cdot 253.5+(\frac{7}{4^{16}d^{12}}-\frac{4}{4^{10}d^6})\cdot 192+(\frac{7}{19^8d^{12}}-\frac{4}{19^5d^6})\cdot 805.5\\ &+(\frac{7}{21^8d^{12}}-\frac{4}{21^5d^6})\cdot 843.75+(\frac{7}{5^{16}d^{12}}-\frac{4}{5^{10}d^6})\cdot 468.75\Big) \qquad (6.51)\end{aligned}$$

Finally, we can obtain

$$\begin{aligned}\lambda &= a_{ljp}\left(\frac{d_0}{d}\right)^{14}-b_{ljp}\left(\frac{d_0}{d}\right)^{8}\\ \mu &= g_{ljp}\left(\frac{d_0}{d}\right)^{14}-h_{ljp}\left(\frac{d_0}{d}\right)^{8} \qquad (6.52)\\ p &= A_{ljp}\left(\frac{d_0}{d}\right)^{14}-B_{ljp}\left(\frac{d_0}{d}\right)^{8} \qquad (6.53)\end{aligned}$$

where

$$\begin{aligned}a_{ljp} &= 2.10787\pm 0.0001\kappa, \quad b_{ljp}=1.48770\pm 0.0001\kappa\\ g_{ljp} &= 1.17103\pm 0.0001\kappa, \quad h_{ljp}=0.49424\pm 0.0001\kappa \qquad (6.54)\\ A_{ljp} &= 0.46841\pm 0.0001\kappa, \quad B_{ljp}=0.49673\pm 0.0001\kappa\end{aligned}$$

or, in more common reduced units,

$$\begin{aligned}\lambda &= 374.732\left(\frac{\sigma}{d}\right)^{14}-132.240\left(\frac{\sigma}{d}\right)^{8} \quad \frac{\epsilon}{\sigma^2}\\ \mu &= 208.183\left(\frac{\sigma}{d}\right)^{14}-43.9324\left(\frac{\sigma}{d}\right)^{8} \quad \frac{\epsilon}{\sigma^2}\\ p &= 83.2729\left(\frac{\sigma}{d}\right)^{14}-44.1538\left(\frac{\sigma}{d}\right)^{8} \quad \frac{\epsilon}{\sigma^2}. \qquad (6.55)\end{aligned}$$

The unique instability point in this system is a spinodal instability at $d = 1.2207\sigma(= 1.0875d_0)$ or $p = -3.8521\epsilon/\sigma^2(= -0.1092\kappa)$. This instability coincides again with the rupture point in our MD computer simulations (see Chapter 7). We therefore can conclude that at zero or very low temperature and compressive hydrostatic pressure, there is no structural transformation for a perfect LJM. We confirm this conclusion by performing a constant pressure MD simulation at $T = 0.0022\epsilon/k_B$ up to $p = 2100\epsilon/\sigma^2$.

6.5.3 4-8P System

With the following choice of unit of length $d_0 = 2^{\frac{1}{4}}\sigma'$ and $\epsilon' = 0.0225\kappa d_0^2$, the 4-8P (Eq. (2.9)) can be written as

$$\phi_{4-8}(r) = \epsilon'\left(\frac{1}{r^8} - \frac{2}{r^4}\right) \tag{6.56}$$

so that

$$\begin{aligned} \frac{\phi''_{4-8}}{r^2} - \frac{\phi'_{4-8}}{r^3} &= 16\epsilon'\left(\frac{5}{r^{12}} - \frac{3}{r^8}\right) \\ r\phi'_{4-8} &= 8\epsilon'\left(\frac{1}{r^4} - \frac{1}{r^8}\right). \end{aligned} \tag{6.57}$$

Also up to the 11th neighbours, we find

$$\begin{aligned} p &= \frac{2\epsilon'}{a}\Big(6(\frac{1}{d^8} - \frac{1}{d^4}) + 6(\frac{1}{3^4d^8} - \frac{1}{3^2d^4}) + 6(\frac{1}{2^8d^8} - \frac{1}{2^4d^4}) + 12(\frac{1}{7^4d^8} - \frac{1}{7^2d^4}) \\ &\quad +6(\frac{1}{3^8d^8} - \frac{1}{3^4d^4}) + 6(\frac{1}{12^4d^8} - \frac{1}{12^2d^4}) + 12(\frac{1}{13^4d^8} - \frac{1}{13^2d^4}) + 6(\frac{1}{4^8d^8} - \frac{1}{4^4d^4}) \\ &\quad +12(\frac{1}{19^4d^8} - \frac{1}{19^2d^4}) + 12(\frac{1}{21^4d^8} - \frac{1}{21^2d^4}) + 6(\frac{1}{5^8d^8} - \frac{1}{5^4d^4})\Big) \\ &= \frac{12\epsilon}{a}\Big(\Big(1 + \frac{1}{3^4} + \frac{1}{2^8} + \frac{2}{7^4} + \frac{1}{3^8} + \frac{1}{12^4} + \frac{2}{13^4} + \frac{1}{4^8} + \frac{2}{19^4} + \frac{2}{21^4} + \frac{1}{5^8}\Big)\cdot\frac{1}{d^8} \\ &\quad + \Big(1 + \frac{1}{3^2} + \frac{1}{2^4} + \frac{2}{7^2} + \frac{1}{3^4} + \frac{1}{12^2} + \frac{2}{13^2} + \frac{1}{4^4} + \frac{2}{19^2} + \frac{2}{21^2} + \frac{1}{5^4}\Big)\cdot\frac{1}{d^4}\Big) \end{aligned} \tag{6.58}$$

and

$$\begin{aligned} \lambda_0 &= \frac{8\epsilon'}{a}\Big((\frac{5}{d^8} - \frac{3}{d^4})\cdot 0.75 + (\frac{5}{3^6d^8} - \frac{3}{3^4d^4})\cdot 6.75 + (\frac{5}{2^{12}d^8} - \frac{3}{2^8d^4})\cdot 12 \\ &\quad +(\frac{5}{7^6d^8} - \frac{3}{7^4d^4})\cdot 37.5 + (\frac{5}{3^{12}d^8} - \frac{3}{3^8d^4})\cdot 60.75 + (\frac{5}{12^6d^8} - \frac{3}{12^4d^4})\cdot 108 \\ &\quad +(\frac{5}{13^6d^8} - \frac{3}{13^4d^4})\cdot 253.5 + (\frac{5}{4^{12}d^8} - \frac{3}{4^8d^4})\cdot 192 + (\frac{5}{19^6d^8} - \frac{3}{19^4d^4})\cdot 805.5 \\ &\quad + (\frac{5}{21^6d^8} - \frac{3}{21^4d^4})\cdot 843.75 + (\frac{5}{5^{12}d^8} - \frac{3}{5^8d^4})\cdot 468.75\Big) \end{aligned} \tag{6.59}$$

and finally

$$\begin{aligned} \lambda &= a_{48p}\left(\frac{d_0}{d}\right)^{10} - b_{48p}\left(\frac{d_0}{d}\right)^6 \\ \mu &= g_{48p}\left(\frac{d_0}{d}\right)^{10} - h_{48p}\left(\frac{d_0}{d}\right)^6 \\ p &= A_{48p}\left(\frac{d_0}{d}\right)^{10} - B_{48p}\left(\frac{d_0}{d}\right)^6 \end{aligned} \tag{6.60}$$

where

$$\begin{aligned} a_{48p} &= 1.10987 \pm 0.0005\kappa, \qquad b_{48p} = 0.97545 \pm 0.0005\kappa \\ g_{48p} &= 0.47548 \pm 0.0005\kappa, \qquad h_{48p} = 0.18909 \pm 0.0005\kappa \\ A_{48p} &= 0.31719 \pm 0.0005\kappa, \qquad B_{48p} = 0.39318 \pm 0.0005\kappa \end{aligned} \tag{6.61}$$

or, in more common units,

$$\begin{aligned} \lambda &= 197.310\left(\frac{\sigma'}{d}\right)^{10} - 86.7067\left(\frac{\sigma'}{d}\right)^{6} \quad \frac{\epsilon'}{\sigma'^2} \\ \mu &= 84.5298\left(\frac{\sigma'}{d}\right)^{10} - 16.8080\left(\frac{\sigma'}{d}\right)^{6} \quad \frac{\epsilon'}{\sigma'^2} \\ p &= 56.3893\left(\frac{\sigma'}{d}\right)^{10} - 34.9493\left(\frac{\sigma'}{d}\right)^{6} \quad \frac{\epsilon'}{\sigma'^2} \end{aligned} \tag{6.62}$$

The unique instability point for this system is again a spinodal instability at $d = 1.2846\sigma'(= 1.0802d_0)$ or $p = -3.1678\epsilon'/\sigma'^2(= -0.1008\kappa)$ and it coincides with the rupture point in our MD simulations (see Chapter 7). We therefore can also conclude that at zero or very low temperature and hydrostatic pressure, there is no structural transformation for a perfect 4-8M.

6.5.4 m-nP System

For a system with interparticle interaction of the form

$$\phi_{nm}(r) = \epsilon\left(\left(\frac{\sigma}{r}\right)^{n} - \left(\frac{\sigma}{r}\right)^{m}\right) \tag{6.63}$$

In the same way one can get the analogous formulae

$$\begin{aligned} \lambda &= a_{nm}\left(\frac{\sigma}{d}\right)^{n+2} - b_{nm}\left(\frac{\sigma}{d}\right)^{m+2} \quad \frac{\epsilon}{\sigma^2} \\ \mu &= c_{nm}\left(\frac{\sigma}{d}\right)^{n+2} - e_{nm}\left(\frac{\sigma}{d}\right)^{m+2} \quad \frac{\epsilon}{\sigma^2} \end{aligned} \tag{6.64}$$

where a_{nm}, b_{nm}, c_{nm} and e_{nm} are some n, m-dependent constants.

6.6 Conclusions and Discussions

The stability of homogeneously deformed systems has been discussed in a thermodynamic framework by requiring that the appropriate thermodynamic potential be minimum with respect to infinitesimal displacements about an equilibrium configuration. The general stability criterion under constant loading conditions is the same as the one derived by Wang et al. [104] through finite deformations; it is the positive definiteness of

$$\begin{aligned} C_{\alpha\beta\sigma\tau} \equiv \mathring{C}_{\alpha\beta\sigma\tau} - \frac{1}{2}(&\mathring{S}_{\alpha\beta}\,\delta_{\sigma\tau} + \mathring{S}_{\sigma\tau}\,\delta_{\alpha\beta} - \mathring{S}_{\alpha\sigma}\,\delta_{\beta\tau} \\ &- \mathring{S}_{\alpha\tau}\,\delta_{\beta\sigma} - \mathring{S}_{\beta\tau}\,\delta_{\alpha\sigma} - \mathring{S}_{\beta\sigma}\,\delta_{\alpha\tau}). \end{aligned} \tag{6.65}$$

Only for unstressed systems ($S_{\alpha\beta} = 0$) or constant $t_{\alpha\beta}$ ensemble do we have the usual condition of a positive definite elastic constant tensor $\mathring{C}_{\alpha\beta\sigma\tau}$. With isotropic stress, the condition is the positive definiteness of $C_{\alpha\beta\sigma\tau} = \mathring{c}_{\alpha\beta\sigma\tau}$, the elastic stiffness tensor. But for arbitrary anisotropic stress $C_{\alpha\beta\sigma\tau}$ will be distinct from both. We also show that stability conditions are dependent on the ensemble used. In particular, we show that a state can be stable in the constant volume ensemble but unstable in the constant pressure ensemble. We also present some simple expressions for elastic moduli in some perfect 2D systems at zero temperature and hydrostatic pressure.

The formalism has been developed assuming rotational invariance, i.e. rotations produce no stress. The need to consider the rotational effects was discussed in the 1950's but not apparently since then [109, 110, 111, 112, 113, 114, 115]. To add the rotational effects will greatly complicate the problem since the independent number of strains increases to 9 and requires a maximum of 45 (instead of 21) independent elastic constants [109]. In this case the definition of the elastic constants is also different from the traditional one [109]. There is, however, no obstacle in generalizing our formalism to systems where rotations produce internal stresses, since the thermodynamic theory must work for any system.

It should be noted that each physical situation may call for a different relevant quantity. Acoustic experiments, related to the stability question, would measure $C_{\alpha\beta\sigma\tau}$ in the absence of stress and for isotropic stress. In direct experiments, such as elongation, the elastic stiffness coefficients $\mathring{c}_{\alpha\beta\sigma\tau}$ are measured. When constructing interatomic potentials, it may be preferable to work with an unstressed system, the

only situation where the elastic constants $\mathring{C}_{\alpha\beta\sigma\tau}$ probe intrinsic properties of the system.

A thermodynamic potential H under constant loading conditions $T_{\alpha\beta}$, can be defined even in the anisotropic case, where the work has a path dependent component, by considering the average over all paths. In principle, therefore we have, for a specific $T_{\alpha\beta}$, an H for all values of strain $\eta_{\alpha\beta}$. In small deformation from a reference configuration, the work for straight line paths are simply obtained, but for more complex deformations, a path dependent term should be also considered.

We have to emphasize again that when using fluctuation formulae for the calculation of the elastic quantities, the reference configuration must be the current (stressed) one, otherwise it may cause some confusion, and limit the validity of the calculations.

About Hill and Milstein's Conclusion

As mentioned in the introductory section of this chapter, Hill and Milstein approached the stability problem essentially by requiring that the internal energy be *convex* [84], [99]-[103], [104] instead of minimum (of thermodynamic potential H). This leads to the conclusion that the mechanical stability is dependent on the *choice of the coordinate system or the definition of strains or the choice of the generalized stresses* since so does the *convexity*. We should note that the minimum of a function is independent of the choice of the coordinate system and the same applies to our stability criteria. They also did not seem to be aware of the difference between the thermodynamic stress tensor $t_{\alpha\beta}$ and the applied stresses $\mathring{S}_{\alpha\beta}$, $T_{\alpha\beta}$. From Eq. (5.24), we know that this confusion leads to the loss of some very important second order terms in the expansion of the free energy.

However, another problem raised by Hill [84] has to be considered, i.e. that stability can be regarded in the sense of a mechanical test or as an intrinsic property of the material. In the former perspective the loading is conditioned by material rotation in the laboratory frame; in the latter the loading is imagined to 'follow' the material independently of any frame. Whether such a view of strength is realistic is not yet apparent. The existing elasticity theories and also the computer simulation work usually neglects this distinction, and therefore assumes that the system is rotationally invariant implying that the loading is to 'follow' the material independently of any frame, or the rotation of the whole system is prohibited. We have to point out

that if the condition of rotational invariance is violated then the Lagrangian strain tensor which contains only 6 independent components is not enough to describe the deformation of a system, three more variables corresponding to the rotation of the system will be needed. As a consequence, stability criteria may become much more complicated.

About Wang et. al. Results

By considering $\Delta\mathcal{G} = \Delta F - \Delta\mathcal{W}$ and requiring $\Delta\mathcal{G} > 0$ for stability, a condition identical to minimizing $\mathcal{G} = F - \mathcal{W}$, Wang et. al. [104] derived exactly the same stability criteria as ours for constant loading systems in the general anisotropic case. However, there are some differences between our results and theirs. Our derivation is based on the thermodynamic framework. By taking a close look at the nature of the path dependent term $T_{\alpha\beta}\xi'_{\alpha\beta}$, we can define a thermodynamic potential in spite of the path dependence of the work and rigorously show that the positiveness of the $C_{\alpha\beta\sigma\tau}$ can be used as stability criteria. Moreover, they did not seem to be aware of the fact that $T_{\alpha\beta}\xi'_{\alpha\beta}$ is of the same order of magnitude as $\eta_{\alpha\beta}\eta_{\sigma\tau}$. This requires some care in dealing with this term.

We also show for the first time that stability conditions are dependent on the ensemble used. In particular, we show that the stability conditions are stronger in the constant pressure ensemble than in the constant volume ensemble, i.e. a state can be stable in the constant volume ensemble but unstable in the constant pressure ensemble.

It could be noted that even in the anisotropic case, a traditional thermodynamic potential could be used to derive stability criteria for an ensemble under constant thermodynamic stress (Eqs. (5.18) and (5.24)) instead of constant external stress (or loading).

Chapter 7

The Rupture of Physical Membranes

7.1 Introduction

The phenomenon of a membrane breaking into several pieces under tension is known as rupture. The rupture of membranes is a common phenomenon and has been extensively studied experimentally especially in biological membranes [116, 117, 118, 119, 120, 121]. But theories have been few and usually focus on the response to the mechanical forces and neglects the effects of thermal fluctuations [122, 123]. The problems of interest to us are: the kinetics of rupture, dependence on temperature, effect of the range of the interparticle interaction and the relationship between rupture and mechanical instability.

In this Chapter we present preliminary work explaining some of these questions on two classes of simple model systems: one dimensional closed membranes (2D vesicles) and two dimensional flat membranes. We show that rupture at zero temperature occurs at the mechanical instability point. We find that at finite temperature thermal fluctuations play an important role in the rupture of solid membranes. The study is done using molecular dynamics simulation and elasticity theory.

7.2 Rupture and Mechanical Instability

In Chapter 6, we have investigated in detail the mechanical stability criteria of homogeneously deformed systems under an arbitrary loading condition. It is natural to ask what is the relationship between mechanical stability and rupture?

To answer this question, we first consider a system at zero temperature and under isotropic tension p. The thermodynamic potential must be the Gibbs' free energy or the enthalpy (note that at zero temperature they are the same)

$$G = E + pV = \sum_{i>j} \phi(\mathbf{r}_{ij}) + pV, \tag{7.1}$$

or equivalently, but more properly, in the thermodynamic limit

$$g = e + pv = \frac{1}{N} \sum_{i>j} \phi(\mathbf{r}_{ij}) + pv, \tag{7.2}$$

where N is the number of particles, E is the internal energy, $e = E/N$, V the volume of the system, $v = V/N$ and $\phi(\mathbf{r}_{ij})$ the interparticle interaction. We assume that $\phi(\mathbf{r}_{ij})$ is continuous up to the second derivatives. With this assumption, at zero temperature, in general e as a function of v will also be continuous up to the second derivatives. For simplicity, we can assume that as a function of v, e has only one minimum, and $e \to 0$ if $v \to \infty$.

It is easy to show that if $p > 0$, there is also only one minimum of g as shown in curve (a) of Fig. 7.1, so no rupture is possible since rupture corresponds to $v \to \infty$ and leads to $g \to +\infty$.

However, if $p < 0$, the situation is completely different. For small $|p|$, we can find two minima of g, as shown in curve (c) of Fig. 7.1. The first one is a local minimum, close to the minimum of e and determined by $\frac{\partial g}{\partial v} = 0$ and $\frac{\partial^2 g}{\partial v^2} > 0$. The second, a global minimum, corresponds to $v \to \infty$ and $g \to -\infty$, i.e. the system breakdowns. It means that *the system under tension is essentially a metastable state.* Correspondingly, we can also find a local maximum of g located between these two minima. This maximum is determined by $\frac{\partial g}{\partial v} = 0$ and $\frac{\partial^2 g}{\partial v^2} < 0$. At zero temperature the system can stay in this metastable state for a long time since there are no thermal fluctuations to overcome the energy barrier (equal to the difference of g at the maximum and g at the local minimum).

The larger the value of $|p|$, the closer the local minimum is to the maximum, as shown in curves (c)-(e) of Fig. 7.1. Therefore, there must be a value of p_c for which the local minimum coincides with the maximum as in curve (e) of Fig. 7.1. For $|p| \geq |p_c|$, there is no longer a local minimum so the system ruptures. At p_c, we must have $\frac{\partial^2 g}{\partial v^2} = 0$ and it is identical to $B = 0$ where B is the bulk modulus. As we have discussed in Chapter 6, $B = 0$ leads to an incipient spinodal instability.

It is not difficult to generalize the above discussion to the anisotropically stressed system. What we should mention here is that under anisotropic stresses $T_{\alpha\beta}$, the variables coupled to the tension will tend to increase without limit to bring the relevant thermodynamic potential $\mathcal{G}/V_o = E/V_o - T_{\alpha\beta}\xi_{\alpha\beta}$ to its global minimum i.e. a ruptured system, and the local minimum coincides with the maximum when

$$C_{\alpha\beta\sigma\tau}\eta_{\alpha\beta}\eta_{\sigma\tau} = 0 \tag{7.3}$$

(see also Eq. (6.37)). Therefore, *the rupture point at zero temperature occurs at the mechanical instability point.* This is a natural conclusion since in this case the external stresses are the only factor in the breakdown of the system.

Even if the second derivative of $\phi(\mathbf{r}_{ij})$ is not continuous, we may also get the same conclusion since in this case, the discontinuous points of e may be both the mechanical instability and rupture points. We can see this from the results of the PLFP potential system in the next section.

We can verify the above discussion by considering a very simple system. This system consists of two particles with the interparticle interaction

$$\phi(r) = \epsilon(r^{-11} - r^{-5}). \tag{7.4}$$

Therefore

$$G = \epsilon(r^{-11} - r^{-5}) + pr. \tag{7.5}$$

From

$$\left(\frac{\partial G}{\partial r}\right)_{r=r_0} = \epsilon(5r_0^{-6} - 11r_0^{-12}) + p = 0 \tag{7.6}$$

we find

$$r_0^6 = \frac{-5\epsilon}{2p} \pm \frac{1}{2}\left(\frac{25\epsilon^2}{p^2} + \frac{44\epsilon}{p}\right)^{1/2} \tag{7.7}$$

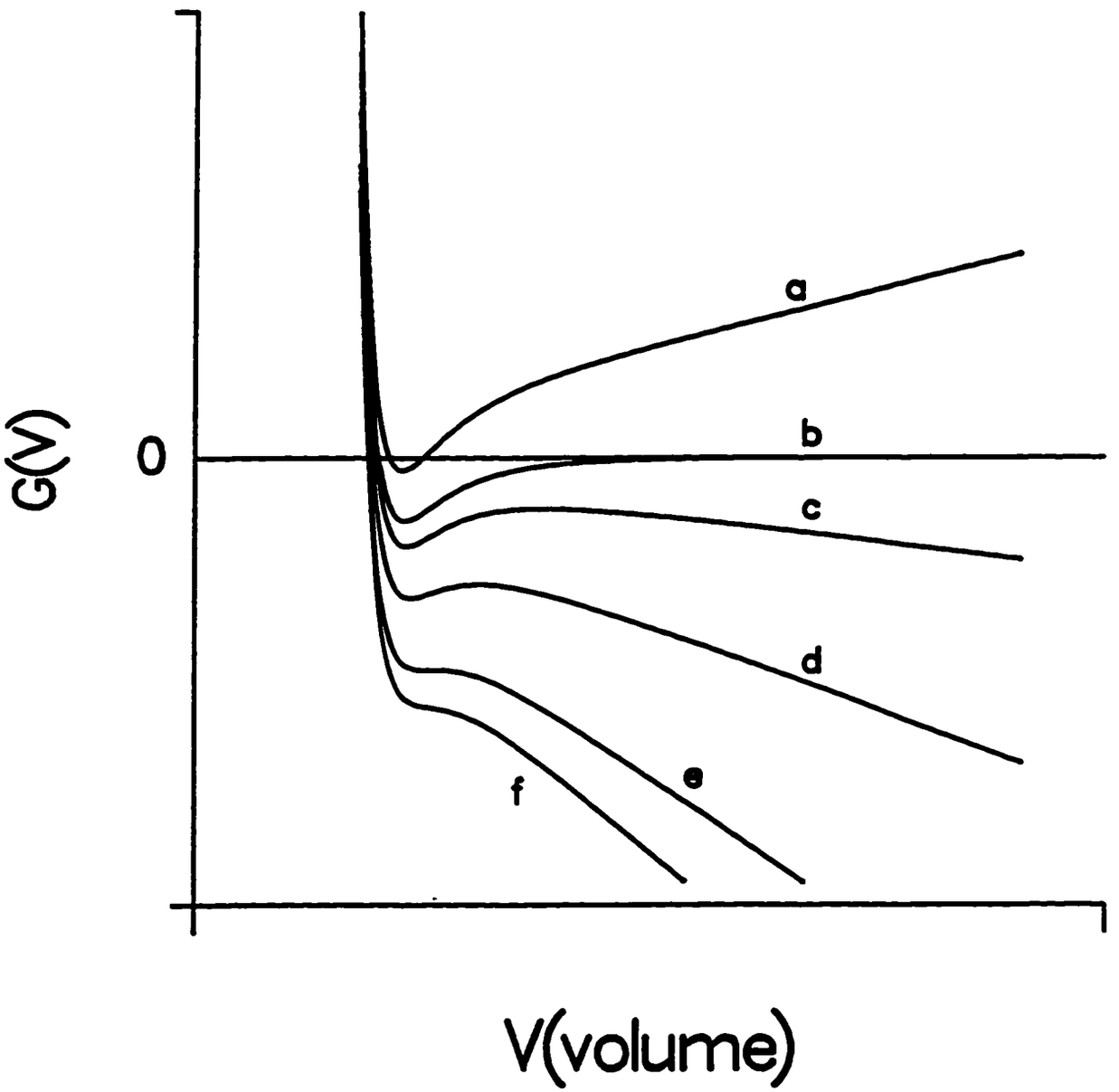

Figure 7.1: The figure showing the rupture at zero temperature. Curve a for $p > 0$; curve b for $p = 0$; curve c for $0 > p = p_1 > p_c$; curve d for $0 > p_1 > p = p_2 > p_c$; curve e for $p = p_c$; curve f for $p < p_c$. The unit in figure is arbitrary.

If $p > 0$, there is only one physical solution for r_0. If $0 > p > \frac{-25\epsilon}{44}$, there are two solutions for r_0, one (by choice '-' in the above equality) gives the local minimum of G and the other gives the maximum. $p_c = \frac{-25\epsilon}{44}$ is the critical pressure where the local minimum coincides with the maximum.

We can expect that at finite T, rupture will in general be different from mechanical instability. This is because for some $|p| < |p_c|$, the free energy barrier can be so small that a local thermal fluctuation is enough to overcome it. Also, at low T, the rupture point should be close to the mechanical instability point. In other words, *the rupture phenomenon is in general not a pure mechanical instability.* This is verified in our simulations.

7.3 One-dimensional Closed Membranes i.e. Two-dimensional Vesicles

7.3.1 Methods of Simulations

The interparticle interaction potentials are given by Eqs. (2.15), where we either use the LJP or 4-8P for the radial dependence. We use the pressurizing gas defined in section 2.2.4 to simulate the effect of an internal pressure in the vesicle.

The basic time step $\tau_0 = 0.005t_0$ in most of our simulations, where $t_0 = \sqrt{m\sigma^2/\epsilon}$. We also tried for some samples $\tau_0 = 0.0025t_0$ but there was no significant change. A critical rupture pressure p_c is defined as the pressure for which the vesicle ruptures in about 10^5 time steps. The definition of p_c is based on the assumption of an exponential decrease of the rupture time with increasing p, a reasonable assumption for a thermally activated process. The above assumption is verified in the simulations. Within 2% of p_c are intervals of p of rapid rupture and no observed rupture over times in excess of 2×10^6 time steps. The initial configuration was a closed circular chain. The p_c and d_c shown in Figs. 7.2 - 7.4 were obtained from several runs with the same initial configuration but different initial velocities. The errors for both p_c and d_c are within $\pm$ 0.005 in reduced unit. The CPU time required in a IBM RISC system/6000 workstation with CPU type 7011 is ranged from a few minuts for rapid rupture to over 5 days for no observed rupture in excess of 2×10^6 time steps.

Since the pressurizing gas is essentially an ideal gas, we used $|p| = N_{gas}k_BT/A$ to

calculate the pressure, where A is the area enclosed by the chain, N_{gas} the number of particles in the pressurizing gas. To calculate the area, we used two methods, one is $A = \pi r^2$ with $r = \frac{Nd}{2\pi}$. N is the number of particles, d the average distance between the nearest neighbours. The justification of this expression is that in our simulations the vesicle is always nearly circular up to rupture. The other method was to use $A = \frac{1}{2}\sum_i^N (y_i + y_{i+1})(x_i - x_{i+1})$ with $x_{N+1} = x_1$ and $y_{N+1} = y_1$. Both methods gave consistent results.

7.3.2 Results

From Figs. 7.2 - 7.4, we can see that there are two regimes, separated by a special temperature named T_1, in the variation of p_c vs. T, and d_c vs. T, where p_c is the rupture pressure and d_c the corresponding critical lattice constant. T_1 is dependent on both the interaction and the size of the system. $T_1 \approx 0.125\epsilon/k_B$ with the LJP and 100 particles, $T_1 \approx 0.120\epsilon/k_B$ with LJP with 150 particles, and $T_1 \approx 0.14\epsilon/k_B$ with the 4-8P and 100 particles.

Figs. 7.2 - 7.4 show that there is a fast decrease of $|p_c|$ and d_c below T_1 for both LJP and 4-8P interactions. This is the expected behaviour for a thermally activated process. However, at high T ($> T_c$), p_c is small and its variation is relatively small for both kinds of interactions. The longer range force leads to a larger variation.

From Figs. 7.2 and 7.4, we can also find that just above T_1, a sudden drop of $|p_c|$ and d_c occur for the LJP. But for the 4-8P, there is no such sudden drop (see Figs. 7.3 and 7.4). The longer range force tends to give a smoother behaviour.

In our simulations, the vesicle is nearly circular up to rupture as shown in Fig. 7.5, but shape fluctuations increase with increasing force range.

Finally, we find that T_d, the zero pressure desintegration temperature, depends on the size of the vesicle. For instance, for the LJM, $T_d = 0.190\epsilon/k_B$ for the 100 particle membrane, $T_d = 0.140\epsilon/k_B$ for 150 particles and $T_d = 0.165\epsilon/k_B$ for 200 particles.

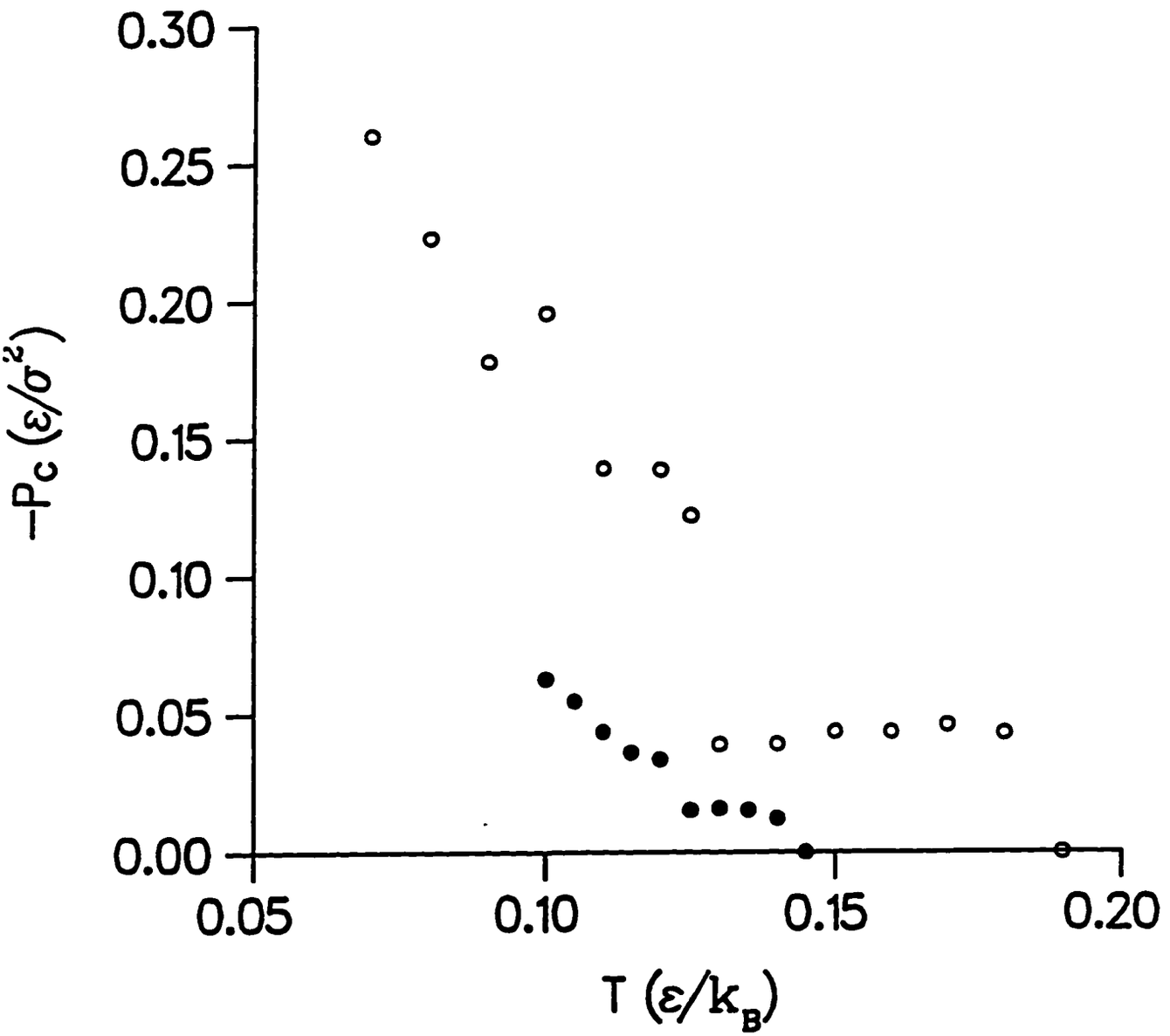

Figure 7.2: The variation of $|p_c|$ vs. T for one-dimensional closed LJM of 100 particles (o) and 150 particles (•).

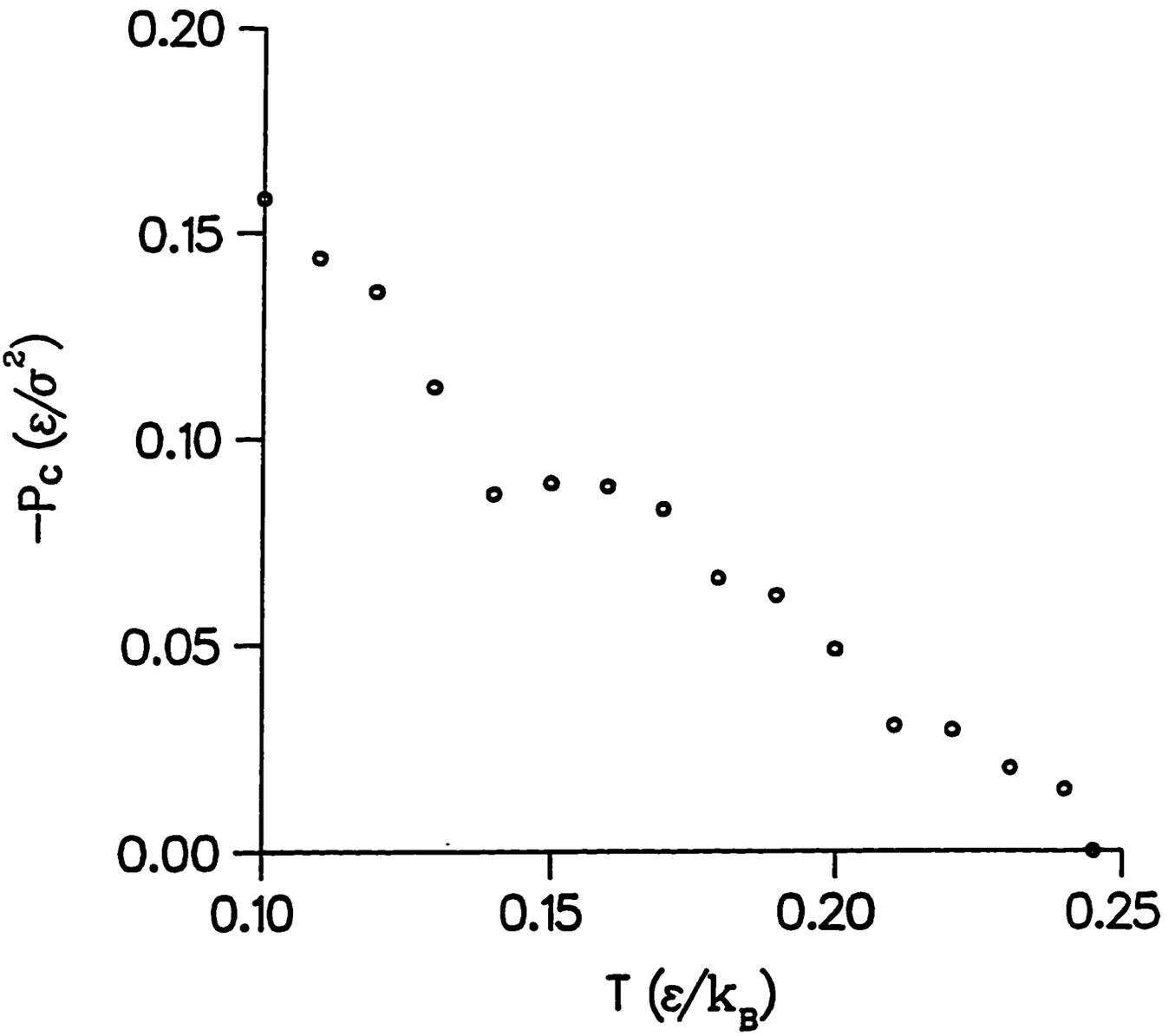

Figure 7.3: The variation of $|p_c|$ vs. T for one-dimensional closed 4-8M of 100 particles.

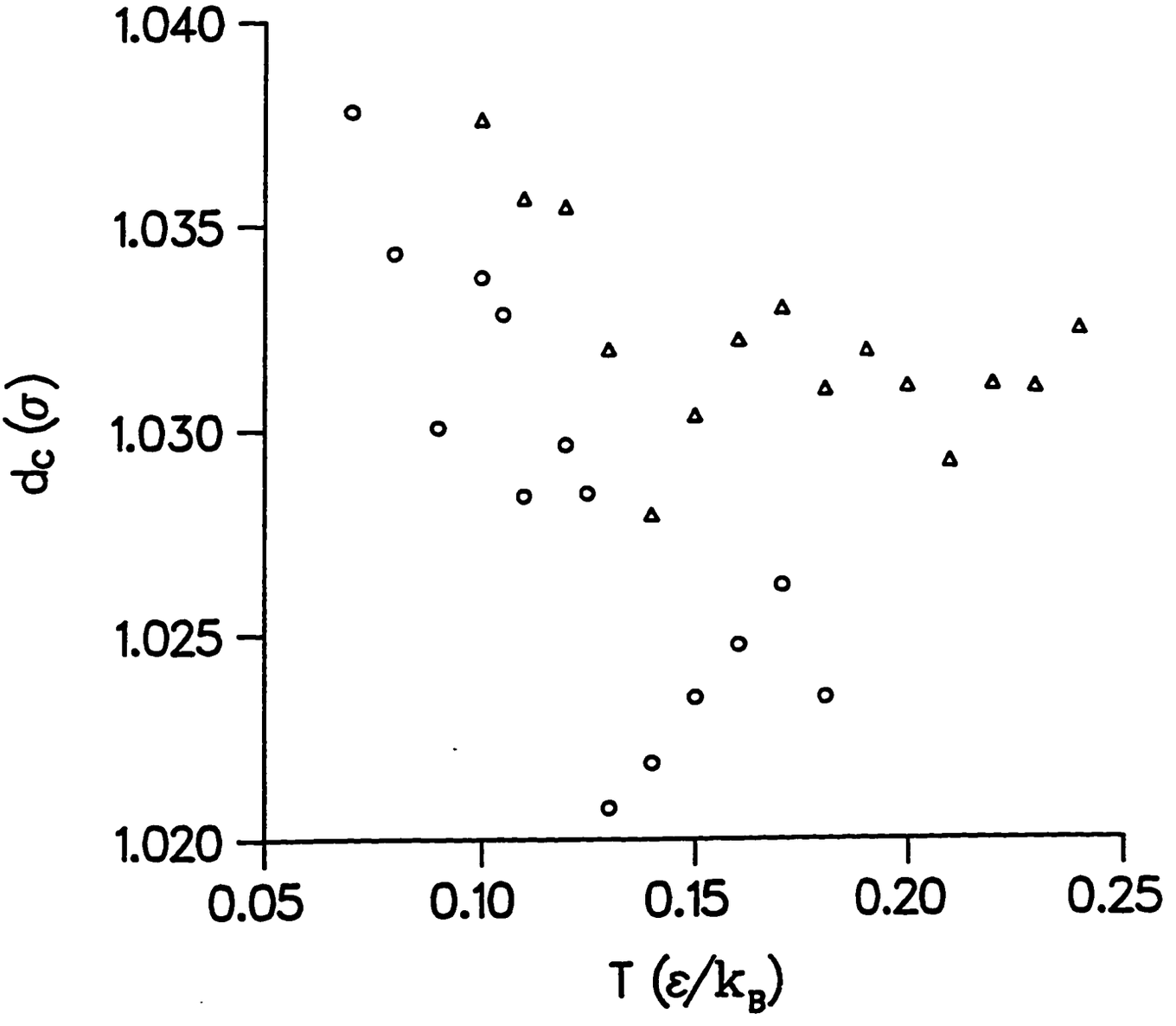

Figure 7.4: The variation of d_c vs. T for one-dimensional closed LJM with 100 particles (o) and a 4-8M with 100 particles (Δ).

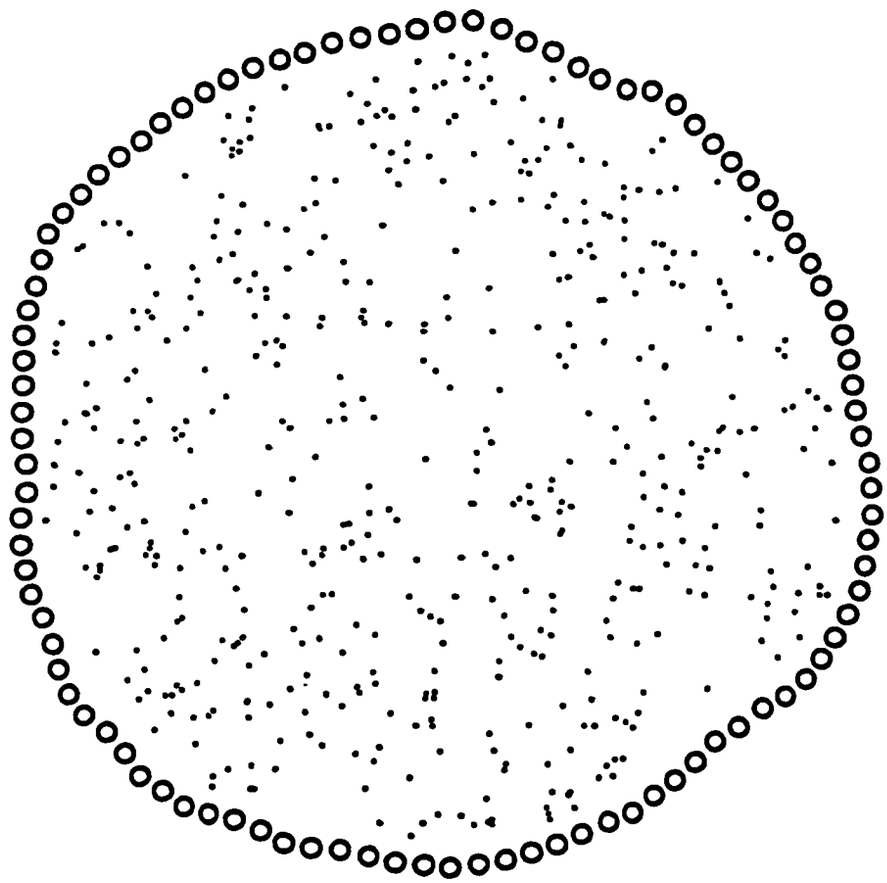

Figure 7.5: Configuration of a two-dimensional 4-8M vesicle at time $t = 2.2 \times 10^6 \tau_0$, $T = 0.14\epsilon/k_B$ and $p \approx -0.039\epsilon/\sigma^2$ (just below $|p_c|$). Symbol '·' in fig. represents the pressurizing gas.

7.4 Two-dimensional Solid Membranes

7.4.1 Methods of Simulations

For the 2D system, the interparticle interaction potentials are given by Eqs. (2.1), (2.7) and (2.9). We use the TPN ensemble with PBC. The data shown in this section were obtained from several runs with the same initial configuration but different initial velocities. The errors for p_c and d_c are within $\pm$ 0.003 in reduced unit.

The shear modulus μ is calculated by Eq. (5.54) and the errors from diffreent runs are within $\pm 0.003\kappa$. But the bulk modulus B is calculated by

$$k_B T A B^{-1} = < A^2 > - < A >< A > \tag{7.8}$$

where A is the area of the system. As we discussed in section 5.3, the rate of convergence of B is unsatisfactory, the errors for LJM and 4-8M can be $\pm 0.05\kappa$ and for PLFM $\pm 0.2\kappa$.

The basic time step $\tau_0 = 0.05 t_0$ in our simulations where $t_0 = \sqrt{m/\kappa}$. Following the same argument as in section 7.3.1, a critical rupture pressure p_c could be easily determined as the pressure separating intervals of p of rapid rupture and no observed rupture over 10^6 time steps. The intermediate region is about 5% of p_c, a little larger than in 1D, which is expected for reasons of dimensionality. The CPU time required in a IBM RISC system/6000 workstation with CPU type 7011 is ranged from a few minuts for rapid rupture to over 10 days for no observed rupture in excess of 5×10^6 time steps.

Most of the simulations are for rhombuses with 28 atoms on the side. We also tried samples with 51 atoms on the side to check size effects.

7.4.2 Rupture at Zero Temperature

We find that, as shown in Figs. 7.6 - 7.10, p_c, d_c B_c (bulk modulus) and μ_c (shear modulus) all tend to their mechanical instability point when $T \to 0$ for all three kinds of potentials, where the values of p_c, d_c B_c and μ_c at zero T are obtained from results in section 6.5. This supports our conclusion in section 7.2 that the rupture point at zero temperature is a mechanical instability point. Combined with the results in section 6.5, we can further conclude that at zero or very low temperature

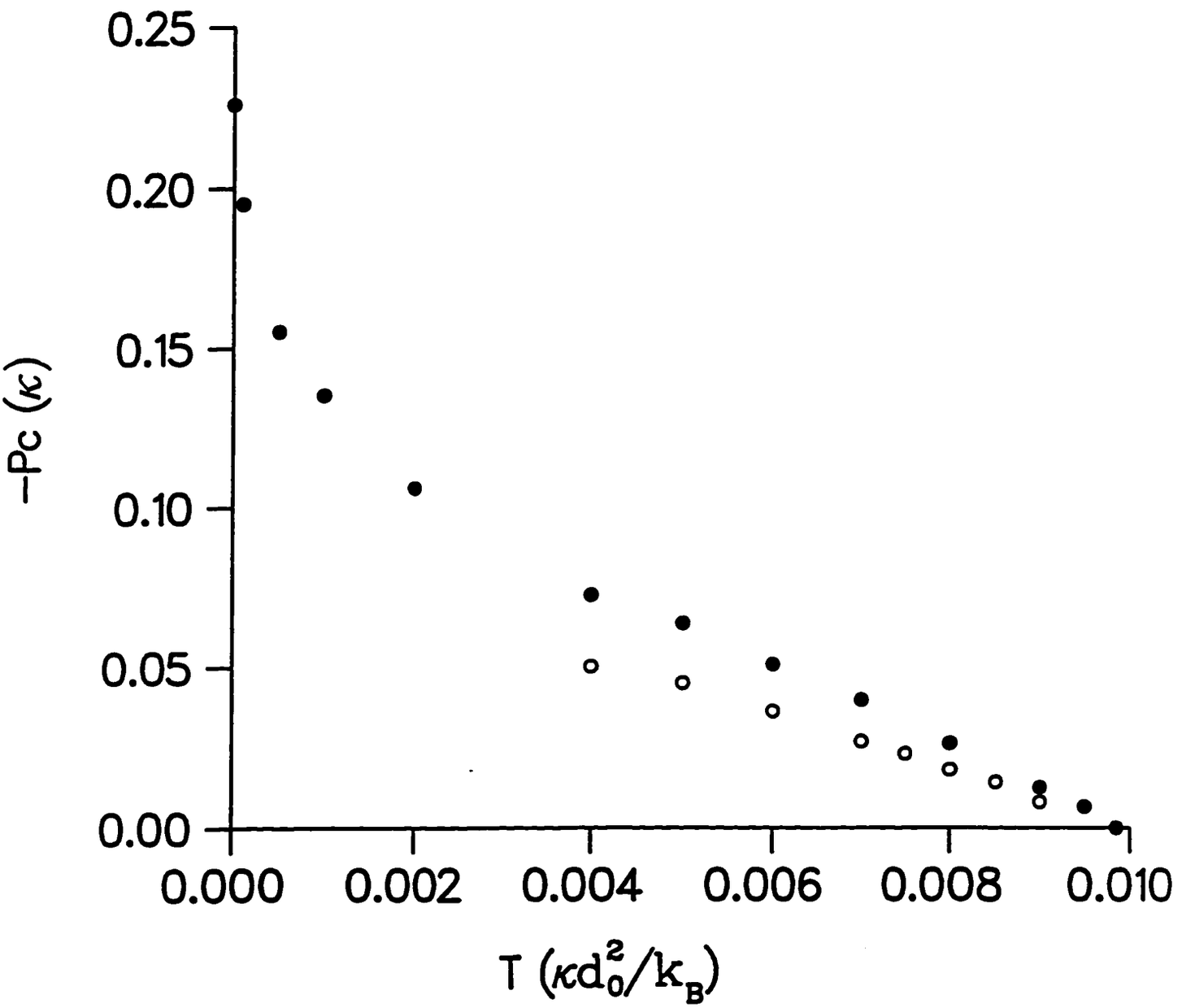

Figure 7.6: The variation of $|p_e|$ vs. T for a two-dimensional perfect solid PLFM (•) and a PLFM with a vacancy concentration of 2.56 at.% (○).

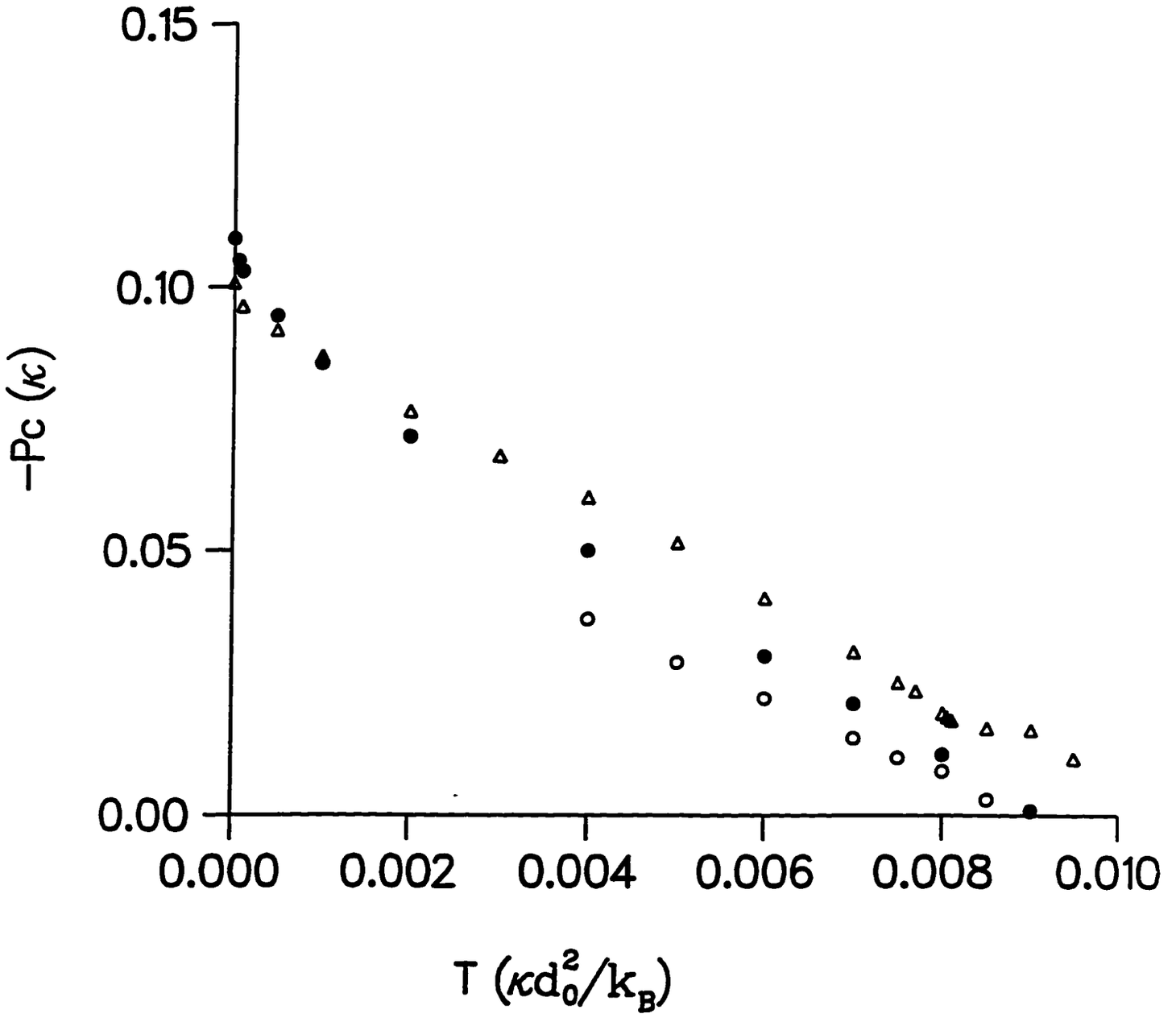

Figure 7.7: The variation of $|p_c|$ vs. T for a two-dimensional perfect solid LJM (•), a LJM with a vacancy concentration of 2.56 at.%(○) and a perfect 4-8M (△).

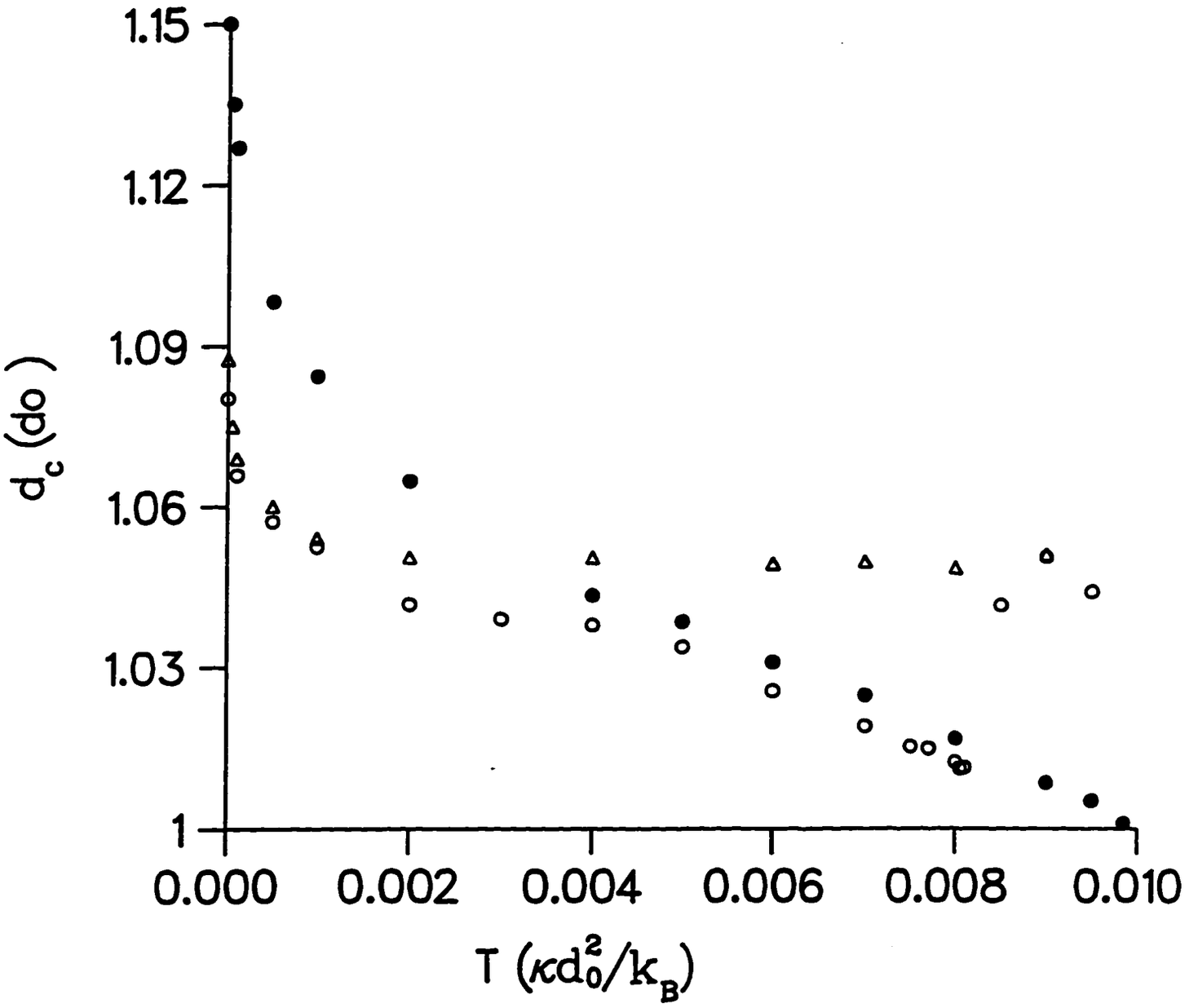

Figure 7.8: The variation of d_c vs. T for a two-dimensional perfect solid PLFM (•), a LJM (△) and a 48M (○).

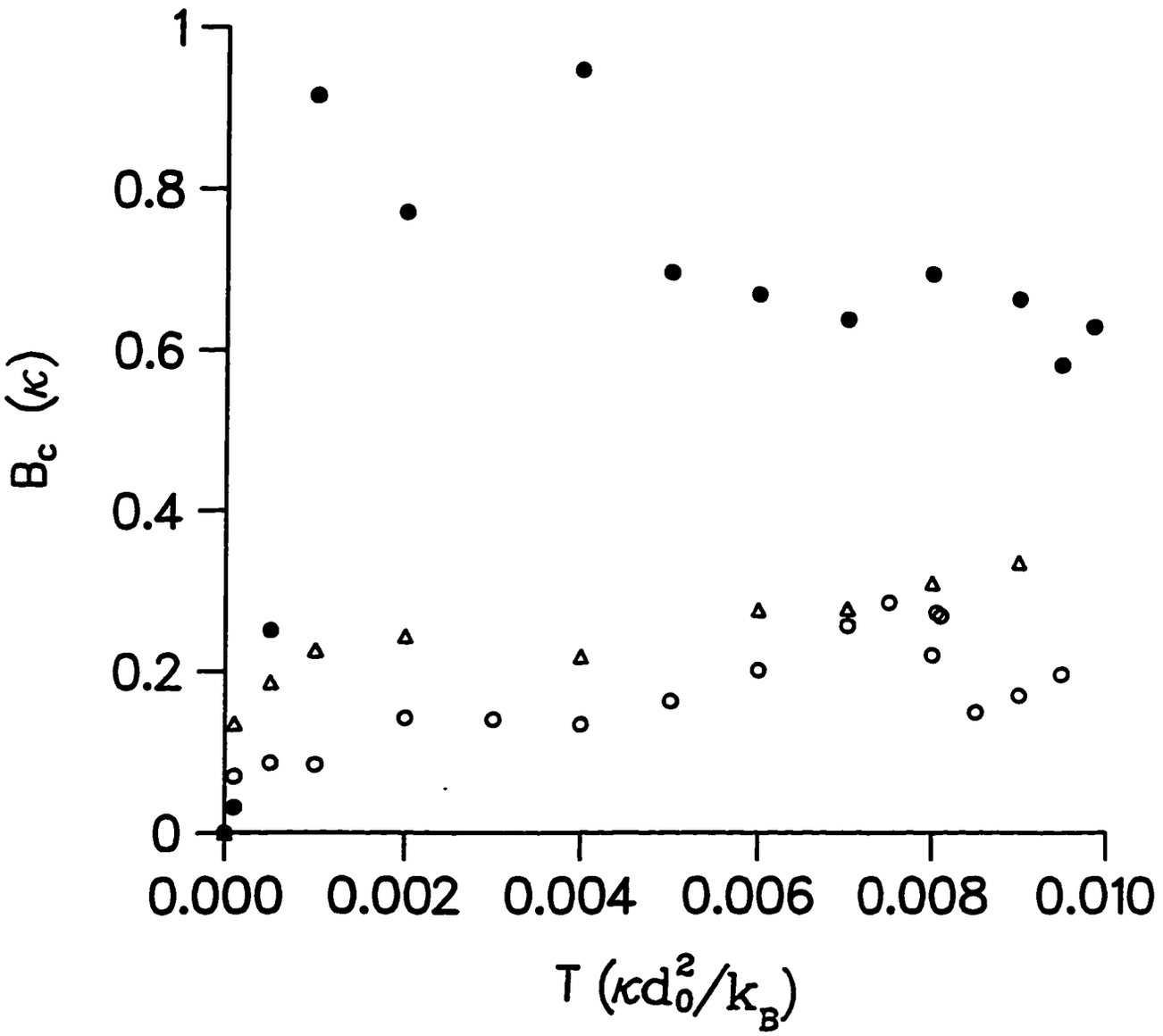

Figure 7.9: The variation of B_c vs. T for a two-dimensional perfect solid PLFM (•), a LJM (△) and a 48M (○).

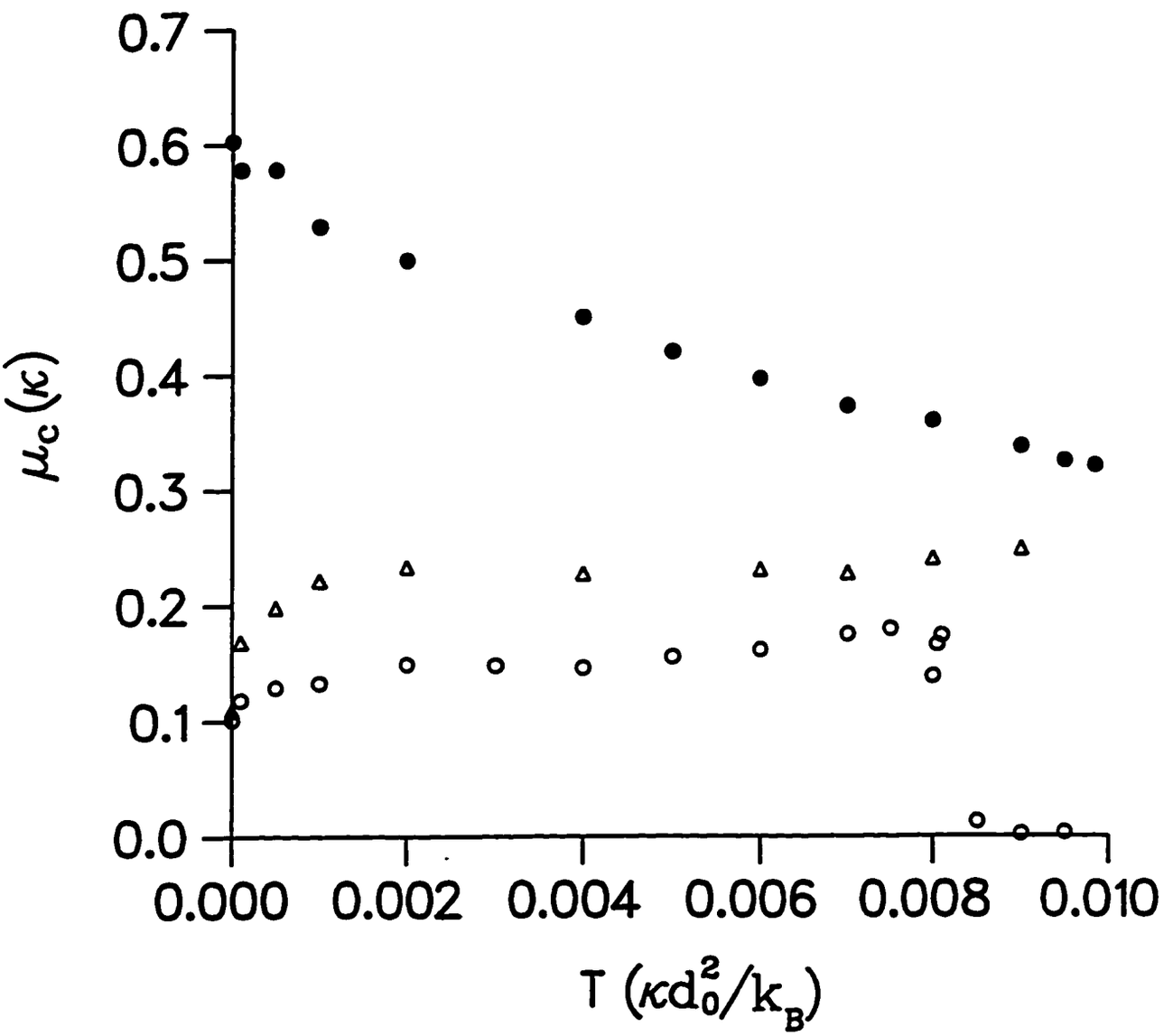

Figure 7.10: The variation of μ_c vs. T for a two-dimensional perfect solid PLFM (•), a LJM (△) and a 48M (○).

and hydrostatic pressure, there is no structural transformation for a perfect LJM and 4-8M since the rupture is the only instability in these two systems.

The second derivative of $\phi(\mathbf{r})$ for the PLFM is discontinuous at $d = 1.15d_0$, its behaviour at this point can be still well predicted with the stability criteria since $B < 0$ for $d > 1.15d_0$.

7.4.3 Finite Temperature Results

Results are shown in Figs. 7.6-7.10. For convenience of comparison for our equal depth potentials, p is in units of κ and T in units of $\kappa d_0^2/k_B$. For the LJM, to convert p to ϵ/σ^2 and T to ϵ/k_B, multiply by 35.2756 and 44.4444, respectively. For the 4-8M, to convert p to ϵ'/σ'^2 and T to ϵ'/k_B, multiply by 31.4270 and 44.4444, respectively.

Figs. 7.6 and 7.7 show a fast drop of $|p_c|$ from the zero temperature instability point at very low T. The shorter the range of the force, the larger the temperature range for this drop.

Figs. 7.6 and 7.7 also show that for all three kinds of interactions, $|p_c|$ decreases almost linearly at high T with or without vacancies.

From 7.9 and 7.10, we can see that as expected at finite temperature, rupture occurs prior to mechanical instability since both $B > 0$ and $\mu > 0$ at the critical pressure. A small finite temperature (a few percents of the melting temperature) is enough to produce a significant difference between rupture and mechanical instability.

We also find that the PLFM and LJM always rupture below the melting temperature ($\mu > 0$ and $B > 0$ for $|p| < |p_c|$). But for $T > 0.008\kappa d_0^2/k_B$, we find that the 4-8M melts first (lattice constant increases suddenly, see Fig. 7.8, and $\mu = 0$) and then ruptures.

It is also interesting to note that the variation of elastic modulus for both the short range (PLFM) and long range (LJM and 4-8M) force systems show quite different tendencies. For instance, the μ_c of the PLFM decreases with T, but the μ_c of the LJM and the 4-8M increase slowly with T.

From Figs. 7.6 and 7.7, we find that vacancies reduce $|p_c|$ more at low T than at high T for both the PLFM and LJM.

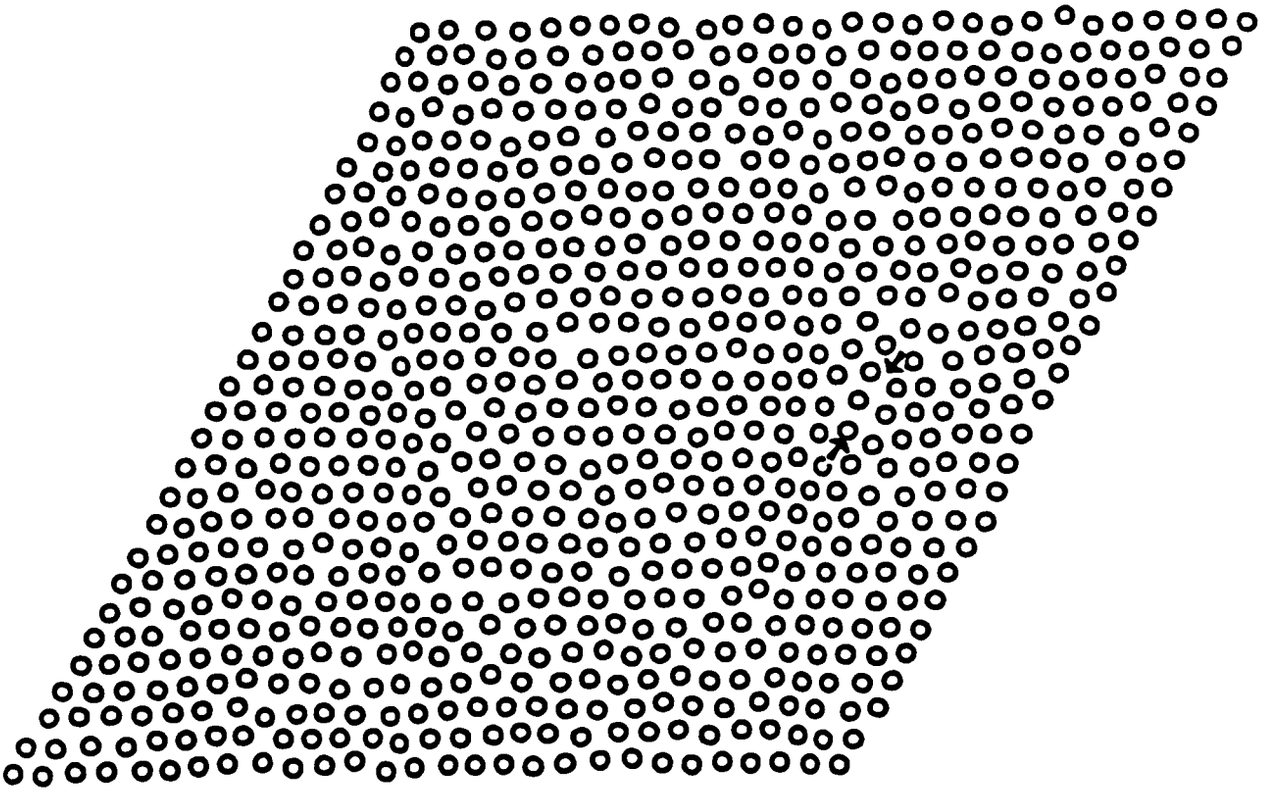

Figure 7.11: Configuration of a two-dimensional perfect solid LJM at $t = 5000\tau_0$, $T = 0.356\epsilon/k_B (= 0.008\kappa d_0^2/k_B)$ and $p = -0.4163\epsilon/\sigma^2 (= -0.0118\kappa$, $|p|$ is just above $|p_c|)$. The arrows placed at the cores of the dislocations are Burgers vectors.

Fig. 7.8 shows that d_c shows quite different behaviour for different range of interactions.

In our simulations, we also find that gliding dislocation dipoles are created just before rupture (Fig. 7.11). But in-grown vacancies reduce the influence of dislocations and can lead to direct cavitation.

We do not observe size effects.

7.5 Conclusions

In summary, we show that rupture at zero temperature occurs at the mechanical instability point. We also verify that in general rupture at finite temperature occurs prior to the mechanical instability point. The effects of the thermal fluctuations are in general not negligible for rupture at finite temperature. We find that in both one and two dimensional systems, the critical rupture pressure $|p_c|$ and bulk modulus drop rapidly at low T. We find that there is no structural transformation for perfect lattice systems with LJP and 4-8P at zero temperature and under hydrostatic pressure.

In 1D, the p_c of the very long range force system varies smoothly vs. T. But the p_c of the short range force system varies discontinuously. The absolute values of p_c, d_c and T_d are dependent on the size of the system, but the same behaviours are observed for every system size.

In 2D, the variation of p_c vs. T of the solid membranes of different force range, with or without vacancies, are alike. $|p_c|$ decreases almost linearly at high T. The gliding dislocation dipoles are created just before rupture for a wide range of interactions.

In 2D and at high T, the system with a very long range force melts first and then ruptures.

Chapter 8

Conclusions

Three related projects are presented in this thesis. They are the kinetics of vacancy annealing in monolayers, the calculation of elastic constants and the mechanical stability criteria for stressed materials, and the rupture of physical membranes. The elastic constants are relevant quantities in all three projects.

On the kinetics of vacancy annealing, we focused on the central force systems. Our studies show that above the self-diffusion temperature the isolated vacancies are unstable, they tend to condense into either larger voids or dislocation dipoles. What exactly happens depends strongly on the range of the interparticle interaction. A short range interaction favours the formation of large voids. However, when the local vacancy concentration is large enough, the vacancy annealing, in monolayers with long range interparticle interaction, is mainly through DMH. For a system with the intermediate range interactions the two behaviours compete. Pressure favours DMH. The mobility of vacancies, which may arise from the third degree of freedom or a higher temperature, also favours the phenomenon.

The DMH process is rapid, of the order of nanoseconds, in a different time scale than the exchange of atoms with the environment for an actual monolayer adsorbed on a substrate [58], when rare gas parameters are used for an infinite system. In contrast, void formation is slow, at least by an order of magnitude, and the more so for the shorter range potential.

Dislocations cause a collapse of the shear strength of the central force monolayers. This is related to the ease with which they anneal out of finite patches. In contrast,

even fairly large voids have no dramatic effect on the shear modulus which seems to be mainly a function of the vacancy concentration.

In an actual monolayer adsorbed on a substrate, the corrugation in the substrate field may have to be considered. The substrate corrugation screens out the interactions between atoms and reduces the diffusion of the vacancies. Consequently, the effects of the substrate modulating field tend to discourage DMH. The high vacancy concentration observed in some rare gas monolayers adsorbed on graphite therefore indicates significant substrate corrugation effects. Structurally these monolayers may be quite different from ideal monolayers.

It would be interesting to investigate the role that vacancies, which are unavoidable in experiments, play in the melting of a physisorbed system, in particular one with a weak substrate corrugation, such as Xe on Ag{111}. The vacancies may condense into clusters. Or, they may play a catalytic role in the creation of dislocation dipoles in a form of DMH, producing a melting transition with persistence of bond orientational order as predicted by the KTHNY theory.

The findings of our work are also helpful for a better understanding of the behaviour reported in bulk materials. In f.c.c. metals, systems with usually long range interactions, experiments observed in the first stage of annealing the clustering of vacancies and the collapse of voids into dislocation loops, the three dimensional equivalent of the dislocation dipole in two dimensions. The specific defect obtained depends on such factors as the stacking fault energy. A low stacking fault energy favours a tetrahedra of {111} planes of stacking faults. With high stacking fault energies, such as in Al, the collapse of the voids into dislocation loops in the {111} plane begins to occur even with clusters of a few vacancies, a behaviour likened to our 4-8P system. In a second stage at a higher temperature the loops are annealed out.

In semiconductors systems, with short range and strong bond angle stiffness, and where dislocations have high Peierls energies due to the covalent bonding, studies have focussed on the kinetics resulting from radiation damage. These kinetics are dominated by interstitials, vacancies, divacancies and other small complexes. The bond angle stiffness seems to reduce the diffusion of the vacancies and does not favour DMH.

There is a related problem, the generation of dislocations by condensation of

vacancies during the growth process. This nucleation process may obey the same physical principles.

With respect to the self-healing of damaged 2D systems, such as membranes, our studies suggest that several conditions permit physical mechanisms to be operative; diffusion of the vacancies, a long range interparticle interaction and pressure. As we saw above for the PLFM with a third degree of freedom or the 4-8M, the predominance of one property can diminish the reliance on the others. In biological membranes enough of the above conditions may be satisfied to have physical mechanisms of self-healing. The molecules usually form liquid phases, which presumably implies high diffusion coefficients. They are embedded in a pressurizing fluid and long range interactions can be present.

On the subject of the calculation of elastic constants, our work clarified the problem of the choice of the reference state for elastic quantities. It is especially important for a system subject to large stress. For a homogeneously deformed material, we obtained general expressions for the elastic constants and stresses in the canonical ensemble under arbitrary deformation and arbitrary interparticle interaction, they are

$$\begin{aligned} \mathring{C}_{\alpha\beta\sigma\tau} &= \mathring{C}^{B}{}_{\alpha\beta\sigma\tau} - \frac{1}{k_B T}\left(\left\langle \tilde{\mathrm{t}}^{U}_{\alpha\beta}\tilde{\mathrm{t}}^{U}_{\sigma\tau}\right\rangle - \left\langle \tilde{\mathrm{t}}^{U}_{\alpha\beta}\right\rangle\left\langle \tilde{\mathrm{t}}^{U}_{\sigma\tau}\right\rangle\right) \\ &\quad + \frac{N k_B T}{V}(\delta_{\alpha\sigma}\delta_{\beta\tau} + \delta_{\alpha\tau}\delta_{\beta\sigma}) \end{aligned} \tag{8.1}$$

$$\mathring{C}^{B}{}_{\alpha\beta\sigma\tau} = S\left(\frac{1}{V}\left\langle \sum_{i,j} 2x_{i\beta}x_{j\tau}\frac{\partial^2 U}{\partial x_{j\sigma}\partial x_{i\alpha}}\right\rangle + \left\langle \tilde{\mathrm{t}}^{U}_{\alpha\sigma}\right\rangle \delta_{\beta\tau}\right) \tag{8.2}$$

$$\tilde{\mathrm{t}}^{U}_{\alpha\beta} = -\frac{1}{V}\sum_{i}\left(x_{i\alpha}\frac{\partial U}{\partial x_{i\beta}} + x_{i\beta}\frac{\partial U}{\partial x_{i\alpha}}\right) \tag{8.3}$$

$$\mathring{S}_{\alpha\beta} = \frac{1}{V}\sum_{i}\left(x_{i\alpha}\frac{\partial U}{\partial x_{i\beta}} + x_{i\beta}\frac{\partial U}{\partial x_{i\alpha}}\right) - \frac{N k_B T}{V}\delta_{\alpha\beta} \tag{8.4}$$

where U is the potential energy of the system, V the volume of the current state. The Greek indices above refer to Cartesian components while Latin indices refer to particle numbers. S is a symmetrizing operator defined by its action on Cartesian coordinates:

$$S(A_{\alpha\beta\sigma\tau}) = \frac{1}{4}\left(A_{\alpha\beta\sigma\tau} + A_{\beta\alpha\sigma\tau} + A_{\alpha\beta\tau\sigma} + A_{\beta\alpha\tau\sigma}\right) \tag{8.5}$$

We also derived the correct fluctuation formulae for the constant shear strain ensembles which include the widely used uniform dilation ensembles.

On the topic of the mechanical stability, we established the thermodynamic foundation for the stability criteria and constructed the appropriate thermodynamic potential for a homogeneously deformed material under constant load. We pointed out that the stability criteria are dependent on the statistical ensemble. This point does not seem to have been made previously. We showed that for a homogeneously deformed material subject to an anisotropic constant load, the most general condition for mechanical stability is the positive definiteness of

$$\begin{aligned} C_{\alpha\beta\sigma\tau} \equiv \mathring{C}_{\alpha\beta\sigma\tau} - \frac{1}{2}(&\mathring{S}_{\alpha\beta}\,\delta_{\sigma\tau} + \mathring{S}_{\sigma\tau}\,\delta_{\alpha\beta} - \mathring{S}_{\alpha\sigma}\,\delta_{\beta\tau} \\ &- \mathring{S}_{\alpha\tau}\,\delta_{\beta\sigma} - \mathring{S}_{\beta\tau}\,\delta_{\alpha\sigma} - \mathring{S}_{\beta\sigma}\,\delta_{\alpha\tau}). \end{aligned} \tag{8.6}$$

We found that stability conditions in the constant pressure ensemble are stronger than in the constant volume ensemble i.e. a state can be stable in the constant volume ensemble but unstable in the constant pressure ensemble. We also derived exact formulae for elastic constants and elastic stiffness constants for two dimensional perfect systems with PLFP, LJP and 4-8P at zero temperature and isotropic stress.

Our studies show the importance in distinguishing $C_{\alpha\beta\sigma\tau}$, $\mathring{c}_{\alpha\beta\sigma\tau}$ and $\mathring{C}_{\alpha\beta\sigma\tau}$ for a stressed system. Acoustic experiments, related to the stability question, would measure $C_{\alpha\beta\sigma\tau}$ in the absence of stress and for isotropic stress. In direct experiments, such as elongation, the elastic stiffness coefficients $\mathring{c}_{\alpha\beta\sigma\tau}$ are measured. When constructing interatomic potentials, it may be preferable to work with an unstressed system, the only situation where the elastic constants $\mathring{C}_{\alpha\beta\sigma\tau}$ probe intrinsic properties of the system.

The stability criteria for a inhomogeneously deformed material are, however, unavailable. In this case, the second law of thermodynamics or Eq. (6.1) still works but the work function $\mathcal{W}$ may no longer be Eq. (6.19).

Finally, we showed that rupture at zero temperature occurs at the mechanical instability points for a homogeneously deformed material. However, in general, rupture at finite temperature takes place prior to mechanical instability due to

thermal fluctuations. We found that there is no structural transformation for a perfect system with LJP or 4-8P at zero temperature and subject to hydrostatic pressure.

We found that in both one and two dimensional systems, the critical rupture pressure and bulk modulus change rapidly at very low temperature but relatively slowly at high temperature. In two dimensions, the critical rupture pressure decreases almost linearly at high temperature and gliding dislocation dipoles are created just before rupture for several interactions, from nearest neighbour PLFP to fairly long range 4-8P. At high temperature and in two dimensional systems, the system with long range force melts first and then ruptures.

The work on rupture is preliminary and raises a number of questions. In the 2D vesicles, there are two regimes separated by a special temperature named T_1. What are the rupture kinetics in these two regimes is an interesting question. In the 2D flat membrane, why the behaviours of B_c, μ_c and d_c are sensitive to the range of the interactions but p_c is not, is still a mystery. Meanwhile, why $|p_c|$ decreases almost linearly, for all three kinds of interactions, at high temperature is also a secret. Furthermore, whether the rupture kinetics of liquid membranes is the same as that of solid membranes is a significant topic for further investigation. Our present work identifies the critical regime and gives a good starting point for further studies.

Appendix A

Molecular Dynamics Simulation Methods

A.1 Introduction

Since the birth of computers it has become possible to solve the classical equations of motion (Newton's equations) numerically for a set of particles. This technique is usually referred to as **Molecular Dymanics (MD)**. The first MD calculations were made by Alder and Wainwright [124] using hard-sphere and square-well potentials.

In this Appendix, we shall introduce some fundamental concepts and techniques used in MD. In section A.3.5, we shall also discuss briefly the correct form of the equations of motion for a system subject to arbitrary stress.

A.2 General Form of the Equations of Motion in Molecular Dynamics

The particle motions in MD simulations are determined by numerically integrating the equations of motion.

The equations of motion in MD can be derived from a Lagrangian by

$$\frac{d}{dt}\left(\frac{\partial \mathcal{L}}{\partial \dot{\mathbf{q}}_k}\right) - \left(\frac{\partial \mathcal{L}}{\partial \mathbf{q}_k}\right) = 0 \tag{A.1}$$

where $\mathbf{q}_k$ are generalized coordinates and $\dot{\mathbf{q}}_k$ their time derivatives. The Lagrangian is in general defined as

$$\mathcal{L}(\mathbf{q}, \dot{\mathbf{q}}) = \mathcal{K}(\mathbf{q}, \dot{\mathbf{q}}) - U(\mathbf{q}), \tag{A.2}$$

where $\mathcal{K}$ is the kinetic energy of the system and U the potential energy.

Equivalently, the equations of motion can also be obtained from the Hamiltonian equations of motion. The generalized momentum conjugate to $\mathbf{q}_k$ are defined as

$$\mathbf{p}_k = \frac{\partial \mathcal{L}}{\partial \dot{\mathbf{q}}_k}. \tag{A.3}$$

The Hamiltonian of the system can be written

$$\mathcal{H} = \sum_{k=1}^{N} \dot{\mathbf{q}}_k \cdot \mathbf{p}_k - \mathcal{L}(\mathbf{q}, \dot{\mathbf{q}}), \tag{A.4}$$

and the equations of motion become

$$\begin{aligned} \frac{d\mathbf{q}_k}{dt} &= \frac{\partial \mathcal{H}}{\partial \mathbf{p}_k} \\ \frac{d\mathbf{p}_k}{dt} &= -\frac{\partial \mathcal{H}}{\partial \mathbf{q}_k}. \end{aligned} \tag{A.5}$$

Different formulations of $\mathcal{L}$ or $\mathcal{H}$ lead to different ensembles, as we shall see in the next section.

A.3 Molecular Dynamics Ensembles

There are many ensembles in molecular dynamics simulations. The microcanonical (EVN) ensemble [13, 14, 15, 16], the canonical (TVN) ensemble [17, 18, 19], the isoenthalpic-isobaric (HPN) ensemble [20, 21] and the isothermal-isobaric (TPN) ensemble [16, 20, 21] are often used to simulate systems of well known symmetry. E is the energy, V the volume, N the particle number, T the temperature, H the enthalpy and P the hydrostatic pressure of the system. To deal with anisotropic solids subjected to arbitrary stress, Ray and Rahman modified Andersen's method for the (HPN) ensemble [20] to develop a new ensemble called the (HtN) ensemble [94, 128, 129], where t is the thermodynamic stress tensor. The following ensembles have also been proposed; (EhN), (ThN) and (TtN) [74, 75, 76, 77, 129, 130, 131], where $h = (\mathbf{a}, \mathbf{b}, \mathbf{c})$, and $\mathbf{a}, \mathbf{b}$ and $\mathbf{c}$ are the three vectors forming the MD cell.

A.3.1 Microcanonical (EVN) Ensemble

The molecular dynamics methods operate most naturally in the microcanonical ensemble i.e. the ensemble of constant energy E, constant volume V and constant particle number N. The Hamiltonian of the system in Cartesian coordinate system is

$$\mathcal{H} = \sum_{i}^{N} \frac{\mathbf{p}_i^2}{2m_i} + U(\mathbf{x}_1, \mathbf{x}_2, ..., \mathbf{x}_N) \tag{A.6}$$

where $\mathbf{x}_i$ is the position vector of particles. The equations of motion are

$$m_k \frac{d^2\mathbf{x}_k}{dt^2} = -\frac{\partial U}{\partial \mathbf{x}_k} \tag{A.7}$$

The half-step Verlet 'leap-frog' algorithm can be directly applied to this ensemble.

A.3.2 Canonical (TVN) Ensemble

The formulation of a rigorous canonical ensemble in MD was proposed first by S. Nosé [132] though some good approximation schemes had been given before. A little later, a different scheme was proposed by W. G. Hoover [133].

Nosé's Scheme - Rigorous Canonical Ensemble

Nosé's introduced some *virtual* variables (coordinate $\mathbf{q}_i$, momentum $\mathbf{p}_i'$ and time t') which are related to the *real* variables ($\mathbf{x}_i, \mathbf{p}_i, t$) by

$$\begin{aligned} \mathbf{q}_i &= \mathbf{x}_i \\ \mathbf{p}_i &= \frac{\mathbf{p}_i'}{s} \\ dt &= \frac{dt'}{s} \end{aligned} \tag{A.8}$$

s is a scaling factor of the real time. The Hamiltonian of the extended system is postulated as

$$\mathcal{H} = \sum_{i} \frac{\mathbf{p}_i'^2}{2m_i s^2} + U(\mathbf{x}) + \frac{p_s^2}{2Q} + gk_B T \ln s \tag{A.9}$$

where p_s is the conjugate momentum of s; Q is a parameter of dimension energy$\times$(time)^2 and behaves as a *mass* for the motion of s, k_B is Boltzmann's constant; the parameter, $g = 3N + 1$, is essentially equal to the number of degrees of freedom of the physical system.

Assuming the Hamiltonian formalism can be applied to Eq. (A.9) with the virtual variables, the equations of motion become

$$\begin{aligned}
\frac{d\mathbf{x}_i}{dt'} &= \frac{\partial \mathcal{H}}{\partial \mathbf{p}_i'} = \frac{\mathbf{p}_i'}{m_i s^2} \\
\frac{d\mathbf{p}_i'}{dt'} &= -\frac{\partial \mathcal{H}}{\partial \mathbf{x}_i} = -\frac{\partial U}{\partial \mathbf{x}_i} \\
\frac{ds}{dt'} &= \frac{\partial \mathcal{H}}{\partial p_s} = \frac{p_s}{Q} \\
\frac{dp_s}{dt'} &= -\frac{\partial \mathcal{H}}{\partial s} = \frac{1}{s}\left(\sum_i \frac{\mathbf{p}_i^2}{m_i} - g k_B T\right)
\end{aligned} \tag{A.10}$$

Or in Lagrangian form,

$$\begin{aligned}
\frac{d^2\mathbf{x}_i}{dt'^2} &= -\frac{1}{m_i s^2}\frac{\partial U}{\partial \mathbf{x}_i} - \frac{2}{s}\frac{ds}{dt'}\frac{d\mathbf{x}_i}{dt'} \\
Q\frac{d^2 s}{dt'^2} &= \frac{1}{s}\left(\sum_i \frac{1}{m_i} s^2 \left(\frac{d\mathbf{x}_i}{dt'}\right)^2 - g k_B T\right)
\end{aligned} \tag{A.11}$$

Though Nosé's scheme yields a rigorous canonical ensemble for real variables, it requires an extra variable s and its equations of motion are a little complex. As a consequence, it requires considerably longer computation time in simulations. Therefore, a good approximate canonical ensemble is sometimes useful.

Approximate Canonical Ensemble: Rescaling of Velocities

The simplest way to construct an approximate canonical ensemble is by scaling the velocities at every time step to keep the total kinetic energy as a constant in according to the required temperature using the same equations of motion as in the microcanonical ensemble. The half-step Verlet 'leap-frog' algorithm can be also applied to this ensemble [16].

Approximate Canonical Ensemble: Damped Force Method

Another simple way to yield a good approximate canonical ensemble is called the damped force method [19]. It involves the integration of a modified set of Hamiltonian equations of motion

$$\begin{aligned} \frac{d\mathbf{x}_i}{dt} &= \frac{\mathbf{p}_i}{m_i} \\ \frac{d\mathbf{p}_i}{dt} &= -\frac{\partial U}{\partial \mathbf{x}_i} - \frac{\alpha \mathbf{p}_i}{m_i} \end{aligned} \tag{A.12}$$

where α is the damped factor determined by requiring that $\frac{dT_{int}}{dt} = 0$ i.e. keeping the instant temperature T_{int} constant, where

$$T_{int} = \frac{1}{3(N-1)k_B} \sum_{i=1}^{N} \mathbf{p}_i \cdot \mathbf{p}_i / m_i \tag{A.13}$$

and so

$$\alpha = \frac{\sum_{i=1}^{N} m_i \mathbf{F}_i \cdot \mathbf{p}_i}{\sum_{i=1}^{N} \mathbf{p}_i \cdot \mathbf{p}_i} \tag{A.14}$$

where $\mathbf{F}_i = -\frac{\partial U}{\partial \mathbf{x}_i}$ is the force on particle i. Note that α is not constant in the simulation.

The half-step Verlet 'leap-frog' algorithm for this ensemble is in the form of

$$\begin{aligned} \mathbf{x}(t+\delta t) &= \mathbf{x}(t) + \dot{\mathbf{x}}(t+\frac{\delta t}{2}) \cdot \delta t \\ \dot{\mathbf{x}}(t+\frac{\delta t}{2}) &= \dot{\mathbf{x}}(t-\frac{\delta t}{2}) + \mathbf{a}(t) \cdot \delta t - \frac{1}{m} \alpha \, \dot{\mathbf{x}}(t) \delta t \end{aligned} \tag{A.15}$$

where $\mathbf{a}(t)$ is the acceleration of the particle. We can simplify the above equation by introducing the projected velocity

$$\begin{aligned} \dot{\mathbf{x}}'(t) &= \dot{\mathbf{x}}(t-\frac{\delta t}{2}) + \mathbf{a}(t) \cdot \delta t \\ \beta^2 &= \frac{3(N-1)k_B T}{m \sum \dot{\mathbf{x}}'^2(t)} \end{aligned} \tag{A.16}$$

so we rewrite

$$\dot{\mathbf{x}}(t+\frac{\delta t}{2}) = \dot{\mathbf{x}}(t-\frac{\delta t}{2})(2\beta - 1) + \beta \mathbf{a}(t) \cdot \delta t \tag{A.17}$$

A.3.3 Isoenthalpic-isobaric (HPN) Ensemble

The rigorous isoenthalpic-isobaric ensemble does not seem to be available in print. The first approximate isoenthalpic-isobaric ensemble was proposed by Andersen [20]. He introduced the scaled coordinate defined by

$$\mathbf{q} = \mathbf{x}/V^{1/3} \tag{A.18}$$

and the Hamiltonian of the system is written as

$$\mathcal{H} = \frac{1}{2}mV^{2/3}\sum_{i=1}^{N}\dot{\mathbf{q}}_i \cdot \dot{\mathbf{q}}_i + \sum_{i<j}^{N}\phi(V^{1/3}\mathbf{q}_{ij}) + \frac{1}{2}M\dot{V}^2 + PV, \tag{A.19}$$

where V is the volume of the system, M a constant which acts as an inertial "mass" for the change in volume, P the external pressure and $\mathbf{q}_{ij} = \mathbf{q}_i - \mathbf{q}_j$. The first two terms of the Hamiltonian (A.19) are equivalent to the internal energy of the particles in the system. The third term is a kinetic energy for the motion of V, and the fourth represents a potential energy associated with V. The momentum of the particles are assumed to be

$$\mathbf{p}_i = mV^{1/3}\dot{\mathbf{q}}_i \tag{A.20}$$

Note that in this ensemble, $\mathbf{p}_i \neq m\dot{\mathbf{x}}_i$. The ensemble average $\langle\mathcal{H}(t)\rangle$ differs from the enthalpy of the N-particle system by $\frac{1}{2}k_BT$ which is the average kinetic energy associated with the volume fluctuations i.e. $\left\langle\frac{1}{2}M\dot{V}^2\right\rangle$.

The equations of motion are of the form

$$\begin{aligned}\frac{d^2\mathbf{q}_i}{dt^2} &= \frac{\mathbf{F}_i}{mV^{1/3}} - \frac{2}{3V}\frac{d\mathbf{q}_i}{dt}\frac{dV}{dt} \\ \frac{d^2V}{dt^2} &= \frac{\mathcal{P}-P}{M}\end{aligned} \tag{A.21}$$

with $\mathcal{P}$ the microscopic pressure given by

$$\mathcal{P} = \frac{1}{3V}\left(\sum_{i=1}^{N}\frac{1}{m}\mathbf{p}_i \cdot \mathbf{p}_i + \sum_{i>j}\mathbf{x}_{ij} \cdot \mathbf{F}_{ij}\right) \tag{A.22}$$

where $\mathbf{x}_{ij} = \mathbf{x}_i - \mathbf{x}_j$, and $\mathbf{F}_{ij}$ is the force on atom i due to atom j.

Transforming the equations of motion from scaled coordinates to real coordinates, they become [16]

$$\frac{d^2\mathbf{x}_i}{dt^2} = \frac{\mathbf{F}_i}{m} + \frac{\mathbf{x}_i}{3V}\left(\frac{d^2V}{dt^2} - \frac{2}{3V}\left(\frac{dV}{dt}\right)^2\right) \tag{A.23}$$

$$\frac{d^2V}{dt^2} = \frac{\mathcal{P} - P}{M} \tag{A.24}$$

(In ref. [16], the last term in Eq. (A.23), their Eq. (4.12), is incorrect. It is easy to see this by checking the dimension).

The Verlet algorithm can be applied to Eqs (A.23)-(A.24) by using

$$\begin{aligned} V(t+\delta t) &= 2V(t) - V(t-\delta t) + \frac{\mathcal{P}(t) - P}{M}\delta t^2 \\ \dot{V}(t) &= \frac{V(t+\delta t) - V(t-\delta t)}{2\delta t} \\ \dot{\mathbf{x}}_i(t+\frac{\delta t}{2}) &= \dot{\mathbf{x}}_i(t-\frac{\delta t}{2}) + \left(\frac{\mathbf{F}_i(t)}{m} + \frac{\mathbf{x}_i(t)}{3V(t)}\left(\ddot{V}(t) - \frac{2}{3V(t)}\dot{V}^2(t)\right)\right)\delta t \\ \mathbf{x}(t+\delta t) &= \mathbf{x}(t) + \dot{\mathbf{x}}(t+\frac{\delta t}{2})\cdot\delta t \end{aligned} \tag{A.25}$$

The trajectory averages or the equilibrium averages in the simulation are independent of the value of M, as long as M is finite and positive [20, 134]. However, the value of M affects the fluctuations and the rate at which the system approaches equilibrium. Andersen has suggested [20] that it would be appropriate to choose M so that the time-scale for the volume fluctuations is approximately equal to the time taken for a sound wave to travel from one end of the sample to the other.

A.3.4 Isothermal-isobaric (TPN) Ensemble

The formulation of a rigorous isothermal-isobaric ensemble in MD was also proposed first by S. Nosé [132]. A different scheme has been put forward by W. G. Hoover [133] which was modified by Melchionna et. al [135].

Nosé's Scheme - Rigorous TPN Ensemble

Combining it with the constant pressure MD method of Andersen [20], Nosé extended his canonical ensemble MD method to the TPN ensemble [132]. In this

scheme, he introduced the virtual variables $(\mathbf{q}_i, \mathbf{p}'_i, t')$ which are related to the *real* variables $(\mathbf{x}_i, \mathbf{p}_i, t)$ by

$$\begin{aligned} \mathbf{x}_i &= \mathbf{q}_i V^{1/3} \\ \mathbf{p}_i &= \frac{\mathbf{p}'_i}{V^{1/3} s} \\ dt &= \frac{dt'}{s} \end{aligned} \tag{A.26}$$

The Hamiltonian of the extended system is postulated as

$$\mathcal{H} = \sum_i \frac{\mathbf{p}'^2_i}{2m_i V^{2/3} s^2} + U(V^{1/3}\mathbf{q}) + \frac{p_s^2}{2Q} + g k_B T \ln s + \frac{p_V^2}{2M} + PV \tag{A.27}$$

where p_V is the momentum conjugate to V. The equations of motion, in Lagrangian form, become

$$\begin{aligned} \frac{d}{dt'}\left(m_i V^{2/3} s^2 \frac{d\mathbf{q}_i}{dt'}\right) &= -\frac{\partial U}{\partial \mathbf{x}_i} V^{1/3} \\ \frac{d}{dt'}\left(Q\frac{ds}{dt'}\right) &= \frac{1}{s}\left(\sum_i \frac{1}{m_i} V^{2/3} s^2 \left(\frac{d\mathbf{q}_i}{dt'}\right)^2 - g k_B T\right) \\ \frac{d}{dt'}\left(M\frac{dV}{dt'}\right) &= \frac{1}{3V}\sum_i \left(\frac{1}{m_i} V^{2/3} s^2 \left(\frac{d\mathbf{q}_i}{dt'}\right)^2 - \frac{\partial U}{\partial \mathbf{x}_i}\cdot \mathbf{x}_i\right) - P \end{aligned} \tag{A.28}$$

Approximate TPN Ensemble: Scaled Coordinates and Damped Force Method

Combining the Andersen method with the damped force method for the canonical ensemble, we can get an approximate TPN ensemble [16]. The algorithm in the simulation can be written as:

$$\begin{aligned} V(t+\delta t) &= 2V(t) - V(t-\delta t) + \frac{\mathcal{P}(t) - P}{M}\delta t^2 \\ \dot{\mathrm{V}}(t) &= \frac{V(t+\delta t) - V(t-\delta t)}{2\delta t} \\ \dot{\mathbf{x}}_i(t+\frac{\delta t}{2}) &= \dot{\mathbf{x}}_i(t-\frac{\delta t}{2})(2\beta - 1) + (1-\beta)\frac{2}{3V(t)}\mathbf{x}_i(t)\dot{\mathrm{V}}(t) \end{aligned}$$

$$+\beta\left(\frac{\mathbf{F}_i(t)}{m}+\frac{\mathbf{x}_i(t)}{3V(t)}\left(\ddot{\mathrm{V}}(t)-\frac{2}{3V(t)}\dot{\mathrm{V}}^2(t)\right)\right)\delta t \qquad \text{(A.29)}$$

$$\mathbf{x}(t+\delta t) = \mathbf{x}(t)+\dot{\mathbf{x}}(t+\frac{\delta t}{2})\cdot\delta t, \qquad \text{(A.30)}$$

where

$$\beta^2=\frac{3(N-1)k_BT}{m\sum_i\dot{\mathbf{x}}_i^2(t)}, \qquad \text{(A.31)}$$

and the projected velocities

$$\dot{\mathbf{x}}_i'(t) = \dot{\mathbf{x}}_i(t-\frac{\delta t}{2})+\left(\frac{\mathbf{F}_i(t)}{m}+\frac{\mathbf{x}_i(t)}{3V(t)}\left(\ddot{\mathrm{V}}(t)-\frac{2}{3V(t)}\dot{\mathrm{V}}^2(t)\right)\right)\frac{\delta t}{2}$$
$$-\frac{\dot{\mathbf{x}}_i(t)}{3V(t)}\dot{\mathrm{V}}(t). \qquad \text{(A.32)}$$

(Again we have to point out that in ref. [16], the last term of Eq. (A.29), their Eq. (5.4), is incorrect.)

In this method the velocity of a particle is dependent on the volume variation

$$\dot{\mathbf{x}}_i=\frac{\mathbf{p}_i}{m}+\frac{\mathbf{x}_i}{3V}\frac{dV}{dt} \qquad \text{(A.33)}$$

Therefore, both the position and the velocity of a particle have to be altered if a boundary is crossed.

Approximate *TPN* Ensemble: Evans and Morriss Scheme

Another approximate *TPN* ensemble was proposed by Evans and Morriss [21]. The equations of motion in this method are

$$\frac{d\mathbf{x}_i}{dt} = \frac{\mathbf{p}_i}{m}+\dot{\mathrm{e}}\mathbf{x}_i$$
$$\frac{d\mathbf{p}_i}{dt} = \mathbf{F}_i-\dot{\mathrm{e}}\mathbf{p}_i-\alpha\mathbf{p}_i \qquad \text{(A.34)}$$

where $\dot{\mathrm{e}}$ is termed the dilation rate and related to the rate of volume change by $\dot{\mathrm{V}}(t)=3V\dot{\mathrm{e}}$ and

$$\alpha = \frac{\sum_i\mathbf{p}_i\cdot\mathbf{F}_i}{\sum_i\mathbf{p}_i\cdot\mathbf{p}_i}-\dot{\mathrm{e}}$$
$$\dot{\mathrm{e}} = -\frac{1}{2m}\sum_{i>j}(\mathbf{x}_{ij}\cdot\mathbf{p}_{ij})(\phi_{ij}''+\phi_{ij}'/r_{ij})\left(\frac{1}{2}\sum_{i>j}\mathbf{x}_{ij}^2(\phi_{ij}''+\phi_{ij}'/r_{ij})+9PV\right)^{-1} \qquad \text{(A.35)}$$

$\mathbf{x}_{ij} = \mathbf{x}_i - \mathbf{x}_j, \mathbf{p}_{ij} = \mathbf{p}_i - \mathbf{p}_j, r_{ij}^2 = \mathbf{x}_{ij}^2$ and the potential energy of the particles is assumed to be pairwise additive.

$$U = \sum_{i>j} \phi_{ij} \tag{A.36}$$

A.3.5 Molecular Dynamics Methods for Anisotropic Systems

So far we have discussed MD ensembles with a fixed shape of the MD cell. These ensembles, however, are not appropriate to describe anisotropic solids subjected to arbitrary stress. To deal with this problem, Parrinelo and Rahman developed two new ensembles called (HtN) and (TtN) ensembles [74, 75, 128, 129].

The Hamiltonian in Ray and Rahman's (TtN) ensemble for a central force system can be written [75]

$$\begin{aligned} \mathcal{H} &= \sum_a \frac{\Pi'(a) G^{-1} \Pi(a)}{2 m'_a s^2} + \sum_{a<b} \phi\left(\mathbf{x}(a) - \mathbf{x}(b)\right) + g k_B T \ln s \\ &\quad + \frac{\Pi_s^2}{2Q} + K_{cell} + V_0 \mathrm{Tr}(t\eta) \end{aligned} \tag{A.37}$$

with

$$K_{cell} = \frac{1}{2W} \mathrm{Tr}(\Pi_h \Pi'_h) \tag{A.38}$$

$$\mathbf{x}(a) = h\mathbf{q}(a) \qquad \mathbf{p}(a) = h'^{-1}\Pi(a) \tag{A.39}$$

$$m_a = m'_a s^2 \qquad G = h'h \tag{A.40}$$

$$\eta = \frac{1}{2}\left(h_0'^{-1} G h_0^{-1} - 1\right) \tag{A.41}$$

$$t = \frac{V}{V_0} h_0 h^{-1} \sigma h'^{-1} h'_0 \tag{A.42}$$

where $\mathbf{x}(a)$ is the coordinate of the particle a in real space, $\mathbf{q}(a)$ the scaled coordinate, $\mathbf{p}(a)$ the real momentum, $\Pi(a)$ the momentum conjugate to $\mathbf{q}(a)$, the real mass of the particle, m'_a the scaled mass, s the scaling factor of the mass, Π_s the momentum conjugate to s. h_0 is the reference value of h, a tensor constructed from the three vectors forming a parallelepiped, which is the periodic MD cell. h' is the transfer of h, $G = hh'$ the metric tensor, η the Lagrangian strain tensor, V_0 the volume $V = \det(h)$ at reference state, σ the applied stress. Π_h the momentum conjugate to

h. Q and W are constants. $g = 3N+1$, N is the number of particles in the system, k_B the Boltzmann constant. The Einstein summation convention for repeated suffices is used.

The equations of motion which follow from this Hamiltonian have the form [75]

$$\ddot{\mathbf{q}}(a) = -\frac{2}{m_a s^3} G^{-1}\Pi(a)\dot{s} - G^{-1}\dot{G}\dot{\mathbf{q}}(a) - \frac{1}{m_a s^2}\sum_{b\neq a} g(r(ab))\mathbf{q}(ab) \quad \text{(A.43)}$$

$$Q\ddot{s} = \frac{1}{s}\left(\sum_a \frac{1}{m_a s^2}\Pi'(a)G^{-1}\Pi(a) - gk_BT\right) \quad \text{(A.44)}$$

$$W\ddot{h} = \mathcal{P}A - h\Gamma \quad \text{(A.45)}$$

with

$$\Gamma = V_0 h_0^{-1} t (h_0')^{-1} \quad \text{(A.46)}$$

$$A = V h'^{-1} \quad \text{(A.47)}$$

$$g(r) = \frac{1}{r}\frac{d\phi(r)}{dr}, \qquad r^2(ab) = (x_i(a) - x_i(b))^2 \quad \text{(A.48)}$$

and $\mathcal{P}$ the microscopic stress

$$\mathcal{P}_{ij} = \frac{1}{V}\left(\sum_a \frac{p_i(a)p_j(a)}{m_a s^2} - \sum_{a>b} g(r(ab))x_i(ab)x_j(ab)\right) \quad \text{(A.49)}$$

If we set $s \equiv 1$ so that $\dot{s} = 0$ and $\ddot{s} = 0$ in Eqs. (A.43) - (A.49), we obtain the equations of motion for the (HtN) ensemble [74, 129].

In Eq. (A.45), a reference value h_0 which comes from the definition of η i.e. Eq. (A.41) is required. Ray and Rahman [74, 75] suggested that h_0 should be the average value of h when the stress is zero. However, in this way one introduces an absolute reference state for strain which creates problems for the expressions of the stress and elastic constants, as we have discussed in Chapter 5. Moreover, the applied stress σ fluctuates in this constant t ensemble as shown in Eq. (A.42) and therefore this ensemble has no proper isotropic limit. To solve these problems, in the same way as the discussion about the elastic constants, one should first choose h_0 as the average of the current state i.e. $h_0 =< h >$. Furthermore, one should change the definition of t i.e. Eq. (A.42). Remembering that the relationship between t and applied stress ([25, 83, 88]) is derived from the elasticity theory - a macroscopic

theory, it is better to use the macroscopic form of h i.e. the ensemble average of h in the definition of t so

$$t = \frac{< V >}{V_0} h_0 < h >^{-1} \sigma < h' >^{-1} h'_0 \tag{A.50}$$

With this choice, we change neither the equations of motion i.e. Eqs. (A.43) - (A.49) nor the conclusion that the average calculated using the trajectories generated by these equations is equal to the (TtN) ensemble average [75]. But Eq. (A.45) can be changed into

$$W\ddot{h} = \mathcal{P}A - h\Gamma' \tag{A.51}$$

where $\Gamma' =< V >< h >^{-1} \sigma < h' >^{-1}$. The reference value h_0 does not appear in the equations of the motion any more and both t and σ are constants now. For the (HtN) ensemble, the new equations of motion are identical to that of reference [129].

Because the new equations of motion need $< h >$, one has to do self-consistent calculations in the simulations. It causes no difficulty for a steady state problem. However, they seem inappropriate if we want to study the kinetics of a structural transformation, since $< h >$ will be highly unstable during this time interval.

A.4 Finite Difference Methods

A standard method for the solution of ordinary differential equations such as Eqs (A.1) and (A.5) is the finite difference approach. The general idea is as follows. Given the particle positions, velocities and other dynamic information at time t, we attempt to obtain the positions, velocities etc. at a later time $t + \delta t$, to a sufficient degree of accuracy. The equations are solved on a step-by-step basis; the choice of the time interval δt (also called the basic time step in MD) will be dependent somewhat on the method of solution, but δt must be small enough so it is of the order of the real microscopic time scales of the system.

Many different algorithms fall into the general finite difference pattern. We present as follows two of the most widely used algorithms in MD. We, have ourselves used both.

A.4.1 The Verlet Leap-frog Algorithm

Perhaps the most widely used method of integrating the equations of motion is that initially adopted by Verlet [14, 15] and modified by Hockney and Potter [125, 126], the so-called half-step Verlet 'leap-frog' algorithm. This method is a direct solution of the second-order Eqs. (A.1). The origin of the name becomes apparent when we write the algorithm down:

$$\begin{aligned} \mathbf{q}(t+\delta t) &= \mathbf{q}(t) + \dot{\mathbf{q}}(t+\frac{\delta t}{2}) \cdot \delta t \\ \dot{\mathbf{q}}(t+\frac{\delta t}{2}) &= \dot{\mathbf{q}}(t-\frac{\delta t}{2}) + \mathbf{a}(t) \cdot \delta t, \end{aligned} \tag{A.52}$$

where $\mathbf{a}(t)$ is the acceleration of $\mathbf{q}$. The stored quantities are the current position $\mathbf{q}(t)$ and acceleration $\mathbf{a}(t)$ together with the mid-step velocities $\dot{\mathbf{q}}(t-\frac{1}{2}\delta t)$. The velocity equation is implemented first, and the velocities leap over the coordinates to give the next mid-step values $\dot{\mathbf{q}}(t+\frac{1}{2}\delta t)$. During this step, the current velocities may be calculated

$$\dot{\mathbf{q}}(t) = \frac{1}{2}\left(\dot{\mathbf{q}}(t+\frac{\delta t}{2}) + \dot{\mathbf{q}}(t-\frac{\delta t}{2})\right). \tag{A.53}$$

This is necessary so that the energy as well as any other quantities dependent on the velocities at time t can be calculated.

This method requires essentially $9N$ words of storage making it very compact and simple to program. The algorithm is exactly reversible in time because $\dot{\mathbf{q}}\,(t+\frac{\delta t}{2})$ and $\dot{\mathbf{q}}\,(t-\frac{\delta t}{2})$ play symmetrical roles. Given conservative forces, it is guaranteed to conserve linear momentum.

A.4.2 The Gear Predictor-corrector Algorithm

The Verlet algorithm can work properly only if the generalized forces or accelerations do not depend on the velocities. In case where the accelerations are dependent on the velocities, the Gear predictor-corrector algorithm is widely used. This method can be illustrated as follows.

For a continuous classical trajectory, an estimate of the positions, velocities etc. at time $t+\delta t$ may be obtained by Taylor expansion about time t:

$$\mathbf{q}^p(t+\delta t) = \mathbf{q}(t) + \dot{\mathbf{q}}(t)\delta t + \frac{1}{2}\mathbf{a}(t)\delta t^2 + \frac{1}{6}\mathbf{b}(t)\delta t^3 + \ldots$$

$$\begin{aligned}
\dot{\mathbf{q}}^p(t+\delta t) &= \dot{\mathbf{q}}(t) + \mathbf{a}(t)\delta t + \frac{1}{2}\mathbf{b}(t)\delta t^2 + \ldots \\
\mathbf{a}^p(t+\delta t) &= \mathbf{a}(t) + \mathbf{b}(t)\delta t + \ldots \\
\mathbf{b}^p(t+\delta t) &= \mathbf{b}(t) + \ldots
\end{aligned} \tag{A.54}$$

The superscript marks these as 'predicted' values: we shall be 'correcting' them shortly. $\mathbf{b}(t)$ denotes the third time derivatives of $\mathbf{q}(t)$. An equation like Eq. (A.54) will not generate correct trajectories as time advances because we have not introduced the equations of motion. These enter through the correction step. We may calculate, from the new position $\mathbf{q}^p$, the force at time $t+\delta t$, and hence the correct accelerations $\mathbf{a}^c(t+\delta t)$. These can be compared with the predicted accelerations from Eqs. (A.54), to estimate the size of the error in the prediction step:

$$\Delta\mathbf{a}(t+\delta t) = \mathbf{a}^c(t+\delta t) - \mathbf{a}^p(t+\delta t) \tag{A.55}$$

This error, and the results of the predictor step, are fed into the corrector step, which reads, typically,

$$\begin{aligned}
\mathbf{q}^c(t+\delta t) &= \mathbf{q}^p(t+\delta t) + c_0\Delta\mathbf{a}(t+\delta t) \\
\dot{\mathbf{q}}^c(t+\delta t) &= \dot{\mathbf{q}}^p(t+\delta t) + c_1\Delta\mathbf{a}(t+\delta t) \\
\mathbf{a}^c(t+\delta t) &= \mathbf{a}^p(t+\delta t) + c_2\Delta\mathbf{a}(t+\delta t) \\
\mathbf{b}^c(t+\delta t) &= \mathbf{b}^p(t+\delta t) + c_3\Delta\mathbf{a}(t+\delta t)
\end{aligned} \tag{A.56}$$

The idea is that $\mathbf{q}^c(t+\delta t)$ etc. are now better approximations to the true values.

For the purpose of optimum stability and accuracy of trajectories, different values of the coefficients $c_0, c_1, c_2, c_3 \ldots$ are required if we include more (or fewer) position derivatives in our scheme, and the coefficients also depend upon the order of the differential equation being solved. Tables A.1 - A.2 give the coefficients proposed by Gear [127].

Therefore, the general scheme of a stepwise MD simulation, based on a predictor-corrector algorithm, may be summarized as follows:

(a) predict the positions, velocities, accelerations etc., at a time $t+\delta t$, using the current values of these quantities;

(b) evaluate the forces and hence accelerations from the new positions and velocities;

Table A.1: Gear corrector coefficients for a first-order equation.

Order	c_0	c_1	c_2	c_3	c_4	c_5
3	5/12	1	1/2			
4	3/8	1	3/4	1/6		
5	251/720	1	11/12	1/3	1/24	
6	95/288	1	25/24	35/72	5/48	1/120

Table A.2: Gear corrector coefficients for a second-order equation.

Order	c_0	c_1	c_2	c_3	c_4	c_5
3	0	1	1			
4	1/6	5/6	1	1/3		
5	19/120	3/4	1	1/2	1/12	
6	3/20	251/360	1	11/18	1/6	1/60

(c) correct the predicted positions, velocities, accelerations etc., using the new accelerations;

(d) calculate any variables of interest such as energy, pressure, order parameters, ready for the accumulation of time averages, before returning to (a) for the next step.

A.4.3 Neighbour Lists

The most time-consuming part of a computer simulation program is the calculation of the forces on the particles. For a system of N particles, forces are computed by sampling, at each time step of the simulation, $N(N-1)/2$ unique r_{ij} distances. But when a truncated potential is used, the force equals zero for any $r_{ij} > r_c$ (where r_c is the potential cutoff distance); consequently, evaluating distances r_{ij} that are greater than r_c wastes computer time.

Time can be saved, especially for a system of over 1000 particles, by using a bookkeeping scheme called cell index method [136, 137]. The computer cell is divided into small mesh cells with length slightly larger than the cutoff distance shown in Fig. A.1. For each particle i, say in mesh cell a, the forces acting on particle i are

nonzero only from particles in cell a and in the neighbouring mesh cells, for 2D, 8 neighbouring mesh cells, and 26 neighbouring mesh cells for 3D.

The cell structure may be set up and used by the method of linked lists [137, 138]. The first part of the method involves sorting all particles into their appropriate cells. This sorting is rapid and may be performed at every step. Two arrays are created during the sorting process. The 'head of chain' array (HEAD) has one element for each cell. This element contains the identification number of one of the particles sorted into that cell. This number is used to address the element of a linked-list array (LIST), which contains the number of the next particle in that cell. In turn, the LIST array element for that particle is the index of the next particle in the cell, and so on. If we follow the trail of link-list references, we will eventually reach an element of LIST which is zero. This indicates that there are no more particles in that cell, and we move on to the head-of-chain particle for the next cell. Sometimes another array is used to record the number of particles in each cell.

The calculation of the force is performed by looping over all cells. For a given cell, the program sorts through the linked list. A particular particle on the list may interact with all particles in the same cell that are further down the list. This avoids counting ij interactions twice.

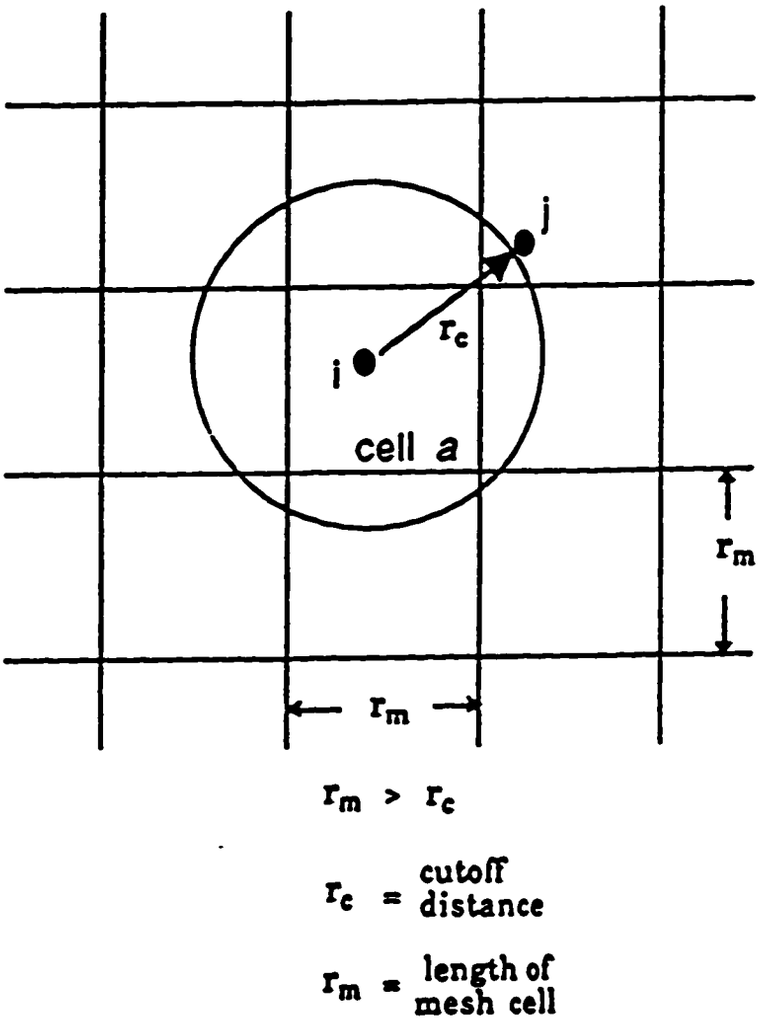

Figure A.1: In the force calculation, the primary cell is divided into smaller mesh cells with size slightly larger than cutoff distance. Contributions to the force f_i on atom i in mesh cell a are nonzero only from atoms j in cell a and 8 neighbouring cells.

Appendix B

Volume Variation and the Relationship Between $t_{\alpha\beta}$ and $T_{\alpha\beta}$

B.1 Introduction

In this Appendix, we derive the expressions for the volume variation and the relationship between $t_{\alpha\beta}$ and $T_{\alpha\beta}$. These expressions are used in Chapters 5 and 6.

B.2 Volume Variation

After deformation, the variation in the volume can be written [25, 83, 88]

$$\begin{aligned}\frac{V}{V_o} &= \det(J) = \det(\delta_{\alpha\beta} + u_{\alpha\beta}) \\ &= (1+u_{11})(1+u_{22})(1+u_{33}) + u_{12}u_{23}u_{31} + u_{21}u_{13}u_{32} \\ &\quad -(1+u_{11})u_{23}u_{32} - (1+u_{22})u_{13}u_{31} - (1+u_{33})u_{12}u_{21} \end{aligned} \tag{B.1}$$

where J is given by Eq. (5.25). Therefore

$$\begin{aligned}\frac{1}{V_0}\left(\frac{\partial V}{\partial u_{ij}}\right)_{u=0} &= \delta_{ij} \\ \frac{1}{V_0}\left(\frac{\partial^2 V}{\partial u_{ii}\partial u_{ii}}\right)_{u=0} &= 0\end{aligned} \tag{B.2}$$

$$\begin{aligned}
\frac{1}{V_0}\left(\frac{\partial^2 V}{\partial u_{ii}\partial u_{jj}}\right)_{u=0} &= 1 \qquad \text{for } i \neq j \\
\frac{1}{V_0}\left(\frac{\partial^2 V}{\partial u_{ij}\partial u_{ji}}\right)_{u=0} &= -1 \qquad \text{for } i \neq j \\
\frac{1}{V_0}\left(\frac{\partial^2 V}{\partial u_{ij}\partial u_{kl}}\right)_{u=0} &= 0 \qquad \text{otherwise}
\end{aligned} \tag{B.3}$$

or

$$\frac{1}{V_0}\left(\frac{\partial^2 V}{\partial u_{ij}\partial u_{kl}}\right)_{u=0} = \delta_{ij}\delta_{kl} - \delta_{il}\delta_{jk} \tag{B.4}$$

Expand $(V - V_0)/V_0$ as a Taylor series of u and η,

$$\begin{aligned}
\frac{V - V_o}{V_o} &= \frac{1}{V_0}\left(\frac{\partial V}{\partial u_{ij}}\right)_{u=0} u_{ij} + \frac{1}{2V_0}\left(\frac{\partial^2 V}{\partial u_{ij}\partial u_{kl}}\right)_{u=0} u_{ij}u_{kl} \\
&= \frac{1}{V_0}\left(\frac{\partial V}{\partial \eta_{ij}}\right)_{\eta=0} \eta_{ij} + \frac{1}{2V_0}\left(\frac{\partial^2 V}{\partial \eta_{ij}\partial \eta_{kl}}\right)_{\eta=0} \eta_{ij}\eta_{kl}
\end{aligned} \tag{B.5}$$

Substituting for

$$\eta_{\alpha\beta} \equiv \frac{1}{2}(u_{\alpha\beta} + u_{\beta\alpha} + u_{\gamma\alpha}u_{\gamma\beta}) \tag{B.6}$$

in Eq. (B.5), it is easy to show that

$$\frac{1}{V_0}\left(\frac{\partial V}{\partial u_{ij}}\right)_{u=0} = \frac{1}{V_0}\left(\frac{\partial V}{\partial \eta_{ij}}\right)_{\eta=0} = \delta_{ij} \tag{B.7}$$

$$\begin{aligned}
\frac{1}{V_0}\left(\frac{\partial^2 V}{\partial \eta_{ij}\partial \eta_{kl}}\right)_{\eta=0} &= \frac{1}{V_0}\left(\frac{\partial^2 V}{\partial u_{ij}\partial u_{kl}}\right)_{u=0} - \delta_{ik}\delta_{jl} \\
&= \delta_{ij}\delta_{kl} - \delta_{il}\delta_{jk} - \delta_{ik}\delta_{jl}
\end{aligned} \tag{B.8}$$

In two dimensions, $A/A_0 = (1 + u_{11})(1 + u_{22}) - u_{12}u_{21}$, where A is the area, Eqs. (B.7) and (B.8) are also valid.

B.3 The Relationship Between $t_{\alpha\beta}$ and $T_{\alpha\beta}$

To first order in u, from Eq. (5.25), it is easy to obtain

$$J^{-1}_{\alpha\beta} = (u_{\sigma\sigma}\delta_{\alpha\beta} + \delta_{\alpha\beta} - u_{\alpha\beta})/\det(J) = \delta_{\alpha\beta} - u_{\alpha\beta}$$

$$\begin{aligned} \det(J) &= 1 + u_{\sigma\sigma} \\ \frac{1}{\det(J)} &= 1 - u_{\sigma\sigma} \end{aligned} \tag{B.9}$$

Therefore, from (5.24) and use $T_{\alpha\beta} = T_{\beta\alpha}$, we find to leading order

$$\begin{aligned} t_{\alpha\beta} &= \det(J) \cdot J^{-1}_{\alpha\sigma} J^{-1}_{\beta\tau} T_{\sigma\tau} \\ &= (1 + u_{ii})(\delta_{\alpha\sigma} - u_{\alpha\sigma})(\delta_{\beta\tau} - u_{\beta\tau}) T_{\sigma\tau} \\ &= (1 + u_{ii})(\delta_{\alpha\sigma}\delta_{\beta\tau} - u_{\alpha\sigma}\delta_{\beta\tau} - u_{\beta\tau}\delta_{\alpha\sigma}) T_{\sigma\tau} \\ &= (\delta_{\alpha\sigma}\delta_{\beta\tau} - u_{\alpha\sigma}\delta_{\beta\tau} - u_{\beta\tau}\delta_{\alpha\sigma} + u_{ii}\delta_{\alpha\sigma}\delta_{\beta\tau}) T_{\sigma\tau} \\ &= T_{\alpha\beta} + T_{\alpha\beta} u_{\sigma\sigma} - T_{\sigma\beta} u_{\alpha\sigma} - T_{\alpha\tau} u_{\beta\tau} \\ &= T_{\alpha\beta} + T_{\alpha\beta} u_{\sigma\sigma} - \frac{1}{2}(T_{\sigma\beta} u_{\alpha\sigma} + T_{\sigma\alpha} u_{\beta\sigma} + T_{\alpha\tau} u_{\beta\tau} + T_{\beta\tau} u_{\alpha\tau}) \\ &= T_{\alpha\beta} + \frac{1}{2}(2T_{\alpha\beta}\delta_{\sigma\tau} - T_{\tau\beta}\delta_{\alpha\sigma} - T_{\tau\alpha}\delta_{\beta\sigma} - T_{\alpha\tau}\delta_{\beta\sigma} - T_{\beta\tau}\delta_{\alpha\sigma}) u_{\sigma\tau} \\ &= T_{\alpha\beta} + \frac{1}{2}(2T_{\alpha\beta}\delta_{\sigma\tau} - T_{\tau\beta}\delta_{\alpha\sigma} - T_{\tau\alpha}\delta_{\beta\sigma} - T_{\alpha\tau}\delta_{\beta\sigma} - T_{\beta\tau}\delta_{\alpha\sigma}) \eta_{\sigma\tau} \\ &\quad - T_{\beta\sigma}\omega_{\alpha\sigma} - T_{\alpha\sigma}\omega_{\beta\sigma} \end{aligned} \tag{B.10}$$

In general, the $\omega_{\alpha\beta}$ are disregarded. This equation is used in section 6.4.3.

Appendix C

Derivation and Simplification of the Expressions for Elastic Constants in the Central Force System

C.1 Introduction

In this appendix, we first derive in detail the expressions for isothermal elastic constants in the central force system by using scaled coordinates and scaled momenta. This derivation is lengthy and it is not found in the literature. We then prove that with the correct reference value, these are exactly the same as Eq. (5.48). The adiabatic elastic constants can be found in an analogous way using Eq. (D.22), but excluding the constraints of $\alpha \neq \beta$ and $\sigma \neq \tau$.

C.2 Fundamental Definitions in Molecular Dynamics

Helmholtz free energy

$$\begin{aligned} F &= E - TS = -k_B T \ln Z \\ Z &= \frac{1}{C} \int e^{-\mathcal{H}/k_B T} d\Gamma \end{aligned} \tag{C.1}$$

where $\mathcal{H}$ is the Hamiltonian of the system, C a constant, $d\tau$ the differential volume element in the 6-N-dimensional phase space and k_B the Boltzmann constant.

For a central force system

$$\mathcal{H} = \sum_a \frac{p^2(a)}{2m} + \sum_{a<b} \phi(|\, \mathbf{x}(a) - \mathbf{x}(b)\, |) \tag{C.2}$$

The conventional definition of isothermal elastic constants in molecular dynamics is written

$$\overset{\circ}{C}{}^T{}_{\alpha\beta\sigma\tau} \equiv \frac{1}{V_o}\frac{\partial^2 F}{\partial\eta_{\alpha\beta}\partial\eta_{\sigma\tau}} \equiv \frac{1}{V_o}\frac{\partial t_{\alpha\beta}}{\partial\eta_{\sigma\tau}} \tag{C.3}$$

where V_0 is the volume of the reference state. Note that the subscript $\eta = 0$ in our Eq. (5.7) is missing in this definition. This may lead to a confusion about the reference state. t is the thermodynamic stress tensor defined by Eq. (5.18). The Lagrangian strain tensor in MD is given in Eq. (5.39). The metric tensor $G = h'h$, or $G_{ik} = h_{li}h_{lk}$, and so $G^{-1}_{mi} = h^{-1}_{mk}h^{-1}_{ik}$. I is the unit tensor.

In MD, the scaled coordinates are given by $\mathbf{s} = h^{-1}\mathbf{x}$ or $s_i(a) = h^{-1}_{ij}x_j(a)$ so $r^2 = s_k G_{kl} s_l$. The scaled momenta are given by $\pi = h'p$ or $\pi_i(a) = h_{ji}p_j(a)$ so $p^2 = \pi_k G^{-1}_{kl}\pi_l$. $s_\alpha(ab) = s_\alpha(a) - s_\alpha(b)$ and $r^2 = x^2_\alpha$. Note that the symbols here are a little different from those in Chapter 5. For convenience, we also introduce

$$\begin{aligned} g(r) &= \frac{1}{r^2}\phi''(r) - \frac{1}{r^3}\phi'(r) \\ \phi'(r) &= \frac{d\phi}{dr} \\ \phi''(r) &= \frac{d^2\phi}{dr^2} \end{aligned} \tag{C.4}$$

C.3 Derivation

First of all, from Eq. (5.39), we can find

$$\begin{aligned} dG_{kl} &= 2h_{0ik}d\eta_{ij}h_{0jl} \\ \frac{\partial G_{kl}}{\partial\eta_{ij}} &= 2h_{0ik}h_{0jl} \end{aligned} \tag{C.5}$$

Using $G_{ij}G^{-1}_{jk} = \delta_{ik}$, we get

$$\begin{aligned} G^{-1}_{jk}dG_{ij} + G_{ij}dG^{-1}_{jk} &= 0 \\ dG^{-1}_{mk} &= -G^{-1}_{mi}G^{-1}_{jk}dG_{ij} \\ \frac{\partial G^{-1}_{ij}}{\partial G_{kl}} &= -G^{-1}_{ik}G^{-1}_{lj} \end{aligned} \tag{C.6}$$

hence

$$\begin{aligned} \frac{\partial p^2}{\partial G_{kl}} &= -\pi_i\pi_j G^{-1}_{ik}G^{-1}_{lj} \\ \frac{\partial \tau}{\partial G_{kl}} &= \frac{1}{2\tau}s_k s_l. \end{aligned} \tag{C.7}$$

Therefore

$$\begin{aligned} M_{kl} \equiv \frac{\partial \mathcal{H}}{\partial G_{kl}} &= -\frac{1}{2m}\sum_a \pi_i(a)\pi_j(a)G^{-1}_{ik}G^{-1}_{lj} + \sum_{a>b}\frac{\phi'}{2\tau}s_k(ab)s_l(ab) \\ &= -\frac{1}{2}Vh^{-1}\mathcal{P}(h')^{-1} \\ 4N_{klmn} \equiv 4\frac{\partial^2\mathcal{H}}{\partial G_{kl}\partial G_{mn}} &= 4N_{mnkl} \\ &= \frac{2}{m}\sum_a \pi_i(a)\pi_j(a)(G^{-1}_{im}G^{-1}_{nk}G^{-1}_{lj} + G^{-1}_{ik}G^{-1}_{lm}G^{-1}_{nj}) \\ &\quad + \sum_{a>b} g(r_{ab})s_k(ab)s_l(ab)s_m(ab)s_n(ab), \end{aligned} \tag{C.8}$$

where $\mathcal{P}$ is the microscopic stress tensor given by

$$\mathcal{P}_{ij} = \frac{1}{V}\left(\frac{1}{m}\sum_a p_i(a)p_j(a) - \sum_{a<b}\frac{\phi'(r_{ab})}{r_{ab}}x_i(ab)x_j(ab)\right). \tag{C.9}$$

Now

$$\mathring{C}^T{}_{ijkl} = \frac{\partial t_{ij}}{\partial \eta_{kl}} = \frac{\partial t_{ij}}{\partial G_{mn}}\cdot\frac{\partial G_{mn}}{\partial \eta_{kl}} = 2h_{0km}h_{0ln}\frac{\partial t_{ij}}{\partial G_{mn}}, \tag{C.10}$$

but

$$\begin{aligned} t_{ij} &= \frac{1}{V_0}\frac{\partial F}{\partial \eta_{ij}} = \frac{1}{V_0}\frac{\partial F}{\partial G_{pq}}\cdot\frac{\partial G_{pq}}{\partial \eta_{ij}} = \frac{2}{V_0}h_{0ip}h_{0jq}\frac{\partial F}{\partial G_{pq}} \\ &= \frac{2h_{0ip}h_{0jq}}{V_0 ZC}\int e^{-\mathcal{H}/k_BT}\frac{\partial \mathcal{H}}{\partial G_{pq}}d\tau = \frac{2h_{0ip}h_{0jq}}{V_0}\langle M_{pq}\rangle \end{aligned} \tag{C.11}$$

Therefore,

$$\begin{aligned}\overset{\circ}{C}^{T}{}_{ijkl} &= \frac{4h_{0km}h_{0ln}h_{0ip}h_{0jq}}{V_0 C}\frac{\partial}{\partial G_{mn}}\left(\frac{1}{Z}\int e^{-\mathcal{H}/k_BT}\frac{\partial \mathcal{H}}{\partial G_{pq}}d\tau\right) \\ &= \frac{4}{V_0}\left(\langle N_{mnpq}\rangle - \frac{1}{k_BT}\Delta(M_{mn}\cdot M_{pq})\right)h_{0km}h_{0ln}h_{0ip}h_{0jq} \qquad \text{(C.12)}\end{aligned}$$

where $\Delta(AB) =< AB > - < A >< B >$. Or

$$V_0 h^{-1}_{0im}h^{-1}_{0jn}h^{-1}_{0kp}h^{-1}_{0lq}\,\overset{\circ}{C}_{mnpq} = 4\langle N_{ijkl}\rangle - \frac{4}{k_BT}\Delta(M_{ij}\cdot M_{kl}). \qquad \text{(C.13)}$$

Using

$$\frac{1}{m}\left\langle \sum_a \pi_i(a)\pi_j(a)\right\rangle = Nk_BTh_{li}h_{lj} \qquad \text{(C.14)}$$

we can finally find the usual expressions for isothermal elastic constants in MD [76],

$$\begin{aligned}V_0 h^{-1}_{0im}h^{-1}_{0jn}h^{-1}_{0kp}h^{-1}_{0lq}\,\overset{\circ}{C}^{T}{}_{mnpq} &= \frac{-4}{k_BT}\Delta(M_{ij}M_{kl}) + 2Nk_BT(G^{-1}_{li}G^{-1}_{jk} + G^{-1}_{ki}G^{-1}_{jl}) \\ &\quad + \left\langle \sum_{a<b} g(r_{ab})s_i(ab)s_j(ab)s_k(ab)s_l(ab)\right\rangle \qquad \text{(C.15)}\end{aligned}$$

If $h_0 \neq h$, Eq. (C.15) is dependent on both h and h_0 so the formulae will be obviously different from Eq. (5.48).

C.4 Special Case of the Isotropic System

C.4.1 Simplification of the Momenta Terms

By using $\frac{1}{m} < p_i p_j >= k_BT\delta_{ij}$ and $\frac{1}{m^2}\langle p^4\rangle = 3(k_BT)^2$, we can find

$$\begin{aligned}&\frac{1}{m^2}\left\langle \left(\sum_a p_\alpha(a)p_\beta(a)\right)\cdot\left(\sum_b p_\sigma(b)p_\tau(b)\right)\right\rangle \\ &= \frac{1}{m^2}\left\langle \sum_{a\neq b} p_\alpha(a)p_\beta(a)p_\sigma(b)p_\tau(b)\right\rangle + \frac{1}{m^2}\left\langle \sum_{a=b} p_\alpha(a)p_\beta(a)p_\sigma(b)p_\tau(b)\right\rangle \\ &= N(N-1)(k_BT)^2\delta_{\alpha\beta}\delta_{\sigma\tau} + N(k_BT)^2(\delta_{\alpha\beta}\delta_{\sigma\tau} + \delta_{\alpha\sigma}\delta_{\beta\tau} + \delta_{\alpha\tau}\delta_{\beta\sigma}) \\ &= (Nk_BT)^2\delta_{\alpha\beta}\delta_{\sigma\tau} + N(k_BT)^2(\delta_{\alpha\sigma}\delta_{\beta\tau} + \delta_{\alpha\tau}\delta_{\beta\sigma}) \qquad \text{(C.16)}\end{aligned}$$

Note that Eq. (C.16) is always valid for an isothermal system.

C.4.2 Isotropic System

In the isotropic case, we can write $h_{ij} = V^{\frac{1}{3}}\delta_{ij}$, so $G_{ij} = V^{\frac{2}{3}}\delta_{ij}$ and $s_i = V^{-\frac{1}{3}}x_i$. It is easy to obtain

$$\begin{aligned} 4V^{\frac{4}{3}}\langle N_{ijkl}\rangle &= 2Nk_BT(\delta_{ik}\delta_{lj}+\delta_{il}\delta_{kj}) + \left\langle \sum_{a>b} g(r_{ab})x_i(ab)x_j(ab)x_k(ab)x_l(ab)\right\rangle \\ 2V^{\frac{2}{3}}\langle M_{ij}\rangle &= -Nk_BT\delta_{ij} + \left\langle \sum_{a>b}\frac{\phi'(r_{ab})}{r_{ab}}x_i(ab)x_j(ab)\right\rangle \end{aligned} \tag{C.17}$$

and

$$\begin{aligned} 4V^{\frac{4}{3}}\langle M_{ij}\cdot M_{kl}\rangle &= \left\langle \left(\sum_{a>b}\frac{\phi'(r_{ab})}{r_{ab}}x_i(ab)x_j(ab)\right)\cdot\left(\sum_{a>b}\frac{\phi'(r_{ab})}{r_{ab}}x_k(ab)x_l(ab)\right)\right\rangle \\ &\quad + \frac{1}{m^2}\left\langle \sum_{ab} p_i(a)p_j(a)p_k(b)p_j(b)\right\rangle \\ &\quad -\frac{1}{m}\left\langle \sum_a p_i(a)p_j(a)\right\rangle\left\langle \sum_{a>b}\frac{\phi'(r_{ab})}{r_{ab}}x_k(ab)x_l(ab)\right\rangle \\ &\quad -\frac{1}{m}\left\langle \sum_a p_k(a)p_l(a)\right\rangle\left\langle \sum_{a>b}\frac{\phi'(r_{ab})}{r_{ab}}x_i(ab)x_j(ab)\right\rangle \\ &= \left\langle \left(\sum_{a>b}\frac{\phi'(r_{ab})}{r_{ab}}x_i(ab)x_j(ab)\right)\cdot\left(\sum_{a>b}\frac{\phi'(r_{ab})}{r_{ab}}x_k(ab)x_l(ab)\right)\right\rangle \\ &\quad + (Nk_BT)^2\delta_{ij}\delta_{kl} + N(k_BT)^2(\delta_{ik}\delta_{jl}+\delta_{il}\delta_{jk}) \\ &\quad -Nk_BT\left\langle \sum_{a>b}\frac{\phi'(r_{ab})}{r_{ab}}x_k(ab)x_l(ab)\right\rangle\delta_{ij} \\ &\quad -Nk_BT\left\langle \sum_{a>b}\frac{\phi'(r_{ab})}{r_{ab}}x_i(ab)x_j(ab)\right\rangle\delta_{kl}, \end{aligned} \tag{C.18}$$

therefore

$$\begin{aligned} 4V^{\frac{4}{3}}\Delta\langle M_{ij}\cdot M_{kl}\rangle &= \Delta\left(\left(\sum_{a>b}\frac{\phi'(r_{ab})}{r_{ab}}x_i(ab)x_j(ab)\right)\cdot\left(\sum_{a>b}\frac{\phi'(r_{ab})}{r_{ab}}x_k(ab)x_l(ab)\right)\right) \\ &\quad + N(k_BT)^2(\delta_{ik}\delta_{jl}+\delta_{il}\delta_{jk}). \end{aligned} \tag{C.19}$$

Finally

$$\left(\frac{V}{V_0}\right)^{\frac{1}{3}} \overset{\circ}{C^T}_{ijkl} = \frac{1}{V_0}\left\langle \sum_{a>b} g(r_{ab}) x_i(ab) x_j(ab) x_k(ab) x_l(ab) \right\rangle$$
$$-\frac{1}{k_B T V_0}\Delta\left(\left(\sum_{a>b}\frac{\phi'(r_{ab})}{r_{ab}} x_i(ab) x_j(ab)\right)\cdot\left(\sum_{a>b}\frac{\phi'(r_{ab})}{r_{ab}} x_k(ab) x_l(ab)\right)\right)$$
$$+\frac{N k_B T}{V_0}\left(\delta_{ik}\delta_{jl}+\delta_{il}\delta_{jk}\right). \qquad \text{(C.20)}$$

Note that the above equation differs from Eq. (5.48) or Eqs. (5.52) - (5.54) by a factor of $\left(\frac{V}{V_0}\right)^{\frac{1}{3}}$.

C.5 Simplification with the Correct Reference Value

Let $h_0 = h$ in Eq. (C.15), and so $V = V_0$, multiply both sides of Eq. (C.15) by $h_{\alpha i}h_{\beta j}h_{\sigma k}h_{\tau l}$ and sum over i, j, k, l, using

$$\begin{aligned}
\overset{\circ}{C^T}_{\alpha\beta\sigma\tau} &= h_{\alpha i}h_{\beta j}h_{\sigma k}h_{\tau l}h^{-1}_{iu}h^{-1}_{jv}h^{-1}_{kw}h^{-1}_{lo}\,\overset{\circ}{C^T}_{uvwo} \\
x_\alpha(ab)x_\beta(ab)x_\sigma(ab)x_\tau(ab) &= h_{\alpha i}h_{\beta j}h_{\sigma k}h_{\tau l}s_i(ab)s_j(ab)s_k(ab)s_l(ab) \\
h_{\alpha i}h_{\beta j}h_{\sigma k}h_{\tau l}G^{-1}_{li}G^{-1}_{jk} &= \delta_{\alpha\tau}\delta_{\beta\sigma} \\
h_{\alpha i}h_{\beta j}h_{\sigma k}h_{\tau l}G^{-1}_{ki}G^{-1}_{jl} &= \delta_{\alpha\sigma}\delta_{\beta\tau} \\
h_{\alpha i}h_{\beta j}h_{\sigma k}h_{\tau l}M_{ij}M_{kl} &= h_{\alpha i}h_{\beta j}h_{\sigma k}h_{\tau l}\cdot\left(-\frac{1}{2}Vh^{-1}_{im}\mathcal{P}_{mn}h^{-1}_{jn}\right)\cdot\left(-\frac{1}{2}Vh^{-1}_{km'}\mathcal{P}_{m'n'}h^{-1}_{ln'}\right) \\
&= \frac{1}{4}V^2\mathcal{P}_{\alpha\beta}\mathcal{P}_{\sigma\tau} \qquad \text{(C.21)}
\end{aligned}$$

we obtain

$$\overset{\circ}{C^T}_{\alpha\beta\sigma\tau}V = -\frac{V^2}{k_B T}\Delta(\mathcal{P}_{\alpha\beta}\mathcal{P}_{\sigma\tau}) + 2Nk_BT(\delta_{\alpha\tau}\delta_{\beta\sigma}+\delta_{\alpha\sigma}\delta_{\beta\tau})$$
$$+\left\langle\sum_{a<b} g(r_{ab})x_\alpha(ab)x_\beta(ab)x_\sigma(ab)x_\tau(ab)\right\rangle \qquad \text{(C.22)}$$

Furthermore, using the fact that the average of momenta is independent of the coordinates, we can find

$$V^2\Delta(\mathcal{P}_{\alpha\beta}\mathcal{P}_{\sigma\tau}) = \Delta\left(\left(\sum_{a<b}\frac{\phi'(r_{ab})}{r_{ab}}x_\alpha(ab)x_\beta(ab)\right)\cdot\left(\sum_{a<b}\frac{\phi'(r_{ab})}{r_{ab}}x_\sigma(ab)x_\tau(ab)\right)\right) + \frac{1}{m^2}\Delta\left(\left(\sum_a p_\alpha(a)p_\beta(a)\right)\cdot\left(\sum_b p_\sigma(b)p_\tau(b)\right)\right) \quad \text{(C.23)}$$

Using Eq. (C.16) again, we finally obtain

$$\overset{\circ}{C}{}^T{}_{\alpha\beta\sigma\tau} = \frac{1}{V}\left\langle\sum_{a<b}g(r_{ab})x_\alpha(ab)x_\beta(ab)x_\sigma(ab)x_\tau(ab)\right\rangle - \frac{1}{k_BTV}\Delta\left(\left(\sum_{a<b}\frac{\phi'(r_{ab})}{r_{ab}}x_\alpha(ab)x_\beta(ab)\right)\cdot\left(\sum_{a<b}\frac{\phi'(r_{ab})}{r_{ab}}x_\sigma(ab)x_\tau(ab)\right)\right) + \frac{Nk_BT}{V}(\delta_{\alpha\tau}\delta_{\beta\sigma}+\delta_{\alpha\sigma}\delta_{\beta\tau}) \quad \text{(C.24)}$$

Eq. (C.24) is exactly the same as Eq. (5.48) and this is what we wanted to prove.

C.6 About Adiabatic Elastic Constants

It may be useful to note that the adiabatic elastic constants can also be simplified, the same way,

$$\overset{\circ}{C}{}^S{}_{\alpha\beta\sigma\tau} = \frac{1}{V}\left\langle\sum_{a<b}g(r_{ab})x_\alpha(ab)x_\beta(ab)x_\sigma(ab)x_\tau(ab)\right\rangle - \frac{1}{k_BTV}\Delta\left(\left(\sum_{a<b}\frac{\phi'(r_{ab})}{r_{ab}}x_\alpha(ab)x_\beta(ab)\right)\cdot\left(\sum_{a<b}\frac{\phi'(r_{ab})}{r_{ab}}x_\sigma(ab)x_\tau(ab)\right)\right) + \left(-\frac{3Nk_BT}{V}+\frac{1}{k_BTVm^2}\left\langle\sum_a p_\alpha^4(a)\right\rangle\right)\delta_{\alpha\beta}\delta_{\beta\sigma}\delta_{\sigma\tau} + \frac{Nk_BT}{V}(\delta_{\alpha\tau}\delta_{\beta\sigma}+\delta_{\alpha\sigma}\delta_{\beta\tau}) \quad \text{(C.25)}$$

where the temperature T is given by

$$3Nk_BT = \left\langle\sum_a\frac{1}{m}p_\alpha^2(a)\right\rangle. \quad \text{(C.26)}$$

If

$$\left\langle\sum_a\frac{1}{m^2}p_\alpha^4(a)\right\rangle = 3N(k_BT)^2, \quad \text{(C.27)}$$

then the expressions for $\mathring{C}^{S}{}_{\alpha\beta\sigma\tau}$ will be in the same form as those for $\mathring{C}^{T}{}_{\alpha\beta\sigma\tau}$ i.e. Eq. (C.24). Our MD simulations confirm Eq. (C.27), but an exact proof is not yet available.

Appendix D

Calculation of Elastic Constants in Constant Enthalpy and Constant Shear Strain Ensemble

D.1 Introduction

In this Appendix, using the same method as used in the microcanonical ensemble and the isoenthalpic-isobaric ensemble [130, 139, 140], we derive the fluctuation formulae of elastic constants for the constant enthalpy and constant shear strain ensemble.

D.2 Formulation of the Constant Enthalpy and Constant Shear Strain Ensemble

First we introduce the definition of the constant enthalpy and constant shear strain ensemble i.e. $(H, t_{\alpha\alpha}, \eta_{\alpha\beta}, \alpha \neq \beta)$ ensemble. The $(H, t_{\alpha\alpha}, \eta_{\alpha\beta}, \alpha \neq \beta)$ ensemble is defined by using the phase volume via

$$\phi(H, t_{\alpha\alpha}, \eta_{\alpha\beta}) = \int_{\mathcal{H} \leq H + V_0 \sum_i t_{\alpha\alpha} \epsilon_{\alpha\alpha}} dq dp d\epsilon_{11} d\epsilon_{22} d\epsilon_{33} \tag{D.1}$$

where H is the enthalpy, $\mathcal{H}$ the Hamiltonian of the system. The integral in Eq. (D.1) is over all $3N$ coordinates, $3N$ momenta and 3 independent diagonal microscopic

strain components $\epsilon_{\alpha\alpha}$.

In this section, we shall use scaled coordinates and scaled momenta as defined in Eqs. (5.37) - (5.38). This is necessary since otherwise Eqs. (D.18) - (D.19) are incorrect.

The enthalpy H is defined by

$$H = E - V_0 \sum_{\alpha} t_{\alpha\alpha}\eta_{\alpha\alpha} \tag{D.2}$$

where E is the energy of the system and $\eta_{\alpha\alpha} = \langle \epsilon_{\alpha\alpha} \rangle$ the macroscopic strains. The phase volume can be written

$$\phi(H, t_{\alpha\alpha}, \eta_{\alpha\beta}) = \int \theta(\mathcal{H} - (H + V_0 \sum_{i} t_{\alpha\alpha}\epsilon_{\alpha\alpha}))d\tau \tag{D.3}$$

where the step function

$$\theta(x) = \begin{cases} 1 & x < 0 \\ 0 & x > 0 \end{cases} \tag{D.4}$$

and $d\tau = dqdpd\epsilon_{11}d\epsilon_{22}d\epsilon_{33}$. The density of states $\omega(H, t_{\alpha\alpha}, \eta_{\alpha\beta})$ is defined by

$$\omega = \left(\frac{\partial \phi}{\partial H}\right)_{t_{\alpha\alpha}, \eta_{\alpha\beta}} = \int \delta(\mathcal{H} - (H + \sum_{\alpha} V_0 t_{\alpha\alpha}\epsilon_{\alpha\alpha}))d\tau \tag{D.5}$$

where δ is the Dirac delta function. The normalized probability density $W(q, p, \epsilon_{\alpha\alpha})$ is

$$W(q, p, \epsilon_{\alpha\alpha}) = \delta(\mathcal{H} - (H + \sum_{\alpha} V_0 t_{\alpha\alpha}\epsilon_{\alpha\alpha}))/\omega \tag{D.6}$$

The average value (ensemble average) of any quantity $f(q, p, \eta_{\alpha\beta}, t_{\alpha\alpha})$ is determined from

$$\langle f \rangle = \int W f d\tau \tag{D.7}$$

The entropy is defined by

$$S(H, t_{\alpha\alpha}, \eta_{\alpha\beta}) = k_B \ln \phi(H, t_{\alpha\alpha}, \eta_{\alpha\beta}) \tag{D.8}$$

We have omitted various constant factors which would render ϕ dimensionless. These constant factors would not appear in any of our final results. From Eq. (D.8), we obtain for the temperature

$$T = \left(\frac{\partial S}{\partial H}\right)_{t_{\alpha\alpha},\eta_{\alpha\beta}} = \frac{\phi}{k_B\omega} \tag{D.9}$$

Following the same arguments as those used in the microcanonical ensemble[139, 141] leads to the equipartition theorem

$$\left\langle x_j \frac{\partial \mathcal{H}}{\partial x_k} \right\rangle = \frac{\phi}{\omega}\delta_{jk} \tag{D.10}$$

where x_i stands for one of the q or p variables.

Next we consider the adiabatic theorem for this ensemble. The Hamiltonian is now assumed to depend on an additional external parameter, say y. The generalized force associated with this parameter is $\frac{\partial \mathcal{H}}{\partial y}$. Calculating the average value of this generalized force, just as we did in the microcanonical ensemble[139, 141], leads to the result

$$\begin{aligned}\left\langle \frac{\partial \mathcal{H}}{\partial y} \right\rangle &= \frac{1}{\omega}\int \frac{\partial \mathcal{H}}{\partial y}\delta(\mathcal{H} - (H + \sum_\alpha V_0 t_{\alpha\alpha}\epsilon_{\alpha\alpha}))d\tau = -\frac{1}{\omega}\left(\frac{\partial \phi}{\partial y}\right)_{H,t_{\alpha\alpha},\eta_{\alpha\beta}} \\ &= \left(\frac{\partial H}{\partial y}\right)_{S,t_{\alpha\alpha},\eta_{\alpha\beta}}\end{aligned} \tag{D.11}$$

which is the adiabatic theorem.

D.3 Calculation of the Elastic Constants

The thermodynamic law in the $(H, t_{\alpha\alpha}, \eta_{\alpha\beta}, \alpha \neq \beta)$ ensemble is

$$dH = TdS - V_0 \sum_\alpha \eta_{\alpha\alpha} dt_{\alpha\alpha} + V_0 \sum_{\alpha\neq\beta} t_{\alpha\beta} d\eta_{\alpha\beta}, \tag{D.12}$$

from which follows

$$\begin{aligned} V_0\eta_{\alpha\alpha} &= -\left(\frac{\partial H}{\partial t_{\alpha\alpha}}\right)_S \\ V_0 t_{\alpha\beta} &= \left(\frac{\partial H}{\partial \eta_{\alpha\beta}}\right)_S . \end{aligned} \tag{D.13}$$

Now we can derive the fluctuation formulae of the adiabatic elastic constants by following the same procedure as Ray et. al. [130, 139, 140] did. Defining a potential

$$X_{\alpha\alpha} = \int \epsilon_{\alpha\alpha}\theta(\mathcal{H} - (H + V_0 \sum_{\alpha} t_{\alpha\alpha}\epsilon_{\alpha\alpha}))d\tau \tag{D.14}$$

by using Eq. (D.13) and the definition of the average value, we obtain

$$\begin{aligned}\left(\frac{\partial X_{\alpha\alpha}}{\partial t_{\beta\beta}}\right)_S &= \int \epsilon_{\alpha\alpha}\delta(\mathcal{H} - (H + \sum_{\alpha} V_0 t_{\alpha\alpha}\epsilon_{\alpha\alpha}))(-V_0 \langle\epsilon_{\beta\beta}\rangle + V_0\epsilon_{\beta\beta})d\tau \\ &= \omega V_0 \left(\langle\epsilon_{\alpha\alpha}\cdot\epsilon_{\beta\beta}\rangle - \langle\epsilon_{\alpha\alpha}\rangle\langle\epsilon_{\beta\beta}\rangle\right).\end{aligned} \tag{D.15}$$

For a system of many degrees of freedom, the approximation $X_{\alpha\alpha} = \langle\epsilon_{\alpha\alpha}\rangle\phi = \eta_{\alpha\alpha}\phi$ is very accurate, hence Eq. (D.15) becomes

$$\langle\epsilon_{\alpha\alpha}\cdot\epsilon_{\beta\beta}\rangle - \langle\epsilon_{\alpha\alpha}\rangle\langle\epsilon_{\beta\beta}\rangle = \frac{\phi}{\omega V_0}\left(\frac{\partial\eta_{\alpha\alpha}}{\partial t_{\beta\beta}}\right)_S$$

or using Eq. (D.9)

$$\langle\epsilon_{\alpha\alpha}\cdot\epsilon_{\beta\beta}\rangle - \langle\epsilon_{\alpha\alpha}\rangle\langle\epsilon_{\beta\beta}\rangle = \frac{k_B T}{V_0}(\mathring{C}^s)^{-1}_{\alpha\alpha\beta\beta}. \tag{D.16}$$

To derive the formula for the elastic constants with $\alpha \neq \beta$ and $\sigma \neq \tau$ we have to define a new function,

$$Z(H, t_{\alpha\alpha}, \eta_{\alpha\beta}) = \int \mathcal{P}_{\alpha\beta}\theta(\mathcal{H} - (H + V_0 \sum_{\alpha} t_{\alpha\alpha}\epsilon_{\alpha\alpha}))d\tau, \quad \alpha \neq \beta \tag{D.17}$$

where $\mathcal{P}_{\alpha\beta}$ is the microscopic stress tensor defined by (also see Eq. (C.9))

$$V_0\mathcal{P}_{\alpha\beta} = \frac{\partial\mathcal{H}}{\partial\eta_{\alpha\beta}} \tag{D.18}$$

We have

$$\begin{aligned}\left(\frac{\partial Z}{\partial\eta_{\sigma\tau}}\right)_S &= \int \frac{\partial\mathcal{P}_{\alpha\beta}}{\partial\eta_{\sigma\tau}}\theta(\mathcal{H} - (H + V_0 \sum_{\alpha} t_{\alpha\alpha}\epsilon_{\alpha\alpha}))d\tau \\ &\quad - \int \mathcal{P}_{\alpha\beta}\delta(\mathcal{H} - (H + V_0 \sum_{\alpha} t_{\alpha\alpha}\epsilon_{\alpha\alpha}))\left(\frac{\partial\mathcal{H}}{\partial\eta_{\sigma\tau}} - \left(\frac{\partial H}{\partial\eta_{\sigma\tau}}\right)_S\right)d\tau \\ &= \frac{1}{V_0}\int \frac{\partial^2\mathcal{H}}{\partial\eta_{\alpha\beta}\partial\eta_{\sigma\tau}}\theta(\mathcal{H} - (H + V_0 \sum_{\alpha} t_{\alpha\alpha}\epsilon_{\alpha\alpha}))d\tau \\ &\quad + V_0 \int \mathcal{P}_{\alpha\beta}\mathcal{P}_{\sigma\tau}\delta(\mathcal{H} - (H + V_0 \sum_{\alpha} t_{\alpha\alpha}\epsilon_{\alpha\alpha}))d\tau \\ &\quad - V_0 \langle\mathcal{P}_{\alpha\beta}\rangle\langle\mathcal{P}_{\sigma\tau}\rangle\omega\end{aligned} \tag{D.19}$$

Again, by using $Z = \langle \mathcal{P}_{\alpha\beta} \rangle \phi$ and

$$\int \frac{\partial^2 \mathcal{H}}{\partial \eta_{\alpha\beta} \partial \eta_{\sigma\tau}} \theta(\mathcal{H} - (H + V_0 \sum_a t_{aa} \epsilon_{aa})) d\tau = \left\langle \frac{\partial^2 \mathcal{H}}{\partial \eta_{\alpha\beta} \partial \eta_{\sigma\tau}} \right\rangle \phi \qquad \text{(D.20)}$$

we get

$$\phi \left(\frac{\partial \langle \mathcal{P}_{\alpha\beta} \rangle}{\partial \eta_{\sigma\tau}} \right)_S = \frac{\phi}{V_0} \left\langle \frac{\partial^2 \mathcal{H}}{\partial \eta_{\alpha\beta} \partial \eta_{\sigma\tau}} \right\rangle - \omega V_0 \langle \mathcal{P}_{\alpha\beta} \mathcal{P}_{\sigma\tau} \rangle + \omega V_0 \langle \mathcal{P}_{\alpha\beta} \rangle \langle \mathcal{P}_{\sigma\tau} \rangle \qquad \text{(D.21)}$$

or

$$\begin{aligned} (\mathring{C}^S)_{\alpha\beta\sigma\tau} &= \frac{1}{V_0} \left\langle \frac{\partial^2 \mathcal{H}}{\partial \eta_{\alpha\beta} \partial \eta_{\sigma\tau}} \right\rangle \\ &\quad - \frac{V_0}{k_B T} (\langle \mathcal{P}_{\alpha\beta} \cdot \mathcal{P}_{\sigma\tau} \rangle - \langle \mathcal{P}_{\alpha\beta} \rangle \langle \mathcal{P}_{\sigma\tau} \rangle) \quad \alpha \neq \beta \text{ and } \sigma \neq \tau \qquad \text{(D.22)} \end{aligned}$$

Note that Eq. (D.22) is exactly the same as the one in the microcanonical ensemble. Using the same procedure as in Appendix C, for the central force system, we can derive the same expressions as in the microcanonical ensemble [76, 77, 131] for the elastic constants with $\alpha \neq \beta$ and $\sigma \neq \tau$.

The remaining elastic constants i. e. the crossover part with $\alpha = \beta$ but $\sigma \neq \tau$ or $\alpha \neq \beta$ but $\sigma = \tau$ cannot be obtained in this way as in the constant T and constant shear strain ensemble.

Appendix E

Extreme deformation paths for $T_{\alpha\beta}\xi'_{\alpha\beta}$

Using Eq. (6.27) with $\epsilon_{\alpha\beta} = \epsilon_{\alpha\beta}(x)$, where x is a path parameter, we have for an arbitrary path

$$T_{\alpha\beta}\xi'_{\alpha\beta} = \int (T_{\alpha\beta}\dot{\epsilon}_{\alpha\beta}\epsilon_{\sigma\sigma} - T_{\alpha\beta}\epsilon_{\alpha\beta}\dot{\epsilon}_{\sigma\sigma})dx. \tag{E.1}$$

The Euler equations for the deformation paths maximizing $T_{\alpha\beta}\xi'_{\alpha\beta}$ are

$$T_{\alpha\beta}\delta_{\sigma\tau}\dot{\epsilon}_{\alpha\beta} - T_{\sigma\tau}\dot{\epsilon}_{\alpha\alpha} = 0. \tag{E.2}$$

For isotropic stress ($T_{\alpha\beta} = -p\delta_{\alpha\beta}$), the above equation is satisfied automatically. But for anisotropic stress, Eq. (E.2) with $\sigma \neq \tau$, yields $\dot{\epsilon}_{\alpha\alpha} = 0$, or $\epsilon_{\alpha\alpha} = 0$, using the initial boundary condition, and $\eta_{\alpha\alpha} = 0$. These are volume preserving deformations, reached by volume preserving paths. The $\sigma = \tau$ terms then give $T_{\alpha\beta}\dot{\epsilon}_{\alpha\beta} = 0$, or $T_{\alpha\beta}\epsilon_{\alpha\beta} = 0$ along the path, and the final value $T_{\alpha\beta}\eta_{\alpha\beta} = 0$. For these special paths, it follows immediately that $T_{\alpha\beta}\xi'_{\alpha\beta} = 0$. The linear deformation paths to the $\eta_{\alpha\alpha}$ satisfying the above two conditions are obviously part of this set. Therefore there may exist in anisotropic cases, a set of volume preserving deformation directions with extreme paths attaining them, which have path independent work with the above constraints. For arbitrary $\eta_{\alpha\beta}$, however, there usually will be no extremum path. If the $\epsilon_{\alpha\beta}$ are bounded, the extremum path will be determined by the boundary.

For the case of uniaxial tension $T_{\alpha\beta} = -p\delta_{1\alpha}\delta_{1\beta}$, and $T_{\alpha\beta}\epsilon_{\alpha\beta} = -p\epsilon_{11} = 0$; or $\epsilon_{11} = 0$ with constant volume. Deformations obeying these constraints have a path independent work with $T_{\alpha\beta}\xi'_{\alpha\beta} = 0$.

References

[1] A. J. C. Ladd and W. G. Hoover, Phys. Rev. B **26**, 5469 (1982).

[2] W. G. Hoover, N. E. Hoover and W. C. Moss, J. Appl. Phys. **50**, 829 (1979).

[3] W. G. Hoover, W. T. Ashurst and R. J. Olness, J. Chem. Phys. **60**, 4043 (1974).

[4] W. G. Hoover, A. J. C. Ladd and N. E. Hoover, in *Interatomic Potentials and Crystalline Defects*, edited by J. K. Lee (Metallurgical Society, Warrendale, Penn., 1981).

[5] F. F. Abraham, Adv. Phys. **35**, 1 (1986).

[6] K. Strandburg, Rev. Mod. Phys. **60**, 161 (1988).

[7] J. A. Combs, Phys. Rev. Lett. **61**, 714 (1988), J. A. Combs, Phys. Rev. B **38**, 6751 (1988).

[8] W. G. Hoover, A. J. de Groot and C. G. Hoover, Comp. Phys. **6**, 155(1992).

[9] B. Joós and M. S. Duesbery, Phys. Rev. Lett. **70**, 2754 (1993).

[10] A. J. C. Ladd and W. G. Hoover, J. Chem. Phys. **74**, 1337(1981).

[11] W. A. Steele, Surf. Sci. **36**, 317(1973).

[12] M. P. Allen and D. J. Tildesley, *Computer Simulation of Liquids*, (Oxford University Press, New York, 1987).

[13] A. Rahman, Phys. Rev. A **136**, 405(1964).

[14] L. Verlet, Phys. Rev. **159**, 98(1967).

[15] L. Verlet, Phys. Rev. **165**, 201(1968).

[16] D. Brown and J. H. R. Clarke, Mol. Phys., **51**, 1243(1984).

[17] L. V. Woodcock, Chem. Phys. Lett., **10**, 257(1970).

[18] Y. Hiwatari, E. Stoll and T. Schneider, J. Chem. Phys. **68**, 3401(1978).

[19] W. Hoover, Pysica **A118**, 111(1983).

[20] H. C. Andersen, J. Chem. Phys. **72**, 2384 (1980).

[21] D.J. Evans and G.P. Morriss, Chem. Phys. **77**, 63(1983); Phys. Lett., **98A**, 433(1983).

[22] K. Huang, *Statistical Mechanics* (New York, John Wiley & Sons Inc. 1965).

[23] L. E. Reichl, *A Modern Course in Statistical Physics* (University of Texas Press 1980).

[24] D. Chandler, *Introduction to Modern Statistical Mechanics* (New York, Oxford, Oxford University Press 1987).

[25] R. N. Thurston, in *Physical Acoustics*, Vol. I., Part A, edited by W. P. Mason (Academic New York, 1964).

[26] F. F. Abraham, Phys. Rep. **80**, 339(1980).

[27] M. P. Allen, D. Frenkel, W. Gignac and J. P. McTague, J. Chem. Phys. **78**, 4206(1983); F. H. Stillinger and T. A. Weber, J. Chem. Phys. **74**, 4015, 4020(1981); J. Q. Broughton, G., H., Gilmer and J. D. Weeks, Phys. Rev. B **25**, 4651(1982).

[28] R.M.J. Cotterill, M. Doyoma, J.J. Jackson and M. Meshii, Eds: *Lattice Defects in Quenched Metals*, (Academic Press, New York,1965).

[29] C.P. Flynn, *Point Deffects and Diffusion*, (Oxford, Oxford University Press, 1972).

[30] C. Kittel, *Introduction to Solid State Physics*, 7th edn (Toronto, John Wiley & Sons, Inc., 1995).

[31] P. Dimon, P. M. Horn, M. Sutton, R. J. Birgeneau and D. E. Moncton, Phys. Rev. B **31**, 437 (1985) (the vacancy concentration at a given point in the phase diagram is obtained by comparing the coverage measured in units of the commensurate $\sqrt{3} \times \sqrt{3}$ density with the expected full coverage calculated from for the lattice constant derived from the structure factor peak.)

[32] J. M. Kosterlitz and D. J. Thouless, J. Phys. C **6**, 1181 (1973).

[33] D. R. Nelson and B. I. Halperin, Phys. Rev. B **19**, 2457 (1979).

[34] A. P. Young, Phys. Rev. B **19**, 1855 (1979).

[35] B. Joós, Z. Zhou and M.S. Duesbery, Phys. Rev. B **50**, 8763 (1994).

[36] M. S. Duesbery and B. Joós, Phil. Mag. A **54**, 145 (1985) (in fig. 1 the labels for λ and μ have been inverted).

[37] V. Volterra, Ann. Sci. Ec. Norm. Sup., Paris **24**, 401(1907).

[38] J. H. Michell, Proc. Lond. Math. Soc. **31**, 100(1900).

[39] G. Weingarten, Atti Accad. Naz. Lincer Rc. **10**, 57(1901).

[40] A. Timpe, Z. Math. Phys. **52**, 348(1905).

[41] A. E. H. Love, *A Treaties on the Mathematical Theory of Elasticity*, 3rd edn (Cambridge, Cambridge Univerisity Press, 1927).

[42] C. Somigliana, Atti Accad. Naz. Lincer Rc. **23**, 463(1914).

[43] C. Somigliana, Atti Accad. Naz. Lincer Rc. **24**, 655(1915).

[44] O. Mügge, Neues Jahb. Min. **13**(1883).

[45] A. Ewingg and W. Rosenhain, Phil. Tans. Roy. Soc. A **193**, 353(1899).

[46] L. Prandtl, Z. angew. Math. Mech. **8**, 85(1928).

[47] U. Delhlinger, Ann. Phys. Lpz. **2**, 749(1929).

[48] G. I. Taylor, Proc. R. Soc. A **145**, 362(1934).

[49] E. Orowan, Z. Phys. **89**, 634(1934).

[50] M. Polanyi, Z. Phys. **89**, 660(1934).

[51] J. M. Burgers, Proc. Koninkl. Ned. Acad. Wet. **42**, 293(1939).

[52] J. P. Hirth and J. Lothe, *Theory of Dislocations*, 2nd edn (Wiley, New York 1982).

[53] J. A. Barker, D. Henderson and F. F. Abraham, Physica **106A**, 226(1981).

[54] M. Manninen and H. Häkkinen, J. Comput. Phys. **100**, 197(1992). in ref. [9].

[55] B. Joós and M. S. Duesbery, Phys. Rev. Lett. **55**, 1997 (1985); Phys. Rev. B **33**, 8632 (1986).

[56] B. Grossmann, B. Joós and M.S. Duesbery, Phys. Rev. B **39**, 7917 (1989).

[57] B. Joós, Q. Ren and M.S. Duesbery, Surf. Sci. **302**, 385 (1994).

[58] Desorption rates for physisorbed monolayers are of the order of $10^8 s^{-1}$(see for instance H. J. Kreuzer and Z. W. Gortel, Physisorption Kinetics (Springer Verlag, Berlin, 1986) vol. 1 of Springer Series in Surface Sciences.

[59] N. Greiser, G. A. Held, R. Frahm, R. L. Greene, P. M. Horn and R. M. Suter, Phys. Rev. Lett. **59**, 1706 (1987) and references therein.

[60] See, for instance, B. Alberts, D. Bray, J. Lewis, M. Raff, K. Roberts and J. D. Watson, *Molecular Biology of the Cell*, 2nd ed. (Garland, New York, 1989).

[61] R.W. Balluffi, J. Nucl. Mat. **69 & 70**, 240 (1978), and others in this two volume issue devoted to a conference on atomic defects in metals.

[62] D.P. Lahiri, T.R. Ramachandra and A.K. Jena, J. Mat. Sci. **11**, 471 (1976).

[63] S. Ceresara, A. Giarda and A. Sanchez, Phil. Mag. **35**, 97 (1977).

[64] E. Hashimoto, Y. Murakami and T. Kino, J. Phys. Soc. Jpn. **49**, 1123 (1980).

[65] A. Parthasarathi and H.L. Fraser, Phil. Mag. A **50**, 89 (1984); **50**, 101 (1984).

[66] A.J. Perry, Phil. Mag. **21**, 743 (1970).

[67] Z. Zhou and B. Joós, Surf. Sci. **323**, 311(1995).

[68] See, e.g. *Deep centers in Semiconductors*, ed. S.T. Pantelides (Gordon and Breach, New York, 1986); S. Dannefaer, G.W. Dean, D.P. Kerr and B.G. Hogg, Phys. Rev. B **14**, 2709 (1976); B.G. Svensson, K.Johnsson, D.-X. Xu, J.H. Svensson and J.L. Lindstrom, in *Radiation Effects and Defects in Solids*, Vol. 111, p. 439 (Gordon and Breach, New York, 1989); S. Roorda, W.C. Sinke, J.M. Poate, D.C.Jacobson, S. Dierker, B.S. Dennis, D.J. Eaglesham, F. Spaepen and P. Fuoss, Phys. Rev. B **44**, 3702 (1991); S. Roorda, Mat. Res. Soc. Symp. Proc. Vol. 316, p. 159 (1994).

[69] B. Mutaftschiev, in *Dislocations in Solids*, Vol. 5, F.R.N. Nabarro ed., (North-Holland, Amsterdam, 1980) p. 57.

[70] K. Huang, Proc. Roy. Soc. **A**, 178 (1950); M. Born and K. Huang, *Dynamical Theory of Crystal Lattice* (Oxford University Press, Oxford, 1954).

[71] D. R. Squire, A. C. Holt and W. G. Hoover, Physica **42**, 388 (1969).

[72] W.G. Hoover, A.C. Holt and D.R. Squire, Physica **44**, 437 (1969).

[73] M. L. Klein and R. D. Murphy, Phys. Rev. B **6**, 2433 (1972).

[74] J. R. Ray and A. Rahman, J. Chem. Phys. **80**, 4423(1984).

[75] J. R. Ray and A. Rahman, J. Chem. Phys. **82**, 4243 (1985).

[76] J. R. Ray, M. C. Moody and A. Rahman, Phys. Rev. B **32**, 733 (1985).

[77] J. R. Ray, M. C. Moody and A. Rahman, Phys. Rev. B **33** 895(1986).

[78] J. Ray, Compt. Phys. Repts. **8**, 109(1988).

[79] J. Lutsko, J. Appl. Phys. **65**, 2991(1989).

[80] A. A. Maradudin, in *Dynamical Properties of Solid*, Vol. 1, ed. by G. K. Horton and A. A. Maradudin (North-Holland, Amsterdam, 1974).

[81] T. H. K. Barron and M. L. Klein, Proc. Phys. Soc., **85**, 523 (1965).

[82] Z. Zhou and B. Joós, Phys. Rev. B, (in press).

[83] D. C. Wallace, *Thermodynamics of Crystals* (Wiley, New York, 1972).

[84] R. Hill, Math. Proc. Camb. Phil. Soc., **77**, 225(1975).

[85] F. Milstein, Phys. Rev. Ser., **B3**, 1130(1971), J. Appl. Phys. **44**, 3833(1973).

[86] F. Milstein, J. Appl. Phys. **44**, 3833(1973).

[87] Z. S. Basinski, M. S. Duesbery, A. P. Pogany, R. Taylor and Y. P. Varshni, Can. J. Phys. **48**, 1480 (1970).

[88] J. H. Weiner, *Statistical Mechanics of Elasticity*, (John Wiley & Sons, Toronto, 1983).

[89] J. Wang, S. Yip, S. R. Phillpot and D. Wolf, Phys. Rev. Lett. **71**, 4182 (1993).

[90] M. Sprik, R. W. Impey and M. L. Klein, Phys. Rev. B **29**, 4368(1984).

[91] S. J. Barsky, M. Plischke, B. Joós and Z. Zhou (to be published).

[92] S. Chapman and T. G. Cowling, *The Mathematical Theory of Nonuniform Gases*, (Cambridge University Press, Cambridge, 1961).

[93] J. M. Haile, *Molecular Dynamics Simulation*, (John Wiley & Sons, Inc., Toronto, 1992).

[94] M. Parrinello and A. Rahman, J. Chem. Phys. **76**, 2662 (1982).

[95] S. Nosé and M. L. Klein, Mol. Phys., **50**, 1055(1983).

[96] M. Born, Proc. Camb. Phil. Soc., **36**, 160(1940).

[97] M. Born and R. Furth, Proc. Camb. Phil. Soc. **36**, 454(1970).

[98] N. H. Macmillan and A. Kelly, Proc. R. Soc. Lond. A

[99] R. Hill and F. Milstein, Phys. Rev. B **15**, 3087(1977).

[100] F. Milstein and R. Hill, J. Mech. Phys. Solids **25**, 457(1977).

[101] F. Milstein and R. Hill, J. Mech. Phys. Solids **26**, 213(1978).

[102] F. Milstein and R. Hill, Phys. Rev. Lett. **43**, 1411(1979).

[103] F. Milstein, in Mechanics of Solids, edited by H. G. Hopkins and M. J. Sewell (Pergamon, Oxford, 1982).

[104] J. Wang, J. Li, S. Yip, S. Phillpot and D. Wolf, Phys. Rev. B **52**, 12627(1995).

[105] H. Goldstein, *Classical Mechanics*, 2nd ed., (Addison-Wesley, Reading, Mass, 1980) p. 339.

[106] O.-Y. Zhong-can and W. Helfrich, Phys. Rev. Lett. **59**, 2486 (1987); Phys. Rev. **A39**, 5280 (1989).

[107] L. Miao, B. Fourcade, M. Rao, M. Wortis and R. K. P. Zia, Phys. Rev. **A43**, 6843 (1991).

[108] M. A. Peterson, Phys. Rev. Lett. **61**, 1325 (1988).

[109] H. B. Huntington, in *Solid State Physics*, Vol. 7, ed. by F. Seitz and D. Turnbull (Academic Press Inc., New York, 1958).

[110] J. Laval, Compt. rend. **232**, 1947(1951); **238**, 1773 (1954).

[111] Y. Le Corre, Compt. rend. **236**, 1903(1953).

[112] Y. Le Corre, Bull. soc. franc. mineral et crist. **76**, 464(1953); **77**, 1363(1954); **78**, 33(1955).

[113] K. S. Viswanathan, Proc. Indian Acad. Sci. **A39**, 196(1954); **A41**, 98(1955).

[114] C. V. Raman and K. S. Viswanathan, Indian Acad. Sci. **A42**, 1, 51(1955).

[115] C. V. Raman and D. Krishnamurti, Indian Acad. Sci. **A42**, 111(1955).

[116] W.T. Coakley and J.O.T. Deeley, Biochim. Biophys. Acta **602**, 355.

[117] D. Gallez and W.T. Coakley, Prog. Biophys. Mol. Biol. **48** (1986).

[118] S. Ohki, *Molecular Mechanisms of Membrane Fusion*, (Plenum, New York, 1988).

[119] L. Song, Q.F. Ahkong, D. Georgescauld and J.A. Lucy, Biochim. Biophys. Acta **1065**, 541(1991).

[120] G.V. Gass and L.V. Chernomordik, Biochim. Biophys. Acta **1023**, 1(1990).

[121] T.Y. Tsong, Biophys. J. **60**, 297(1991).

[122] D. Gallez, N.M. Costa Pinto and P.M. Bisch, J. Colloid. Interface. Sci. **160**, 141(1993).

[123] M.J. Grimson, J. Phys.: Condens. Matter **5**, 4749(1993).

[124] B. J. Alder and T. E. Wainwright, Phys. Rev. **127**, 359(1962).

[125] R. W. Hockney, Methods Comput. Phys., **9**, 136(1970).

[126] D. Potter, in *Computational Physics*, (Wiley, New York 1972).

[127] C. W. Gear, in *Numerical initial value problems in ordinary differential equations*, (Prentice-Hall, Englewood Cliffs, NJ 1971).

[128] M. Parrinello and A. Rahman, Phys. Rev. Lett. **45**, 1196(1980).

[129] M. Parrinello and A. Rahman, J. Appl. Phys. **52**, 7182 (1981).

[130] J. R. Ray, J. Appl. Phys., **53**, 6441(1982).

[131] T. Cagin and J. R. Ray, Phys. Rev. B **38**, 7940(1988).

[132] S. Nosé , Mol. Phys. **52**, 255(1984); J. Chem. Phys. **81**, 511(1984).

[133] W. G. Hoover, Phys. Rev. A **31**, 1695(1985).

[134] J. M. Hail and H. W. Graben, J. Chem. Phys. **73**, 2412(1980).

[135] S. Melchionna, G. Ciccotti and B. L. Holian, Mol. Phys., **78**, 533(1993).

[136] B. Quentrec and C. Brot, J. Comput. Phys. **13**, 430(1975)

[137] R. W. Hockney and J. W. Eastwood, in *Computer simulation using particles*, (McGraw-Hill, New York 1981).

[138] D. Knuth, in *The art of computer programming*, 2nd edn, (Addison-Wesley, Reading, MA 1973).

[139] J. R. Ray, and H. W. Graben, Mol. Phys. **43**, 1293(1981).

[140] J. R. Ray, H. W. Graben and J. M. Haile, Nuovo Cimento B **64**, 191(1981).

[141] R. Becker, in *Theory of Heat*, 2nd ed. (Springer-Verlag, 1967) Chap. 2.